nature

THE INTERNATIONAL WEEKLY JOURNAL OF SCIENCE

JUMP FOR IT

Modern lizards model velociraptor motion and inspire robot design

PAGES 148 & 181

REGENERATIVE MEDICINE

TRIALS AND TRIBULATIONS

The business of embryonic stem-cell research

PAGE 130

EXTRASOLAR PLANETS

WONDERFUL WORLDS

'Super-Earths' plentiful in the Milky Way

PAGE 167

CLIMATE POLICY

REACH FOR THE SUMMIT

With Durban a memory it's time to plan for 2015

PAGE 137

NATURE.COM/NATURE

12 January 2012 £10

Vol. 481, No. 7380

02

9 770028 083095

EPITOMICS®

BETTER ANTIBODIES • BETTER SCIENCE

SPECIAL OFFER

$99 ANTIB SPECI

Find out more @ www.epitomics.com/product

ANTIBODIES for AUTOPHAGY

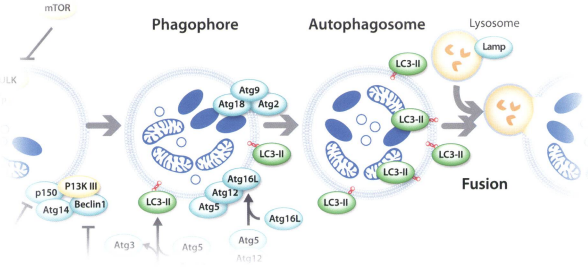

- **High quality antibodies to autophagy targets:** Atg family members, LC3 and more
- **Validated in WB, IHC, IF, IP and FACS**
- **Over 7000 antibodies and counting**

Epitomics provides a wide range of high quality antibodies for autophagy-related targets. Using our patented Rabbit Monoclonal Antibody (RabMAb®) technology, we have developed a collection of high quality autophagy-specific antibodies. This includes RabMAbs to several important autophagy markers, such as Atg family members and LC3 (MAP1LC3).

Every RabMAb is validated in western blot, immunohistochemistry, immunofluorescence, immunoprecipitation and flow cytometry before release, so you can be assured which assays the antibody will work for before purchasing.

Find out more @ www.epitomics.com/autophagy

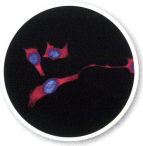

Atg3

Immunofluorescent staining of HeLa cells using anti-Atg3 RabMAb (cat. # 3580-1).

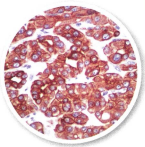

Atg5

Immunohistochemical analysis of paraffin-embedded human hepatocellular carcinoma tissue using anti-Atg5 RabMAb (cat. # 3167-1).

Antibody Satisfaction Guarantee

www.epitomics.com

US & Canada | 1-877-772-2622

Outside NA | 650-583-6688

info@epitomics.com

This month in *Nature Reviews*

Neural mechanisms of atrial arrhythmias
M. J. Shen, E. Choi, A. Y. Tan, S. Lin, M. C. Fishbein, L. S. Chen & P. Chen

Ectopic foci in pulmonary veins can trigger episodes of atrial fibrillation (AF), but how these foci arise remains unclear. This review highlights the role of the autonomic nervous system in the induction and maintenance of atrial arrhythmias, and explores neural modulation as a treatment strategy for AF.

www.nature.com/nrcardio

The worldwide epidemiology of type 2 diabetes mellitus—present and future perspectives
L. Chen, D. J. Magliano & P. Z. Zimmet

Zimmet and colleagues review the current worldwide trends of the diabetes epidemic and discuss the associated major risk factors, particularly genetic and epigenetic factors. The authors also discuss the potential impact of the use of HbA_{1c} as an alternative diagnostic tool on global diabetes surveillance.

www.nature.com/nrendo

MRI in Crohn's disease—current and future clinical applications
G. Fiorino, C. Bonifacio, A. Malesci, L. Balzarini & S. Danese

Fiorino *et al.* discuss the development of objective MRI-based scores to evaluate the extent of intestinal damage in patients with Crohn's disease and speculate about how this could form part of a 'damage-driven' treatment paradigm.

www.nature.com/nrgastro

The podocyte cytoskeleton—key to a functioning glomerulus in health and disease
G. I. Welsh & M. A. Saleem

This Review outlines the most recent concepts and advances in podocyte biology, and discusses how an improved understanding of the podocyte cytoskeleton is starting to shape advances in delineating the pathogenesis of common glomerular diseases.

www.nature.com/nrneph

Depression in Parkinson disease—epidemiology, mechanisms and management
D. Aarsland, S. Påhlhagen, C. G. Ballard, U. Ehrt & P. Svenningsson

Depression is common in patients with Parkinson disease (PD). Aarsland *et al.* discuss the course of depression and the mechanisms that contribute to enhanced susceptibility to depression in PD. Management strategies are also highlighted.

www.nature.com/nrneurol

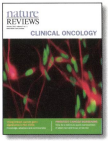

Cancer immunology—analysis of host and tumor factors for personalized medicine
S. Ogino, J. Galon, C. S. Fuchs & G. Dranoff

Cancer immunology is an interactive field that requires the skills of oncologists and immunologists, in addition to other aspects, such as pathology. This Review uses colorectal cancer as a prototypical cancer and describes how molecular features and immune reactions are inter-related.

www.nature.com/nrclinonc

Cardiovascular safety of biologic therapies for the treatment of RA
J. D. Greenberg, V. Furer & M. E. Farkouh

Comorbid cardiovascular disease is a substantial problem for patients with rheumatoid arthritis (RA). Here, the authors summarize the evidence—and knowledge gaps—regarding the influence of biologic therapies on cardiovascular risk parameters in patients with RA.

www.nature.com/nrrheum

Image-guided radiation therapy for muscle-invasive bladder cancer
J. Thariat et al.

The hollow and mobile nature of the bladder causes variations in its volume, shape and position, making delivery of radiation therapy to bladder tumors challenging. Here, Thariat *et al.* describe using imaging to improve the accuracy and effectiveness of radiation therapy for bladder cancer.

www.nature.com/nrurol

nature REVIEWS
www.nature.com/reviews
nature publishing group npg

"There's a way to do it better — **find it.**"

Thomas Edison

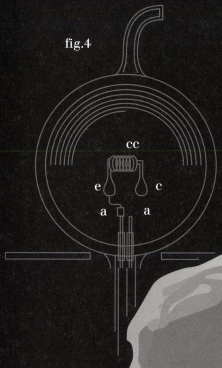

ReadCube is a better way to **read**, **search**, **organize** and **find** your research literature.

Digital Science –
software that understands science

DIGITAL science

www.digital-science.com

readcube

www.readcube.com

CONTENTS

12 January 2012 / Vol 481 / Issue No 7380

THIS WEEK

EDITORIALS

113 NUCLEAR POWER
Get tough on nuclear safety
The Fukushima disaster means that the nuclear industry needs fresh standards

113 UK SCIENCE
A long stretch
Can the UK government's plans for new-style universities be realized without investment?

114 WHALING
Whales for sale
Quota trading may be the best way to save the whale

WORLD VIEW

115 **Don't censor life-saving science**
Peter Palese
Restricting access to research on bird flu does not serve the greater good

RESEARCH HIGHLIGHTS

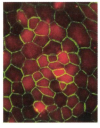

116 SELECTIONS FROM THE SCIENTIFIC LITERATURE
Life without centrosomes / Extinction threat grows / Why see in colour? / Lost connections in the brain / Making silk

SEVEN DAYS

118 THE NEWS IN BRIEF
China improves information on Beijing smog / Forest fires ravage national park in Chile / Airlines protest over Europe's emissions fee / Bristol-Myers Squibb joins the drive for hepatitis C drugs / China endures severe drought

CAREERS

225 BRIDGE FUNDING
How to stay afloat
There are ways to bridge that funding gap — but it's tough out there

227 TURNING POINT
Europe beckons for climate researcher Saffron O'Neill despite the air miles

227 CAREER BRIEFS

NEWS IN FOCUS

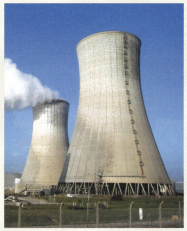

ENERGY

Power play

France sets high bar for nuclear safety
PAGE 121

123 POLICY
Greece pins hopes on university reforms

124 ECONOMICS
Financial cost of natural disasters soars

125 PUBLIC HEALTH
US clamps down on use of antibiotics on farm animals

127 ASTRONOMY
Dutch radio telescope takes pole position as probe for early Universe

128 THERAPEUTICS
US centre for translational medicine gears up for action

FEATURES

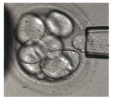

130 STEM CELLS
Never say die
Can Advanced Cell Technology bring embryonic stem-cell therapies to the clinic?

134 MISCONDUCT
Zero tolerance
A Chinese university's drive to clean up its act

COMMENT

137 CLIMATE CHANGE
Deadline 2015
Michael Jacobs
It's time to prepare for a climate summit meeting to set new policy goals

139 CONSERVATION
A market approach to saving the whales
Christopher Costello, Leah R Gerber & Steven Gaines
The toll of whaling could be reduced by allowing quotas to be bought and sold

BOOKS & ARTS

141 CONSERVATION
Harpoons and heartstrings
Philip Hoare

142 ENERGY
Curbing urban greed
David Orr

143 BOOKS IN BRIEF

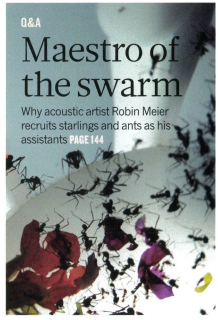

Q&A

Maestro of the swarm

Why acoustic artist Robin Meier recruits starlings and ants as his assistants PAGE 144

CORRESPONDENCE

145 Global genomic health-check / Flood control / Sun and wind could power India / A manufactured MMR dispute

FUTURES

230 **The driver**
Rahul Kanakia

Scitable
by nature EDUCATION

As many as 1,209 butterfly species have been documented in 55 square kilometers of the Tambopata Reserve in southeastern Peru.

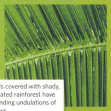

Once-verdant hills covered with shady, beautifully variegated rainforest have given way to unending undulations of dusty oil palm rows.

Tropical forests have the highest primary productivity of any of the terrestrial biomes.

In the 1950s, MIT physicist Harold Edgerton used a strobe light flash to produce stunningly beautiful images of, amongst other things, a hummingbird flapping its wings.

Rapid nutrient uptake is facilitated by mycorrhizae, which are fungal mutualists associated with plant roots.

Dengue infection is caused by any of four related viruses that are transmitted to humans by the mosquitoes *Aedes albopictus* (Asian tiger mosquito) and *Aedes aegypti*.

A new ecosystem for learning

www.nature.com/scitable

Open science resources for faculty and students

• Genetics • Cell Biology • Ecology

... and more!

For Students. For Faculty. For Science

nature publishing group npg

CONTENTS

12 January 2012 / Vol 481 / Issue No 7380

RESEARCH

NEW ONLINE

147 Papers published this week at nature.com

NEWS & VIEWS

148 BIOMECHANICS
Leaping lizards and dinosaurs
Aerial lizard manoeuvres
R McNeill Alexander SEE LETTER P.181

149 ASTROPHYSICS
Progenitors of type Ia supernovae
No sign of a companion star for a type Ia supernova remnant
Pilar Ruiz-Lapuente
SEE LETTER P.164

150 ANGELMAN SYNDROME
Drugs to awaken a paternal gene
Use of topoisomerase inhibitors to induce expression of *UBE3A* gene
Arthur L Beaudet SEE LETTER P.185

152 APPLIED PHYSICS
Nanowire electronics comes of age
Three-dimensional nanowire structures gain ground
Tomás Palacios

153 EARTH SCIENCE
Limits of the power law
Multi-scale modelling of the deformation of magnesium oxide
Andrew M Walker
SEE LETTER P.177

154 COGNITION
Your face looks familiar
Wasps learn to identify their peers
Lars Chittka & Adrian Dyer

ARTICLE

157 CANCER **The genetic basis of early T-cell precursor acute lymphoblastic leukaemia**
J Zhang et al.

LETTERS

164 ASTRONOMY **An absence of ex-companion stars in the type Ia supernova remnant SNR 0509-67.5**
B E Schaefer & A Pagnotta
SEE N&V P.149

167 ASTRONOMY **One or more bound planets per Milky Way star from microlensing observations**
A Cassan et al.

ON THE COVER

Giant leap

This agama lizard, leaping to a vertical surface from a low-friction vault, is using its tail to stabilize its trajectory. This 'swinging appendage' method may have been used by velociraptors, and is ideal for incorporation into highly manoeuvrable tailed robots.
PAGES 148 & 181

170 PHYSICS **Implementation of a Toffoli gate with superconducting circuits**
A Fedorov, L Steffen, M Baur, M P da Silva & A Wallraff

173 CHEMISTRY **Charge order and three-site distortions in the Verwey structure of magnetite**
M S Senn, J P Wright & J P Attfield

177 GEOPHYSICS **Modelling the rheology of MgO under Earth's mantle pressure, temperature and strain rates**
P Cordier, J Amodeo & P Carrez
SEE N&V P.153

181 EVOLUTION **Tail-assisted pitch control in lizards, robots and dinosaurs**
T Libby et al. SEE N&V P.148

185 NEUROSCIENCE **Topoisomerase inhibitors unsilence the dormant allele of *Ube3a* in neurons**
H-S Huang et al. SEE N&V P.150

190 CANCER **A microRNA regulon that mediates endothelial recruitment and metastasis by cancer cells**
K J Png, N Halberg, M Yoshida & S F Tavazoie

195 STEM CELLS **Ars2 maintains neural stem-cell identity through direct transcriptional activation of *Sox2***
C Andreu-Agullo, T Maurin, C B Thompson & E C Lai

199 IMMUNOLOGY **Acquisition of a multifunctional IgA$^+$ plasma cell phenotype in the gut**
J H Fritz et al.

204 MICROBIOLOGY **Cysteine methylation disrupts ubiquitin-chain sensing in NF-κB activation**
L Zhang et al.

209 CELL BIOLOGY **Basic amino-acid side chains regulate transmembrane integrin signalling**
C Kim et al.

214 STRUCTURAL BIOLOGY **Subnanometre-resolution structure of the intact *Thermus thermophilus* H$^+$-driven ATP synthase**
W C Y Lau & J L Rubinstein

219 STRUCTURAL BIOLOGY **An unanticipated architecture of the 750-kDa $\alpha_6\beta_6$ holoenzyme of 3-methylcrotonyl-CoA carboxylase**
C S Huang, P Ge, Z H Zhou & L Tong

224 ERRATUM **Thermalization and its mechanism for generic isolated quantum systems**
M Rigol, V Dunjko & M Olshanii

STRUCTURAL BIOLOGY

Power pack

The structure of the molecule that powers rotary ATPases. PAGE 214

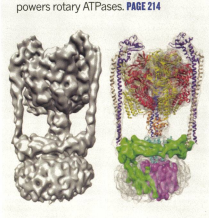

Manpei Suzuki Diabetes Foundation

Calling for 2012 nominations for Manpei Suzuki International Prize for Diabetes Research

Go to www.manpeisuzukiprize.org

Deadline: July 1, 2012

- The Manpei Suzuki Diabetes Foundation is pleased to call for a nomination of a researcher who has accomplished creative, innovative researches of highest quality in Diabetes Research.
- Award comprises of a Certificate of Honor, US$150,000 and a Japanese objet d'art.
- A member of ADA, EASD, JDS or other scientific societies can submit one nomination yearly.

2011 Winner

Masato Kasuga, MD, PhD

Director-General, Research Institute
National Center for Global Health and Medicine

2008
C. Ronald Kahn, MD

2009
Donald F. Steiner, MD

2010
Carl Erik Mogensen, MD

2011
Masato Kasuga, MD, PhD

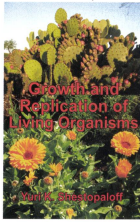

GROWTH AND REPLICATION OF LIVING ORGANISMS

GENERAL LAW OF GROWTH AND REPLICATION AND THE UNITY OF BIOCHEMICAL AND PHYSICAL MECHANISMS

BY YU. K. SHESTOPALOFF

A SOURCE OF IDEAS AND STRATEGIES FOR BIOLOGISTS AND BIOENGINEERS

www.akvypress.com/growth/book.html

nature jobs

Like to switch to a non-traditional science career?

- Wide selection of vacancies, such as science communications, marketing, sales, and regulatory affairs
- Browse Non-traditional career articles and news

Find out more on nature jobs.com

nature

12 January 2012 / Vol 481 / Issue No. 7380

EDITORIAL

LONDON, MUNICH, WASHINGTON DC, NEW YORK, BOSTON, PARIS, SAN FRANCISCO, TOKYO nature@nature.com

EDITOR-IN-CHIEF: Philip Campbell
MANAGING EDITOR: Nick Campbell
PUBLISHING EXECUTIVE EDITOR: Maxine Clarke **EXECUTIVE EDITOR:** Véronique Kiermer
CHIEF MAGAZINE EDITOR: Tim Appenzeller
THIS WEEK/NEWS/FEATURES: Alison Abbott, David Adam, Ananyo Bhattacharya, Geoff Brumfiel, Declan Butler, Ewen Callaway, Erika Check Hayden, Daniel Cressey, David Cyranoski, Natasha Gilbert, Eric Hand, Heidi Ledford, Corie Lok, Brendan Maher, Emma Marris, Richard Monastersky, Brian Owens, Helen Pearson, Mark Peplow, Eugenie Samuel Reich, Ivan Semeniuk, Quirin Schiermeier, Jeff Tollefson, Richard Van Noorden, Meredith Wadman, M Mitchell Waldrop **COMMENT:** Sara Abdulla, Joanne Baker, Rosalind Cotter, Barbara Kiser, Alison McCook, Lucy Odling-Smee, Sarah Tomlin **NATURE PODCAST/VIDEO:** Adam Rutherford, Eric Olson, Kerri Smith, Charlotte Stoddart **NEWS AND VIEWS:** Sadaf Shadan, Ania Lopes, Andrew Mitchinson, Cesar Sanchez, Marian Turner **RESEARCH:** Ritu Dhand, Karl Ziemelis, Francesca Cesari, I-han Chou, Tanguy Chouard, Rosamund Daw, Alex Eccleston, Angela Eggleston, Joshua Finkelstein, Henry Gee, Patrick Goymer, Noah Gray, Marie-Thérèse Heemels, Magdalena Helmer, Karen Howell, Claudia Lupp, Barbara Marte, Andrew Mitchinson, Juliane Mössinger, Deepa Nath, Leslie Sage, Magdalena Skipper, Clare Thomas, John VanDecar, Liesbeth Venema, Ursula Weiss, Michael White **INSIGHTS/REVIEWS/PERSPECTIVES:** Ursula Weiss **CAREERS:** Gene Russo, Karen Kaplan **TECHNOLOGY FEATURES:** Monya Baker **FUTURES:** Henry Gee **SUPPLEMENTS:** Herb Brody, Michelle Grayson, Tony Scully **SUBEDITORS:** Colin Sullivan, Sarah Archibald, Nicola Bailey, Anne Blewett, Nicolas Fanget, Isobel Flanagan, Paul Fletcher, Afsaneh Gray, Dinah Loon, Anna Novitzky, Yukie Ozawa, Katherine Perry, David Price, Jenny Rooke, Chris Simms, David Winters, Anna York **PRODUCTION:** Jenny Henderson, Gemma Carder, Leonora Dawson-Bowling, Dan Foley, Stewart Fraser, Susan Gray, Simon Gribbin, James McQuat, Emilia Orviss, Yvonne Strong, Robert Sullivan, Roberta Tarran, Charles Wenz **ART AND DESIGN:** Kelly Buckheit Krause, Wesley Fernandes, Madeline Hutchinson, Barbara Izdebska, Paul Jackman, Jasiek Krzyszkofiak, Annthea Lewis, Nik Spencer, Claire Welsh, Mark Wood **JAPAN EDITION:** Mika Nakano, Akemi Tanaka, Mitsuyo Utsugi **PRESS OFFICE:** Ruth Francis, Neda Afsarmanesh, Lisa Boucher, Rachel Twinn, Rebecca Walton **ADMINISTRATION:** Paul Sng, Helen Anthony, Liz Bankes, Roseann Campbell, Ffion Cleverley, Faye Fornasier, Amy Invernizzi, Diane Kempinski, Hazel Mayhew, Katie McGoldrick, Jenny Meyer, Rina Nozawa, Kenneth Simpson, Claire Smith

PUBLISHING

LONDON feedback@nature.com
MANAGING DIRECTOR & PUBLISHER: Steven Inchcoombe
ASSOCIATE PUBLISHER: Arash Hejazi
PUBLISHING PROJECT MANAGER: Christian Manco
PROJECT MANAGER: Helen Anthony

TOKYO feedback@natureasia.com
PUBLISHING DIRECTOR — ASIA-PACIFIC: David Swinbanks
ASSOCIATE DIRECTOR — ASIA-PACIFIC: Antoine E Bocquet

DISPLAY ADVERTISING, SPONSORSHIP & NATUREJOBS

GLOBAL HEAD: Andrew Douglas a.douglas@nature.com

DISPLAY ADVERTISING AND SPONSORSHIP
GLOBAL HEAD: Gerard Preston g.preston@nature.com
ASSISTANT SPONSORSHIP MANAGER: Reya Silao Tel: +44 (0)20 7843 4977 (r.silao@nature.com)

EUROPE/REST OF WORLD display@nature.com Tel: +44 (0)20 7843 4960
GERMANY/SWITZERLAND/AUSTRIA: Sabine Hugi-Fürst Tel: +41 52761 3386
UK/IRELAND/SCANDINAVIA/SPAIN/PORTUGAL: Evelina Rubio Hakansson Tel: +44 (0)20 7843 4079
FRANCE/BELGIUM/THE NETHERLANDS/LUXEMBOURG/ITALY/OTHER EUROPE: Nicola Wright Tel: +44 (0)20 7843 4959

NORTH AMERICA display@natureny.com
NEW ENGLAND/ EASTERN CANADA: Sheila Reardon Tel: +1 617 494 4900
NEW YORK/MID-ATLANTIC/SOUTHEAST: Jim Breault Tel: +1 212 726 9334
MIDWEST: Mike Rossi Tel: +1 212 726 9255
WEST COAST/ WESTERN CANADA: George Lui Tel: +1 415 781 3804
WEST COAST NORTH: Kayla McCutchan Tel: +1 415 403 9038

ASIA-PACIFIC display@natureasia.com
ASIA-PACIFIC HEAD: Kate Yoneyama
JAPAN: Ken Mikami Tel: +81 3 3267 8765
GREATER CHINA/SINGAPORE: Gloria To Tel: +852 2811 7191
INDIA: Vikas Chawla Tel: +91 124 288 1057

SPONSORSHIP
BUSINESS DEVELOPMENT MANAGER: David Bagshaw Tel: +1 212 726 9215 **BUSINESS DEVELOPMENT MANAGER:** Patrick Murphy Tel: +1 617 475 9216

NATUREJOBS naturejobs@nature.com
EUROPEAN HEAD OFFICE, LONDON: Tel: +44 (0)20 7843 4961
EUROPEAN SALES MANAGER: Nils Moeller (n.moeller@nature.com) **BUSINESS DEVELOPMENT MANAGER, MIDDLE EAST:** Jon Giuliani (j.giuliani@nature.com) **ADVERTISING PRODUCTION MANAGER:** Stephen Russell **NATUREJOBS ONLINE PRODUCTION:** Dennis Chu
US HEAD OFFICE, NEW YORK: naturejobs@natureny.com **US SALES MANAGER:** Ken Finnegan
JAPAN HEAD OFFICE, TOKYO: Tel: +81 3 3267 8765 **ASIA-PACIFIC HEAD:** Kate Yoneyama
ASIA-PACIFIC SALES & BUSINESS DEVELOPMENT MANAGER: Yuki Fujiwara **BUSINESS DEVELOPMENT MANAGER, GREATER CHINA, SINGAPORE:** Gloria To Tel: +852 2811 7191
INDIA: Vikas Chawla Tel: +91 1242881057 (v.chawla@nature.com)

MARKETING & SUBSCRIPTIONS

USA/CANADA/LATIN AMERICA **subscriptions@us.nature.com**
Tel: (USA/Canada)+1 866 363 7860; (outside USA/Canada) +1 212 726 9223
MARKETING: Sara Girard **FULFILMENT:** Karen Dawson

JAPAN/CHINA/KOREA **subscriptions@natureasia.com**
Tel: +81 3 3267 8751 **MARKETING/PRODUCTION:** Keiko Ikeda, Takesh Murakami

EUROPE/REST OF WORLD **subscriptions@nature.com**
Tel: +44 (0)1256 329242
MARKETING: Elena Woodstock, Marcus Parker, Hannah Phipps **FULFILMENT:** Jean Burrows

INDIA **npgindia@nature.com**
Tel: +91 124 2881053/54
HEAD OF BUSINESS DEVELOPMENT, INDIA: Debashish Brahmachari **MARKETING:** Harpal Singh Gill

ANNUAL SUBSCRIPTIONS (UK/Europe, including post and packing)
FULL RATE: £1,400
PERSONAL RATES: UK £135; Europe €209; Rest of World £210
STUDENT RATES: UK £79; Europe €122; Rest of World £125
Individual rates apply to payments by personal cheque or credit card. Back issues: £20.00.

ANNUAL SUBSCRIPTIONS (USA, including post and packing)
INSTITUTIONAL/CORPORATE RATE: $2,730 ; **PERSONAL RATE:** $199; **STUDENT RATE:** $99;
POSTDOC RATE: $119
Printed in USA. Individual rates available only to subscribers paying by personal check or credit card. Orders for student/postdoc subscriptions must be accompanied by a copy of student ID. Rates apply to USA, Canada, Mexico/Central & South America. Add 7% GST tax in Canada (Canadian GST number 140911595). **BACK ISSUES:** US$20.00.

ANNUAL SUBSCRIPTIONS (Asia, including post and packing)
JAPAN: 年間購読料金: *Nature* のみ 437,800 円 +21,890 円 (消費税) =459,690 円 (合計)
Nature + *Nature Digest* 466,550 円 +23,328 円 (消費税) =489,878 (合計)
お問い合わせ 日本出版貿易株式会社 国内営業 1 部
〒101-0064 東京都千代田区猿楽町1-2-1 Tel: 03-3292-3767 Fax: 03-3292-8766
個人/学生購読について
NPG ネイチャー アジア・パシフィック フルフィルメント & カスタマーサービス
〒162-0843 東京都新宿区市谷田町2-37 千代田ビル Tel: 03-3267-8759 Fax: 03-3267-8752
CHINA: www.natureasia.com/cn/subscribe; **KOREA:** www.natureasia.com/korea/subscribe

NATURE ONLINE

WWW.NATURE.COM/NATURE

CHIEF TECHNOLOGY OFFICER: Howard Ratner **ASSOCIATE DIRECTOR, NATURE.COM:** Daniel Pollock **PLATFORM DEVELOPMENT:** Jeremy Macdonald **WEB PRODUCTION:** Alexander Thurrell, Deborah Anthony **WEB DESIGN:** Juan-Carlos Sobrino, Luke Stavenhagen **PLATFORM INTERFACES:** Amanda Ward

SITE LICENCES, FULFILMENT & CUSTOMER SERVICES

SITE LICENCES: npg.nature.com/libraries feedback@nature.com
CHIEF OPERATIONS OFFICER: John Carroll **ASSOCIATE DIRECTOR OF OPERATIONS:** Dominic Pettit
CUSTOMER SERVICE: Gerald Coppin **ORDER PROCESSING OPERATIONS:** Steve Poulter

NATURE PUBLISHING GROUP OFFICES

LONDON: The Macmillan Building, 4 Crinan Street, London N1 9XW Tel: +44 (0)20 7833 4000 Fax: +44 (0)20 7843 4596/7
BASINGSTOKE: Nature Publishing Group, Subscriptions, Brunel Road, Basingstoke, Hants RG21 6XS, UK Tel: +44 (0)1256 329242
WASHINGTON DC: 968 National Press Building, 529 14th St NW, Washington DC 20045-1938 Tel: +1 202 737 2355
NEW YORK: 75 Varick St, 9th Floor, New York, NY 10013-1917 Tel: +1 212 726 9200
BOSTON: 25 First Street, Suite 104, Cambridge, MA 02141 Tel: +1 617 475 9275
SAN FRANCISCO: 225 Bush Street, Suite 1453, San Francisco, CA 94104 Tel: +1 415 403 9027
MUNICH: Nymphenburger Strasse 14, D-80335 München Tel: +49 89 549057-13
PARIS: Moulin de Malicorne, Sainte Maure de Touraine, Paris 37800 Tel: +33 2 47 35 72 15
TOKYO: Chiyoda Building, 2-37 Ichigaya Tamachi, Shinjuku-ku, Tokyo 162-0843 Tel: +81 3 3267 8751
INDIA: Nature Publishing Group, 3A, 4th Floor, DLF Corporate Park, Gurgaon 122002 Tel: +91 124 2881053/54

Nature® (ISSN 0028-0836) is published by Nature Publishing Group, a division of Macmillan Publishers Ltd (The Macmillan Building, 4 Crinan Street, London N19XW). Registered as a newspaper at the British Post Office. North and South American orders to subscriptions@naturenj.com (Tel: +1 866 363 7860). Other orders to subscriptions@nature.com (Tel. +44 (0)1256 329242; Fax +44 (0)1256 812358). Authorization to photocopy material for internal or personal use, or internal or personal use of specific clients, is granted by *Nature* to libraries and others registered with the Copyright Clearance Center (CCC) Transactional Reporting Service, provided the relevant copyright fee is paid direct to CCC, 222 Rosewood Drive, Danvers MA 01923, USA. Identification code for *Nature*: 0028-0836/03. CPC PUB AGREEMENT #40032744. In the US, *Nature* (ISSN 0028-0836) is published weekly on Thursday, except the last week in December by Nature Publishing Group, 75 Varick St, 9th Fl, New York NY 10013-1917, USA. US Periodicals postage paid at New York NY, and additional mailing post offices. US POSTMASTER: send address changes to *Nature*, Subscription Dept, 75 Varick St, 9th Fl, New York NY 10013-1917, USA. Published in Japan by NPG Nature Asia-Pacific, Chiyoda Building, 2-37 Ichigayatamachi, Shinjuku-ku, Tokyo 162-0843, Japan. © 2012 Macmillan Publishers Limited. All rights reserved.

SCIENTIFIC AMERICAN™

Publishing the latest in science and technology for more than 165 years

A site license provides online access to *Scientific American*, *Scientific American Mind* and Special Issues

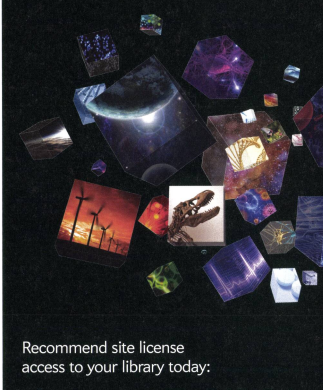

Recommend site license access to your library today:

www.nature.com/libraries/scientificamerican

nature publishing group npg

© Scientific American, Inc.

nature EDUCATION

ANNOUNCING

Principles of Biology

An interactive textbook solution by Nature Education

A learning solution designed to bridge students from the classroom to the lab.

200 customizable mini-chapters created by dozens of scientists, instructors, and editors	200+ online interactive exercises to give students a hands-on way to apply their knowledge	50 Science Techniques units cultivating real scientific skills, including data analysis	3000+ assessment questions integrated into lessons
Synopses and links to milestone research papers from *Nature* and other journals	Affordably priced for all students	Optional color print companion	Access on all devices:

Learn more at **www.nature.com/principles**

nature publishing group npg

THIS WEEK

EDITORIALS

CONSERVATION Why the world should start a great whale sale **p.114**

WORLD VIEW Journals must not censor papers on virulent flu **p.115**

VISION Life in black and white helps primates to find food **p.116**

Get tough on nuclear safety

A refreshingly frank and forward-looking report on the safety of French nuclear power plants in the wake of Fukushima should spur other countries to take a hard look at regulation of their own reactors.

The Three Mile Island and Chernobyl nuclear accidents each prompted profound rethinks of safety requirements. But as the incidents slipped into history, the nuclear industry, regulators and governments tended to revert to reassuring refrains that atomic energy was once again safe and in expert hands.

So it is probably too early to be confident about the impact of the Fukushima accident in Japan last March. But it is clear that, as the defences at the Fukushima Daiichi power plant crumbled, so too did the fundamental dogma of modern nuclear safety: that a series of back-up and redundant safety systems, combined with physical defences strong enough to resist expert estimates of external threats, was enough to make impossible a catastrophic meltdown and release of radioactivity into the environment.

As the first anniversary of the disaster approaches, and supporters and opponents of nuclear power prepare to use it to underscore their positions, will Fukushima mark a turning point for the nuclear enterprise, or will industry return to business as usual?

André-Claude Lacoste, head of France's Nuclear Safety Authority (ASN) in Paris, suggested at a press conference last week that things have already changed. "There will be a before and an after Fukushima," he promised.

Is he right? Some in industry will always oppose the costs of tougher regulation, and shortsighted or ideological politicians and companies will continue to insist that a repeat of Fukushima is impossible in their own backyards. But many in the nuclear industry were genuinely and deeply shocked to see at Fukushima a sequence of events that they believed impossible. The world's main nuclear operators have an interest in establishing the causes of the disaster and learning the lessons — they know too well that if another major accident were to occur, then in many people's eyes the already-struggling industry would be finished.

The World Association of Nuclear Operators, for example, has stressed the need for its members to respond properly to Fukushima, and has beefed up its own inspection and oversight of plants (see *Nature* **472,** 274 and http://doi.org/hj5; 2011).

So to France, the world's leading user of nuclear power and arguably the nation with the most to lose from a global rejection of it. Last week, the ASN released a report announcing a sweeping safety upgrade to all the country's reactors (see page 121). The planned multi-billion-euro improvements are part of a programme of tests to assess how well French reactors would stand up to extreme events, and how prepared plants are to deal with a major accident. The ASN's report is written with stunning candour, stating plainly that a loss of coolant or electricity could, in the worst cases, see meltdowns at reactors in hours. It also lists many shortcomings found during 'stress tests', in which some safety aspects of plants were found not to conform to existing standards.

Critics will wonder why the ASN didn't spot these problems earlier, given that it is responsible for regulating the plants. Others will question how the authority can reconcile its statement that France's reactors are fundamentally safe with its insistence that they must be upgraded on safety grounds. But it would be a mistake to penalize France for listing its nuclear shortcomings, especially when other nations seem less enthusiastic about publicly discussing problems with their own reactors and regulations. The French report makes for a breath of fresh air in a post-Fukushima climate in which worldwide public reassurance has too often taken priority over transparent debate.

> ***"It would be a mistake to penalize France for listing its nuclear shortcomings."***

The ASN has also come up with an elegant technical solution to get around the (universal) dilemma of how to protect a plant from external threats, such as natural disasters. The report recommends that all reactors, irrespective of their perceived vulnerability, should add a 'hard core' layer of safety systems, with control rooms, generators and pumps housed in bunkers able to withstand physical threats far beyond those that the plants themselves are designed to resist.

There will, rightly, be scepticism about whether France will ultimately implement the new measures. The bunker concept may prove technically difficult, and Électricité de France — the operator of the reactors — would need to pay for systems that some in the company will probably feel are an expensive luxury.

Whatever happens in the long term, the French plans have an immediate benefit: they raise the post-Fukushima safety bar for other countries. Those governments, regulators and companies that have yet to propose anything close to such far-reaching measures must now explain why not. ■

A long stretch

The UK government hopes to squeeze even more out of science — without paying a penny extra.

David Willetts may not be familiar with the film *Jerry Maguire*, in which Tom Cruise yells: "Show me the money!" But the UK science minister has been on the receiving end of a number of similar quips this week.

By most measures, the United Kingdom has always achieved greater research output than might be expected from the amount of government funding its science base receives. Last week, in a speech to the London-based think-tank Policy Exchange, Willetts said that he wants to stretch this relationship even further.

For starters, he wants the number of British universities rated among the world's top 100 to grow from the current figure of

between 10 and 19, depending on the rankings used. To help make that happen, he announced that his coalition government was "inviting proposals" for "a new type of university" that would focus on science and postgraduates. But there was a catch. "There will," Willetts stated, "be no additional government funding." This triggered a storm of protest from experts and several (poor) impressions of Cruise.

During his speech, Willetts was keen to reference plans for a huge university campus in New York being pushed forward by Cornell University (see *Nature* http://doi.org/hj9; 2011). And private higher education is clearly on the rise, albeit probably more in teaching than the research arena. But, as critics quickly pointed out, the Cornell project is receiving at least US$100 million in public funding.

Experts contacted by *Nature* said that the idea that private finance and business sponsorship alone can create a new institution — as Willetts suggested — seems fanciful. "I don't think this is likely to fly without very, very substantial amounts of new money," says Paul Nightingale, a science and technology policy expert at the University of Sussex in Brighton, UK. And Roger Geiger, who studies research universities at Pennsylvania State University in University Park, says: "Industry has its own research labs and if they're going to invest their own money, that's where they're going to put it."

Neither Willetts nor his Department for Business, Innovation and Skills was willing to elaborate on the plans this week, saying only that much depends on the proposals that the department receives. The government insists that there has been "a lot of interest", but without government incentive, will that interest go any further?

In his speech, given just a stone's throw from the Houses of Parliament, Willetts also highlighted the good that his government has done. As the United Kingdom stumbles through one of the worst economic climates in living memory, the fact that the country's research budget has been largely protected from the severe cuts inflicted on other public sectors (including university teaching) is something to be thankful for.

And it is a shame that Willetts' high-profile but extremely brief mention of the universities idea distracted from other points in the speech, such as an admission that the government is involved in "picking winners" — investing in technologies underpinned by science and research that could bring economic benefit — something that politicians have been reluctant to acknowledge previously.

> ***"Private higher education is clearly on the rise, albeit probably more in teaching than the research arena."***

"The noises are positive. Every time he speaks about science and innovation the thinking seems to get a little more sophisticated," says Kieron Flanagan, a lecturer in science and technology policy at the University of Manchester, UK. This is a welcome shift from previous Conservative policies, which tended towards generic initiatives. However, the rhetoric has yet to be matched with much action, Flanagan says, although increased efforts to link businesses and research in key areas are a good start.

Many will be happy to be proved wrong if a number of world-leading finance-free universities do arise in the United Kingdom, as Willetts hopes. Meanwhile, discussion of the idea certainly has one thing in its favour: it's not costing anything. ■

Whales for sale

A quota-trading scheme could end conflict between whalers and conservationists.

In the chilly waters of the Southern Ocean, an annual drama is under way once more. The Japanese whaling fleet has set to sea again. So has a flotilla of vessels crewed by conservationists and activists, determined to keep the hunters from their prey.

Three Australian anti-whaling campaigners boarded the *Shonan Maru No. 2* whaling ship on Sunday. After negotiations, the Japanese government has agreed to release them to an Australian customs ship. The incident came just days after the conservation ship *Brigitte Bardot* was smashed by a giant wave and seriously damaged while pursuing the ship *Nisshin Maru*, some 2,400 kilometres from the Australian coast. Sea Shepherd Conservation Society, a group based in Friday Harbour, Washington, that operates the stricken vessel, is counting the cost of its principles. This isn't the first time: in January 2010, the group's powerboat *Ady Gil* sank after a collision with the *Shonan Maru No. 2*. The skirmishes and confrontations continue, with campaigners maintaining their high-risk pursuit and their attempts to foul the propellers of the whaling ships with ropes, and the whalers responding with water cannon. Surely there is a better way?

Perhaps. On page 139 of this issue, three environmental scientists outline a plan to introduce tradable quotas for whale catches. Under the scheme, conservationists could buy (and retire) the quotas from whalers, giving industry a way to profit from the animals without killing them. In return, anti-whaling campaigners could be more certain that their actions were reducing the slaughter. Theoretically, such a scheme would allow both sides to benefit with no loss of face. As the researchers say, it could "open the door to reducing mortality without needing to battle over whether whaling is honourable or shameful". And both the number of whales killed and the associated costs would go down.

The article's authors — Christopher Costello and Steven Gaines of the University of California, Santa Barbara, and Leah Gerber of Arizona State University in Tempe — use the per-animal profit of whaling ships to decide that about US$13,000 would be a fair price to buy the life of a minke whale, and $85,000 should secure a fin whale. "Whale prices should therefore be within reach of conservation groups and even some individuals," they suggest.

The idea first surfaced in 1982, to little effect. But perhaps, three decades on, its time has come. Market approaches to environmental problems are now common, with carbon offsets bought by individuals to neutralize their greenhouse-gas emissions. Such systems have even been shown to be effective, reducing sulphur dioxide pollution from US power plants.

To put a price on the head of a whale would be a different matter, of course. Committed anti-whaling campaigners would have to put aside moral objections and accept such a scheme's tacit legitimation of whaling as an enterprise to be rewarded, as well as the de facto official approval for the heavily disputed notion that whales (and other animals) are a resource to be exploited. Pro-whaling nations would need to be persuaded that the scheme would have more strategic benefit than their continuing political efforts to lift, or find ways to work around, the current commercial whaling moratorium. Then there is the need for scrutiny and verification of the quota market, not to mention getting such a plan through the political quagmire that bogs down annual meetings of the International Whaling Commission, the body that would be best placed to put a market mechanism into action. (And what of the world's scientists, denied information from some of the 1,000 or so whales slaughtered each year for 'scientific purposes'? *Nature* suspects that they would manage.)

Still, with political will and goodwill, the idea could work. At the very least, it deserves proper consideration from all involved. As events in the Southern Ocean show, pro- and anti-whaling groups will both go to extraordinary lengths to pursue their agendas. To those in peril on the sea, the middle ground should seem just as secure as the moral high ground. ■

➲ **NATURE.COM**
To comment online, click on Editorials at:
go.nature.com/xbunqv

Cellular & Molecular Immunology

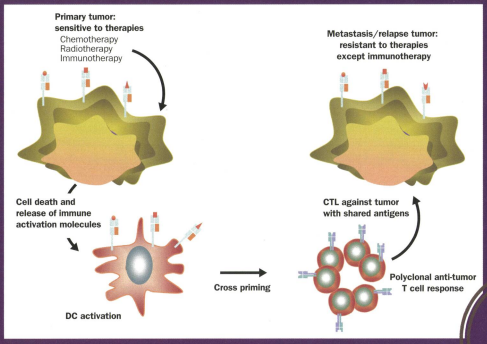

Special issue and Web Focus

Cancer Immunology

The January special issue of *Cellular & Molecular Immunology* presents two important strategies for generating potent and lasting anti-tumor immunity. Further background information on this important topic is available through the accompanying web focus which links to related articles from across Nature Publishing Group.

Featured articles include:

Bone marrow and the control of immunity
Ende Zhao, Huanbin Xu, Lin Wang, Ilona Kryczek, Ke Wu, Yu Hu, Guobin Wang and Weiping Zou

Targeting and utilizing primary tumors as live vaccines: changing strategies
Xuanming Yang, Eric D Mortenson and Yang-Xin Fu

Optimal culture conditions for the generation of natural killer cell-induced dendritic cells for cancer immunotherapy
Je-Jung Lee *et al.*

Anti-γδ TCR antibody-expanded γδ T cells: a better choice for the adoptive immunotherapy of lymphoid malignancies
Jianhua Zhou, Ning Kang, Lianxian Cui, Denian Ba and Wei He

To access the Special Issue and Web Focus on Cancer Immunology visit:
www.nature.com/CMI/focus/cancer_immunology/

nature OUTLOOK

Published in the 22/29 December issue of *Nature* and available free online for six months

TRADITIONAL ASIAN MEDICINE

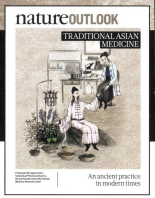

Using scientific techniques to investigate the claims of traditional medicine as practised in countries such as China and Japan can help sort effective treatments from unfounded superstitions — and perhaps give modern medicine a few insights into holistic approaches borne from thousands of years of herbal remedies.

Access the Outlook free online for six months.
nature.com/nature/outlook/asian_medicine

Produced with support from

SAISHUNKAN

Scan this tag to access the Outlook on your smartphone

If you would be interested in partnering with *Nature* on a similar project please contact: **sponsorship@nature.com**

nature publishing group npg

PETER PALESE

Don't censor life-saving science

Controlling who is allowed access to information about mutations in the H5N1 bird flu virus is unacceptable, says **Peter Palese**.

The recent arguments over the creation of a transmissible form of the bird flu virus (H5N1) feel very familiar. My colleagues and I were at the centre of a similar controversy in 2005, when we reconstructed the 1918 flu virus, which had killed up to 50 million people worldwide. News stories around the globe debated the merits of our research and television pundits argued opposing viewpoints. Naturally, the US government was concerned — as it is now. Yet our research was published in full. So why are similar concerns being used now to demand unacceptable censorship of the H5N1 scientific papers?

I have spent my career studying potentially dangerous pathogens — 20 years ago, my lab developed the technique that has enabled the H5N1 researchers to insert the mutations that render the virus more easily transmissible. In the 1990s, researchers discovered degraded samples of the 1918 virus in lung tissue from US soldiers who had died from the 'Spanish flu'. Using polymerase chain reaction technology, they amplified and sequenced the virus's RNA. We then took an existing influenza virus and, one by one, swapped its genes with those from the 1918 virus, eventually recreating a live version.

As we prepared our results for publication, the US government convened the National Science Advisory Board for Biosecurity (NSABB), which advises the community about research using agents that pose threats to national security or public health. Our experiments had made some people nervous.

During our discussions with members of the NSABB, we explained the importance of bringing such a deadly pathogen back to life. Although these experiments may seem dangerously foolhardy, they are actually the exact opposite. They gave us the opportunity to make the world safer, allowing us to learn what makes the virus dangerous and how it can be disabled. Thankfully, the discussions were largely constructive — within a week, the NSABB recommended that we continue to study the virus under biocontainment conditions, and publish the results so that other scientists could participate in the research. After we published our full paper in 2005 (T. M. Tumpey *et al. Science* **310,** 77–80; 2005), researchers poured into the field who probably would not otherwise have done, leading to hundreds of papers about the 1918 virus. As a result, we now know that the virus is sensitive to the seasonal flu vaccine, as well as to the common flu drugs amantadine (Symmetrel) and oseltamivir (Tamiflu). Had we not reconstructed the virus and shared our results with the community, we would still be in fear that a nefarious scientist would recreate the Spanish flu and release it on an unprotected world. We now know such a worst-case scenario is no longer possible.

WHO WILL WANT TO ENTER A FIELD IN WHICH YOU CAN'T PUBLISH YOUR MOST SCIENTIFICALLY INTERESTING RESULTS?

NATURE.COM
Discuss this article online at:
go.nature.com/yexx2z

This experience has made the NSABB's latest recommendation — that the H5N1 researchers not reveal the mutations behind the virus's transmissibility — all the more frustrating. I make the same argument today that we made in 2005 — publishing those experiments without the details is akin to censorship, and counter to science, progress and public health. Why did the (different) members of the committee come to a different conclusion in this case? I can only hope that they take a more sensible stance and change their minds, or that the scientific community at large convinces them to do so. Certainly, the authors of the papers, as well as the journals considering them for publication (including this one), should resist the committee's unworkable compromise that the full information should be released only to approved experts, and insist on full disclosure.

Giving the full details to vetted scientists is neither practical nor sufficient. Once 20–30 laboratories with postdoctoral fellows and students have such information available, it will be impossible to keep the details secret. Even more troublesome, however, is the question of who should decide which scientists are allowed to have the information. We need more people to study this potentially dangerous pathogen, but who will want to enter a field in which you can't publish your most scientifically interesting results?

Knowing which mutations render the virus more dangerous could help on a public-health level — if an outbreak of bird flu occurs in Taiwan, for instance, and researchers sequence the virus and see those mutations, we would know to ramp up the production of appropriate vaccines and antiviral drugs.

Incidentally, I believe that the risk of future outbreaks in humans is low: H5N1 has had the opportunity to cause widespread pandemics for many, many decades, yet it has not done so. Although we know the virus is transmissible between ferrets, little is known about how it will behave in other animals, including humans.

The more danger a pathogen poses, the more important it is to study it (under appropriate containment conditions), and to share the results with the scientific community. Slowing down the scientific enterprise will not 'protect' the public — it only makes us more vulnerable. ■

Peter Palese *is the Horace W. Goldsmith professor and chair of the Department of Microbiology at the Mount Sinai School of Medicine, New York.*
e-mail: peter.palese@mssm.edu

Editor's note: *Nature* is considering one of the papers and the NSABB's recommendations. It is also involved in consultations about how restricted access to the scientific methods and data might be implemented.

PHYSICS

'Nanoear' hears small sounds

By using laser beams to trap a gold nanoparticle, researchers in Germany have developed a sensitive sound-wave detector.

Tightly focused laser beams, known as optical tweezers, have been used to manipulate microscopic objects for two decades. Andrey Lutich, Jochen Feldmann and their co-workers at the Ludwig–Maximilians University in Munich used a similar approach: they suspended a 60-nanometre gold nanoparticle in water in the focal spot of a laser beam. They sent sound waves through the water and measured changes in the particle's constrained motion. The authors calculate that the nanoparticle can pick up sounds as low as –60 decibels, making the set-up a million times more sensitive than the human ear.

Phys. Rev. Lett. 108, **018101 (2012)**

CARDIOVASCULAR BIOLOGY

Stranded cells fuel plaques

One contributor to the build-up of fatty plaques in artery walls is a signalling protein that blocks the emigration of a major plaque constituent from the deposits.

Fat-laden white blood cells called macrophages are abundant in atherosclerotic plaques. Kathryn Moore at New York University and her colleagues found that these cells produce netrin-1, a protein that can guide the migration of white blood cells and the growing tips of neurons. But expression of netrin-1 in plaques blocked macrophage responses to chemical cues that would normally direct them out of the plaques.

Furthermore, mice lacking the netrin-1 gene had less atherosclerosis. These findings suggest that netrin-1 could provide a new drug target.

Nature Immunol. **http://dx.doi.org/10.1038/ni.2205 (2012)**

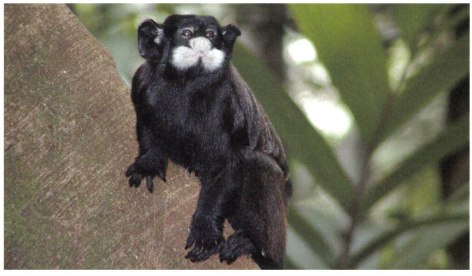

J. DIEGMANN

EVOLUTION

Colour vision aids the hunt

Primates with three types of colour receptor in their eyes capture more insect prey than those whose eyes have two. But the latter are not without advantage — they are better at detecting and catching camouflaged prey.

The primates of mainland Africa and Asia all have three types of colour receptor, making them 'trichromats'. Some in the Americas can be trichromat or dichromat. Hannah Buchanan-Smith at the University of Stirling, UK, and her colleagues studied trichromatic and dichromatic tamarins (*Saguinus* spp.; pictured) in captivity and in the field.

Other research has shown that trichromacy may also assist primates in spotting ripe fruits and young leaves. The persistence of dichromacy may result from the advantage it provides in detecting concealed prey, the authors say.

Anim. Behav. **http://dx.doi.org/10.1016/j.anbehav.2011.11.023 (2012)**

CELL BIOLOGY

No centrosome, no problem

Planarian flatworms have rid their cells of centrosomes, organelles that are found in nearly every animal cell. The structures anchor microtubule filaments that control cell division, cell migration and cell orientation.

Juliette Azimzadeh and Wallace Marshall at the University of California, San Francisco, and their team noticed that the flatworm *Schmidtea mediterranea* lacks centrioles — which make up the centrosomes — in dividing cells. They found centrioles only in certain cells that help the worms to glide across surfaces, feed and sense their environment.

The *S. mediterranea* genome is missing several genes needed to form centrioles; most flatworms have a full suite of centrosome genes. The authors suggest that planarians shed their centrosomes because, unlike many other animals, they rely on a form of embryonic development that does not depend on a cell's orientation.

Science **http://dx.doi.org/10.1126/science.1214457 (2012)**

CLIMATE-CHANGE ECOLOGY

Extinctions underestimated

More species may become extinct as a result of climate change than previously thought, a modelling study suggests.

As the climate warms, many species are predicted to shift their ranges to stay within comfortable temperature zones. However, some species will be better able to do so than others. Mark Urban at the University of Connecticut in Storrs and his colleagues have created a model that takes into account the competition that species face for habitats when they move to new ecosystems. They modelled the effect of 4 °C of warming over 100 years on 40 simulated species, and found a much higher number of extinctions than did models that do not account for species competition and species' differing dispersal abilities.

Even species with broad heat tolerances might be outcompeted — either by the arrival of newcomers in their current habitats or by native species in ecosystems that become habitable to them in future.

Proc. R. Soc. B **http://dx.doi.org/10.1098/rspb.2011.2367 (2012)**

DEVELOPMENTAL BIOLOGY

Stem cells of the eye

Retinal cells that are normally dormant *in vivo* are still capable of dividing *in vitro*, and can even take on properties seen in stem cells.

Retinal pigment epithelial (RPE) cells form a supporting layer in the retina and are implicated in various eye diseases, including some that lead to blindness. Sally Temple at the Neural Stem Cell Institute in Rensselaer, New York, and her colleagues isolated RPE cells, which are normally dormant throughout life, from human donor eyes. When cultured in certain growth conditions, the cells divided and showed characteristics of stem cells. The cells could also produce RPE and develop into neural, bone and fat cells, and displayed markers of some of these cells after being injected into chick embryos.

These RPE-derived cells represent a new type of stem cell from the central nervous system, the authors say.

Cell Stem Cell **10, 88–95 (2012)**

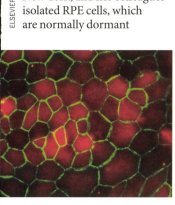

D. LENCER

CANCER

Immune cell boosts cancer

Skin immune cells that present fragments of invaders to the immune system also promote skin cancer in response to a powerful carcinogen.

Michael Girardi at Yale University in New Haven, Connecticut, and his colleagues exposed the skin of mice to DMBA, a laboratory chemical representative of common carcinogens in industrial pollution. Mice engineered to be deficient in Langerhans cells, the immune cells in question, were almost completely resistant to developing skin cancer. By contrast, the Langerhans cells of normal mice metabolized DMBA to an intermediate that induced a cancer-causing mutation in the DNA of adjacent skin cells.

When the intermediate was applied directly to the skin of the mice, both types developed skin cancer.

Science **335, 104–108 (2012)**

NEURODEVELOPMENT

Culprit in deafness

Age-related hearing loss often results from damage to the outer hair cells in a highly specialized component of the inner ear called the organ of Corti. Researchers at Washington University in St. Louis, Missouri, looked at how the development of these cells is regulated and identified a protein that is required for their normal development in mice.

David Ornitz and his colleagues discovered that mice lacking the protein FGF20 are deaf but otherwise healthy. The protein functions at a particular developmental stage to prime specific cells in the organ of Corti for further maturation. Without this factor, the outer hair cells and supporting cells in this part of the inner ear fail to develop, resulting in congenital deafness.

The authors speculate that mutations in the *FGF20* gene could be a cause of deafness in humans.

PLoS Biol. **10, e1001231 (2012)**

COMMUNITY CHOICE

The most viewed papers in science

NEUROSCIENCE

How the brain slows with age

HIGHLY READ on www.jneurosci.com in December

In the brain, a drop in the activity of just one gene decreases neurons' ability to change the strength of their connections — a hallmark of age-related cognitive decline.

The gene, *Bdnf*, encodes a protein that helps neurons in cognitive centres of the brain to form connections called synapses. Cui-Wei Xie and her colleagues at the University of California, Los Angeles, analysed brain slices from young, middle-aged and aged rats. Aged rat brains showed a decrease in the addition of acetyl groups to histones — proteins that package up DNA — in the regulatory regions of the *Bdnf* gene, reducing the gene's expression. Treating the brain slices with chemicals that mimic the BDNF protein or inhibit histone deacetylation increased the density and strength of neuronal connections.

J. Neurosci. **31, 17800–17810 (2011)**

F. PUPPA/FLPA

BIOTECHNOLOGY

Silkworms spin spider-like silk

Spider silk is tough and has many potential applications, but spiders' territorial nature makes them hard to farm. Researchers have therefore engineered silkworm moths that can produce threads of comparable strength.

Donald Jarvis at the University of Wyoming in Laramie and his colleagues built a silk gene that combines sequences from the golden silk orb-weaver spider (*Nephila clavipes*) and the silkworm moth (*Bombyx mori*; **pictured**). The team transferred the genetic construct into the genome of *B. mori* and then harvested the resulting larvae's silks, which comprise a mixture of natural and synthetic silk proteins.

The material is stronger and stretchier than normal *Bombyx* silks and is as tough as spider draglines. It could be harvested for biomedical applications such as surgical sutures.

Proc. Natl Acad. Sci. USA **http://dx.doi.org/10.1073/pnas.1109420109 (2012)**

NATURE.COM

For the latest research published by *Nature* visit:
www.nature.com/latestresearch

SEVEN DAYS *The news in brief*

POLICY

Stem-cell regulation

China has ordered a halt to unapproved stem-cell treatments, and says that it will stop accepting new applications for clinical trials using stem-cell products until July. The 10 January announcement by the government's health ministry was viewed as an effort to crack down on a flourishing trade in unproven stem-cell therapies, which are widely offered and loosely regulated in the country.

Telescope rivals

The US National Science Foundation (NSF) has launched a competition for a giant ground-based telescope — even though it can't provide funds to build or operate such an instrument until at least 2020 (see *Nature* **479**, 18–19; 2011). Two rival US projects, the Thirty Meter Telescope and the Giant Magellan Telescope, hope to earn some backing from the government agency, despite the lack of spare cash. The NSF intends to announce the winning proposal by October 2012.

Indian overhaul

India needs to transform its scientific landscape if it is to avoid falling further behind other nations, says the country's Prime Minister, Manmohan Singh. His remarks, at the country's largest annual science congress, in Bhubaneswar on 3 January, were triggered by a December 2011 report from his scientific advisory council, which urged him to make structural administration changes, send people abroad for PhD studies and create centres of excellence. India's scientists have heard calls for reform before — but the council's chair, C.N.R. Rao, thinks that the government will take the panel's advice seriously. See go.nature.com/cksmj6 for more.

PURAVIDA FOTOGRAFÍA/DEMOTIV/CORBIS

Chilean reserve scorched by wildfires

Forest fires in Chile have ravaged almost 15,000 hectares of native forest and steppe in the Torres del Paine National Park in Patagonia — burning more than 8% of one of Chile's most important protected areas. The fires began on 27 December, allegedly caused by a tourist, and by 5 January, five of six pockets of fire in the park region had been controlled. Chile continues to battle fires in other regions. Fires in 2005 and 1985 caused similar destruction in the park, which the United Nations Educational, Scientific and Cultural Organization has designated as a biosphere reserve. See go.nature.com/ubvjvq for more.

Beijing smog

Residents of China's capital can expect to get more realistic assessments of the city's air quality. The municipal government said on 5 January that it would publicly report data on levels of particles smaller than 2.5 micrometres across ($PM_{2.5}$), and would report hourly (rather than daily) on other pollutants, such as sulphur dioxide. Without $PM_{2.5}$ monitoring, public assessments had always underestimated Beijing's air pollution, much to residents' anger. China is working towards a stricter nationwide air-quality standard that includes measurements on ozone and $PM_{2.5}$, but this will not be rolled out until 2016.

Antibiotic ban

The US Food and Drug Administration is restricting some uses of a major class of antibiotic in farm animals, to slow down the rate at which microbes acquire resistance to the drugs. On 4 January, the agency banned unapproved uses of cephalosporins in cattle, pigs, chickens and turkeys — a ban that it had already ordered in 2008, but revoked after protests from farmers, drug firms and veterinary surgeons. The new order is less strict than the 2008 rule. See page 125 for more.

Airline carbon row

Global airlines are protesting a European law that requires them to pay for some of the carbon emissions from their flights using European airports. Last week, China's airlines said they would not pay the charges; US airlines have raised prices for European flights, but the country's government is said to be looking at ways to counter the policy. From 1 January, aviation was included in the European Union's Emissions Trading System, with airlines

expected to buy permits covering 15% of their carbon dioxide emissions in 2012. First payments will not be collected until next year.

Safer reactors

France's nuclear regulator is demanding stringent safety upgrades for the country's reactors in response to the disaster at Japan's Fukushima nuclear plant. Its 3 January report was sent to the European Commission, which had asked for 'stress tests' of its member states' reactors. By contrast, a 4 January report from the UK nuclear regulator did not find any fundamental weaknesses in its nation's power stations. See page 121 for more.

PEOPLE

MMR lawsuit

Disgraced medical researcher Andrew Wakefield is suing the *British Medical Journal* (*BMJ*), its editor Fiona Godlee, and journalist Brian Deer over a string of articles that branded him a fraud (F. Godlee *et al. Br. Med. J.* **342**, c7452; 2011). Wakefield's work posited a now-discredited link between autism and the combined measles, mumps and rubella (MMR) vaccine; in 2010, his 1998 research paper on the subject was retracted and he was struck off the UK medical register for serious professional misconduct.

Wakefield filed the suit on 3 January in a district court in Texas, where he now lives.

EPA research head

The US Environmental Protection Agency's research head and chief science adviser, Paul Anastas, is leaving the agency after two years in charge. Anastas, a pioneer of green chemistry, spent much of his time reforming the agency's programme for assessing the risks of individual chemicals, while also trying to shift its research focus to a more holistic view of sustainability. He told staff on 5 January that he would be returning in mid-February to his research position at Yale University in New Haven, Connecticut.

EVENTS

JEWANA PHOTOSHOT

Drought in China

After a decade-long dry spell, China's largest freshwater lake has shrunk to its smallest size in years, state media said on 5 January. The area of Poyang Lake, in the eastern Jiangxi province, was 183 square kilometres early this year, nearly half the average of 344 square kilometres recorded since 1951. The drought has left thousands of fishing boats stranded on the exposed lake bed (**pictured**).

BUSINESS

Cheap genomes

The US$1,000 genome has arrived — according to US biotech firm Life Technologies of Carlsbad, California, which promised on 10 January that its new bench-top sequencing device could break the symbolic cost barrier. The company said that its $149,000 Ion Proton sequencer, the latest version of the Ion Personal Genome Machine that it launched late in 2010 (see *Nature* **475**, 278; 2011), would be able to sequence a genome in a day for $1,000.

Hepatitis C hopefuls

Pharmaceutical giant Bristol-Myers Squibb of New York City has become the latest company to spend billions on the promise of hepatitis C treatments. On 7 January, the firm said that it would pay US$2.5 billion to acquire Inhibitex, a biopharmaceutical company based in Alpharetta, Georgia. Inhibitex's main asset is a compound against hepatitis C that is in phase II trials. Last November, Gilead Sciences in Foster City, California, splashed out $11 billion on biotech firm Pharmasset of Princeton, New Jersey, which has three treatments for hepatitis C in clinical trials. See go.nature.com/qjoqfn for more on hepatitis C drugs.

Teva rethink

Israeli pharmaceutical firm Teva, the world's largest maker of generic drugs, may shift its focus towards branded medicines after it announced a new chief executive. Jeremy Levin, former head of strategy and alliances at Bristol-Myers Squibb in New York City, has a reputation for making external partnerships and acquisitions and is expected to continue his approach at Teva, which is headquartered near Tel Aviv. "Medicines are medicines," he told investors in a conference call on 3 January. "It doesn't matter if they are branded or generic."

COMING UP

12 JANUARY
The *British Medical Journal* and Britain's Committee on Publication Ethics host a London meeting on how best to manage research misconduct in the United Kingdom.

13 JANUARY
India may have gone a year without reporting a case of polio — a milestone that could see it removed from the list of countries where the disease is still endemic.

14–16 JANUARY
Russia's failed Mars mission, Phobos-Grunt, is expected to fall back to Earth.

TREND WATCH

Companies in the gene-sequencing industry — such as Illumina of San Diego, California — are suffering because of slack demand for their machines. But one of the hardest hit is Pacific Biosciences, based in Menlo Park, California, whose share price has fallen more than 82% since its initial public offering in October 2010. The firm has also been hit with a class-action lawsuit alleging that it made misleading statements about its technology in a prospectus shown to potential investors.

GENE-SEQUENCING STOCK SUFFERS

Pacific Biosciences has fared worse than other sequencing companies since it went public in 2010.

SOURCE: NASDAQ

NATURE.COM
For daily news updates see:
www.nature.com/news

nature REVIEWS NEUROSCIENCE

November 2011

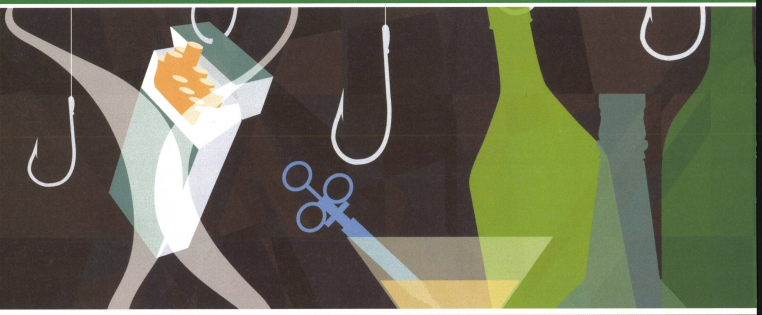

Focus on Addiction

Addiction incurs enormous medical, economic and social costs. The currently available pharmacotherapies for addiction are only moderately effective, which further emphasizes the need to improve our understanding of the changes induced in the brain by addictive substances. In this special Focus issue of *Nature Reviews Neuroscience* five articles discuss recent insights into the neurobiology of addiction — from the molecular to the behavioural level — and highlight the importance of these findings for the development of new treatments.

Articles include:

Transcriptional and epigenetic mechanisms of addiction
Alfred J. Robison and Eric J. Nestler

Common cellular and molecular mechanisms in obesity and drug addiction
Paul J. Kenny

Dysfunction of the prefrontal cortex in addiction: neuroimaging findings and clinical implications
Rita Z. Goldstein and Nora D. Volkow

Pharmacogenetic approaches to the treatment of alcohol addiction
Markus Heilig, David Goldman, Wade Berrettini and Charles P. O'Brien

Opiate versus psychostimulant addiction: the differences do matter
Aldo Badiani, David Belin, David Epstein, Donna Calu and Yavin Shaham

Read for FREE online at:
www.nature.com/nrn/focus/addiction

Produced with support from NIAAA NATIONAL INSTITUTE ON ALCOHOL ABUSE AND ALCOHOLISM NIDA NATIONAL INSTITUTE ON DRUG ABUSE

nature publishing group npg

NEWS IN FOCUS

GREECE Europe's financial crisis spurs research shake-up **p.123**

RADIO ASTRONOMY Giant array will listen for whispers from the first stars **p.127**

THERAPEUTICS NIH launches its translational-medicine institute **p.128**

CHINA University president leads the fight against misconduct **p.134**

M. EULISS/AP

Nuclear plants such as Tricastin will need to build fail-safe systems that operate even after an accident.

NUCLEAR POWER

France 'imagines the unimaginable'

Regulator demands safety upgrades for nuclear plants to guard against a Fukushima-like disaster.

BY DECLAN BUTLER

Nowhere did the alarm bells sounded by the Fukushima nuclear disaster ring more loudly than in France, which leads the world in nuclear energy. About three-quarters of its electricity comes from nuclear power stations, and it is one of the main exporters of reactors and related technology.

Now it is leading the way in setting radical safety standards for the industry, in an effort to ensure that the disaster in Japan on 11 March 2011 could never be replayed on French soil.

Last week, the country's nuclear regulator imposed what are perhaps the toughest safety measures so far in response to the Fukushima accident. In a novel approach, it will require all power plants to build a set of safety systems of last resort, contained in bunkers that will be hardened to withstand more extreme earthquakes, floods and other threats than plants themselves are designed to cope with.

It will also adopt a proposal by Électricité de France (EDF), France's sole nuclear power plant operator, to create an elite force that is specifically trained to tackle nuclear accidents and could be deployed to any site within hours. Both moves respond to the main lessons of Fukushima: that the magnitude of external threats can far exceed those anticipated; that these threats can knock out multiple safety measures; and that to prevent a serious accident degenerating into a catastrophe, it is vital to ensure that key safety capacities — such as a control room, emergency generator and coolant system — remain in working order.

These and a raft of other measures are outlined in a 336-page report published by France's independent Nuclear Safety Authority (ASN), based in Paris, on 3 January (see go.nature.com/ytktvo). The report has been submitted to the European Commission as part of ongoing European Union (EU) 'stress tests' of all its member countries' reactors. The ASN report bluntly states that despite existing safety measures, a loss of power or cooling systems at some French plants could result in a "core meltdown within a few hours in the most unfavourable cases".

Keeping systems running in the crucial hours after an accident will be a core doctrine of French nuclear safety in the future. "If you can get the water flowing, you can buy time" and thus avoid the meltdown that made the Fukushima accident so serious, says Martial Jorel, director of reactor safety at the Institute of Radioprotection and Nuclear Safety (IRSN) in Fontenay-aux-Roses near Paris, which gives scientific advice to the ASN. The ASN report incorporates many IRSN recommendations made in November 2011 (see go.nature.com/b3tjru). "In France, we're saying, 'imagine the unimaginable'," says Jorel. The current basis of nuclear safety is 'defence-in-depth', in which multiple levels of protection and redundancy are intended to guard against a serious accident, he adds. "But at Fukushima, all of those lines of defence collapsed. The accident has thrown into question all of our safety rules, our ways of thinking."

Like nuclear regulators in other countries, which are also taking stock of safety, the ASN intends to review and reinforce ▶

NATURE.COM
Nature's interactive graphic of the world's nuclear plants:
go.nature.com/hglcgt

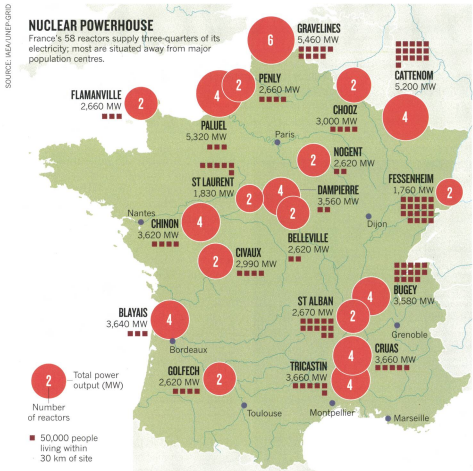

conventional measures such as flood-protection barriers. It has also ordered better safety and emergency-response training of plant staff, and a complete review of reactor cooling systems.

The bunker concept is different, however, because it short-circuits the traditional approach to safeguarding against estimated levels of risk. Irrespective of their perceived vulnerability to external threats, plants will need to be equipped with this 'hard core' of protected control rooms, generators and pumps, as well as hardened reservoirs of coolant.

This circumvents the delays and compromises inherent in setting new estimates of seismic, flood or other risks, which requires years of discussions between the regulator, industry and expert advisers, says Jorel. Predicting risk is an imperfect art, and the bunker concept should protect against any other unforeseen, low-probability event. "It's far easier to design and build a system of last resort than to try to address every potential problem," he says.

The new measures are part of a shift in the emphasis of nuclear safety in the wake of Fukushima, from preventing a nuclear accident to stopping one from spiralling out of control — and mitigating the damage should the worst occur, says nuclear engineer Laurent Stricker, chairman of the World Association of Nuclear Operators (WANO) and a senior adviser to EDF. WANO, which was created as an international forum on nuclear safety in the aftermath of the 1986 Chernobyl accident, announced in November that it would increase its staff from 140 to 415 to address this broader mandate.

France's strategy is also likely to influence the global debate on nuclear safety, with the bunker safety system and rapid-response team possibly gaining traction internationally, say experts. Stricker endorses both concepts, and adds that WANO will encourage its members to consider creating such specialist response teams in key regions around the world.

Many of the national reports for the EU stress test have been published only in the past few weeks, to meet the commission's deadline of 31 December 2011. But it already seems clear that France's proposals are the most comprehensive. They contrast sharply with those from the United Kingdom, for example, which were released last week and concluded that no major changes were immediately needed at the country's ten plants.

This may reflect differences in the reactors used by each nation, says Andrew Sherry, director of the Dalton Nuclear Institute at the University of Manchester, UK. France uses pressurized water reactors (see 'Nuclear powerhouse'), whereas almost all of Britain's are advanced gas-cooled reactors, which progress to meltdown more slowly in the event of an accident, buying more time to mount an emergency response. "What might be appropriate in France might not be appropriate in the United Kingdom," Sherry says. Experts from EU member states will now peer-review each other's reports and carry out site inspections of nuclear plants, to assess the safety of nuclear reactors across the EU. That exercise is scheduled to be completed in June.

Meanwhile, EDF has said that it fully backs the new rules, but its initial estimate is that adopting them will cost €13 billion (US$16.6 billion). It must submit initial designs for its new safety features to the ASN by 30 June. The big question, says Jorel, is how fully the planned measures will be implemented.

Yves Marignac, a Paris-based consultant on nuclear and energy issues, says that the French report is a "thorough analysis", particularly in its assessment of the existing safety shortcomings at plants. But he says that the concepts of a protected bunker and rapid-response force will take time to flesh out, and are not likely to be a quick solution. "It's technically wrong to sell politically the idea that billions of euros could fix the problem in the coming months," he says.

Sherry is convinced, however, that the Fukushima accident has been a wake-up call for the nuclear industry. "What's quite clear to me is that they are taking things very seriously." ■

MORE ONLINE

P. ZBOROWSKI/AAP/PA

TOP STORY

Modified mosquitoes set to quash dengue fever
go.nature.com/olakko

MORE NEWS

- Return of the super ants go.nature.com/eisrm3
- Mathematician claims breakthrough in Sudoku puzzle go.nature.com/q6tnyj
- Thawing permafrost reduces runoff into China's Yangtze River go.nature.com/i1amsy

PODCAST

Resurrecting ancient proteins, a new hormone and whale markets
go.nature.com/sqovzn

POLICY

Greek science on the brink

Financial woes spur controversial reforms of the country's research system.

BY ALISON ABBOTT IN ATHENS

"We are trying to survive and go along as if nothing is happening," says Dimitra Thomaidou, a microscopist at the Hellenic Pasteur Institute in Athens.

Despite Greece's financial crisis, optimism was the prevailing mood at last month's meeting of the Hellenic Society for Biochemistry and Molecular Biology in Athens, where Thomaidou coordinated a session. Meeting attendance was at a record high, and chat was full of references to fancy equipment purchases and Greek success in winning participation in European research-infrastructure programmes.

But as the financial crisis deepens and university and research spending, already among the lowest in Europe, shrink further, staying optimistic is a constant battle. Academic salaries have been cut by 20% and university budgets have halved since the crisis began about two years ago. Still, money from the European Commission and international grants is keeping the best Greek scientists committed to their work. "It may sound irrational, but we just don't think we can live without our research," says Thomaidou.

Closer conversation, however, reveals anxiety — not about money, but about reforms spurred by the crisis. Just a handful of Greece's universities and research institutions are internationally competitive. A massive restructuring of the system would modernize their governance, giving them more autonomy while introducing greater competition and transparency. Some institutes and universities would be merged to reduce the fragmentation that has arisen in the past 30 years. Expected to take effect this year, the plan also aims to break down barriers that make it difficult for scientists to move between institutions.

"It may sound irrational, but we just don't think we can live without our research."

Scientists' main concern, says Thomaidou, is that mid-career researchers like herself will survive the upheavals only to find that there is no new generation of researchers to succeed them, because poorly paid and financed research careers are unattractive. "We keep our thoughts firmly on science and hope that things will get better — and that if everything is to be restructured, it will be done appropriately," she says.

T. STAVRAKIS/AP

Despite rallies against austerity in Greece, there is growing acceptance of the need for university reform.

Many scientists in Greece accept that their research system needs restructuring. Previous governments failed to win parliamentary support for reform, but the financial crisis has helped to break down resistance, says Achilleas Gravanis, a pharmacologist at the University of Crete in Heraklion and chairman of the biosciences section of the National Council for Research and Technology, which advises the government. A new law for higher education was approved with a huge majority by the Greek parliament on 24 August 2011, and next month a draft law for research should be presented to parliament, where it is expected to have an easy ride.

The academic leadership of the 18 publicly funded research centres in Greece is generally positive about the reforms. "Only good things are likely to happen," says Dimitris Thanos, a molecular biologist and research director at the Bioacademy in Athens. But scientists in smaller research institutes dread being told to merge with universities, saying that their agility could be crushed by university bureaucracy.

The rectors of Greece's 24 public universities, for their part, seem appalled by the law, which radically changes university governance, depoliticizing it and bringing it into line with European norms. Students will lose their right to vote for department chairs, deans and rectors. Each university will be responsible for its own budget and must appoint a powerful governing council with 15 members: six from outside the university, and just one student representative. The council will draw up a shortlist for the position of rector, on which faculty members will vote.

REBELLIOUS RECTORS

Implementation of the law has stalled because rectors are appealing to the Constitutional Court, claiming that the presence of external council members violates their academic independence. Gravanis disagrees with this opposition: "It is shocking that academic leaders would show no respect for a law passed with huge parliamentary majority," he says. The law was designed with input from a constitutional-court judge, he adds.

Only the University of Crete is complying with the changes. It is to hold elections for internal members of its council on 22 February. "We'll just have to see how we can make the law work well in practice," says its rector, Euripides Stephanou. But he is nervous. The financial crisis may have encouraged the approval of reform laws, he says, but cash shortages may encourage the incoming governing councils to close faculties that have no revenue-generating potential — such as the University of Crete's prestigious ▶

archaeology and history departments.

The proposed law on research would also need solid financial backing, say scientists. It designs a system in which researchers in different types of institution and in industry would be able to collaborate easily, administration would be efficient and there would be regular calls for competitive research grants. The law would create a mandatory line for research spending in the state budget for the first time. But parliament would have to approve the actual budget each year, and scientists fear that parliament might not be generous.

Greece does not have a dedicated research funding agency, but that absence is offset by the €0.9 billion (US$1.14 billion) earmarked for research from the country's 2007–13 European Union (EU) Structural Funds, which are effectively subsidies for poorer regions in the union. After years of providing almost no research funding, the Greek government has in the past year put out a handful of calls for infrastructure and competitive-research grant proposals that would use the EU money. Most calls invite applications from academic networks and industry collaborations, but one, made last May, is aimed at individual researchers. Modelled on grants offered by the European Research Council, the calls are worth up to €1 million each. But competition is harsh: of 1,200 applications, fewer than 200 will be funded.

The money will be a life-saver for established researchers, but the future of the system as a whole remains uncertain. Over the next five years, 30% of current faculty members and researchers will retire from Greek universities and research centres, and replacing them may be difficult. Thanks again to EU funding, Greece produces large numbers of PhDs, but most of those who continue on to postdoctoral research do so abroad. In the past, many have returned to seed competitive research groups at home. The proposed law provides schemes to encourage that, but few believe that it will work, given the very low salaries and uncertain funding that researchers can expect.

Vasso Kostourou, a cell biologist at the Alexander Fleming Biomedical Sciences Research Center in Vari, is an exception. She returned to Greece from London in 2008, and recalls colleagues encouraging her because they thought that project funding was about to resume. Instead, she arrived as the crisis hit. At 37 years old, Kostourou thinks that she may be among the last scientists to return to academia in Greece for the foreseeable future. "That's a shame because the quality of science that can be done here is high," she says. "It's only the funding that's bad." ■

NATURE.COM
Listen to an interview about the Greek crisis at: go.nature.com/kwsh4c

ECONOMICS

Disaster toll tallied

The soaring cost of natural catastrophes is due more to socio-economic than climatic factors.

BY QUIRIN SCHIERMEIER

Natural disasters around the world last year caused a record US$380 billion in economic losses. That's more than twice the tally for 2010, and about $115 billion more than in the previous record year of 2005, according to a report from Munich Re, a reinsurance group in Germany. But other work emphasizes that it is too soon to blame the economic devastation on climate change.

Almost two-thirds of 2011's exceptionally high costs are attributable to two disasters unrelated to climate and weather: the magnitude-9.0 earthquake and tsunami that hit Japan in March, and February's comparatively small but unusually destructive magnitude-6.3 quake in New Zealand.

And the long-term rise in the costs of global disasters is probably due mainly to socio-economic changes, such as population growth and development in vulnerable regions. That conclusion is backed up by a forthcoming study — supported by Munich Re — by economists Fabian Barthel and Eric Neumayer at the London School of Economics. Their analysis of events worldwide between 1990 and 2008 concludes that "the accumulation of wealth in disaster-prone areas is and will always remain by far the most important driver of future economic disaster damage" (F. Barthel and E. Neumayer *Climatic Change*; in the press). Any major weather event hitting densely populated areas now causes huge losses because the value of the infrastructure has increased tremendously, they note, adding that if the 1926 Great Miami hurricane happened today, for example, it would cause much more damage than it did at the time.

However, weather-related events are generally on the rise. Thanks to a relatively quiet Atlantic hurricane season, damage caused by extreme weather was actually lower in 2011 than in four of the previous five years. But weather accounted for about 90% of the year's 820 recorded natural disasters, which caused at least 27,000 deaths. These disasters include flooding in Thailand, a series of tornadoes that hit the United States Midwest and southern states last spring, and storms and extreme rainfall over parts of the Mediterranean in November.

Since 1980, the report notes, the number of severe floods has almost tripled, and storms have nearly doubled, which insurance experts link, in part, to the impact of climate change (see 'Catastrophe count'). "It would not seem

P. BROWN/PANOS

Heavy rains turned roads into rivers last year as Thailand experienced its worst flooding in 50 years.

plausible that climate change doesn't play a role in the substantial rise in weather-related disasters," says Ernst Rauch, head of Munich Re's Corporate Climate Centre.

Climate scientists believe that the frequency and severity of extreme-weather events will increase as temperatures continue to rise. The summary of a report published in November by the Intergovernmental Panel on Climate Change supports that view and warns that some areas could even become "increasingly marginal as places to live in".

But attempts to attribute specific events to global warming are in their infancy (see *Nature* **477,** 148–149; 2011). "Disasters are a tempting image for advocacy, but the science is just not there to support strong claims," says Roger Pielke Jr, a climate-policy researcher at the University of Colorado in Boulder. "We cannot yet attribute increasing dollar losses to human-caused climate change. Maybe we will one day, but not at present." ■

SOURCE: MUNICH RE

CATASTROPHE COUNT

An increase in severe storms is helping to drive up the number of recorded disasters, but this cannot be conclusively attributed to climate change.

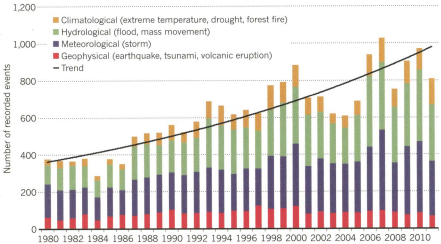

PUBLIC HEALTH

Rules tighten on use of antibiotics on farms

Clampdown aims to stop spread of drug-resistant microbes.

BY NATASHA GILBERT

Alarmed at signs that the overuse of antibiotics in farm animals is blunting these key weapons against human disease, governments are taking action.

In industrial farming, antimicrobials are commonly given to farm animals to treat infections, and prophylactically to prevent disease or spur growth. But there is growing concern that excessive use on farms is helping to breed antibiotic-resistant microbes, from *Salmonella* (see 'Rising resistance') to *Escherichia coli*, which are harder to treat when they infect people.

The US Food and Drug Administration (FDA) is now moving to protect key antibiotics known as cephalosporins, which are used in humans to treat a range of infections, including pneumonia. On 4 January, the agency said that it would prohibit certain uses of cephalosporins in farm animals including cattle, pigs, chickens and turkeys, because overuse of the drugs is "likely to contribute to cephalosporin-resistant strains of certain bacterial pathogens". If cephalosporins become ineffective in treating human diseases, the FDA said, "doctors may have to use drugs that are not as effective, or that have greater side effects".

The new rules, to come into effect on 5 April, restrict veterinary surgeons to using the two cephalosporin drugs specifically approved for food-producing animals — ceftiofur and cephapirin — and ban prophylactic use. In animals not listed in the FDA order, such as ducks or rabbits, vets will have more discretion to use the drugs.

Most antibiotic classes are used both in animals and in humans, so the FDA is also considering tightening controls on all classes of antimicrobials used on farms. It is reviewing comments on rules that would prohibit the use of any antimicrobial drug to promote animal growth, a move that would be welcomed by many vets. "We would support greater veterinary oversight of antimicrobial drugs," says Christine Hoang, assistant director of scientific activities at the American Veterinary Medical Association in Schaumburg, Illinois.

The European Union (EU), which already forbids the use of antimicrobials to promote growth, plans to strengthen its own rules. Its new antibiotic-resistance strategy, published in November 2011, calls on EU countries to ensure that antibiotics are only available on prescription, and to strengthen surveillance systems to track and report cases of resistance (see *Nature* http://doi.org/cshmhv; 2011).

Although it is widely accepted that overusing antibiotics can be a major driver of resistance in microbes, the evidence linking antibiotic use in farm animals with resistance in humans is still controversial (A. E. Mather *et al. Proc. R. Soc. B* http://doi.org/hj8; 2011). A research programme coordinated by Europe's Innovative Medicines Initiative could provide some answers: in the next few months it will call for proposals for €350 million (US$445 million) in grants to understand how resistance arises, and to develop new antimicrobial drugs.

Antimicrobial resistance is also this year's top priority for the intergovernmental World Organisation for Animal Health (OIE), based in Paris. Bernard Vallat, director-general of the OIE, says that it is working with the FDA and the World Health Organization to help developing countries to improve their legislation covering the control, distribution and use of veterinary antimicrobials. The three organizations plan to urge governments to put vets in charge of allocating the drugs and to ban preventative use.

"There are over 100 countries worldwide without legislation. Antibiotics are sold like sweets," Vallat told *Nature*. "There is no control and this is a major risk to animal and human health." ■

RISING RESISTANCE

Farms in the United States have seen an alarming rise in *Salmonella*'s resistance to ceftiofur.

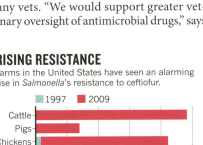

SOURCES: NATIONAL ANTIMICROBIAL RESISTANCE MONITORING SYSTEM; FDA

Technical University of Denmark

DTU

PROFESSOR (AND CENTER DIRECTOR)

Center for Microbial Biotechnology (CMB)

DTU Systems Biology. Applications are invited for a professorship in Cell Factory Design, Cellular Physiology and Metabolic Engineering. The professor will, for the research into microbial and cellular physiology, benefit from an advanced small-scale fermentation platform established at CMB. This fermentation platform is currently based on yeast, fungi and gram positive bacteria, and lately, mammalian cells and stem cells have been included.

Application deadline: **27 January 2012**

DTU is a technical university providing internationally leading research, education, innovation and public service. Our staff of 5,000 advance science and technology to create innovative solutions that meet the demands of society; and our 7,000 students are educated to address the technological challenges of the future. DTU is an independent academic university collaborating globally with business, industry, government, and public agencies.

Further details: dtu.dk/career

W219818R

NATURAL ENVIRONMENT RESEARCH COUNCIL

CHAIR OF THE NERC SCIENCE AND INNOVATION STRATEGY BOARD

The Natural Environment Research Council (NERC) is seeking a part-time non-executive Chair for its Science and Innovation Strategy Board (SISB). SISB is the key source of advice to NERC Council on science and innovation strategy, policy and investments.

You will have extensive experience and understanding of research, business or policy related to environmental science or engineering at national and international levels. With an excellent record of achievement, influence and personal credibility in your field, you will be able to evaluate complex issues and make balanced strategic recommendations. Board-level experience and understanding of finance would be beneficial.

We offer a remuneration package of £9,000 per annum for 20-25 days work, plus reasonable travel expenses. The appointment is for three years commencing 1st April 2012.

NERC supports the full range of atmospheric, earth, biological, terrestrial and aquatic sciences, from the deep oceans to the upper atmosphere and from the poles to the equator.

Further information and an application pack are available at http://www.nerc.ac.uk/about/work/boards/science/.

For enquiries contact Mark Hinder on 01793 411537, e-mail mark@nerc.ac.uk.

Closing date: **Monday 13th February 2012.** Interviews will be held in London on **7th and 9th March 2012.**

U220117N

---

hhc human health care

Eisai

Eisai Ltd. (ESL), part of Eisai Co., Ltd., focuses on the development of innovative medicines for the treatment of neurodegenerative diseases.

As part of our continued commitment to Neuroscience Product Creation at the European Knowledge Centre (Hatfield, UK), an opportunity exists for a Senior Medicinal Chemist with outstanding scientific and personal leadership qualities.

(SENIOR) PRINCIPAL SCIENTIST, MEDICINAL CHEMISTRY

The successful candidate will be instrumental in leading and advancing projects to critical decision making milestones, from Target Validation to Candidate Selection and beyond. The primary purpose of the role is the delivery of tangible Project outcomes through the formation of strong internal cross-functional interactions and key external collaborations rather than line management and administration, to allow for the application of science of the highest quality in a timely manner. Given the critical importance of the role, the candidate will also be expected to contribute to the development of our scientific strategy, and the identification and prosecution of novel targets for disease intervention. Proactive contribution to problem solving and scientific cross-fertilisation of the laboratories beyond the immediate area of project responsibility will be expected.

You will be able to demonstrate a strong record of creativity and delivery in drug discovery, exemplified by the identification of high quality development candidates through the application of excellent science and leadership of multidisciplinary teams. You will have a significant number of publications, presentations and patents that support your international status in the scientific community. You will have a track record of taking intelligent risks, a sense of urgency and tenacity in the prosecution of project goals, courage in decision making and a willingness to be held accountable for decisions. A track record of leading by example and motivating teams with vision, integrity, flexibility, passion and forthright/clear communication is a must.

To apply, please send your curriculum vitae, a covering letter and details of two professional referees to: HR Department, Recruitment GC001/2012, Eisai Europe Ltd, European Knowledge Centre, Mosquito Way, Hatfield, Hertfordshire, AL10 9SN or by email to Recruitment@eisai.net.

The deadline for receipt of applications is **20th Jan 2012**.
For more information about our company, please visit: ***www.eisai.co.uk***

U220186R

To advertise here please contact – US tel. +1 800 989 7718, naturejobs@natureny.com or Europe/ROW tel. +44 20 7843 4961, naturejobs@nature.com

ASTRONOMY

Radio array starts work

Giant low-frequency sensor system on track to probe the birth of the first stars.

BY ERIC HAND

LOFAR/ASTRON

At the heart of the LOFAR telescope is a collection of tile-like and dipole antennas.

The Netherlands, one of the most densely populated countries in Europe, would seem to be an inauspicious place to detect radio whispers from the distant Universe. Mobile-phone towers, television transmissions, planes overhead and even the odd burst of noise from a windmill create a background din in the radio sky.

But the builders of LOFAR, the Low-Frequency Array of radio receivers centred around the tiny village of Exloo, say that they have found ways to ignore the noise. In doing so, Dutch astronomers at ASTRON, the Netherlands Institute for Radio Astronomy in Dwingeloo, are opening up a region of the electromagnetic spectrum that should hold clues to one of the earliest phases of cosmic history, when the first stars formed — an era beyond the ken of even the biggest optical telescopes.

"Many of the radio astronomers said this couldn't be done," says Heino Falcke, an astronomer at Radboud University in Nijmegen and chairman of the International LOFAR Telescope Board, the five-nation foundation that governs the €150-million (US$192-million) project. Yet Falcke and his colleagues defied the doubters by presenting their first results on 9 January at a meeting of the American Astronomical Society in Austin, Texas. "The message today is: the basic things all work. We can do this," he said.

Mapping the low-frequency sky requires an expansive telescope as well as the ability to tune out noise. When completed later this year, the array will contain 2,700 slender dipole antennas tuned to 30–80 megahertz, and 43,000 antennas embedded in flat tiles a few metres square that are sensitive to 120–240 megahertz. The antennas will be concentrated in 40 stations across the Netherlands; 8 other stations in the United Kingdom, France, Germany and Sweden give the array extra angular resolution for fine-scale imaging. The fibre-optic data network that links the LOFAR antennas will also support sensor webs for geoscience and agricultural monitoring (see 'A multi-purpose array').

A MULTI-PURPOSE ARRAY

The Low Frequency Array was designed for astronomy — but its fibre-optic data links will also be used for seismic monitoring, water management and agricultural sensing.

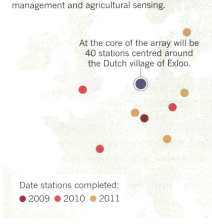
At the core of the array will be 40 stations centred around the Dutch village of Exloo.
Date stations completed:
2009
2010
2011

LOFAR has already turned up surprises. Its observations of four pulsars — spinning neutron stars that emit regular radio pulses — show that the emissions at a wide range of frequencies are bunched together in time, implying that they emanate from a narrow region near the pulsar. The finding challenges a common picture in which pulsars generate their radio signal in a much wider region, says ASTRON's Jason Hessels, co-principal investigator of LOFAR's pulsar working group.

But the real prize would be the detection of a signal from the epoch of re-ionization. That was roughly 400 million to 800 million years after the Big Bang, when radiation from the first stars and galaxies ionized the primordial hydrogen gas that filled the newborn Universe, creating bubbles of ionized gas like the holes in a Swiss cheese. By mapping the gradual disappearance of the faint 21-centimetre emission line from the primordial hydrogen, LOFAR astronomers hope to distinguish between two re-ionization mechanisms: one driven by the stars' ultraviolet light and one by X-rays from super-massive black holes in newborn galaxies. That would allow the astronomers to watch the first stars and galaxies being born.

Based on an initial run of ten hours spent staring at several quiet corners of the radio sky, ASTRON's Ger de Bruyn suspects that the re-ionization signal could be detected with 400 hours of devoted observing time — a campaign he plans to begin by the end of the year.

That schedule would put LOFAR ahead of rival re-ionization projects in remote parts of Australia, South Africa and New Mexico, locations chosen partly for their lack of radio noise. Greg Taylor, an astronomer at the University of New Mexico in Albuquerque and director of the Long Wavelength Array being built in New Mexico, acknowledges that LOFAR is the array to beat in the race to detect re-ionization — but says that would be just the beginning. "If you make the discovery, then it's a Nobel prize for somebody," he says. But afterwards, "it has the potential to explode into a field of study". ■

THERAPEUTICS

US translational-science centre gets under way

Mission of newly formed NCATS is to dramatically speed up production of drugs and other therapies, but sceptics question agency's ability to deliver.

BY MEREDITH WADMAN

Scarcely a year after plans to establish it were made public, the National Center for Advancing Translational Sciences (NCATS), the newest branch of the US National Institutes of Health (NIH) in Bethesda, Maryland, is up and running. On 4 January the centre's 230 employees gathered for their first 'all-hands' meeting, at which they heard an exhortation from NIH director Francis Collins and his lieutenants about the importance of the centre's mission: finding ways to radically speed up the development of new drugs, devices and diagnostics.

"Patients suffering from debilitating and life threatening diseases do not have the luxury to wait the 13 years it currently takes to translate new scientific discoveries into treatments," Collins said on 23 December, the day President Barack Obama signed the law creating NCATS. Congress had for months expressed concerns that NCATS could infringe on the private sector, and that the NIH was rushing it into existence. But the critics relented, and Congress approved the US$576-million centre on 17 December as part of a massive government funding bill.

"Getting drugs that work in people is a very hard thing to do."

The law creates NCATS from several existing NIH programmes — most notably, the Clinical and Translational Science Awards (CTSA; see table). In the new law, Congress directs the NIH to spend at least $488 million on the awards in 2012. At the same time, it dissolves the National Center for Research Resources (NCRR), where the CTSA programme has been housed, and parcels out that centre's programmes to other parts of the NIH. NCATS will also administer a Cures Acceleration Network (CAN), authorized in the 2010 health-reform law and now funded for the first time under the new law. CAN, a competitive grant programme that will allow the agency to circumvent bureaucratic obstacles and push promising drugs forward, received just $10 million, one-tenth of what Collins had requested. The minimal funding nonetheless means that the programme "can get up and running", says Margaret Anderson, executive director of FasterCures, a think tank in Washington DC that actively supported the creation of NCATS.

ASSEMBLING THE PUZZLE

NCATS will be created from pre-existing NIH programmes. Their budgets give a sense of their relative scale.

Programme	Original NIH home	Funding in 2011
Clinical and Translational Science Awards	National Center for Research Resources (NCRR)	$460.5 million (from NCRR); $22.7 million (from NIH Common Fund*)
Components of the Molecular Libraries Program	National Human Genome Research Institute (NHGRI)	$21.4 million (from Common Fund)
Therapeutics for Rare and Neglected Diseases	NHGRI	$24 million (from all NIH institutes and centres)
Bridging Interventional Development Gaps (formerly called RAID)	NHGRI	$15 million (from Common Fund)
Office of Rare Diseases Research	Office of the director	$17.8 million
NIH–FDA Regulatory Science Initiative	Office of the director	$2.7 million (from Common Fund)
Cures Acceleration Network	New	$0 ($10 million for 2012)

*The NIH Common Fund is a discretionary fund for short-term, trans-institute programmes, administered through the office of the director.

But the new centre has its sceptics — some of whom have voted with their feet. At the NCRR, 26 employees left during 2011 while Congress was debating their centre's future — more than twice the turnover in 2010. The dismantling "was a complete shock and surprise", says Barbara Alving, the former NCRR director, who resigned in September.

Others say that Collins is naive to suggest that the NIH can fix bottlenecks in the drug pipeline when the far-better-funded pharmaceutical industry has failed to do so. Creating NCATS "is sort of like declaring the war on cancer", says one critic. "Now what? Getting drugs that work in people is a very hard thing to do." But Congress wants NCATS to steer clear of industry prerogatives anyway: the legislation establishing it pointedly insists that the centre should "not create duplication, redundancy and competition with industry activities". And Congress explicitly forbids it from sponsoring late-stage clinical trials.

In a separate report, Congress instructs NCATS to protect both the money and the mission of the CTSA programme, which funds recipients at 60 academic medical centres nationwide — even though the recipients' activities do not always overlap with the new centre's mission. The CTSA programme would comprise at least 80% of the NCATS budget. Lawmakers have instructed the agency to enlist the Institute of Medicine to assess the CTSA's current mission, and to decide within 18 months whether changes are needed. Mark Lively, a biochemist at Wake Forest Baptist Medical Center in Winston-Salem, North Carolina, who served on the NCRR external advisory council, worries that, in the interim, NIH leaders will boost the rest of NCATS's budget by dipping into basic-science funding. NIH officials insist that this will not happen.

Meanwhile, at the top of the new centre's to-do list is finding a director. "We are thrilled with the applicants and are going to start interviews this month," says Kathy Hudson, acting deputy director of NCATS. ■

CLARIFICATION

The News story 'Last-minute wins for US science' (*Nature* **480,** 423; 2011) implied that the total US contribution to the Global Fund to Fight AIDS, Tuberculosis and Malaria is $298 million. This is just how much the National Institutes of Health was set to provide in 2012, and which will now be given instead by the Department of State.

CORRECTION

The News story '2011 in review' (*Nature* **480,** 426–429; 2011) confused its melanoma treatments: 'ipilimumab' should read 'vemurafenib'.

nature REVIEWS GENETICS

ARKITEK STUDIOS

Animation on RNA interference

RNA interference (RNAi) has enormous scientific implications, from shaping our understanding of how gene expression is regulated to providing new tools for basic and clinical research. Now you can learn about the principles RNAi through an up-to-date animation that introduces you to gene regulation by small interfering RNAs (siRNAs) and microRNAs (miRNAs).

Nature Reviews Genetics, in association with Arkitek Studios, has brought RNAi to life in this vivid, audio-visual journey into the cell.

See RNAi in action by viewing the animation for FREE at:
www.nature.com/nrg/multimedia/rnai

Also, download a **FREE** poster on tools for studying and using small RNAs at:
www.nature.com/nrg/posters/small-rna

The Animation and Poster are freely available thanks to support from:

Thermo SCIENTIFIC
Part of Thermo Fisher Scientific

nature publishing group npg

Never say die

With a history of public blunders, can Advanced Cell Technology make embryonic stem-cell therapies a reality?

BY CORIE LOK

"Oh crap, this really puts us in the spotlight!" thought Robert Lanza when he first heard the news. Advanced Cell Technology (ACT), the biotechnology company in Marlborough, Massachusetts, of which Lanza is chief scientific officer, had for more than a year been operating in the shadow of Geron, a rival company in Menlo Park, California. Geron was bigger and better funded than ACT, and it was the first company to be approved by the US Food and Drug Administration (FDA) to test a therapy in humans based on embryonic stem (ES) cells. ACT was second. But in November, Geron announced that it was halting its trial to focus instead on cancer drugs. And with the announcement, Lanza says, he felt the weight of the ES-cell field fall on his shoulders.

Lanza and his company have had plenty of experience in the spotlight, but the attention has not always been flattering. Since the late 1990s, ACT has gained a reputation as a renegade company, accused of overhyping results to raise attention and money. Critics say that the company has damaged the field more than once with its high-profile, controversial announcements, such as one describing the company's attempts to clone a human embryo[1] in 2001. ACT's actions — and the

SAM OGDEN

Robert Lanza has been a public face for Advanced Cell Technology's many ups and downs.

highly politicized nature of stem-cell research — scared off investors, leaving the company teetering on the verge of bankruptcy for most of the past decade.

But the scrappy biotech refused to die, in part because of Lanza's doggedness. ACT is now performing early-phase clinical trials testing the safety of implanting retinal cells derived from human ES cells into the eye to treat certain types of blindness.

Lanza says that this time, he aims to do things right: direct good science focused on treating disease, publish in reputable journals with rigorous peer-review processes and work with high-quality collaborators and clinical centres for its trials. "We're a different company now," says Lanza.

Not everyone is convinced. Even if positive results emerge from these trials, ACT will still face major challenges in getting an ES-cell-based therapy approved for wider use. And some in the field are sceptical about ACT's reformation. "Can you really trust a company that has a spotty record?" says Arthur Caplan, a bioethicist at the University of Pennsylvania in Philadelphia.

It's not just Lanza who has a stake in the answer. With Geron out of the game, ACT's success or failure will be important for a field looking to prove itself worthy of further research funding. "If the trials are positive, that would fundamentally transform the debate," says Christopher Thomas Scott, director of the Program on Stem Cells and Society at Stanford University in California.

PROBLEM CHILD

ACT began in the mid-1990s as an animal-cloning outfit owned by Avian Farms, a Maine-based poultry genetics company. ACT quickly shifted focus when Michael West — who founded Geron — became its chief executive in 1998. Human ES cells had just been isolated for the first time, and researchers were excited about their potential use in regenerative medicine.

But many were concerned that patients' immune systems would reject cells derived from unrelated embryos. To solve this, West proposed 'therapeutic cloning' — taking the nucleus out of a patient's cell, transferring it into an egg cell to create a cloned embryo, then using that embryo to derive patient-matched stem-cell lines.

In 1999, using money he had made at Geron, West bought ACT. Lanza, a physician who had spent the past 20 years working in academic research and biotech on organ and cell transplantation, was one of West's first recruits. The team moved quickly to try to make therapeutic cloning a reality.

If the American public had not yet heard of human cloning or ACT by the fall of 2001, it could hardly have missed the hype that began on 25 November that year. West appeared on *Meet the Press*, a nationally televised US political talk show, to discuss a paper, published that day, in which ACT scientists described the first cloning of a human embryo. "We've taken the first halting steps toward what we think is going to be a new area of medicine," West said.

West appeared on several other news shows in the following days. CNN and *US News and World Report* heralded the work as a breakthrough, and West and his team hailed the "dawn of a new age in medicine" in a report for *Scientific American* (now owned by Nature Publishing Group).

In the paper[1], published in the now-defunct online journal *e-biomed*, West, Lanza and their colleagues showed that they could pull a nucleus from a human egg cell, replace it with a whole adult ovarian cell and generate an embryo that divided into six cells. It then stopped growing, far short of the 100-cell blastocyst stage from which stem cells can be derived.

> "It was our policy not to hide what we were doing and why. We wanted to be honest, accurate and open."

The work pressed a political hot button. That summer, President George W. Bush had approved federal funding for human ES-cell research, but only for a small number of cell lines that had already been created. He also voiced staunch opposition to human cloning of any kind, and a bill to ban it had been advancing through the US Congress, much to the chagrin of researchers who saw promise in therapeutic cloning.

ACT's announcement stoked fears that scientists were trying to clone humans for reproductive purposes — and conflated reproductive cloning and human-embryonic-stem-cell research in many people's minds. "It gave critics plenty of ammunition to insist that if stem-cell research was funded, human reproductive cloning would be funded too," says Caplan. "It had a huge deleterious impact for years."

Scientists, meanwhile, dismissed the finding. The ACT team hadn't gained new insight into the human developmental process, says George Daley, a stem-cell researcher at Children's Hospital Boston in Massachusetts. "I was not in a position to defend the cloning that they were doing because it was ineffective in what they were trying to do," he says. "It was more for publicity than for science."

Jose Cibelli, who was first author on the paper and left ACT in 2002 for a faculty position at Michigan State University in East Lansing, says that in an ideal world he would have waited until the team could grow the embryos to the blastocyst stage before publishing the work. But he had heard rumours that other groups were pursuing the same goal, and he was worried about getting scooped. (A successful derivation of stem cells from a cloned human embryo was not reported until October 2011, and these stem cells had three sets of chromosomes rather than two[2].)

West says that he pushed ahead with publication in the interest of transparency. "It was our policy not to hide what we were doing and why," he says. "We wanted to be honest, accurate and open."

The announcement ended up hurting the company, however. ACT was trying to raise a needed round of venture-capital financing when the cloning news broke. The negative attention combined with the political uncertainty around stem-cell funding killed the deal, says Greg Bonfiglio, who was with Anthem Venture Partners of Santa Monica, California, at the time, and would have been the lead investor on that round.

SCRAPING BY

The disappearance of the venture funding sent ACT on a financial downward slide from which it would take nearly ten years to recover, says Bonfiglio, who has dealt with the company on several more occasions. Researchers at Geron, meanwhile, had successfully derived neurons from human embryonic stem cells[3] and were pursuing research that would eventually look to repair the damage caused by spinal-cord injuries, a possible use for embryonic stem cells that was much touted at the time. ACT was largely dismissed as a sideshow.

Lanza is now the longest-serving employee of the company. He says that a "tough childhood" in Stoughton, a town south of Boston, Massachusetts, helped him to develop a thick skin.

Unlike many Boston-area academics, Lanza has the 'R'-dropping accent of the region, most noticeable when he talks about one of his main preoccupations: Stargardt's disease. "Stahgahdt's" — as he says it — is one of the two types of degenerative blindness his company is targeting in its clinical trials. The other, the 'dry' form of age-related macular degeneration, is the most common cause of age-related blindness. Both diseases result from the death of retinal cells, a process that Lanza suspects can be slowed or even halted using stem-cell-derived replacements.

After the venture funding fell through, West sold ACT's animal-cloning division to generate revenue. By 2004, however, money had again started to run low. But Lanza and West had recently hired Irina Klimanskaya, who, as a researcher at Harvard University in Cambridge, Massachusetts, had helped to derive many of the institution's first human ES-cell lines and who had a knack for working with scant resources. At ACT, she began optimizing a protocol for transforming ES cells (derived from embryos donated through

ADVANCED CELL TECHNOLOGY/AP

1998 ACT scientists and collaborators announce the successful generation of cloned transgenic cattle.

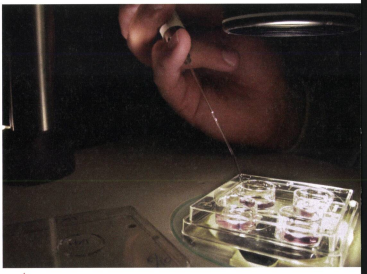

E. AMENDOLA/AP

2001 With a full media blitz, ACT publishes its efforts to clone a human embryo for the purpose of growing stem cells.

fertility clinics) into retinal pigmented epithelial (RPE) cells. These are lost in both Stargardt's and dry age-related macular degeneration[4].

Stopping vision loss didn't quite have the dramatic appeal of Geron's goal of reversing paralysis. But focusing on the eye may have been a wise decision, say experts.

"The eye is an ideal place to begin this type of experimental work," says Michael Young, an ophthalmology researcher at the Schepens Eye Research Institute in Boston. Surgeons already have protocols for injecting cells directly into the eye, and they can measure changes in the retina just by peering into it. The eye is relatively sealed off from the immune system compared with other parts of the body, which may reduce the risk of cell rejection.

Moreover, transplanted RPEs do not need to form synapses, or connections, with neurons, unlike other retinal cell types. "If cell-based therapy in the eye is going work, it's got to work with the RPEs," says Thomas Reh, a neurobiologist at the University of Washington in Seattle.

By 2004, Lanza and his team were ready to start testing the RPE cells in animals — but they were paralysed by a lack of money. The cells sat in a freezer for almost a year. Meanwhile, the company's phone service was turned off, purchases of basic lab supplies grew harder to justify and the skeleton crew of remaining scientists wondered week to week whether they would get paid.

Some left, but Klimanskaya opted to stay on. "I believe in the company, in the cells, in the technology and in my own skills," she says. "Why should I quit?"

Out of desperation, West agreed at the end of 2004 to take the company public to gain access to a new source of funding. But the legal, accounting and marketing costs of going public through an initial public offering (IPO) were far beyond the company's reach. Instead, in early 2005, ACT merged with Two Moons Kachinas, an obscure, Utah-based outfit that sold Native American dolls. Two Moons was essentially a 'shell' company, allowing ACT to take it over and become a publicly traded firm. This 'reverse merger' was much cheaper than an IPO, but the US$8 million it raised had more strings attached.

As part of the deal, investors required the company to name a new chief executive. "The issue with ACT at that time was never about the quality of the science team," says Bonfiglio, who led the deal. "The business skills were not resident on that team." The new chief executive, William Caldwell, had more than 30 years of experience in banking, transportation and telecommunications, but none in biotech.

OUT OF THE ASHES

With the infusion of cash, ACT went on a hiring spree. West, who became the company's president and chief scientific officer, moved to California and recruited several researchers in hope of starting a lab that could tap into funding from the San Francisco-based California Institute for Regenerative Medicine (CIRM), a $3-billion, state-backed fund for stem-cell research.

Meanwhile, Lanza built up his team in Massachusetts and forged ahead with the RPE transplantation studies in rats. In 2006, positive results began to materialize[5] and ACT opened its new headquarters, a 1,400-square-metre research facility in Alameda, California, which included a lab capable of growing cells according to the strict standards required for human trials.

Just as optimism was running high, the company made another very public stumble. In August 2006, Lanza and his co-authors published a paper[6] in *Nature* showing that a single cell could be plucked from an 8–10-cell human embryo and grown into stem cells. Lanza wanted to show that it was possible to derive stem cells without destroying the embryo, to sidestep ethical concerns.

In fact, the embryos were destroyed in the experiments, but that had not been made clear in the original version of the paper, the press releases about it or in some of Lanza's press interviews. *Nature* issued two clarifications after its original press release, but many news organizations had already reported that the embryos were unharmed. When the truth became clear, critics pounced.

Opponents of ES-cell research saw the debacle as an attempt to mislead the public, and scientists criticized the method as impractical and still ethically problematic. Biopsying embryos puts them at risk, says Daley, so some will be lost.

Lanza says that the *Nature* paper was only meant to be a proof of principle and that the company soon perfected the technique so that embryos survived. But the episode reinforced perceptions that the company hyped its results, this time to boost its stock value. If that was the intent, the effect was short-lived. The increase in share price on the day of the announcement — from $0.42 to $1.83 — would be reversed in the weeks and months that followed.

Unable to raise enough money from conventional sources, Caldwell turned to last-resort financing. ACT borrowed cash from investors and then repaid them in shares on a monthly basis, using the lowest share price of the previous month. As that price dropped, ACT had to issue more and more shares, forcing the price down even further. Caldwell completed several rounds of this 'death-spiral financing' between 2005 and 2010 to keep Lanza's RPE research going, and the company sank further into debt.

ADVANCED CELL TECHNOLOGY/AP

2006 ACT scientists demonstrate a possible way to derive stem cells from embryos without destroying them.

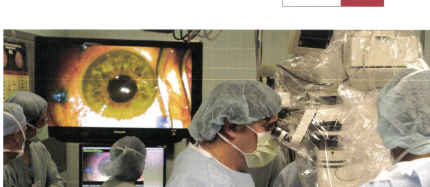

R. HUTCHINSON/UCLA

2011 ACT begins a clinical trial testing surgical implantation of retinal cells derived from embryonic stem cells as a treatment for blindness.

By 2007, West says, he was not getting along with Caldwell and left ACT to head another company to develop products for ES-cell research. In 2008, ACT closed its Alameda facility — the CIRM funding never materialized — but Caldwell stayed in Los Angeles. By the time the markets crashed later that year, ACT's stock price had dwindled to pennies. Caldwell lost all of his executives, and the entire RPE development team left.

Still, Lanza was convinced that RPE therapy held the key to the company's survival. He was, moreover, impressed with Caldwell's dedication to the project. "He got all excited [about the science], and that was important," Lanza says. "He was really my partner." The two worked tirelessly throughout 2009 to rebuild the company. Caldwell eked out funding so that Lanza and his team could do the studies needed for FDA approval of the clinical trials. "We knew we had one chance," says Lanza.

In November 2010, when a fax arrived saying that the trial had been approved, a cheer went through the office. "We came out of the ashes," says Lanza. "It was a long time coming."

There was little time for celebration, however. The team still needed approval from the clinical centres conducting the trials before they could start treating patients.

Lanza usually began each morning by answering a slew of e-mails from Caldwell, who often worked later hours in Los Angeles. So he was concerned when, on the morning of 14 December, his inbox was empty. The call came later that afternoon from Caldwell's wife. The man who had kept ACT afloat for the past six years had died unexpectedly, aged 63. Describing the loss now, Lanza becomes quite emotional and almost can't continue. "It was like I lost a father," he says.

The company faced yet another bleak period. But Gary Rabin, an investment banker who had been on ACT's board since 2007, stepped in as interim leader. Within two weeks, he had secured $25 million in financing from two firms that Caldwell had been courting. Rabin, who is now ACT's chairman and chief executive, says that the funding is enough to pay for the company's two ongoing trials and should last through 2012.

THE CHALLENGES AHEAD

Now, the company's future hinges on the outcome of the trials. Final results won't be out until 2013, and they will show mainly whether the cell transplants are safe. The patients enrolled in the trial are in the late stages of vision loss, so the chances of dramatic improvement are remote, experts say.

Still, Rabin and Lanza are optimistic. If the treatment is safe and even moderately effective, they say they would consider partnering with a pharmaceutical company to help take the programme forward — although they are still working out their plan. Scott, with Stanford's Program on Stem Cells and Society, says that positive results could fire up patient advocacy groups, which can be powerful in building support. And a good outcome could encourage investment in other stem-cell therapy companies, says Bonfiglio, who is now managing partner at Proteus Venture Partners in Palo Alto, California.

But even if the trial results are positive, ACT will face enormous challenges in commercializing the technology. The company will have to show the FDA that its RPE cells can slow vision loss in bigger and more expensive clinical trials.

And even if the treatment works, storing and distributing the cells, which often have short shelf-lives, is expensive and logistically difficult, says Chris Mason, head of the Stem Cell and Regenerative Medicine Bioprocess Group at University College London.

These challenges were thrown into stark relief when Geron halted its stem-cell trial in November, having decided that the hurdles to commercializing the therapy were too great. Now, it is up to ACT to face them. "The departure of Geron from the field will ultimately place a greater burden on ACT in terms of educating the FDA and establishing standards for safety and efficacy," Bonfiglio says.

ACT is not entirely alone: other stem-cell-based therapies are moving towards the clinic. For example, a consortium of research groups called the London Project to Cure Blindness aims to test RPE transplants from embryonic stem cells in patients with macular degeneration this year. A group in Japan hopes to test a similar approach in humans using stem cells from reprogrammed adult cells within the next three years.

Still, some who have tracked ACT's trajectory say that the company might have what it takes to succeed. "What has kept ACT going is persistence, tenacity and vision," says Ronald Green, ACT's long-time ethics adviser and a professor of religion and ethics at Dartmouth College in Hanover, New Hampshire.

Lanza says that at times he considered giving up and working on something less controversial. "If I wasn't a stubborn Italian," he says, "I would have thrown up my hands at least 25 times." ■

Corie Lok *is* Nature*'s Research Highlights Editor.*

1. Cibelli, J. B. *et al. E-Biomed* **2,** 25–31 (2001).
2. Noggle, S. *et al. Nature* **478,** 70–75 (2011).
3. Carpenter, M. K. *et al. Exp. Neurol.* **172,** 383–397 (2001).
4. Klimanskaya, I. *et al. Cloning Stem Cells* **6,** 217–245 (2004).
5. Lund, R. D. *et al. Cloning Stem Cells* **8,** 189–199 (2006).
6. Klimanskaya, I., Chung, Y., Becker, S., Lu, S.-J. & Lanza, R. *Nature* **444,** 481–485 (2006).

ZERO TOLERANCE

A UNIVERSITY CRACKS DOWN ON MISCONDUCT IN CHINA.

BY DAVID CYRANOSKI

Yang Wei has an easy smile and a carefree, even distracted, air — but he takes such a solemn approach to life that his wife sometimes tells him to relax. "I take everything seriously," he says.

The former materials scientist certainly took it seriously when, two years after he became president of Zhejiang University (ZJU) in Hangzhou, China, he faced a case of scientific misconduct that became a turning point for his presidency. In early October 2008, the editor of the *International Journal of Cardiology* discovered that figures in a manuscript by He Haibo, a scientist researching traditional Chinese medicine who had been hired by the ZJU only months before, were suspiciously similar to those in an article that He had published elsewhere. Confronted, He quickly owned up, submitting a 12-page confession to Yang on 26 October.

But the case, which eventually led to the retraction of eight papers, spiralled into an international media catastrophe for the ZJU, one of China's oldest and largest universities, as well as one of the most successful in publishing science. Articles attacked the laxity of a system that gave leadership roles to the likes of Li Lianda, dean of the department of pharmaceutical sciences and He's supervisor, who was largely absent from the lab and unfamiliar with the work, but was last author on some of He's papers. "There was plagiarism, fabrication and falsification. It was a showcase of every kind of problem," says Yang.

Facing one of the best-publicized misconduct cases in China's recent history, Yang knew he had to act quickly. He personally wrote to all the editors of the journals involved. They supplied copies of copyright-transfer forms with all the co-authors' signatures, and Yang sent them to the national calligraphy centre. "Most signatures were identical to He's own," says Yang. "Even I could tell that."

In March 2009, the ZJU fired He, terminated the contract of Wu Limao, a co-author on several of He's papers and the laboratory head in Li's absence, and took away Li's dean-ship and graduate students.

Yang didn't stop there: he launched a campaign to make the ZJU more responsive to misconduct. With an energetic companion named Yuehong (Helen) Zhang cracking down on the university's journals (see 'Policing the plagiarists'), and assistance from a group of university administrators who share his determination and commitment to a zero-tolerance policy for misconduct, Yang hopes to make the ZJU into a role model that can help to clean up China's reputation for rife scientific misconduct. That reputation, exacerbated in the past five years by a string of high-profile cases (see *Nature* **441,** 392–393; 2006), has made observers and journal editors increasingly sceptical of the ability of Chinese research institutions to ensure trustworthy science.

Yang, who now tours the country giving lectures on scientific integrity, has established a reputation as the most evangelical of the reformers. His collaborators are impressed. "He is committed to cleaning things up at Zhejiang," says Mark Frankel, director of the Scientific Freedom, Responsibility and Law Program at the American Association for the Advancement of Science (AAAS) in Washington DC, who is working with Yang to improve

OLIVIER MUNOZ

research ethics. Frankel says that efforts such as Yang's are driving change. "What is most impressive is how open and willing the people with whom I work in China are to admit that a serious problem exists, and that they are committed to turning things around for the younger generation of scientists," he says.

THE SCALE OF THE PROBLEM

There are no comprehensive statistics on the extent of research misconduct in China — and few ministries, agencies or universities make cases public. Surveys and anecdotal evidence, however, reveal a deep-rooted problem, and suggest that students are learning unethical behaviour alongside their science. In an unpublished 2008 survey of 1,641 students at 10 universities, Cao Nanyan, a research-integrity specialist at Tsinghua University in Beijing, found that more than 20% of students admitted to changing data that didn't match their expectations. Some 60% of PhD students said that they sometimes witnessed misconduct, yet only 5% would report it — and Cao found evidence that the students' tolerance of misconduct increased the longer they stayed in education.

"It suggests that the more entangled you are in the system, the less able or motivated you are to pursue good practices," says Daniele Fanelli, a social scientist at the University of Edinburgh, UK, who has studied the frequency of scientific misconduct. Fanelli says that Cao's figures are "clearly worrying, because they would suggest much higher rates of misconduct, and lower rates of reporting, compared to what is usually reported in surveys in Western countries".

Cao and other experts on misconduct point to specific contributing factors. China's research system has developed very rapidly, and universities are scrambling to train the influx of students, scientists and administrators. "As a large, newly developed system of research, China does not have the control of its research programmes that is found in the West," says Nicholas Steneck, who studies research integrity at the University of Michigan in Ann Arbor. Some researchers are simply oblivious to the rules, says Zhong Haining, a neuroscientist who trained at Tsinghua University and is now starting a lab at Oregon Health and Science University in Portland. "The official guideline for scientific misconduct may (or may not) exist, but it's not very well publicized, at least not emphasized so much in training," he says.

Steneck adds that these issues may be rooted in a broader lack of honesty in governance, and that this makes it tough to build a culture of honest research. "It is difficult to have integrity in research if integrity in other aspects of life is questionable," he says.

NATURE.COM
Ten experts give their opinions on how to stop plagiarism:
go.nature.com/jiqv0d

The government, universities and research institutions have introduced a cornucopia of integrity policies over the past decade. But enforcement is problematic, says Mu-ming Poo, director of the Institute of Neuroscience in Shanghai. Most Chinese funding organizations do not, for example, have permanent offices to deal with misconduct in a systematic and transparent fashion, as the Office of Research Integrity at the US Department of Health and Human Services attempts to do. "Very few people in the funding agency or in the scientific community are willing to be the 'bad guy' and enforce the regulations," says Poo. He points to an investigation into what he considered a clear-cut case of misconduct. A researcher was dismissed, but soon found a job elsewhere and continued to get large grants. "There's essentially no punishment for scientific misconduct," says Poo. "The tolerance and appeasement within the community — that really worries me."

QIU A SHEN/PANOS

Yang Wei wants to reform attitudes towards research ethics at Zhejiang University and across the country.

"IT IS DIFFICULT TO HAVE INTEGRITY IN RESEARCH IF INTEGRITY IN OTHER ASPECTS OF LIFE IS QUESTIONABLE."

TAKING ACTION

Yang had encountered misconduct before he became president of the ZJU — as a reviewer of manuscripts in fracture mechanics, and in roles such as director-general of the academic degrees committee of the State Council of China, a post that he held from 2004 to 2006. But when the He case came to light, Yang says he felt the weight of responsibility for the ZJU and its students, and this compelled him to act. "It's not that I want to do this. I have to do this," he says.

In January 2009, on the basis of lessons learned in the He case, Yang created a research-integrity committee and an investigation task force at the ZJU. That March, at a conference to discuss the He situation, the Chinese minister of education called for a zero-tolerance policy towards misconduct — and Yang signed up. He issued a series of codes to guide behaviour on authorship, citations and submission procedures, including one that forbids electronic submissions of papers by a non-corresponding author. This addressed one of the key problems in the He case, in which He and some graduate students had submitted papers from an account under the name of the corresponding author, Wu. Yang replaced most of the ZJU's adjunct deans with full-time executive deans in an attempt to avoid the problems created by Li's absentee leadership. And he introduced new investigative procedures and spelled out disciplinary actions.

All this helped Yang to prepare for a second big case, in mid-2010. The editor-in-chief of a journal published by Springer contacted Yang to say that plagiarism and fabrication in an article from a ZJU researcher were so egregious that Springer was considering blocking all submissions from the university to its 2,000 science,

technology and medicine journals. (Yang declines to name the researcher or editor.) "It put pressure on. We had to convince them that we could handle the case," says Yang.

This time, Yang was ready. He dismissed the main scientist involved, and cut the salary and PhD-student allocation of the corresponding author. "Springer was satisfied," says Yang.

Over the past two years, Yang says, he has dealt just as briskly with another 40 or so misconduct cases at the ZJU. More than 20 researchers have been found guilty of wrong-doing after discussion by the university administration. For the ten cases involving recent graduates, more than half lost their degrees. One sued the ZJU to overturn the ruling of plagiarism. She lost. If work done during your training is fraudulent, "your degree should be taken away", says Yang firmly.

In cases involving faculty members, three had their employment terminated, four faced disciplinary action including a pay cut, and the rest were issued with public or internal warnings. Some have been temporarily forbidden from taking on PhD students.

But laws and punishment go only halfway towards tackling the problem — prevention is also essential. At the ZJU, Yang has established a system for mentoring young faculty members on research ethics, and since 2009 the university has held more than ten seminars and lectures on research integrity, with attendance at some surpassing 1,000. Yang also continues his talks at universities around the country. "We have to train them to be honest. It's not enough to be aware of the ethics code. You need to really understand it," says Gong Ke, president of Nankai University in Tianjin, who, with Yang and the AAAS, is preparing a book of scientific-misconduct cases that can be used to teach research integrity in China and the United States.

SLOW PROGRESS

Yang says it is too early to tell whether his efforts are really paying off. Most misconduct cases are several years old by the time they come to light, so the researchers involved haven't been exposed to the education and enforcement efforts. And there is always the fear that teaching people about misconduct might simply make some determined individuals craftier — as in the case of those who try to outwit plagiarism-detection software with software of their own. "But at least they are more aware that they are doing something wrong," says Yang.

Yang is not cleaning up Chinese science on his own. Other universities have established ethics courses and strengthened their investigation procedures. And China's aggressive 'online police' have been rooting out frauds — the XYS blog run by Fang Shimin has become famous for its tenacity. Posts on the website discuss problems with data, as well as discrepancies between researchers' CVs and their actual achievements. Fang is not yet convinced that the ZJU is rigorously investigating all the misconduct cases that it should. "I don't think he takes his own words seriously," he says of Yang. But Fang notes that he has seen improvements in the 11 years since he started his own "fight" against misconduct. The media are more willing to report misconduct and appeal for reform, he says, "and the government at least admits there are problems".

Real change will take more time and effort. At a 2007 meeting on research integrity with the China Association for Science and Technology, Frankel recalls, one Chinese speaker after another presented data on how bad the situation was and "openly worried about its effects on how science coming out of China would be perceived". The professional guidelines that are surfacing now, he says, are "merely a first step. They have adopted investigative practices and procedures similar to the United States but lack experience and manpower needed to be truly effective. This will take time."

Even the best efforts of administrators such as Yang might not be enough to change deep-rooted behaviours, says Sheila Bonde, an archaeologist and historian at Brown University in Providence, Rhode Island, who is collaborating with the ZJU to create a course in ethics. "Training graduate students about ethics as they enter research laboratories is too little, too late and too specific," she says. "There is a critical need for broader discussion of ethical choices across the spectrum of Chinese academic, political and economic issues, and this has to begin much earlier in students' lives."

Still, the passion for cleaning up China's science is tangible. Frankel says that reformers such as Yang have a different kind of drive from those in the United States, where "the emphasis is on accountability for spending the public's money, its impact on research progress, and public trust. My Chinese colleagues view research misconduct as a stain on their country," says Frankel. "It's almost personal there."

The reason, suggests Steneck, is that the stakes for China are so high. "If other countries lose confidence in the integrity of Chinese science, it is the Chinese who will suffer the most," he says. ■

David Cyranoski *is* Nature's *Asia-Pacific correspondent.*

POLICING THE PLAGIARISTS

A software arms race

In October 2008, Yuehong (Helen) Zhang became the first journal editor in China to introduce CrossCheck, a tool that compares text against published articles to flag up plagiarism. Two years later, she had found that 31% of the 2,233 submissions over that time to her publication, the *Journal of Zhejiang University — Science*, contained unoriginal material. After reporting the number in *Nature* (Y. Zhang *Nature* **467,** 153; 2010), Zhang was harassed on blogs. "Many people criticized me. They say I am unpatriotic. I don't care. I think I'm doing the right thing. I think it could make science stronger in China."

Zhang, who is also vice-president of the Society of China University Journals in Beijing, has been working to build a journal that is run to international standards. Unlike many Chinese journals, hers insists on peer review. In December 2010, she became the first Chinese person to win a grant from the International Committee on Publication Ethics, for a project to analyse types of plagiarism. But the biggest reward, she says, has been the improvement: only 15% of submissions in the first half of 2011 contained unoriginal content.

There are 5,000 science and technology journals in China, but only 200 are in English and can use CrossCheck. Zhang says that some 20 do so. A separate effort is under way to police Chinese-language journals. In 2009, the China National Knowledge Infrastructure (CNKI) in Beijing, which shares information about research from the country, launched a system called the Academic Misconduct Literature Check (AMLC). Sun Xiongyong, director of the CNKI Academic Integrity Research Center, says that the organization was pushed by publishers and universities to develop the AMLC, which now includes about 80 million Chinese articles, conference proceedings and doctoral theses. Its subscribers include some 4,500 publishers and 600 universities.

Sun says that a crucial component of the system is the ability to check Chinese articles against the 30 million or so English articles in the database, and vice versa. "It's the only multi-language check system," notes Sun.

The systems can be cheated. For example, students who are given access to the AMLC to check their theses before submission might find passages that trigger the plagiarism warning and then tweak them until the text scrapes through. "AMLC is abused," says Sun. In response, the CNKI has established a monitoring system that can check, for example, whether the AMLC was being used before submission. But the arms race continues: Sun's latest headache is the use of software available outside China — such as Turnitin — to defeat the check system. D.C.

COMMENT

CONSERVATION Buying shares in whales could help to save them **p.139**

SUSTAINABILITY A vision of more energy-efficient American cities **p.142**

MUSIC Composer of mosquito love songs and firefly symphonies **p.144**

GENOMICS A network for linking DNA and geographic location **p.145**

ILLUSTRATION BY PHIL DISLEY

Deadline 2015

A summit meeting of heads of government is needed to strengthen global ambition on climate change — we should start preparing now, says **Michael Jacobs**.

Climate change has a new target date. The agreement reached last month at the United Nations (UN) conference in Durban, South Africa, specifies that negotiations towards a new, legally binding regime should be concluded by 2015.

At the same time, countries have committed to raising their collective ambition for capping greenhouse-gas emissions, in order to close the gap between their present emissions targets and the pathway likely to achieve the globally agreed goal of limiting global warming to 2 °C above pre-industrial temperatures. No timetable has been set for that process, but because almost all present targets are for 2020, 2015 is the very latest that such a change would have to be agreed.

Bringing these 'legal' and 'ambition' strands of global climate policy together in 2015 will require more than the usual UN conference attended by environment ministers. International decisions of this magnitude can only be made by heads of government. 2015 must be a leaders' summit.

Calls for such a summit will no doubt induce scepticism: the last one, in Copenhagen in 2009, failed spectacularly to yield universal agreement. But Copenhagen was badly undercooked: it became a leaders' meeting only three months before it happened. For a summit in 2015 there is ample time to prepare.

Indeed, 2015 seems particularly opportune for such an event. The year before will have seen the publication of the fifth assessment report of the Intergovernmental Panel on Climate Change (IPCC). The IPCC's fourth assessment report in 2007 catalysed a wave of public concern about climate change, which in turn forced a build-up of diplomatic pressure on the Copenhagen conference; the 2014 report is likely to dramatize the issue once again. 2015 is also when the UN Framework Convention on Climate Change will ▶

conclude its own review of global climate-change efforts, which will inevitably find present mitigation commitments inadequate to meet the 2 °C goal.

Moreover, 2015 is the year in which China will set its next five-year plan, which will determine its emissions targets for 2016–20. Given China's central role both in the future trajectory of global emissions and in international climate politics, its willingness to raise its own emissions-cuts targets for 2020 would do much to encourage higher ambition in the rest of the world. It might even influence the United States: 2015 is the year that a second Obama administration, if it occurs, would have the best chance of finally pushing climate and energy legislation through Congress.

One could argue that to increase ambition for 2020, decisions must be made now. That would of course be desirable, and in the case of the European Union, it could still happen. Europe will this year again consider raising its present emissions-cuts target from 20% by 2020 — which, in the wake of the recession, will be achieved with very little effort — to 30%, which would prop up its now wilting carbon price. But few other countries are likely to tighten their targets so soon after setting them in 2009–10.

CONFIDENCE BUILDING

Waiting until 2015 to strengthen targets offers some advantages. By then, the worst of the present economic storm should have passed, and countries will have had several years of experience in planning and implementing low-carbon policies — which in most cases should show that cutting carbon is not as difficult or costly as once imagined.

This is particularly true for the big emerging economies such as China and India, which have been understandably nervous about making future commitments without the evidence of actual implementation. If by 2015 countries feel more confident of the potential for emissions reductions, they may be more willing to strengthen their targets.

At the same time, the business community will be clamouring for greater investment certainty. Investors will demand clarity from governments on emissions targets beyond the current 2020 timetable — to 2030 at least.

Making progress towards 2015 will require continued efforts, both 'top-down', through international diplomacy, and 'bottom-up', through national policy.

These are not mutually exclusive, as some have claimed. Since the apparent failure of the climate conference in Copenhagen, it has become fashionable in some circles to discount the possibility of progress under the United Nations, and to argue that the focus should now be entirely on domestic policy in the high-emitting countries. But this is to misunderstand the interdependence of these processes. International agreement is limited by the feasibility of domestic policy in the major economies, but international pressure helps to determine national ambition.

This was actually demonstrated best at Copenhagen itself. The hyping of diplomatic and media pressure in the run-up to that event has since been widely decried as contributing to its failure. But it was precisely that pressure that led almost every country in the world to adopt radical climate targets in the months before the conference.

Many of those — among them the European Union, China, India, Brazil, Indonesia, Korea, Mexico, South Africa, Japan, Australia and even the United States — would not have announced new targets at all during that period were it not for the elevated expectations for Copenhagen. And they would certainly not have been as ambitious. In this respect, Copenhagen must go down as one of the most successful failures in the history of multilateral diplomacy.

> *"Copenhagen must go down as one of the most successful failures in the history of multilateral diplomacy."*

These Copenhagen-induced targets are now the bases for bottom-up domestic climate policies. Implementing these policies successfully must be the top priority for the next few years: the experience of achieving (or not achieving) present targets will determine countries' willingness to raise them next time around.

Perhaps surprisingly, success seems most likely in developing countries. Rapid economic growth is generating considerable resources for investment. Building new low-carbon infrastructure — notably in energy, urban transport and waste management — creates more opportunities than retrofitting existing systems. The costs of low-carbon technologies are falling rapidly — solar power is on its way to reaching parity with coal in India, and wind power has already achieved that in China. Brazil has had remarkable success in cutting deforestation.

In developed countries, by contrast, low growth and high debt make it seem hard to give priority to climate policy. But here there is a growing case for using low-carbon investment as a means of economic recovery. Green infrastructure can stimulate short-term economic demand and employment while boosting productivity and innovation over the longer term. The EU 2050 road maps for climate and energy provide a powerful blueprint for such 'green growth' that need not be confined to Europe.

The key to this is financing. Even the most competitive renewable energy sources, such as solar and wind, are more expensive in the short term. This is partly because of high upfront capital expenditure and partly because of the policy risks that investors face. There is plenty of finance available in the world at the moment — pension funds, sovereign wealth funds and other investors are sitting on large sums that are earning very little. Mobilizing these resources for low-carbon infrastructure is one of the great challenges facing governments today. To do so, they need to reduce policy risk by guaranteeing their own low-carbon policies. Over the past three years, governments have put up large sums of public funds to bail out banks and guarantee sovereign debt. Doing the same now for low-carbon investment would boost both economic and climate goals.

MOMENTOUS DECISIONS

It is in this way, through national (and in the case of Europe, multinational) policy, that emissions reduction will occur. But even if present policies are successful, they are insufficient to meet the 2 °C goal. And it is implausible that, through solely domestic political and economic processes, every major country will simultaneously increase its targets by enough to close the gap. Only international pressure will do that. And that is why the focal point of such pressure needs to be a leaders' summit.

The decisions required in 2015 will be momentous: to raise collective global ambition for 2020–30 to meet the 2 °C pathway; to agree a new, legally binding framework; to identify the sources of finance that can meet the goal of providing US$100 billion in climate assistance to the poorest countries by 2020; and to agree a new international collaboration on the development, demonstration and deployment of low-carbon technologies.

These decisions are not within the powers of environment ministers, and they will not happen of their own accord. They require the direct engagement of heads of government, under the full glare of a summit spotlight. And that summit requires the kind of pressure that only the coordinated mobilization of global civil society — including the scientific community, businesses, non-governmental organizations and youth movements — can achieve.

So the first task of such a campaign is to persuade governments to hold a summit meeting in 2015. The UN Conference on Sustainable Development (Rio+20) in Brazil this June would be a good place for that to be agreed. ■

Michael Jacobs *is a visiting professor at the Grantham Research Institute on Climate Change and the Environment, London School of Economics and Political Science, London WC2A 2AE, UK. He was special adviser to former British Prime Minister Gordon Brown.*
e-mail: m.u.jacobs@lse.ac.uk

A. ANKOMAH/GETTY

Introducing tradeable permits for commercial whaling could actually reduce the number of whales that are caught by countries including Japan.

A market approach to saving the whales

The future of the International Whaling Commission is tenuous. A 'whale conservation market' might rescue it, say **Christopher Costello**, **Leah R. Gerber** and **Steven Gaines**.

Despite the International Whaling Commission's (IWC) moratorium on commercial whaling beginning in 1986, the number of whales taken has more than doubled since the early 1990s. Almost 2,000 whales are now harvested each year — roughly 1,000 for 'scientific purposes' (by Japan), 600 by countries that object to the ban (Norway and Iceland), and 350 for subsistence (mainly by Denmark, Russia and the United States)[1]. Many populations of large whales have been severely depleted and continue to be threatened by commercial whaling[2].

The persistence of largely unregulated whaling has sparked heated debate about whether the IWC, long hamstrung by management and ethics issues, should again permit formally sanctioned whaling. In 2010, some anti-whaling nations proposed a compromise: establishing quotas for sanctioned whaling that would still reduce the overall number of whales taken. After much wrangling, the deal fell through — largely because many anti-whaling groups had a fundamental problem with setting quotas at all, because they felt that these would appear to legitimize commercial whaling. Some people blame Japan for the deal's collapse, because the country refused to sign up to a proposed zero quota on whale catches in the Southern Ocean.

We propose an alternative path forward that could break the deadlock: quotas that can be bought and sold, creating a market that would be economically, ecologically and socially viable for whalers and whales alike. Because conservationists could bid for quotas, whalers could profit from whales even without harvesting the animals. A market would therefore open the door to reducing mortality without needing to battle over whether whaling is honourable or shameful.

TRIED AND TESTED

Market approaches to environmental protection have expanded substantially over the past 20 years. When carefully designed, they can be remarkably successful. Emissions trading markets for air pollutants such as sulphur dioxide and nitrogen oxides have reduced emissions more, and at a lower cost, than traditional regulations in the United States. Conservation and wetland mitigation-banking programmes have resulted in more than 200,000 protected acres of habitat and have catalysed investment in conservation by the private sector. And fisheries managed with individual transferable quotas, in which sustainable levels of catch are divided and traded between permit-holding fishermen, in countries such as New Zealand, Iceland and Canada, have simultaneously allowed fisheries to continue and stopped stocks from collapsing.

The concept of auctioning annual whale catch quotas through a 'World Whaling Authority' was suggested in 1982 (ref. 3). It was never implemented, however, perhaps because the concept was ahead of its time (the first such tools — in fisheries, air pollution and biodiversity — were not established until the 1990s), and perhaps because it would have required whalers to purchase a privilege that they were used to receiving for free.

A whale-conservation market would be different. In such a system, 'whale shares' would be allocated in sustainable numbers to all member nations of the IWC, who would have the choice of exercising them, leaving them unused for a year or retiring them in perpetuity. The shares would be tradable in a carefully controlled global market, perhaps with the restriction that members could not trade whale products with non-members. The number of whales hunted would depend on who owned the shares. At one extreme (in which whalers purchase all the shares), whales would be harvested to the agreed sustainable level. At the other extreme (where conservationists purchase all the shares), all whales would be protected from harvest.

There are multiple challenges in getting such a scheme to work, including agreeing on sustainable quotas and on how shares should be allocated. We believe that the IWC is up to the task.

KILLER QUESTION

Various well-established algorithms could be used to identify sustainable harvest levels for whales[5]. For example, the IWC's 'catch limit algorithm', which sets commercial quotas for baleen whales, could be applied more broadly. The US Marine Mammal Protection Act mandates a more conservative approach, known as 'potential biological removal', to establish sustainable take levels for marine mammals in US waters. Although negotiations to set binding catch quotas, such as the deliberations by IWC members in 2010, have not led to consensus, the major reason has not been objections to the proposed quota numbers per se, but a more philosophical objection to the idea of setting quotas at all. Allowing the quotas to be traded, as we advocate, means that they would not necessarily lead to whale deaths or national caps on takes, appeasing both parties.

The initial allocation of whale shares is a potentially challenging issue. In the realm of climate change, the process of divvying up global emissions targets into national responsibilities has proven intractable, with developing nations arguing that stringent targets will inhibit growth, and others arguing that their circumstances, from particularly cold winters to vast forests acting as carbon sinks, justify higher targets. Allocation has been contentious in fisheries too, where it gives a highly valuable asset to the recipient. In practice, in both the emissions and fisheries markets, the initial allocations almost always coincide with historical use. Research into the global markets for air pollutants[5] and fish[6] offers many potential solutions to the whaling allocation problem. One possibility would be to divide the majority of the quota between whaling and non-whaling nations based on historical whaling patterns, leaving the rest for open auction, the proceeds of which would go to whale conservation.

Handing out shares within nations has had a greater history of success, and is likely to be less contentious. Initial allocations within non-whaling countries would probably go to conservation trusts that are focused on protecting particular species. Quota rights could be limited in duration, say for ten years with the possibility of renewal, or in perpetuity for subsistence groups.

Policing such a market would not be simple. But a global vessel registry and carefully monitored trading would help to ensure system integrity. Requiring prices and trades to be made public would bring transparency to an industry that has long been accused of back-room deals and vote trading.

The 'whale share' approach stands a good chance of being acceptable both to anti- and to pro-whaling constituents. If quotas are set properly, transactions would reduce the number of whales harvested, quite possibly to zero, unlike existing protocols, which seem to be increasing the catches. Whalers would be suitably compensated. And because trades are voluntary, the market would have the potential to make all parties better off, and simultaneously improve whale conservation.

A fervent anti-whaler will be quick to argue that you cannot and should not put a price on the life of a whale; a species should be protected irrespective of its economic value. But unless all nations can be convinced or forced to adopt this view, whaling will continue. It is precisely because of the lack of a real price tag in the face of different values that anti-whaling operations have had such limited success.

A generous estimate of the total annual profit from all global commercial whaling activity is US$31 million. Whalers spend millions of dollars to harvest these whales, many of which are then sold on global markets. Recent reports suggest that even some whales hunted for subsistence may end up for sale elsewhere[7], suggesting that whale meat is replaceable as a necessary source of protein for some communities.

Simple calculations based on current market prices, whale sizes and whaling costs, suggest that the per-whale profit for whalers is in the ballpark of $13,000 for a minke whale to $85,000 for a fin whale. Whale prices should therefore be within reach of conservation groups and even some individuals.

A conservative estimate of the amount spent annually by non-profit organizations on anti-whaling (based on the expenditures of Greenpeace USA, Greenpeace International, Sea Shepherd Conservation Society, WWF International and WWF UK) is $25 million. Rather than supporting anti-whaling protests and movements (and their accompanying carbon footprint), this money could be used to purchase whales, arguably with the same or better effect. Sea Shepherd, for example, estimates that its multimillion-dollar 2008 campaign saved about 350 minke whales in Antarctic waters. By our calculations, those whales could have been purchased for less than $4 million.

"If quotas are set properly, transactions would reduce the number of whales harvested."

Properly designed, a whale market could accommodate important concerns such as the by-catch of whales in fisheries or whale ship strikes. It could even be integrated with other market approaches, such as a recent proposal to apply carbon credits to live whales[8]. By placing an appropriate price tag on the life of a whale, a whale conservation market provides an immediate and tangible way to save them. ■

J. WATSON/AFP/GETTY

In a market system, charities could 'buy' whales, rather than spending money campaigning.

Christopher Costello *and* **Steven Gaines** *are at the Bren School of Environmental Science and Management, University of California, Santa Barbara, California 93106, USA.* **Leah R. Gerber** *is in the Ecology, Evolution and Environmental Sciences faculty, School of Life Sciences, Arizona State University, Tempe, Arizona 85281, USA.*
e-mail: costello@bren.ucsb.edu

1. International Whaling Commission *Catch Limits & Catches Taken*; available at http://go.nature.com/rcnfq5
2. Gerber, L. R., DeMaster, D. & Roberts, S. *Am. Sci.* **88,** 316–324 (2000).
3. Clark, C. W. & Lamberson, R. *Mar. Pol.* **6,** 103–120 (1982).
4. Haltuch, M. A., Punt, A. E. & Dorn, M. W. *Fish. Res.* **100,** 42–56 (2009).
5. Goulder, L., Hafstead, M. & Dworsky, M. *J. Environ. Econ. Manage.* **60,** 161–181 (2010).
6. Anderson, T., Arnason, R. & Libecap, G. *Annu. Rev. Res. Econ.* **3,** 159–179 (2011).
7. Black, R. Greenland whale hunt 'commercial' *BBC News* (17 June 2008); available at http://go.nature.com/vspyt5
8. Pershing, A. J. *et al. PLoS ONE* **5,** e12444 (2010).

F. BAHR/OCEANS-IMAGE/IMPACT PHOTOGRAPHY

Scientific studies of humpback and other whales in the 1920s were first to reveal their dwindling numbers.

CONSERVATION

Harpoons and heartstrings

A history of cetacean research highlights its precarious place between whaling and politics, finds **Philip Hoare**.

Historian of science D. Graham Burnett is sly in his provocations. In *The Sounding of the Whale*, he has painstakingly gathered evidence for science's conflicted role in providing rigorous data for the preservation — if not always conservation — of whales. He wonders whether the competing interests in this tale have reduced the science, buried under the cumulative weight of that evidence, to an "elaborate form of rhetoric".

This is a characteristically wry sentiment from Burnett, whose book provides a synoptic survey of a century of human and natural history. The fact that it is about whales seems almost accidental; its subject matter has more to do with the human response to whales than the creatures themselves.

Burnett begins with whaling in the early twentieth century, when only the United Kingdom and Norway remained major players. The heyday of US whaling, extolled in Herman Melville's 1851 novel *Moby-Dick*, had long passed. With northern stocks of sperm and right whales reduced, the whalers' attention had swung south to the Falkland Islands and South Georgia, where fast boats and grenade harpoons enabled the hunting of species such as blue and fin whales.

The scientific response to this multi-million-pound industry (worth even more during the First World War, when whales were a source of glycerine for munitions) was led by zoologist Sidney Harmer, director of the British Museum (Natural History). Harmer was the first 'statesman-scientist' to voice concerns over dwindling whale numbers, some species of which seemed about to become extinct before they had been studied.

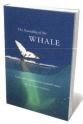

The Sounding of the Whale: Science and Cetaceans in the Twentieth Century
D. GRAHAM BURNETT
University of Chicago Press: 2012. 824 pp. $45, £29

In the early 1920s, Harmer's deft lobbying of the British government produced generous funds for the Discovery research expeditions, using the ship that had taken explorer Robert Scott to the Antarctic. The scientists' aims were to establish breeding patterns, migratory routes and possible populations of blue, fin and humpback whales. They discovered that, far from being as numerous as whalers claimed, many whale populations were diminished as a result of whaling in both their breeding and feeding grounds.

These scientists moulded themselves in the guise of the great polar explorers, bribing the whaling-station butchers with whisky in exchange for whale fetuses and ovaries to study. Meanwhile, on *Discovery*'s sister ship, *William Scoresby*, other scientists were shooting whales with metal darts to track their movements. It was a Faustian pact, Burnett relates, "buying whale science with whale oil".

The 1920s also saw the first stirrings of the public's conscience over whaling (but not its stomach: 42% of margarine made in Britain contained whale oil at the time), with "Save the Whales" appearing in a 1924 headline in the *Liverpool Daily Courier*. Here Burnett shifts his attention across the Atlantic to US naturalist Remington Kellogg, assistant curator of mammals at the Smithsonian Institution in Washington DC. No longer a whaling nation, the United States could take the moral high ground in the move towards whale conservation. Pelagic fleets run by Russia, Japan and the Netherlands were taking up to 50,000 great whales (including blue, fin, sperm and humpback) each year. Kellogg and his colleagues struggled to assess population sizes in the face of such slaughter.

The League of Nations took up the issue as early as 1930, in a committee chaired by the Argentinian academic José León Suárez, who declared that "the riches of the sea, and especially the immense wealth of the Antarctic region, are the patrimony of the whole human race". With the founding of

the International Whaling Commission (IWC) in 1946 — the machinations of which Burnett lays out using newly uncovered archival material — matters became more complicated as cold-war politics kicked in.

By 1965, a crisis point had been reached. Soviet whaling fleets were exceeding their allotted quota, and seriously under-reporting their catch. The IWC, and the uncertainty of cetacean science, sat uneasily in this sorry story of 'cetapolitics'. Radical conservationists suspected some scientists of perpetuating whaling because it supplied them with the subjects for their studies; other researchers found their work being used as a delaying tactic by the whalers, who could continue their culls under the pretence of aiding science. Thus, the obsessive collection of data, Burnett writes, ended up "obscuring the seriousness of the problem" by becoming an end in itself rather than addressing the pressing issue of population depletion.

Enter the contentious physician John Lilly, whose idea of cetaceans as 'alien species' and wild experiments (culminating in dosing dolphins with the drug LSD) have been seen by some as setting the field back by years. But Burnett shows how Lilly's work was the crucial interface between military bioscience and a new countercultural attitude towards cetaceans. That paved the way for the astonishing effect of a 1971 recording of humpback whale songs by researchers Scott McVay and Roger Payne, which sensitized a generation and galvanized the anti-whaling movement.

The same battle for the fate of the whale is still being fought, three decades after the implementation of the IWC's moratorium on commercial whaling. The scope and weight of Burnett's book symbolizes that continuing inertia.

Perhaps that is why, after his ten years of research, Burnett is left with a Melvillean sense of existential defeat even in his groundbreaking conclusion: "The fundamental lesson I have taken from the research and writing of this book amounts to nothing less than a kind of sweeping epistemological humiliation." Yet by questioning the very nature of our scientific interest in the whale, he has set the tone for a new century of discovery — and, one hopes, recovery. ■

Philip Hoare *is the Leverhulme artist-in-residence at the Marine Institute at Plymouth University, and a visiting fellow at the University of Southampton, UK. He is the author of* Leviathan or, The Whale.
e-mail: phoare@soton.ac.uk

ENERGY

Curbing urban greed

An overview of resource-guzzling US cities has lessons for us all, finds **David Orr**.

Austin Troy concludes *The Very Hungry City* by writing: "Good cities are good places to live. But they take work." In the United States, that is both the promise and the problem. With few exceptions, such as Washington DC, US cities grew by happenstance, contrivance and often by connivance. The same is increasingly true of megacities worldwide. Growth without planning — as Troy shows in his trek through conurbations from Los Angeles to Copenhagen to Masdar City in Abu Dhabi — has huge implications for energy use and the natural resources that support it.

Troy, an environmental economist, gives us a sure-handed, cogent treatment of urban challenges, focusing on 'urban energy metabolism' — a city's pattern of energy use determined by its location, culture, history and size. Most US cities need massive energy inputs per capita compared with many of their European, Chinese or developing-world counterparts. The price they pay is a vulnerability to scarcity, rising costs and environmental decay. Troy traces energy use through water consumption, transport, construction, the heating and cooling of homes, and the creation of workable communities, and includes sidebars on energy choices from renewables, natural gas and coal to nuclear power, oil and biofuels.

He describes a drearily familiar pattern that has accelerated since the mid-twentieth century. With little planning or foresight, inner cities are forsaken for suburbs, from which people flee to yet more distant 'exurbs' — a pattern of urban greed that consumes land, infrastructure, people and energy. The United States is littered with extreme examples: on the one hand is Detroit, Michigan, a proud industrial city of around 2 million people in 1950 that is now reduced to a beleaguered population of 700,000 circled by affluent suburbs; on the other is glittering, overbuilt Phoenix, Arizona, facing a future of extreme heat and dessication.

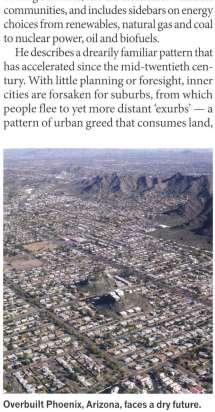

Overbuilt Phoenix, Arizona, faces a dry future.

A. MAGLEAN/GETTY

The Very Hungry City: Urban Energy Efficiency and the Economic Fate of Cities
AUSTIN TROY
Yale University Press: 2012. 384 pp. $28, £25

Elsewhere, notably in the US Sun Belt, 'zombie' urban subdivisions built far from city centres drive up energy and resource use. Even urban success stories elsewhere, such as Stockholm, face the challenges of energy and resources that come with continued growth.

How did we get to this point? Americans have traditionally regarded cities as places where you make money fast and move on. The combination of greed and devil-take-the-hindmost economic theories led to the abandonment of whole sectors of urban economies when people found their mobile capital could earn them a bit more somewhere else. Racism also played a large part. Banks refused to invest in minority-dominated inner cities, resulting in segregated poverty and crime. And then there is the car, an indiscriminate wrecker of urban fabric, air quality and climate stability.

As a result of all this, the United States still does not have a coherent urban policy. That has cost the country dear — not least in terms of the human cost of wars fought over the oil needed to subsidize inefficient urban growth.

Underpriced and oversubsidized fossil fuels made energy cheap, but that era is stumbling to an end. Accelerating climate destabilization, peak oil extraction, water shortages and rapidly growing urban populations are looming global challenges. More than half the people in the world live in cities, and it is here that humanity's future will be decided — albeit in a global economy with a diminishing margin for waste and policy mistakes.

➲ NATURE.COM
Nature's Science and the City special:
go.nature.com/9233vu

Yet we can curb the urban energy appetite. Troy covers a growing list of successes — stories of improved energy and resource efficiency, better technology, collective solutions and foresight. For example, semiconductor manufacturer Intel is pumping three-quarters of the water it uses in its New Mexico facility back into local aquifers. The city of Los Angeles is belatedly resuscitating its once-extensive urban light-rail system. Vermont has deployed a highly successful statewide energy-efficiency programme.

Policy tools such as location-efficient mortgages — which encourage people to buy houses in areas that have abundant public transport — can help to recalibrate economic incentives with energy and climate realities. Congestion-charge schemes such as that in London are reducing traffic in dense urban areas, and time-of-day charges for electricity cut energy use. Even the Empire State Building in New York has been refurbished to lower its energy use by 38%, hinting at potential changes for older buildings everywhere.

Energy-efficient developments are proving to be popular and economically viable. Denver, Colorado, for instance, has revitalized derelict properties in the lower downtown area. Portland in Oregon set up a growth boundary for the city in 1973, deflecting investment downtown with dramatic results. And creative urban designers such as Peter Calthorpe — a pioneer of community models that integrate principles such as environmental sustainability and mixed-use building — continue to push the boundaries. The keys to making smart development the default setting and not an anomaly are creative, long-term public policies and investment strategies that stress energy efficiency and the deployment of renewable energy.

We may even be seeing the start of a global urban renaissance in places such as Masdar City. Once finished, it will house 50,000 people and get all of its energy from sunlight and other renewable sources. But this does not mean abandoning existing urban settlements. Many older European cities are prosperous, attractive and increasingly sustainable because they have preserved a coherent core and developed a robust urban infrastructure for bikes and light-rail systems. In short, cities in many other countries are doing a great deal better than those in the United States.

There are two models of our urban future. One is a dystopian nightmare of crowded, decaying, violent cities. Troy presents the other: a vision of lean, efficient, human-scaled, sustainable cities fed by efficiency, better design and renewable energy. ■

David Orr *is the Paul Sears Distinguished Professor of Environmental Studies at Oberlin College, Oberlin, Ohio 44074, USA. e-mail: dorr@oberlin.edu*

Books in brief

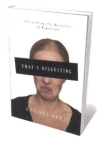

That's Disgusting: Unraveling the Mysteries of Repulsion
Rachel Herz W. W. NORTON *288 pp. $26.95 (2012)*
The emotion of disgust has its evolutionary roots in avoiding poisonous food, notes psychologist Rachel Herz. It has penetrated many areas of human life, as shown by lawyers' and politicians' efforts to incite disgust about their opponents. But that doesn't explain why the things that one culture or individual finds repulsive — such as sea-urchin sushi or horror films — are delightful to another. In her lively tour of vileness, Herz argues that disgust is in the mind of the beholder, and explains how studies of Huntington's disease pinpointed the brain areas involved in this emotion.

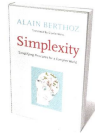

Simplexity: Simplifying Principles for a Complex World
Alain Berthoz (translated by Giselle Weiss) YALE UNIVERSITY PRESS *288 pp. $38 (2012)*
Living things navigate their complex worlds superbly, making tasks such as walking — which thwart the most sophisticated machines — look like child's play. Simplexity, says physiologist Alain Berthoz, allows life to achieve such feats. It involves transforming "a rich combination of simple rules" into a model of reality that aids action and decision-making, yet respects complexity. Berthoz uses examples from perception, locomotion and neuroscience, but argues that simplexity is at work on all levels, from cells to societies and even in love.

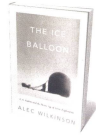

The Ice Balloon: S. A. Andrée and the Heroic Age of Arctic Exploration
Alec Wilkinson ALFRED A. KNOPF *256 pp. $25.95 (2012)*
In 1897, the Swedish explorer Salomon August Andrée sought to use a hydrogen balloon to become the first man to reach the North Pole. Alec Wilkinson's tenth book opens in 1930 with the discovery of Andrée's corpse on a remote Arctic island. It recounts the ill-fated journey through the diaries and photographs of Andrée and his two companions. Wilkinson shows how science and exploration went hand in hand, and how Arctic explorers were celebrities, with the balloonists meriting waxworks in Madame Tussauds museum.

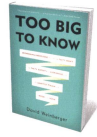

Too Big to Know: Rethinking Knowledge Now That the Facts Aren't the Facts, Experts Are Everywhere, and the Smartest Person in the Room Is the Room
David Weinberger BASIC BOOKS *256 pp. $25.99 (2012)*
Once, says philosopher David Weinberger, experts mastered knowledge and controlled what the rest of us made of it. Now, disciplines such as climate science and molecular biology contain too much data for humans to parse or for theories to explain. Instead, the network is the expert, and anyone can join in. This is creating new forms of communication for science, both educating more people and enabling us to be more emphatically wrong.

Together: The Rituals, Pleasures and Politics of Co-operation
Richard Sennett ALLEN LANE *336 pp. £25 (2012)*
Societies are increasingly complex. Yet we still at mingling with other 'tribes', a trend exacerbated by politicians calling for cultural homogenization. Sociologist Richard Sennett says that the key is learning how to cooperate. In the second of his trio on constructive living, case studies reveal how the upheavals of the early modern era and unethical work practices have broken down cooperation. As a route to remaking it, Sennett advocates 'everyday diplomacy', an essential craft that could heal societal rifts from the inside out.

A. CENNO

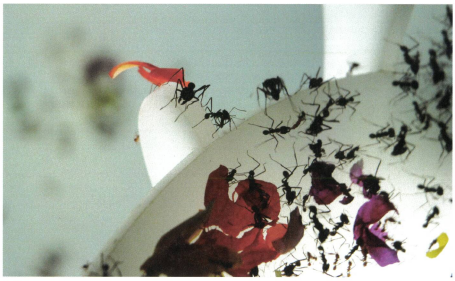

In *The Tragedy of the Commons*, artists Robin Meier and Ali Momeni recorded the sounds of foraging ants.

Q&A Robin Meier

Maestro of the swarm

Swiss acoustic artist Robin Meier manipulates the sounds of insects and birds to create ethereal soundscapes. As his mosquito-inspired musical installation Truce *is aired in the French city of Nantes, he talks about firefly synchrony and setting up feedback loops in nature.*

Why did you choose to work with mosquitoes?

Male mosquitoes serenade potential mates with a 'love song' by vibrating their wings. They synchronize their wingbeats with those of the females to mate in mid-air. I first read about this in a 2006 paper by entomologist Gabriella Gibson and neurobiologist Ian Russell (*Curr. Biol.* **16,** 1311–1316; 2006). The constant *glissandi* — gliding from one pitch to another — and 'tuning in' of mosquito wingbeats reminded me of *dhrupad*, an ancient form of Indian classical music often sung by brothers in unison. My collaborator Ali Momeni and I played male mosquitoes some *dhrupad* and, sure enough, they tuned in. We call the piece *Truce: Strategies for Post-Apocalyptic Computation* because we see it as one way that computation could evolve. In the future, the environment could become an extension of our cognitive processes.

How did you become interested in this area?

I'm a musician but studied cognitive philosophy, and am very interested in artificial intelligence. One of my first installations, with French experimental musician Frédéric Voisin in 2004, involved manipulating artificial neural networks to make music. The idea of collective intelligence is a theme that is common to all my work. Intelligence isn't just an intrinsic property; it lies in the interaction between organisms and environment. It is all around us, and I want to harness it to make music.

How did that lead you to work with ants?

With the help of scientists at the Laboratory of Experimental and Comparative Ethology at the University of Paris 13, I conditioned leafcutter ants to associate quinine — which they dislike — with different smells and foods. We built a star-shaped installation called *The Tragedy of the Commons*, which provides a choice of six foods, each in one arm of the star [see go.nature.com/mvbswm]. Here we manipulate the ants' foraging decisions through smell. Once they associate quinine with a certain food, we take the quinine away and the smell of that food alone will put them off. They communicate this to other ants, partly through sound signals called stridulation, when they rub body parts together. Using strategically placed microphones and loudspeakers, we have created a soundscape of their foraging decisions on two levels: an amplification of the stridulation, and an amplification of the sounds of ants eating at the positions they choose. The sound therefore varies spatially across the installation.

Truce: Strategies for Post-Apocalyptic Computation
ROBIN MEIER AND ALI MOMENI
Musée des Beaux-Arts de Nantes. Until 15 January.

And what about your firefly work?

My virtual firefly project hinges on synchrony. Fireflies synchronize their flashing for courtship purposes. Groups of males of the same species seem to do this so that the passing females can see them better — the flashing pattern is species-specific. When it happens, you see distributed pockets of synchronous flashing appear before they join up and an overall synchrony emerges. Although the behaviour itself is complex, all you need to generate it virtually is a number of identical 'organisms', each equipped with some basic perceptual apparatus and an internal mechanism for adjusting the flashing speed. We have simulated this on a computer.

How do you turn virtual firefly synchrony into music?

You could think of the fireflies as a sort of amateur orchestra and me as their conductor, only I go further by tinkering with their virtual brains. We manipulate their flashing by altering those underlying parameters — the ones that determine how they perceive and generate flashes — and so change the rhythm or even break up the synchrony completely. My collaborator on this project, Canadian artist Yan Breuleux, is interested in the visual effects that this allows him to create. I transform the flashes into sound and create audio effects using standard music-sampling software.

NICK HIGGINS

What other projects are in the pipeline?

I've long been interested in the neurobiology of songbirds. Starlings are fascinating because they're such good learners. They imitate car alarms, mobile phones, anything. This year, we intend to build birdhouses in the Camargue nature park in the south of France, and we hope that starlings will nest in them. We'll install speakers and play melodies to them. Because starlings are migratory, the fledglings could carry the tunes far and wide.

Are you 'playing God' with animals?

No: God is top-down, we're bottom-up. I think of what we do as more like hacking. We may end up manipulating a few starlings, for example, and our manipulation may be transmitted, but probably only in a small way before it fades like a ripple on a pond. It's not just us manipulating the organism. The organism reacts to our manipulation, we react to its reaction, and so on. We set up feedback loops. ■

INTERVIEW BY LAURA SPINNEY

Correspondence

A genomic network to monitor Earth

We propose that a network of genomic observatories should be established to take the planet's 'biological pulse'. We invite participants to assist in the shaping of this network (see genomicobservatories.org).

DNA sequences are becoming core components of Earth-monitoring systems, and data output is soaring from genomics and other observing technologies. But sequence data alone are of limited value without the context of time and location.

Genomic observatories would integrate genomic information with environmental, socio-ecological and other biological data. Sequencing model ecosystems would accelerate ecological understanding.

Despite reduced sequencing costs, genomic studies are still expensive to analyse and interpret, and the expense of field collection of DNA samples remains incompressible. Genomic observatories would consolidate these efforts.

These observatories must be supported by field stations, marine labs, museums, standards organizations, research networks and sequencing centres. They should be established at existing scientifically important sites.

Neil Davies *Gump South Pacific Research Station, University of California Berkeley, Moorea, French Polynesia.*
Dawn Field *Centre for Ecology and Hydrology, Wallingford; and University of Oxford, UK. dfield@ceh.ac.uk*
The Genomic Observatories Network *(see go.nature.com/rcusv3 for a list of co-authors).*

Reduce urban flood vulnerability

Increasing numbers of people live in flood-prone areas worldwide. With continued development, flooding will become more frequent. Acceleration of the hydrological cycle and sea-level rise resulting from climate change could worsen the problem. We must therefore address the social, economic and political factors that force or allow some people to inhabit high-risk areas.

For example, monsoon flooding last year of Thailand's Chao Phraya River caused damage to Bangkok and surrounding areas estimated at US$45 billion. A failure to prepare for this recurrent hazard, which has occurred in each of the past four decades, is partly to blame.

Short-term engineering approaches are not enough. Building higher dykes or cascades of dual-purpose dams may maximize water storage and reduce flood risk, but they can make people complacent and thus more vulnerable to floods.

Long-term development solutions are needed. Vulnerable cities need to be redesigned, for example by supplying transport links to metropolitan areas on higher ground.

Alan D. Ziegler ** National University of Singapore, Singapore. adz@nus.edu.sg*
**On behalf of 4 co-authors (see go.nature.com/vhe7ur).*

India should exploit renewable energy

Japan's Fukushima disaster has spurred public protest in India against government plans to build new nuclear power plants, despite the Atomic Energy Commission's reassurances. We should instead be considering solar energy — a safe and sustainable option.

India receives 5,000 trillion kilowatt-hours of solar energy equivalent every year, more than the total energy the country consumes (see go.nature.com/g89snn). India could also easily exploit wind energy to meet its power needs. Yet only a fraction of this potential is being used.

Nuclear power plants are in decline worldwide. India should follow the lead of countries such as Germany and abandon the nuclear option.

A tsunami in 2004 flooded the Kalpakkam Atomic Reprocessing Plant in Chennai. It was promptly shut down, preventing a disaster. But what if there is another tsunami? Until we abandon nuclear power, that question will continue to haunt India's policy-makers, politicians and scientists.

Govindasamy Agoramoorthy *Gujarat Institute of Desert Ecology, Bhuj, Gujarat, India. agoram@mail.tajen.edu.tw*

Latest MMR 'dispute' is a straw man

Journalists have for years manufactured baseless controversy over the measles, mumps and rubella (MMR) vaccine. The latest example is Eugenie Samuel Reich's report 'Fresh dispute about MMR 'fraud'' (*Nature* **479,** 157–158; 2011). Truly a classic of the genre.

You rely on one David Lewis, a retired environmental microbiologist who claims to refute findings of research fraud against Andrew Wakefield contained in my report in the *British Medical Journal* (*BMJ*) last January and in an accompanying editorial. You say that Lewis analysed a pathologist's bowel-histology grading sheets: these were supplied to him by Wakefield, a now struck-off former surgeon. These data underlay the claims in Wakefield's 1998 study of a "new inflammatory bowel disease" associated with MMR, based on alleged "histological diagnoses" of "non-specific colitis" (*Lancet* **351,** 637–641, 1998; retracted, 2010).

Your report fails to identify where the *BMJ*'s conclusions (that Wakefield's work was "an elaborate fraud" (F. Godlee *et al. Br. Med. J.* **342,** c7452; 2011)) were reliant on bowel histopathology. I invoked patient selection, clinical histories and reporting with regard to autism. These were different aspects of the study, and therefore your suggestion that somebody's opinion on the histology might "complicate" the debate about Wakefield's 'integrity' is an obvious straw-man fallacy.

You also wrongly claim that Lewis had a letter in the *BMJ* "arguing that Wakefield did not commit research fraud". A letter was published, behind a report by me, in which I quoted five gastroenterological specialists who noted that the grading sheets indicate essentially healthy findings, where Wakefield reported disease (B. Deer *Br. Med. J.* **343,** d6823; 2011). In his *BMJ* letter, Lewis then merely remarks: "I do not believe that Dr Wakefield intentionally misinterpreted the grading sheets as evidence of 'non-specific colitis'."

As no such proposition was advanced (histopathology was almost the only area where, until recently, we lacked critical raw data), why did you publish an article founded upon its denial? The denier, moreover, has no qualifications in medicine or pathology; misread the grading sheets, according to their author (see go.nature.com/b9e5gu); and began working with Wakefield at a meeting of vaccine-campaign activists in Montego Bay, Jamaica, which he attended at the organizers' expense.

To breathe life into your shameless straw man, you claim that "no institution has yet ruled on the matter". You note ethics findings of a statutory tribunal of the UK General Medical Council last year, but fail to report that it found Wakefield guilty, against a criminal standard, of four counts of dishonesty over the research. These included his dishonest publication of "a misleading description of the patient population" which was "fundamental to the understanding of the study and the terms under which it was conducted" (see go.nature.com/hg9dvs).

Brian Deer *London, UK. http://briandeer.com*

BoneKEy Reports

NEW TO NPG IN 2012

BoneKEy Reports: a new monthly online journal in the field of bone and mineral metabolism

Part of the *IBMS BoneKEy* platform, ***BoneKEy Reports*** serves the international community of researchers and physicians with in-depth coverage on all scientific and clinical aspects of bone health and disease.

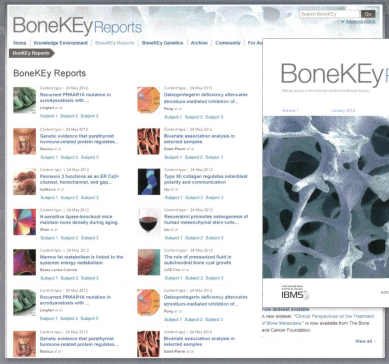

- High-quality reviews
- **BoneKEy Watch** – weekly research highlights of key content across the bone field
- Basic science subjects such as bone cell and molecular biology
- Clinical topics including: osteoporosis diagnosis/management, genetics, and biomechanics
- Multimedia article templates

Access to *BoneKEy Reports* is available through IBMS membership, a personal subscription, or a site license through your institution.

www.nature.com/bonekeyreports

IBMS BoneKEy

nature publishing group npg

RESEARCH

NEW ONLINE

Papers published this week at Nature.com/nature

ARTICLE The genetic basis of a severe acute childhood leukaemia **p.157**

LETTER Gravitational micro-lensing shows that most stars in our Galaxy host planets **p.167**

LETTER Modelling magnesium oxide flow in the extremes of the Earth's mantle **p.177**

PUBLISHED 9 JANUARY 2012

EVOLUTION

Step-by-step route to complexity

In real-lab variation on the 'Jurassic Park' theme, ancestral proteins have been resurrected from synthetic DNA using sequences inferred from current versions of their genes. Gregory Finnigan *et al.* take the idea further with the reconstruction of a multiprotein complex — the transmembrane ring of the proton pump V-ATPase — using a protocol that mimics millions of years of evolution. Starting from a two-component 'ancestral' version of the protein, gene duplication and purely degenerative mutations are sufficient to trigger the observed increased complexity in V-ATPase.

Evolution of increased complexity in a molecular machine
G C Finnigan *et al.*
doi:10.1038/nature10724

A ratchet for protein complexity
W F Doolittle
doi:10.1038/nature10816

STRUCTURAL BIOLOGY

Cardiac ion channel structure

The KCNH family of potassium ion channels is crucial for repolarization of the cardiac action potential and the regulation of neuronal excitability. Brelidze *et al.* report the X-ray crystal structure of the cyclic nucleotide-binding homology domain of the zebrafish *ether-à-go-go*-like potassium channel. They find that the overall structure of the domain is similar to that of the cyclic-nucleotide-binding domain in the related HCN channel. However, the presence of a negatively charged electrostatic region explains the lack of binding and regulation of KCNH channels by cyclic nucleotides. These findings clarify aspects of the regulation of an important group of ion channels and suggest design features for targeted drugs.

Structure of the carboxy-terminal region of a KCNH channel
T I Brelidze *et al.*
doi:10.1038/nature10735

STRUCTURAL BIOLOGY

Structure of HDAC3 bound to co-repressor and inositol tetraphosphate
P J Watson *et al.*
doi:10.1038/nature10728

IMMUNOLOGY

Cysteinyl leukotriene type I receptor desensitization sustains Ca^{2+}-dependent gene expression
S-W Ng *et al.*
doi:10.1038/nature10731

NEUROSCIENCE

X-ray structures of LeuT in substrate-free outward-open and apo inward-open states
H Krishnamurthy & E Gouaux
doi:10.1038/nature10737

BIOCHEMISTRY

Molecular recognition of a single sphingolipid species by a protein's transmembrane domain
F-X Contreras *et al.*
doi:10.1038/nature10742

PUBLISHED 11 JANUARY 2012

ASTRONOMY

Dual 'Suns' are no novelty

Most Sun-like stars in the Milky Way are found in gravitationally bound pairs, or binaries. The discovery of exoplanet Kepler-16 b showed that planets can orbit around a binary. Now, two further 'circumbinary' planets have been found. Kepler-34 b and Kepler-35 b are low-density gas giants with orbits closely aligned with their parent stars. Kepler-34 b orbits two Sun-like stars every 289 days; Kepler-35 b orbits a pair of smaller stars every 131 days. The observed rate of circumbinary planets implies that at least 1% of close binary stars have giant planets in nearly coplanar orbits — equivalent to several million such bodies in the Milky Way.

Transiting circumbinary planets Kepler-34 b and Kepler-35 b
W F Welsh *et al.*
doi:10.1038/nature10768

A new class of planet
J Southworth
doi:10.1038/nature10818

CANCER

SYK is a target in retinoblastoma

Retinoblastoma is a rare and aggressive childhood cancer caused by the loss of the *RB1* gene. Whole-genome sequencing of four retinoblastomas now shows that the retinoblastoma genome is relatively stable, with a mutational rate among the lowest reported in human cancer. However, *RB1* loss is associated with epigenetic deregulation of several cancer pathways. Significantly, the proto-oncogene *SYK* is upregulated in retinoblastoma and is required for tumour cell survival. A small-molecule inhibitor of SYK induced retinoblastoma tumour cell death *in vitro* and *in vivo*.

A novel retinoblastoma therapy from genomic and epigenetic analyses
J Zhang *et al.*
doi:10.1038/nature10733

MEDICAL RESEARCH

Irisin in diabetes and obesity

Exercise is an effective therapy for obesity and type II diabetes. The transcriptional coactivator PGC1-α mediates many of the effects of exercise in skeletal muscle, and this paper shows that its expression in muscle stimulates the expression of the membrane protein FNDC5 in mice. FNDC5 is cleaved and secreted in the circulation as a hormone, dubbed irisin, after Iris, the Greek messenger of the gods. Irisin levels are elevated in the blood of humans and mice after exercise and the hormone is a powerful activator of a thermogenic programme in primary white fat cells, causing a 'browning' of such cells and an increase in in expression of UCP1 and in respiration. These data identify irisin as a possible treatment for metabolic disorders.

A PGC1-α-dependent myokine that drives brown-fat-like development of white fat and thermogenesis
P Boström *et al.*
doi:10.1038/nature10777

CANCER

Clonal evolution in relapsed acute myeloid leukaemia revealed by whole-genome sequencing
L Ding *et al.*
doi:10.1038/nature10738

BIOCHEMISTRY

Complete subunit architecture of the proteasome regulatory particle
G C Lander *et al.*
doi:10.1038/nature10774

BIOMECHANICS

Leaping lizards and dinosaurs

Tightrope walkers use poles to keep their balance. A study reveals that agama lizards use their tails much like balancing poles as they leap through the air — and that some dinosaurs may have done the same. SEE LETTER P.181

R. MCNEILL ALEXANDER

Agama lizards jump quite well, and have a remarkable ability to land safely. On page 181 of this issue, Libby *et al.*[1] describe a study in which they filmed agamas jumping from a horizontal platform to a vertical wall. The lizards used mid-air tail movements to ensure that their trunk was tilted at an appropriate angle for landing as they approached the wall*.

The manoeuvre depends on the principle of conservation of angular momentum, which states that the angular momentum of a system remains constant unless external torques act on it. For example, some tightrope walkers carry a balancing pole. By tilting the pole, the performer can make his or her body lean in the opposite direction to that tilt; any change of angular momentum of the pole must be matched by an opposite change of angular momentum of the body, to keep the overall angular momentum constant (Fig. 1a). Small movements of the pole can therefore keep the performer's centre of mass where it needs to be, vertically above the rope. A long, slender pole works better than a short, thick one because it has a larger moment of inertia for the same weight (the angular momentum of a body is its angular velocity multiplied by its moment of inertia). This simple explanation assumes that any transverse movements of the centre of mass are so small that the moment of body weight about the rope is negligible.

In their study, Libby *et al.* found that if a lizard needed to tilt its trunk 'nose-up' during a jump to ensure that it landed correctly on a vertical surface, it bent its long, slender tail upwards (Fig. 1b). This, for example, gave the tail clockwise momentum and the trunk equal anticlockwise momentum, leaving the total angular momentum unchanged, as the conservation principle requires. To find out whether a lizard could adjust its tail movements to compensate for errors at launch, the authors put a slippery surface on the take-off platform for some of the trials. They observed that if a lizard's foot skidded, the angle of the body at take-off was affected, but the animal corrected the error using an appropriate tail movement.

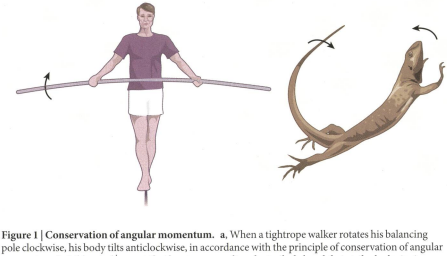

Figure 1 | Conservation of angular momentum. a, When a tightrope walker rotates his balancing pole clockwise, his body tilts anticlockwise, in accordance with the principle of conservation of angular momentum. **b**, Libby *et al.*[1] report that leaping agama lizards similarly bend their tails clockwise in mid-air, to tilt their bodies anticlockwise.

Libby *et al.* used a mathematical model to confirm that their explanation of tail control worked quantitatively. As a further check, they built a delightful toy: a wheeled robot with a tail, which leapt like a ski jumper from a ramp. During each jump, the front wheels of the robot left the ramp first and started falling while the rear ones were still on the ramp, causing the robot to tilt nose-down. But the machine corrected the angle of its body before landing using tail movements that were controlled by feedback from a gyroscope. The robot compensated for its imperfect launch posture brilliantly, even better than did the lizards.

As with all good research, Libby and colleagues' findings raise new questions. The authors considered a lizard's use of its tail as a two-dimensional problem: they considered only the pitch of the body (whether its nose was up or down). But can the tail also be used to adjust the angle of yaw (turning to left or right) and roll? Pitch is paramount when jumping onto a vertical wall, but jumping between irregularly shaped rocks or branches would require adjustments in three dimensions. The same group has previously considered all three dimensions in a paper[2] on body-righting responses of falling geckos, but there are opportunities for more quantitative work along these lines.

Apart from lizards, Libby *et al.* cite several examples of animals that exploit the moment of inertia of an appendage, including lemurs, kangaroo rats and cats. The authors go on to suggest that some dinosaurs may have jumped, using their tails as agamas do to control the angle of the body. Any dinosaurs that did this, however, must have been relatively small. Very large animals cannot jump far because — assuming that their anatomy is geometrically similar to that of their smaller kin — their weights are proportional to the cube of their lengths, whereas the strengths of their bones and muscles are proportional only to cross-sectional areas, and so to their lengths squared. Horses and elands (a very large species of antelope) are, at around 500 kilograms each, among the largest animals that can jump well. Calculations based on measurements of dinosaur bones[3] and on the estimated dimensions of their muscles[4] show that large dinosaurs cannot have been very agile.

So is there any evidence that smaller dinosaurs jumped? The carnivorous dinosaur *Deinonychus* is estimated to have had a mass of about 70 kilograms — in the size range of leopards, and well within the feasible range

*This article and the paper[1] under discussion were published online on 4 January 2012.

for jumping. Some fossil evidence has been interpreted[5] as suggesting that *Deinonychus*, hunting in packs, may have preyed on dinosaurs much larger than themselves. Although this suggestion has been challenged[6], it has been widely assumed that *Deinonychus* leapt onto the backs and flanks of their victims, using enormous claws to get a firm grip[7]. Similarly, lions and other big cats use their sharp claws to grip the hide of their prey, while using their teeth to attack the vulnerable structures of the throat.

There are several drawings on the Internet showing *Deinonychus* in mid-air, jumping onto large prey. Some of the drawings show the animal jumping improbably high, but it is pleasing to see that several of them show the tail swung upwards in the manner used by agamas, as reported by Libby and colleagues[3]. ■

R. McNeill Alexander *is at the Institute of Integrative and Comparative Biology, University of Leeds, Leeds LS6 4BU, UK.*
e-mail: r.m.alexander@leeds.ac.uk

1. Libby, T. *et al. Nature* **481,** 181–184 (2012).
2. Jusufi, A., Goldman, D. I., Revzen, S. & Full, R. J. *Proc. Natl Acad. Sci. USA* **105,** 4215–4219 (2008).
3. Alexander, R. M. *Zool. J. Linn. Soc.* **83,** 1–25 (1985).
4. Hutchinson, J. R. & Garcia, M. *Nature* **415,** 1018–1021 (2002).
5. Maxwell, W. D. & Ostrom, J. H. *J. Vert. Paleontol.* **15,** 707–712 (1995).
6. Roach, B. T. & Brinkman, D. L. *Bull. Peabody Mus. Nat. Hist.* **48,** 103–138 (2007).
7. Manning, P. L., Payne, D., Pennicott, J., Barrett, P. M. & Ennos, R. A. *Biol. Lett.* **2,** 110–112 (2006).

ASTROPHYSICS

Progenitors of type Ia supernovae

A study of the remains of a type Ia supernova whose light swept past Earth about 400 years ago finds no sign of a companion star. The result indicates that the supernova's progenitor was a pair of white dwarfs. SEE LETTER P.164

PILAR RUIZ-LAPUENTE

Type Ia supernovae are not just another class of star explosion. They have a pivotal role in cosmology. Measurements of their brightness as a function of their distance from Earth have provided evidence[1,2] that the Universe is expanding at an accelerating rate. However, from the very beginning of the study of these objects, one major worry has been that we do not know exactly what their progenitors are. On page 164 of this issue, Schaefer and Pagnotta[3] describe an analysis that provides insight into the progenitor of a type Ia supernova.

Type Ia supernovae are thought to originate from a white dwarf and a companion star in relatively close proximity to one another. According to this hypothesis, the white dwarf — a dense remnant star, composed of carbon and oxygen, that marks the final evolutionary stage of the vast majority of stars — accretes matter from its companion until it reaches a limit known as the Chandrasekhar mass (about 1.4 times the mass of the Sun). At this point, explosive thermonuclear reactions take place at its centre and the resulting flames propagate all the way to the star's surface, completely disrupting the star and ejecting its material at high speeds.

But the nature of the white dwarf's companion star is unknown. It could be anything: a main-sequence star, which is powered by the fusion of hydrogen into helium; a star in a more advanced evolutionary stage than the main-sequence phase, such as a subgiant, a red giant or a supergiant; or another white dwarf. In the case of a white-dwarf companion, the two-star system, which is technically known as a double-degenerate progenitor, is destroyed in the runaway accretion process that precedes the explosion. In all other cases, known as single-degenerate progenitors, the companion should survive the explosion. This distinction has led astronomers to search for surviving companion stars at the sites where type Ia supernovae have occurred.

In their study, Schaefer and Pagnotta set out to look for a companion star to the supernova remnant SNR 0509–67.5 (Fig. 1) in the Large Magellanic Cloud, a satellite galaxy of the Milky Way. SNR 0509–67.5 is the aftermath of a type Ia supernova whose light swept past Earth about 400 years ago. To search for the companion, the authors analysed archive images of the supernova remnant taken with the Hubble Space Telescope. On the basis of their image analysis, they discard the possibility of a companion star with a luminosity greater than 3% of that of the Sun. This means that stars ranging from supergiants (which are at least 8,000 times more luminous than the Sun) and red-giant stars (about 100 or more times the Sun's luminosity) down to main-sequence stars of the cool type K (with luminosities roughly 10% of that of the Sun) can all

NASA, ESA, CXC, SAO, HUBBLE HERITAGE TEAM (STSCI/AURA) & J. HUGHES (RUTGERS UNIV.)

Figure 1 | Supernova remnant SNR 0509–67.5. Schaefer and Pagnotta's analysis[3] of SNR 0509–67.5 indicates that the progenitor of this system was a pair of white dwarfs. The remnant, which consists of a rapidly expanding bubble of hot gas, is seen here in an image that combines visible-light observations from the Hubble Space Telescope (pink and surrounding star field) with X-ray data from the Chandra X-ray Observatory (blue and green). The bubble is about 7 parsecs (23 light years) across.

be excluded as possible companions.

Stars that are less luminous than main-sequence K-type stars are not massive enough to feed a white dwarf until it reaches the Chandrasekhar mass, so they, too, are not plausible candidates. What's more, because the impact of the supernova ejecta would not make a putative companion less luminous than it was before the explosion, a companion more luminous than a type-K star, if it existed, should have been seen in the images. Because no companion has been detected by their search, Schaefer and Pagnotta conclude that the progenitor of the system that left behind SNR 0509–67.5 was a pair of white dwarfs that merged and exploded as a supernova. This conclusion seems sound.

As a follow-up to the present study, the authors have examined other type Ia supernova remnants in the Large Magellanic Cloud (personal communication). They can exclude, as progenitors for the supernovae that produced these remnants, systems involving companion stars that are at an evolutionary stage beyond the main-sequence phase. An investigation[4] of the remnant of type Ia supernova SN 1572, which was first observed by Tycho Brahe in 1572, ruled out a red-giant companion. It also ruled out the very luminous objects that are predicted by hydrodynamic simulations[5] of the impact of the supernova ejecta on a companion star, and it pointed to a subgiant star as the companion. A later study[6] confirmed that identification, although the issue is still debated[7].

On the basis of comparisons between hydrodynamic simulations[8] and supernova data, red giants (and supergiants) are unlikely candidates for the companion stars of type Ia supernovae. The impact of the supernova ejecta on a red-giant companion — which could form a system (called symbiotic) in which the white dwarf accretes mass from the stellar wind of its companion, a recurrent nova (a repeatedly bursting star) or some other kind of system with the white dwarf — would produce a bump in the ultraviolet–optical light emission of the supernova at its very early stages. But, so far, this bump has never been seen in any type Ia supernova. Failure to detect this signature would suffice to rule out red-giant companions. However, in a number of type Ia supernovae, such as supernova SN 2006X (ref. 9), the detection of narrow spectral features, associated with sodium moving away from the supernova site at about only 50 kilometres per second, indicates that recurrent novae could be progenitors of at least some type Ia supernovae. This slow-moving sodium would probably come from matter ejected from the system before the white-dwarf explosion. But it could also come from other sources.

A recent theoretical study[10] has shown that the double-degenerate route should produce subluminous type Ia supernovae, which are dimmer than their typical counterparts. And the single-degenerate path has been successful[11] in explaining observations of standard type Ia supernovae. All in all, it seems that neither the single-degenerate nor the double-degenerate hypothesis for type Ia supernovae can currently be rejected. What seems clear from Schaefer and Pagnotta's results[3] is that the double-degenerate progenitor path does work in some cases — for SNR 0509–67.5 at least. ■

Pilar Ruiz-Lapuente *is in the Department of Astronomy and the Institut de Ciències del Cosmos (IEEC–UB), University of Barcelona, Barcelona 08028, Spain.*
e-mail: pilar@am.ub.es

1. Perlmutter, S. *et al. Astrophys. J.* **517**, 565–586 (1999).
2. Riess, A. G. *et al. Astron. J.* **116**, 1009–1038 (1998).
3. Schaefer, B. E. & Pagnotta, A. *Nature* **481,** 164–166 (2012).
4. Ruiz-Lapuente, P. *et al. Nature* **431,** 1069–1072 (2004).
5. Marietta, E., Burrows, A. & Fryxell, B. *Astrophys. J. Suppl.* **128,** 615–650 (2000).
6. González Hernández, J. I. *et al. Astrophys. J.* **691,** 1–15 (2009).
7. Kerzendorf, W. E. *et al. Astrophys. J.* **701,** 1665–1672 (2009).
8. Kasen, D. *Astrophys. J.* **708,** 1025–1031 (2010).
9. Patat, F. *et al. Astron. Astrophys.* **530,** A63 (2011).
10. Pakmor, R., Hachinger, S., Röpke, F. K. & Hillebrandt, W. *Astron. Astrophys.* **528,** A117 (2011).
11. Hachisu, I., Kato, M. & Nomoto, K. *Astrophys. J.* **679,** 1390–1404 (2008).

ANGELMAN SYNDROME

Drugs to awaken a paternal gene

Mutations in the maternal copy of the *UBE3A* gene cause a neurodevelopmental disorder known as Angelman syndrome. Drugs that activate the normally silenced paternal copy of this gene may be of therapeutic value. SEE LETTER P.185

ARTHUR L. BEAUDET

Angelman syndrome is characterized by intellectual disability, epilepsy, impaired coordination and a characteristic joyful demeanour. Most commonly, it is caused by a deletion of five to six megabases of DNA from chromosome 15, although 'loss-of-function' mutations, or other abnormalities, in the maternal copy of the *UBE3A* gene also result in Angelman syndrome. In all cases, the outcome is very low expression levels of the enzyme UBE3A in neurons.

UBE3A is one of a handful of human genes that are subject to genomic imprinting, whereby either the maternal or the paternal copy of a gene is active, with the other copy remaining silent. In the case of *UBE3A*, only the maternal copy is active in neurons. So a child develops Angelman syndrome if they inherit mutant *UBE3A* from their mother. Indeed, in all cases of the disorder, the paternal copy of *UBE3A* is normal. On page 185 of this issue, Huang *et al.*[1] use drug screening to identify compounds that activate the paternal copy of *UBE3A* in a mouse model of Angelman syndrome*.

Inherited neurological disabilities in children are notoriously resistant to treatment. For some disorders that are characterized by overt abnormalities in the brain (for example, holoprosencephaly, lissencephaly and agenesis of the corpus callosum), the prospects for major interventions after birth remain gloomy. But there may be more room for optimism in conditions in which the brain architecture and function seem quite normal in early infancy — for example, as in fragile X syndrome, Rett syndrome, Angelman syndrome and Prader–Willi syndrome. In these cases, one could hope that the disorder might be cured by restoring normal gene expression.

Other than gene therapy, or perhaps gene correction or recovery of function of a mutant protein, a potential strategy for treating some disorders might be activating the alternative copy of a mutant gene or a gene related to it. For instance, activating the expression of fetal haemoglobin has been a long-term goal for the treatment of sickle-cell anaemia and β-thalassaemia. For many disorders involving genomic imprinting, activating the silenced copy of the gene on the related chromosome may correct the defects associated with the mutant gene.

Mice are useful models for testing whether postnatal restoration of gene expression can overcome the pathological features of a disease. A mouse model of Rett syndrome has, for instance, been tested[2] in this way, with favourable results. Angelman syndrome seems another viable candidate disorder for such treatment, because the brain anatomy in this condition seems normal at birth, and some electrophysiological abnormalities can be reversed in cultured cells[3].

*This article and the paper[1] under discussion were published online on 21 December 2011.

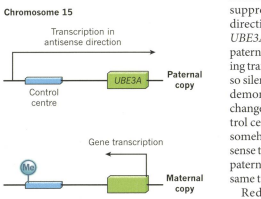

Figure 1 | Differential regulation of maternal and paternal *UBE3A*. Of the two copies of the *UBE3A* gene, only the maternal copy is expressed in neurons, with the paternal copy being silenced by genomic imprinting. Specifically, expression of paternal *UBE3A* is inhibited by transcription in the antisense direction of a long sequence that includes not only this gene but also the control centre that regulates its expression. In the equivalent maternal chromosome, the sequence encoding the control centre is methylated (Me) and so is not expressed. This inhibits transcription in the antisense direction and allows expression of *UBE3A*. Huang *et al.*[1] identify drugs that can activate expression of paternal *UBE3A*. Such drugs could be useful for treating Angelman syndrome, a disorder in which maternal *UBE3A* expression is absent or very low.

To search for compounds that could activate the silent paternal copy of *UBE3A*, Huang *et al.*[1] used a mouse model that had an altered copy of *UBE3A*, isolating cortical neurons from the brains of the animals shortly before birth. The mice were engineered so that their neurons expressed a fluorescently tagged version of UBE3A in response to drugs that activated the paternal copy of its gene. The screen focused on drugs already approved for human use — so that a future clinical trial might be undertaken more readily — and it identified 16 inhibitors of topoisomerase enzymes that were positive in the assay.

The authors focused on topotecan, the most active of the compounds. When they infused the drug into the lateral-ventricle region of the brains of living mice for two weeks, they found that the paternal copy of *UBE3A* was activated throughout the brain. Remarkably, a brief exposure to the drug also gave persistent *UBE3A* activation in spinal-cord neurons for at least 12 weeks after the termination of treatment.

Silencing of the paternal copy of *UBE3A* is probably mediated by an 'antisense' RNA transcript encompassing *UBE3A* on the paternal chromosome (but transcribed in the opposite direction to the gene sequence). Expression of this transcript is regulated by an imprinting control centre on the maternal chromosome (Fig. 1). The sequence functioning as the control centre, together with its promoter region, is methylated on the maternal chromosome, suppressing transcription in the antisense direction, which would silence the maternal *UBE3A*. The equivalent control centre on the paternal chromosome is unmethylated, allowing transcription of the antisense sequence and so silencing the paternal *UBE3A*. Huang *et al.* demonstrate that topotecan causes minimal change in methylation of the imprinting control centre on the paternal chromosome, but somehow still reduces expression of the antisense transcript for *UBE3A*, as well as for other paternally expressed genes that are part of the same transcript.

Reduced expression of paternally expressed genes is a potential drawback. If the 5–6-megabase deletion of chromosome 15 is inherited from the father, the child will develop Prader–Willi syndrome, because the deletion includes the genes involved in this disorder. Therefore, treatment with drugs such as topotecan could convert cells that have a molecular status characteristic of Angelman syndrome into cells with a Prader–Willi molecular status. Clearly, it would be preferable to reduce expression of the *UBE3A* antisense transcript while leaving expression of the other paternally expressed genes intact. But it is reasonable to hope that, after treatment with a topoisomerase inhibitor, cells would express a mixture of maternal and paternal transcripts — a situation that might greatly improve the symptoms of Angelman syndrome without causing notable symptoms of Prader–Willi syndrome. Of course, such treatment could also alter the expression of other genes across the genome, with unknown consequences. On all counts, a sequence-specific knock-down of the antisense transcript seems preferable.

An obvious question is how quickly a topoisomerase inhibitor could be prescribed for patients with Angelman syndrome. It is noteworthy that Huang and colleagues did not demonstrate any reversal of the symptoms in their mouse model, and so this is the next step before proceeding further in this direction.

Other issues concern risk–benefit assessments and regulatory processes. In the United States, topotecan has been injected into the cerebrospinal fluid of adults with neoplastic meningitis[4]. So at least in that country, a physician could theoretically inject topotecan into the cerebrospinal fluid of a patient with Angelman syndrome as a compassionate, off-label use of the drug. However, this seems quite risky in the absence of additional safety and dosage information in children. Presumably, the youngest infants would benefit most from the treatment, because normal brain development could then start as early as possible rather than being delayed by some years.

Systematic trials would require a regulatory process for investigating new drugs, and that would take at least a few months. Because the symptoms of Angelman syndrome are quite severe, and as there are no effective treatments

50 Years Ago

On December 19 Lord Mills announced in the House of Lords that the Government, after considering the question of decimal coinage … thought real advantage would follow from adopting a decimal currency. In view of the widespread use of accounting and other monetary machinery, the transitional cost would be substantial, but could be limited by choice of the size of the new units and careful timing of the change-over.
From *Nature* 13 January 1962

100 Years Ago

Mr. E. C. Snow, in his paper entitled "The Intensity of Natural Selection in Man" … has set himself to answer the following question: Has heavy infantile mortality any selective value or tendency to eliminate the more sickly and to spare the hardier children? Of the data available for the investigation of this problem, the most satisfactory are derived from the annual volumes of Prussian statistics … Thirty rural districts in Prussia were taken, and all the children in them born in the year 1881 were considered. It was ascertained for each district how many of these children died in the first two years of life and how many in the next eight … If the infantile mortality tends to weed out the weaker children, then in those districts in which the mortality among the children born in 1881 was highest in the years 1881 and 1882 it should tend to be lowest in the years 1883–90, since stronger children less likely to succumb to the ailments of childhood would have survived their first two years … We are of the opinion that, on the whole, the author is justified in saying: "Natural selection in the form of a selective death-rate is strongly operative in man in the earlier years of life."
From *Nature* 11 January 1912

for the disorder, the risk–benefit ratio may be viewed as quite favourable for giving topotecan to patients on an experimental basis. The infrastructure for a clinical trial is already in place, because clinical trials (albeit unsuccessful ones) using other drugs for treating Angelman syndrome have already been conducted[5]. Moreover, it is feasible to diagnose almost all cases of Angelman syndrome at birth or even *in utero*[6], so all that is needed is development of a successful treatment. If topoisomerase inhibitors can indeed reverse disabilities associated with Angelman syndrome, Huang and co-workers' data[1] may lead to clinical trials before too long. ■

Arthur L. Beaudet *is in the Department of Molecular and Human Genetics, Baylor College of Medicine, Houston, Texas 77030, USA.*
e-mail: abeaudet@bcm.edu

1. Huang, H.-S. *et al. Nature* **481,** 185–189 (2012).
2. Guy, J., Gan, J., Selfridge, J., Cobb, S. & Bird, A. *Science* **315,** 1143–1147 (2007).
3. Weeber, E. J. *et al. J. Neurosci.* **23,** 2634–2644 (2003).
4. Gammon, D. C. *et al. Am. J. Health-Syst. Pharm.* **63,** 2083–2086 (2006).
5. Bird, L. M. *et al. Am. J. Med. Genet. A* **155,** 2956–2963 (2011).
6. Williams, C. A., Driscoll, D. J. & Dagli, A. I. *Genet. Med.* **12,** 385–395 (2010).

APPLIED PHYSICS

Nanowire electronics comes of age

Three-dimensional nanowire-like electronic devices are gaining ground over conventional planar technology. They may be the means to improve the performance of the electronic circuitry of the future.

TOMÁS PALACIOS

For many years, semiconductor nanowires have offered the prospect of enabling the next generation of electronic devices. But despite this promise, and some exciting preliminary developments[1,2], nanowire electronics has been hampered by technological limitations. It is extremely challenging to develop a nanowire-based fabrication technology for transistors — the building blocks of electronics — that is compatible with the requirements of future microprocessors. Writing in *Applied Physics Letters*, Dhara and co-workers[3] describe a simple technique that may change the way nanowire-based transistors are made.

Transistors are electric switches. In field-effect transistors, which are ubiquitous in modern electronic circuitry, the flow of current between two metal electrodes (source and drain) is controlled by a voltage applied to a third electrode called the gate. The current typically flows through a two-dimensional planar region called the channel. However, the performance of the device could be greatly improved by the use of a three-dimensional nanowire-based channel, in which the gate electrode is wrapped around the channel.

To make their nanowire wrap-gate transistors, Dhara *et al.*[3] first sandwiched a layer of indium arsenide nanowires between two layers of a polymer film that changes its structure when exposed to an electron beam. Next, the authors selectively removed some of the polymer film by exposing it to the electron beam of a lithography system. This procedure made the nanowires — which are horizontal and constitute the transistors' channels — free-standing and ready for subsequent fabrication of the drain and source electrodes as well as the wrap-gate.

The transistor fabrication technology developed by Dhara and colleagues is much simpler than that traditionally pursued for wrap-gate nanowire transistors, which typically involves several lithography steps as well as chemical-etching procedures. In addition, with the authors' technology, the devices have a tenfold larger electron mobility than that previously reported[4] for horizontal wrap-gate nanowire devices.

In spite of the beautiful simplicity of Dhara and co-workers' technique, their work does not solve the second challenge for nanowire electronics, which is how to integrate the billions of closely packed nanowire devices that will potentially be needed in future microprocessors. But the past year has witnessed several breakthroughs that overcome this problem. In combination with the authors' technology[3], these advances may take nanowire research in fresh directions and bring nanowire devices closer to the market.

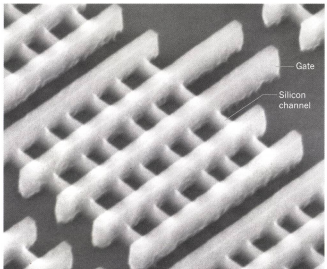

INTEL

Figure 1 | Tri-gate transistors. This scanning electron micrograph shows an intermediate step in the fabrication of Intel's high-performance 22-nm transistors, each of which is made of multiple parallel, nanowire-like silicon channels, or fins. The electrical conductivity of the channels is controlled by a voltage applied to 22-nm-long gate electrodes, which are oriented perpendicularly to the channels. In this technology, only three sides (top, left and right) of the channels are in contact with the gate electrodes. For further improvements in performance, a technology such as the one developed by Dhara *et al.*[3], which consists of gate electrodes that wrap around the entire channel, is necessary.

One way to integrate billions of nanowire transistors on the same chip is to relax the nanowire's geometry: instead of free-standing nanowires, one side of the nanowire can be made to touch the surface of an underlying substrate. Last year, Intel announced[5] that its future microprocessors will incorporate transistors in which nanowire-like channels have three sides in contact with 22-nanometre-long gate electrodes, to improve the control of the transistors' current over that of two-dimensional planar devices. These tri-gate devices (Fig. 1) are effectively rectangular nanowires that have one side attached to the substrate. Although their geometry is slightly different from that of prototypical, free-standing nanowire devices, their operating principle is similar. This innovative geometry allows such nanowire-like devices to be made with a technology that is compatible with that used in the microelectronics industry.

The good news for nanowire-based devices does not stop with tri-gate transistors and Dhara and colleagues' nanowire fabrication technology. The successful integration of transistors based on indium arsenide nanowires — or, more precisely, nanoribbons — on silicon substrates has recently been demonstrated[6]. Nanoribbon structures a few hundreds of nanometres wide have been patterned, and then etched, on an 18-nm-thick layer of indium arsenide semiconductor. Thanks to these structures' outstanding mechanical properties, they were successfully transferred to a silicon wafer, in which transistors with excellent electrical performance were made. This nanoribbon technology allows transistors made from III–V semiconductors, such as indium arsenide, and transistors made from silicon to be integrated on the same chip. Such an advance may help push the performance of electronic systems to higher levels than those achieved using only silicon.

In addition to these improvements, nanowire and nanoribbon structures have been used to enhance the electronic transport properties of semiconductors[7,8]. For example, use of gallium nitride nanoribbons attached to a substrate increases the charge density in the transistors' channels by more than 50% compared with planar devices of the same total channel width, increasing the device's current and improving the overall performance[7].

Silicon–germanium nanowires have also allowed the manufacture[9] of transistors with improved performance. The use of a thin germanium layer to wrap the silicon channel in these devices introduces tensile stress into the channel, increasing hole mobility by 40% (where a hole is a charge carrier produced by the absence of an electron). Both gallium nitride- and silicon–germanium-nanostructured transistors, which integrate thousands of parallel nanoribbons or nanowires on the same device, will soon be used in digital as well as analog circuits to improve wireless communications, low-power electronics and high-performance computing.

In summary, nanowire devices are quickly finding their way into high-performance electronics and commercial products. The current trend of nanowire electronics is based on novel fabrication technologies and three-dimensional nanowire or nanoribbon structures in which only three sides of the structure are exposed, with the bottom one being closely coupled to the substrate. These devices will this year be used in microprocessors and memory devices[5], and should soon improve the performance of mobile phones, radars and other wireless systems. Further improvements will come from technologies such as Dhara and colleagues' technique[5], which enable truly free-standing devices to be made. Electronics is no longer planar. Three-dimensional nanowire structures are here to stay. ■

Tomás Palacios *is at the Massachusetts Institute of Technology, Cambridge, Massachusetts 02139, USA.*
e-mail: tpalacios@mit.edu

1. Li, Y., Qian, F., Xiang, J. & Lieber, C. M. *Mater. Today* **9**, 18–27 (2006).
2. Hashemi, P., Teherani, J. T. & Hoyt, J. L. *Proc. IEEE Int. Electron Device Meet.*, San Francisco (IEEE, 2010).
3. Dhara, S. *et al. Appl. Phys. Lett.* **99**, 173101 (2011).
4. Storm, K. *et al. Nano Lett.* **11**, 1127 (2011).
5. Kuhn, K. J. *Proc. Int. Symp. VLSI Technology, Systems Applications* (IEEE, 2011).
6. Ko, H. *et al. Nature* **468**, 286–289 (2010).
7. Azize, M. & Palacios, T. *Appl. Phys. Lett.* **98**, 042103 (2011).
8. Hashemi, P. *et al. Appl. Phys. Lett.* **96**, 063109 (2010).

EARTH SCIENCE

Limits of the power law

Multi-scale modelling of the deformation of magnesium oxide reveals the need for a re-examination of the way in which laboratory data are used to estimate the strength of Earth's lower mantle. SEE LETTER P.177

ANDREW M. WALKER

For billions of years, convective currents in Earth's solid mantle have cooled and stirred our planet's deep interior and caused tectonic plates to drift centimetres each year. This process is slow, powerful and, given the presumed physical properties of mantle rocks, inevitable[1]. A fundamental controlling factor in mantle convection is how quickly mantle minerals deform. This parameter is expressed as the relationship between the rate of change of strain of the mantle and the stress imposed on it. Despite progress towards laboratory measurement of this relationship under the conditions of temperature (1,800–4,300 kelvin) and pressure (20–130 gigapascals) found in the lower mantle (660–2,900 kilometres beneath Earth's surface), experiments that reach the low strain rate expected in Earth's mantle have not been possible. The use of experimental data for studies of mantle convection thus requires extrapolation.

On page 177 of this issue, Cordier *et al.*[2] test the reliability of this approach by building a multi-scale model of deformation that works at both the low strain rate found in the mantle and the much higher rate used in experiments. The results suggest that the usual power-law extrapolation is not reliable over the wide range of strain rates that must be considered, potentially changing our view of the way in which the deep mantle deforms.

By focusing on magnesium oxide, with its high melting point and simple rock-salt structure, Cordier and colleagues were able to examine deformation processes in one of the best studied and most clearly understood of all mantle minerals. In magnesium oxide, deformation should be accommodated by the movement of dislocations — imperfections in the crystal structure that allow changes in shape to occur in a similar manner to the way that the smooth surface between playing cards permits a deck to be easily sheared. By modelling the details of this process at several length scales, the authors created an impressive predictive model of deformation based only on atomic-scale calculations of the interactions between electrons in a faulted crystal[3].

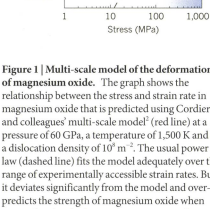

Figure 1 | Multi-scale model of the deformation of magnesium oxide. The graph shows the relationship between the stress and strain rate in magnesium oxide that is predicted using Cordier and colleagues' multi-scale model[2] (red line) at a pressure of 60 GPa, a temperature of 1,500 K and a dislocation density of 10^8 m^{-2}. The usual power law (dashed line) fits the model adequately over the range of experimentally accessible strain rates. But it deviates significantly from the model and over-predicts the strength of magnesium oxide when extrapolated to the low strain rates expected to exist in Earth's lower mantle. Both axes are logarithmic. (Modified from ref. 2.)

Cordier *et al.* then used these atomic-scale calculations to parameterize a larger-scale, semi-continuum model of an isolated, straight dislocation, based on a simple description conceived[4] in 1940 and more recently updated[5] to handle potentially complex dislocation structures. Results from this parameterization in turn informed a model of the motion of a single dislocation that is permitted to curve

under the action of an applied stress and that includes the effect of temperature. Finally, the largest length scale involved modelling the elastic interactions between a network of dislocations, a process that becomes important at high temperature. The overall approach thus avoids the use of experimental data and seeks to predict the relationship between stress and strain rate for a single crystal of magnesium oxide at high temperature and pressure without assuming a particular functional form for that relationship.

Because experiments are time limited, accessible measurable strain rates are typically around 10^{-6} per second (where a sample doubles in length in about two weeks). This is much higher than the maximum strain rate expected in the mantle (perhaps 10^{-12} s^{-1}; at this rate, a sample would take more than 30,000 years to double in length). The usual approach for dealing with such low strain rates is to extrapolate experimental data using a power law — a straight line on a plot of the logarithm of stress against the logarithm of the strain rate. This is assumed to be valid over many orders of magnitude. Cordier and colleagues' multi-scale model[2] makes no such assumption, but, importantly, it reproduces laboratory data at high strain rate over a wide range of temperatures even though these data are not used in the model.

The authors' model can also be used at the low strain rate found in the mantle, allowing the power-law assumption to be tested. Cordier *et al.* found that results from the model differ greatly from the usual power-law extrapolation of laboratory data. The model predicts that magnesium oxide deforming under lower-mantle conditions is significantly weaker than the power-law extrapolation would suggest (Fig. 1).

The most direct implication of this work is that methods used to extrapolate experimental data need to be re-examined. It might be possible to find a way of using experimental data showing the dependence of strain rate on stress, over a wide range of temperatures, to parameterize a non-power-law description of deformation that is consistent with the weakening at very low strain rates predicted by the multi-scale modelling. It remains to be seen whether experiments performed at high enough strain rates for them to be completed in a realistic time-frame can provide enough information to do this.

Magnesium oxide makes up only about 20% of the lower mantle, which is dominated by silicate minerals. A pivotal question is whether Cordier and colleagues' model will be as successful in describing the deformation of these structurally more complex materials as it is for magnesium oxide. One consideration is that the melting point of the silicate phases is lower than that of magnesium oxide, opening up the possibility that deformation is controlled by the motion of isolated atoms rather than by the movement of dislocations[3]. Which of these two processes controls deformation is crucially dependent on the size of individual crystal grains in lower-mantle rocks, a key geophysical parameter that has stubbornly resisted elucidation.

A second concern is that an increasing list of materials, including some that share the structure adopted by silicates in the lower mantle, show dislocations that have a complex, non-planar structure not found in magnesium oxide[2]. If such dislocations occur in silicates in the lower mantle, the authors' multi-scale model would need modification to properly capture the deformation process.

We now have the tools needed to simulate, from first-principles calculations, the deformation of minerals in the lower mantle by the two most likely underlying mechanisms — the motion of atoms[4] and of dislocations[2]. With careful handling of the interaction between adjacent crystals, it may at last be feasible to simulate mantle convection with full feedback between geodynamics, deformation and thermodynamics. These more realistic geodynamical simulations would be expected to exhibit history-dependent deformation and strain weakening. If, for example, regions of strong mantle material surrounded by weak shear zones were to develop, the mantle could resist mixing and allow chemical heterogeneity to be retained over geological time. Such effects complicate our view of mantle convection, but detailed determination of the consequences must await the results of such simulations. ■

Andrew M. Walker *is at the School of Earth Sciences, University of Bristol, Bristol BS8 1RJ, UK.*
e-mail: andrew.walker@bristol.ac.uk

1. Tozer, D. C. *Phil. Trans. R. Soc. Lond. A* **258,** 252–271 (1965).
2. Cordier, P., Amodeo, J. & Carrez, P. *Nature* **481,** 177–180 (2012).
3. Christian, J. W. & Vítek, V. *Rep. Prog. Phys.* **33,** 307–411 (1970).
4. Peierls, R. *Proc. Phys. Soc. Lond.* **52,** 34–37 (1940).
5. Denoual, C. *Phys. Rev. B* **70,** 024106 (2004).
6. Ammann, M. W., Brodholt, J. P., Wookey, J. & Dobson, D. P. *Nature* **465,** 462–465 (2010).
7. Vítek, V. & Paidar, V. in *Dislocations in Solids* Vol. 14 (ed. Hirth, J. P.) 439–514 (Elsevier, 2008).

COGNITION

Your face looks familiar

Paper wasps of the species *Polistes fuscatus* live in strict hierarchical societies in which the ability to identify superiors and subordinates is crucial. Like humans, these insects have a cognitive tool kit for recognizing familiar faces.

LARS CHITTKA & ADRIAN DYER

The ability to recognize individuals can convey significant benefits to social animals. In humans, the capacity to recognize different faces is crucial for making individual behaviour predictable for other members of a group — for keeping track of who is aggressive, bold or wise — and so for knowing everyone's place in a family or society. Moreover, there is strong evidence[1,2] that primate brains contain specialized modules for face processing and recognition. Writing in *Science*, Sheehan and Tibbetts[3] present evidence that an insect, the paper wasp *Polistes fuscatus*, not only recognizes the faces of individuals of the same species, but is a veritable expert at face discrimination.

Individual queens of many social insects, including *Polistes metricus* — a species closely related to *P. fuscatus* — found colonies in the spring, a perilous and challenging enterprise for a single insect. By contrast, several *P. fuscatus* queens typically join forces to build, defend and provide for a new nest. This boosts the chances of the project's success, but, for many of the hopeful foundresses, there is a price to pay: a linear hierarchy is established through a series of one-on-one fights. Consequently, the strongest queen dominates egg-laying, whereas subordinates do more menial tasks. After a duel, individuals recognize their opponents by their distinct facial markings, which helps to avoid the repetition of potentially costly battles.

Sheehan and Tibbetts studied face recognition in *P. fuscatus* and *P. metricus*. They trained the insects to choose one of two arms of a maze, each marked by an image (Fig. 1). If the wasp turned to the 'wrong' image, it experienced an electric shock, whereas choosing the 'correct' arm provided safety. The image pairs consisted of normal wasp faces, manipulated wasp faces, simple geometric patterns or caterpillars — the typical prey of these wasps.

The authors report that the face-learning ability of *P. fuscatus* was greater than that of *P. metricus*. Moreover, *P. fuscatus* wasps learned to recognize wasp faces more quickly and more accurately than they did other image types. Intriguingly, this insect had difficulties recognizing faces that lacked antennae or that

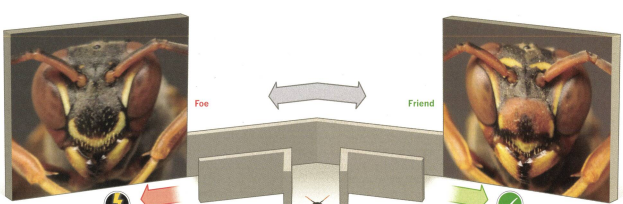

Figure 1 | Face learning by paper wasps. Sheehan and Tibbetts[3] tested the learning abilities of two closely related wasp species, *Polistes fuscatus* and *P. metricus*, in a T-shaped maze. When an individual wasp entered the maze, it had two possible routes to take, which were marked by different images. One (Foe) resulted in punishment with an electric shock, whereas the other (Friend) granted entry to a safety zone. The authors found that *P. fuscatus* is especially skilled at learning to distinguish between correctly configured facial patterns — a unique adaptation to its social environment, in which these wasps use face recognition to establish and enforce dominance hierarchies. In *P. metricus*, individual recognition is not part of social life, and this species failed the face-learning task. (Images, M. J. Sheehan, Univ. Michigan.)

contained scrambled features. This indicates that face learning in *P. fuscatus* is specific to correctly configured faces, and cannot be explained by a general pattern-recognition system.

Because Sheehan and Tibbetts[3] used wasps caught in the wild, it is not clear whether the insects' expertise at face recognition was acquired through evolution, individual experience before capture or an interaction of both. Nonetheless, at the behavioural level, face recognition in *P. fuscatus* shares some features with that in humans. For humans, too, the configuration of facial features is important for reliable recognition[4]. Elemental features such as eyes, nose and mouth are not processed individually but as a whole, and their rearrangement significantly impairs recognition performance.

Several types of processing of facial configurations that have been identified in humans could be explored in wasps. These include detection of a face on the basis of its overall arrangement of features; face processing where certain elemental features are bound together; and sensitivity to second-order relationships, whereby the relative distances between various elemental features enhance recognition[5].

Neurophysiological investigation of specialized brain areas mediating face processing in humans[1,6] and monkeys[2] confirmed the existence of bespoke neural mechanisms for analysing the arrangement of facial features. Studies in other mammals[7] also indicated that the ability to process configural face information involves specialized neural circuitry and extensive experience. However, work in insects on visual processing of compound patterns (including face images) suggests[8] that species without specialized face-processing abilities may also be capable of configural processing. In terms of gross neuroanatomy[9], there are no discernible differences between the visual system of *P. fuscatus* and those of related species that do not use face recognition.

It is therefore likely that neural circuitry similar to that used by insects for prey recognition is co-opted in *P. fuscatus* for face recognition owing to the insect's social lifestyle. This might require only fairly minor adjustments in neural circuitry to embed visual pattern recognition into the appropriate (social) context. Sheehan and Tibbetts's observation[3] that *P. metricus* lacks specialized face recognition lends further support to the view that specialized cognitive capacities can evolve relatively easily in response to pertinent selection pressures.

The finding that a small-brained insect shares the ability to recognize faces with humans and other primates may come as a surprise to adherents of the 'social brain' hypothesis[10] — the idea that group-living and complex social interactions require large brains. However, in asking questions about brain size and cognitive capacity, one must focus on what the computational nature of the task is, and what neural circuitry is actually required to accomplish it. In this view, the specific task that requires a large brain has yet to be discovered.

Analyses of neuronal networks[11] show that reliable face recognition can be achieved with a network of only a few hundred neurons — a circuitry that could be easily accommodated in an insect brain — especially because much of the neural hardware for pattern recognition would also be used for other visual tasks such as recognition of landmarks or prey. Small-brained invertebrates, such as insects, are thus exceptionally useful models for studying how social and cognitive abilities can be mediated by modest neural circuitry[12], and of the evolutionary adjustments necessary to generate such abilities. As for bigger brains, many of their advantages might relate to higher memory storage capacity (equivalent to bigger hard drives rather than better processors), more parallel processing, or more precision and detail in sensory information, but not necessarily to more complex cognitive processes[12]. ■

Lars Chittka *is in the Biological and Experimental Psychology Group, School of Biological and Chemical Sciences, Queen Mary University of London, London E1 4NS, UK.* **Adrian Dyer** *is in the School of Media and Communication, RMIT University, Melbourne, Victoria 3000, Australia.*
e-mails: l.chittka@qmul.ac.uk; adrian.dyer@rmit.edu.au

1. Kanwisher, N. *Nature Neurosci.* **3,** 759–763 (2000).
2. Tsao, D. Y., Freiwald, W. A., Tootell, R. B. H. & Livingstone, M. S. *Science* **311,** 670–674 (2006).
3. Sheehan, M. J. & Tibbetts, E. A. *Science* **334,** 1272–1275 (2011).
4. Collishaw, S. M. & Hole, G. J. *Perception* **29,** 893–909 (2000).
5. Maurer, D., Le Grand, R. & Mondloch, C. J. *Trends Cogn. Sci.* **6,** 255–260 (2002).
6. Lobmaier, J. S., Klaver, P., Loenneker, T., Martin, E. & Mast, F. W. *NeuroReport* **19,** 287–291 (2008).
7. Peirce, J. W., Leigh, A. E. & Kendrick, K. M. *Neuropsychologia* **38,** 475–483 (2000).
8. Avarguès-Weber, A., Portelli, G., Benard, J., Dyer, A. & Giurfa, M. *J. Exp. Biol.* **213,** 593–601 (2010).
9. Gronenberg, W., Ash, L. E. & Tibbetts, E. A. *Brain Behav. Evol.* **71,** 1–14 (2008).
10. Dunbar, R. I. M. *Evol. Anthropol.* **6,** 178–190 (1998).
11. Aitkenhead, M. J. & McDonald, A. J. S. *Eng. Appl. Artif. Intell.* **16,** 167–176 (2003).
12. Chittka, L. & Niven, J. *Curr. Biol.* **19,** R995–R1008 (2009).

nature

12 January 2012 / Vol 481 / Issue No. 7380

Publication policies, author guidelines and information

This is a summary of *Nature*'s guide to authors, publication policies and other author information, available in full on the web via our main author information page at www.nature.com/nature/authors.

Getting published in *Nature*

Please read www.nature.com/nature/authors/get_published before finalizing any original scientific research manuscripts you intend to submit. This section explains *Nature*'s editorial criteria, and how manuscripts are handled by the editors after submission and before acceptance for publication.

Formatting guide

Please read www.nature.com/nature/authors/gta before finalizing and submitting your contribution. This section provides instructions for preparing, formatting and writing all types of contribution published by *Nature*.

Publication policies

This section, at www.nature.com/authors, describes *Nature*'s conditions of publication, including policies on authorship; competing financial interests; duplicate publication; prepublicity and embargoes; materials and data availability; research on animal (including human) subjects; referees; corrections, retractions, errata and addenda to published papers; the complaints procedure and refutations; and copyright/licence to publish. All contributions, for whatever section of the journal, are considered for publication and published on the condition that authors agree to these policies.

Submissions

These sections, at www.nature.com/nature/authors/submissions, contain our online service for presubmission enquiries and submission and tracking of Articles, Letters and Review-type manuscripts. Authors should read the formatting guide before using this service. Authors who cannot submit online can submit by post, but *Nature* strongly recommends the online service. **Authors must not submit by both methods.** Authors experiencing operational difficulty in using the online submission service can send an enquiry to mtshelp@nature.com, with a brief explanation of the problem.

Editorial contacts and author services

This section, at www.nature.com/nature/about/contact, provides the addresses of *Nature*'s editorial offices; names of editorial staff; and contact details for advice, reprints, permissions, press office (press@nature.com), and other author-related contact information, including postal addresses for mailed submissions. Short biographies of editors are also available at www.nature.com/nature/about/editors.

Final submissions

This section, at www.nature.com/nature/authors/submissions/final, applies only if an Article or Letter has been accepted in principle for publication and the author has been asked by the editor for a final version. Authors will need to upload electronic files of the text, production-quality figures and supplementary information (if any) to our database. Authors must include a completed manuscript checklist and all relevant signed forms and declarations as requested by the editor.

Short version of guide to authors

See www.nature.com/nature/authors for full version. Contributors not used to *Nature*'s format are advised to read some papers in published issues before submission, to familiarize themselves with *Nature*'s style. *Nature*'s main formats for original research are Articles and Letters.

ARTICLES are original reports whose conclusions represent a substantial advance in understanding of an important problem and have immediate, far-reaching implications. They do not normally exceed **5 pages** of *Nature* and have **no more than 50** references. (One page of undiluted text is about 1,300 words.)

Articles have a summary for readers outside the discipline, separate from the main text and containing no references, of up to 150 words. The summary does not contain numbers, abbreviations, acronyms or measurements unless essential. It contains a brief account of the background and rationale of the work, followed by a statement of the main conclusions, introduced by the phrase 'Here we show' or its equivalent.

The Article itself typically has about 3,000 words of text, beginning with up to 500 words of referenced text expanding on the background to the work, followed by a concise, focused account of the findings, and ending with one or two short paragraphs of discussion. The text can contain a few short subheadings consisting of about 20 but no more than 40 characters (including spaces) each.

LETTERS are short reports of original research focused on an outstanding finding whose importance means that it will be of interest to scientists in other fields. They do not normally exceed **4 pages** of *Nature*, and have **no more than 30** references. They begin with a **fully referenced paragraph** of not more than 300 words, aimed at readers in other disciplines. This paragraph contains a summary of the background and rationale for the work, followed by a one-sentence statement of the main conclusions introduced by the phrase 'Here we show' or its equivalent, and ending with two to three sentences describing the implications in context.

The main text which follows is typically up to 1,500 words long. This text can, if the author requires, start with a further brief paragraph of introductory material. A description of the research then follows. Any discussion at the end of the text should be as succinct as possible.

FIGURES in both Articles and Letters are as small as possible: Articles typically have 5 or 6 figures, Letters typically have 3 or 4 figures. Legends and/or methods are additional to the main text. Methods Summaries (which are published in print only) are no longer than 300 words; Methods sections (which are published online) can be up to 1,000 words; legends should not exceed 100 words each and start with a one-sentence title for the figure, followed by a brief explanation of the parts and symbols.

See www.nature.com/nature/authors/gta/others.html for details of other types of contribution to *Nature*, including Brief Communications Arising; Reviews and Perspectives (presubmission enquiries to reviewsandinsights@nature.com); and Correspondence (submit to corres@nature.com).

See Authors and Referees @ NPG (www.nature.com/authors) for details of Nature journals' publication policies, author and referee services, author benefits and for links to Nautilus and Peer to Peer blogs.

ARTICLE

doi:10.1038/nature10725

The genetic basis of early T-cell precursor acute lymphoblastic leukaemia

Jinghui Zhang[1]*, Li Ding[2,3]*, Linda Holmfeldt[4]*, Gang Wu[1], Sue L. Heatley[4]†, Debbie Payne-Turner[4], John Easton[5], Xiang Chen[1], Jianmin Wang[6], Michael Rusch[1], Charles Lu[2], Shann-Ching Chen[4], Lei Wei[4], J. Racquel Collins-Underwood[4], Jing Ma[4], Kathryn G. Roberts[4], Stanley B. Pounds[7], Anatoly Ulyanov[3], Jared Becksfort[6], Pankaj Gupta[6], Robert Huether[1,8], Richard W. Kriwacki[8], Matthew Parker[2], Daniel J. McGoldrick[6], David Zhao[6], Daniel Alford[6], Stephen Espy[6], Kiran Chand Bobba[6], Guangchun Song[4], Deqing Pei[7], Cheng Cheng[7], Stefan Roberts[5], Michael I. Barbato[5]†, Dario Campana[9]†, Elaine Coustan-Smith[9]†, Sheila A. Shurtleff[4], Susana C. Raimondi[4], Maria Kleppe[10]†, Jan Cools[10], Kristin A. Shimano[11], Michelle L. Hermiston[11], Sergei Doulatov[12,13], Kolja Eppert[12,13], Elisa Laurenti[12,13], Faiyaz Notta[12,13], John E. Dick[12,13], Giuseppe Basso[14], Stephen P. Hunger[15], Mignon L. Loh[11], Meenakshi Devidas[16], Brent Wood[17], Stuart Winter[18], Kimberley P. Dunsmore[19], Robert S. Fulton[2,3], Lucinda L. Fulton[2,3], Xin Hong[2], Christopher C. Harris[2], David J. Dooling[2,3], Kerri Ochoa[2], Kimberly J. Johnson[2], John C. Obenauer[6], William E. Evans[20], Ching-Hon Pui[9], Clayton W. Naeve[6], Timothy J. Ley[2,21,22], Elaine R. Mardis[2,3,22], Richard K. Wilson[2,3,22], James R. Downing[4] & Charles G. Mullighan[4]

Early T-cell precursor acute lymphoblastic leukaemia (ETP ALL) is an aggressive malignancy of unknown genetic basis. We performed whole-genome sequencing of 12 ETP ALL cases and assessed the frequency of the identified somatic mutations in 94 T-cell acute lymphoblastic leukaemia cases. ETP ALL was characterized by activating mutations in genes regulating cytokine receptor and RAS signalling (67% of cases; *NRAS*, *KRAS*, *FLT3*, *IL7R*, *JAK3*, *JAK1*, *SH2B3* and *BRAF*), inactivating lesions disrupting haematopoietic development (58%; *GATA3*, *ETV6*, *RUNX1*, *IKZF1* and *EP300*) and histone-modifying genes (48%; *EZH2*, *EED*, *SUZ12*, *SETD2* and *EP300*). We also identified new targets of recurrent mutation including *DNM2*, *ECT2L* and *RELN*. The mutational spectrum is similar to myeloid tumours, and moreover, the global transcriptional profile of ETP ALL was similar to that of normal and myeloid leukaemia haematopoietic stem cells. These findings suggest that addition of myeloid-directed therapies might improve the poor outcome of ETP ALL.

Acute lymphoblastic leukaemia (ALL) is the most common malignancy of childhood, with 85% of cases being of B-cell lineage, and 15% T-cell lineage[1]. Recent studies have identified a subtype of T-cell acute lymphoblastic leukaemia (T-ALL) termed "early T-cell precursor" (ETP) ALL that comprises up to 15% of T-ALL, and is associated with a high risk of treatment failure[2]. ETP ALL is characterized by lack of expression of the T-lineage cell surface markers CD1a and CD8, weak or absent expression of CD5, aberrant expression of myeloid and haematopoietic stem cell markers (for example, CD13, CD33, CD34 and CD117), and a gene expression profile reminiscent of the murine early T-cell precursor[3]. The normal ETP, or double negative 1 (DN1) thymocyte retains the ability to differentiate into cells of both the T-cell and myeloid, but not B-cell, lineages[4].

Somatic genetic alterations in ETP ALL

ETP ALL cases commonly exhibit a high burden of DNA copy number alterations, but lack a known unifying genetic alteration[2]. To define the landscape of genetic alterations in ETP ALL, the St Jude Children's Research Hospital–Washington University Pediatric Cancer Genome Project performed whole-genome sequencing (WGS) for matched leukaemic and normal DNA from 12 children with ETP ALL (Supplementary Tables 1–4 and 7, Supplementary Figs 2–4), and determined the frequency of mutations in a separate cohort of 52 ETP and 42 non-ETP childhood T-ALL cases, 82 of which had matched remission DNA. Transcriptome sequencing was performed for two WGS cases, and whole-exome sequencing for three ETP samples in the recurrence cohort (Supplementary Table 8). Putative somatic sequence mutations, and structural alterations identified using CREST[5], were validated by PCR and sequencing. We identified an average of 1,140 sequence mutations (range 235–1,929) and 12 structural variations (range 0–25) per case (Supplementary Tables 9, 11 and 12, Supplementary Fig. 5), including 154 non-silent sequence variants. Fifty-four per cent of the missense mutations were predicted to be deleterious (Supplementary

[1]Department of Computational Biology and Bioinformatics, St Jude Children's Research Hospital, Memphis, Tennessee 38105, USA. [2]The Genome Institute at Washington University, St Louis, Missouri 63108, USA. [3]Department of Genetics, Washington University School of Medicine, St Louis, Missouri 63110, USA. [4]Department of Pathology, St Jude Children's Research Hospital, Memphis, Tennessee 38105, USA. [5]Pediatric Cancer Genome Project Laboratory, St Jude Children's Research Hospital, Memphis, Tennessee 38105, USA. [6]Department of Information Sciences, St Jude Children's Research Hospital, Memphis, Tennessee 38105, USA. [7]Department of Biostatistics, St Jude Children's Research Hospital, Memphis, Tennessee 38105, USA. [8]Department of Structural Biology, St Jude Children's Research Hospital, Memphis, Tennessee 38105, USA. [9]Department of Oncology, St Jude Children's Research Hospital, Memphis, Tennessee 38105, USA. [10]Department of Molecular and Developmental Genetics, Center for Human Genetics, VIB, K.U.Leuven, 3000 Leuven, Belgium. [11]Department of Pediatrics, University of California School of Medicine, San Francisco, California 94143, USA. [12]Department of Stem Cell and Developmental Biology, Campbell Family Cancer Research Institute, Ontario Cancer Institute, University Health Network, Toronto, Ontario M5G 2M9, Canada. [13]Department of Molecular Genetics, University of Toronto, Toronto, Ontario M5S 1A8, Canada. [14]Onco-Hematology Laboratory, Department of Pediatrics, University of Padua, 35122 Padua, Italy. [15]Section of Pediatric Hematology/Oncology/Bone Marrow Transplantation and Center for Cancer and Blood Disorders, University of Colorado Denver School of Medicine, Children's Hospital Colorado, Aurora, Colorado 80045, USA. [16]Department of Biostatistics, University of Florida College of Medicine, Gainesville, Florida 32603, USA. [17]Department of Laboratory Medicine, Seattle Children's Hospital, Seattle, Washington 98105, USA. [18]University of New Mexico, Albuquerque, New Mexico 87131, USA. [19]Pediatric Hematology Oncology, University of Virginia, Charlottesville, Virginia 22903, USA. [20]Department of Pharmaceutical Sciences, St Jude Children's Research Hospital, Memphis, Tennessee 38105, USA. [21]Division of Oncology, Washington University, St Louis, Missouri 63110, USA. [22]Siteman Cancer Center, Washington University, St Louis, Missouri 63110, USA. †Present addresses: Human Immunology, Centre for Cancer Biology, SA Pathology, Adelaide, South Australia, 5000 Australia (S.L.H.); Department of Paediatrics, Yong Loo Lin School of Medicine, National University of Singapore, 119077 Singapore (D.C., E.C.-S.); Human Oncology and Pathogenesis Program, Memorial Sloan Kettering Cancer Center, New York, New York 10065, USA (M.K.); Jefferson Medical College, Thomas Jefferson University, Philadelphia, Pennsylvania 19107, USA (M.L.B.).
*These authors contributed equally to this work.

Table 12), indicating that many of these variants are involved in leukaemogenesis.

Structural rearrangements in ETP ALL

We detected 181 structural variations across the WGS cases (Supplementary Results and Supplementary Tables 13, 14, Fig. 1 and Supplementary Fig. 6). Most abnormalities identified by cytogenetics were also evident on analysis of WGS data (Supplementary Table 15). We also observed evidence of telomere shortening on analysis of WGS data (Supplementary Fig. 7). Three cases (SJTALL001, SJTALL002, SJTALL003) had multiple complex rearrangements with breakpoints suggestive of a single cellular catastrophe ("chromothripsis"[6]; Supplementary Figs 6 and 8). Case SJTALL001 had a nonsense mutation in *MLH3*, a DNA mismatch repair gene with a role in DNA double strand break repair, and SJTALL003 had a missense mutation in *DCLRE1C*, which encodes the non-homologous end-joining factor ARTEMIS, indicating a potential causal relationship between these mutations and the acquisition of structural variations. Case SJTALL007 had a deletion disrupting the mismatch repair gene *MSH5*, and also harboured multiple structural rearrangements.

Remarkably, 51% (77 out of 151) of the validated structural variations had breakpoints in coding genes, including genes with known roles in haematopoiesis and leukaemogenesis, or genes also targeted by sequence mutations (for example, *MLH3*, *SUZ12* and *RUNX1*). A majority of these structural variations (65 out of 77, 84%) are predicted to result in loss-of-function of the involved genes, or occur as part of complex translocations that result in the formation of chimaeric fusion proteins. Ten chimaeric genes encoding six fusion proteins were detected in five cases (Supplementary Table 16) which resulted in the expression of chimaeric in-frame novel fusion genes disrupting haematopoietic regulators, including *ETV6–INO80D* (case SJTALL002), *NUP214–SQSTM1* (SJTALL009) and *NAP1L1–MLLT10* (SJTALL013) (Supplementary Figs 9–12). Case SJTALL012 harboured a *RUNX1–EVX1* rearrangement arising from transpliciing (SJTALL012; Supplementary Figs 10 and 11). No additional cases with these chimaeric fusions were identified upon testing 77 ETP and non-ETP ALL cases with available RNA by PCR with reverse transcription. However, exome sequencing identified *ETV6–INO80D* in case SJTALL208 (Supplementary Fig. 13). *ETV6* encodes a transcription factor required for definitive haematopoiesis that is frequently altered in leukaemia[7–9]. Deletions and mutations of *ETV6* were present in 33% of ETP and 10% of non-ETP T-ALL cases (Supplementary Fig. 14).

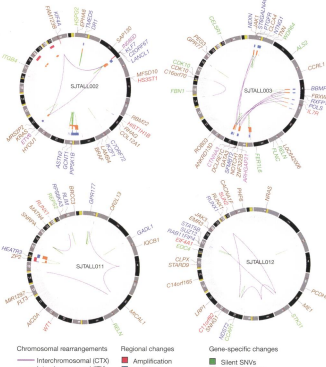

Figure 1 | Circos[43] plots of genetic alterations in four representative ETP ALL cases depicting structural genetic variants, including DNA copy number alterations, intra- and inter-chromosomal translocations, and sequence alterations. Loss-of-heterozygosity, orange; amplification, red; deletion, blue. Sequence mutations in RefSeq genes: silent single-nucleotide variants (SNVs), green; non-silent SNVs, brown; indels, red. Genes at structural variant breakpoints: genes involved in in-frame fusions, pink; others, blue. Circos plots for all cases are provided in Supplementary Fig. 6.

Sequence mutations in ETP ALL

In addition to genes known to be mutated in T-ALL, including *NRAS*[10,11] ($N = 3$ out of 12 WGS cases) *JAK1* (ref. 12, $N = 2$), *NOTCH1* (ref. 13, $N = 1$), *FLT3* (refs. 14–16, $N = 1$), *PHF6* (ref. 17, $N = 3$) and *WT1* (ref. 18, $N = 1$), (Supplementary Fig. 15), we identified multiple novel recurring targets of mutation. These included *DNM2* ($N = 2$), *ECT2L* ($N = 2$), *EP300* ($N = 2$), *GATA3* ($N = 2$), *IL7R* ($N = 2$), *JAK3* ($N = 3$), *RELN* ($N = 2$) and *RUNX1* ($N = 4$) (Table 1, Fig. 2, Supplementary Tables 17 and 18, Supplementary Fig. 15). For the two cases also analysed by transcriptome sequencing (SJTALL002 and SJTALL012), 21 out of 38 mutations were expressed. We did not observe selective expression of mutant alleles, with the exception of those with a concomitant deletion of the wild-type allele (for example, *KRAS* in SJTALL002).

Of 42 genes analysed by Sanger sequencing and single-nucleotide polymorphism microarray analysis in the recurrence cohort, 27 were recurrently mutated (Supplementary Table 19, Figs 2 and 3a, and Supplementary Figs 15 and 16). Of 254 validated non-silent mutations (Supplementary Table 17), 40.7% were indel mutations and 9.4% were nonsense mutations. Eighty-two per cent of missense mutations were predicted to be deleterious, a marked enrichment compared with mutations identified in the WGS samples, consistent with the majority being driver mutations.

We observed a high frequency of mutations known or predicted to result in aberrant cytokine receptor and RAS signalling in ETP ALL. Forty-three out of 64 (67.2%) of ETP cases had mutations in these pathways, compared to 8 out of 42 (19%) non-ETP cases ($P < 0.0001$; Table 1, Fig. 3b and Supplementary Table 20). Known or predicted activating mutations were identified in *BRAF*, *FLT3*, *IGFR1*, *JAK1*, *JAK3*, *KRAS* and *NRAS* (Supplementary Results). Three cases

Table 1 | Recurring mutations in 12 WGS ETP ALL cases

Gene	*N*	Case (mutation)
JAK1	2	003 (S703I), 005 (I631>RGI)
JAK3	3	012 (M511I), 013 (M511I), 007 (A573V)
NRAS	3	008 (Q61H), 012 (Q61P), 001 (Q61H)
KRAS	1	002 (G60D)
BRAF	1	002 (G466E)
FLT3	1	011 (D835Y)
RUNX1	3	006 (R166*), 011 (V124fs), 012 (V164A, translocation involving chrs 8,7,21,10)
PHF6	3	012 (R274Q) 013 (M125I) 005 (exon 8 splice)
ECT2L	2	009 (V588G), 007 (E384D)
EP300	2	006 (L1639P), 007 (exon 10 splice)
GATA3	2	003 (R276Q), 007 (R276Q)
GATA2	1	011 (R307W)
RELN	2	003 (S1719S) 011 (A2114A)
IL7R	2	007 (GCinsL243) 003 (V253>GFSV)
EED	3	001 and 006 (deletion), 004 (S259F)
EZH2	2	009 (deletion) 013 (R684H)
SUZ12	3	006 and 012 (deletion), 013 (S369fs)
HNRNPA1	1	005 (F298fs)
HNRNPR	1	013 (S202fs)

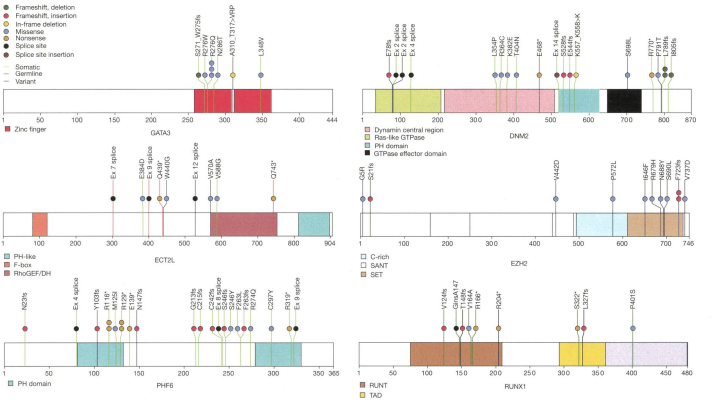

Figure 2 | Recurring sequence mutations in T-ALL. Recurring mutations in ETP-ALL. The figures show mutations for the 12 WGS cases, and the recurrence cohort of 94 cases sequenced by Sanger sequencing. The majority of cases had matched remission DNA to distinguish somatic from inherited variants. Where remission DNA was not available, but variants are known or predicted to be deleterious, mutations are shown as 'variants'. The results of recurrence screening for additional genes sequenced are shown in Supplementary Table 17 and Supplementary Figs 14–17 and 20). The schematics are based on the following NCBI protein reference sequences: GATA3, NP_001002295; DNM2, NP_001005360; ECT2L, NP_001071174; EZH2, NP_001190176; PHF6, NP_001015877.1 and RUNX1, NP_001745.

harboured the JAK3 M511I mutation located adjacent to the pseudokinase domain that has been identified previously in acute myeloid leukaemia and is transforming when introduced into murine haematopoietic progenitor cells[19]. The pseudokinase domain mutation, A573V, has previously been identified in acute megakaryoblastic leukaemia and is transforming[20]. The mutations identified in JAK1 are novel, but are in close proximity to sites of activating mutations previously identified in ALL[12].

Seven cases (five ETP and two non-ETP) harboured mutations in *IL7R* encoding the IL7RA (interleukin 7 receptor alpha) chain (Fig. 4a). IL7RA forms a heterodimer with IL2RG (common gamma chain) for the cytokine IL7, and with CRLF2 (cytokine receptor like factor 2) forms a receptor for TSLP (thymic stromal lymphopoietin). IL7R and CRLF2 signalling are important in early lymphoid maturation[21]. Rearrangement of *CRLF2* is observed in B-progenitor ALL[22,23], and *IL7R* mutations have recently been identified in ALL[24]. All seven cases had an in-frame insertion or substitution at residues I241–V253 of the IL7R transmembrane domain. Consistent with prior data, expression of several of the IL7R mutant alleles in the cytokine-dependent murine haematopoietic Ba/F3 and MOHITO[25] cell lines resulted in transformation to cytokine-independent cell growth (Fig. 4b, c). In six cases the mutations introduced a cysteine into the transmembrane domain that induces dimerization of the receptor in the absence of ligand (Fig. 4d). The mutations also induced Stat5 phosphorylation that was attenuated by Jak inhibition (Fig. 4e). Expression of mutant, but not wild type Il7r in primary murine haematopoietic progenitors resulted in enhanced colony replating *in vitro* (Fig. 4f, g), indicating that the IL7R alterations are transforming events in T-ALL.

We also identified a high frequency of alterations of genes with roles in haematopoietic and lymphoid development, including *RUNX1*, *IKZF1*, *ETV6*, *GATA3* and *EP300* (57.8% of ETP cases versus 16.7% of non-ETP T-ALL cases, $P < 0.0001$). Importantly, several of these genes were targeted by multiple mechanisms of alteration across the cohort: sequence mutation, deletion and chromosomal translocations. Six cases (all ETP) had inactivating mutations of *GATA3*, four of which were biallelic due to either biallelic sequence mutations (SJTALL179, R276Q and A310_T317>VRP; SJTALL010 N286T and S271_W275fs) (Fig. 2) or due to concomitant deletion of the second allele (Supplementary Table 18). *GATA3* encodes GATA binding protein 3, a member of a family of highly conserved zinc-finger transcription factors that is required for the development of early T-lineage progenitors[26], and is mutated in the hypoparathyroidism with sensorineural deafness and renal dysplasia syndrome (HDR)[27]. In four cases the mutation was at R276, a residue also mutated in HDR[27]. The R276P mutation results in impaired DNA-binding affinity of GATA3 for its DNA targets, indicating that the mutations observed in T-ALL are likely to be loss of function. An additional case, SJTALL011, harboured a somatic mutation in *GATA2*, R307W, which is also located in the highly conserved GATA zinc-finger domain and is homologous to the GATA3 R276W mutation.

Twelve cases (ten ETP, and two non-ETP) harboured alterations of *RUNX1*. Two cases had concomitant deletion of the non-mutated allele, and three had *RUNX1* deletions but no sequence mutation. *RUNX1* is required for definitive haematopoiesis[28] and normal T-lymphoid development, and is commonly rearranged and mutated in myeloid and lymphoid malignancies (Supplementary results)[8,29–32].

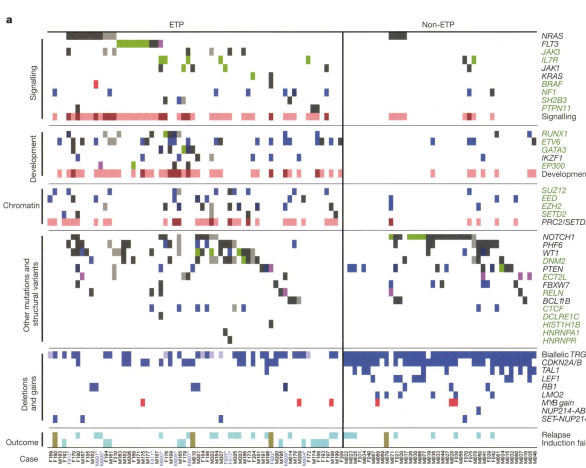

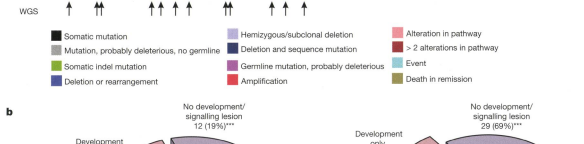
b
No development/ signalling lesion 12 (19%)***
Development only 9 (14%)
Signalling only 15 (23%)
ETP N = 64
No development/ signalling lesion 29 (69%)***
Development only 5 (12%)
Signalling only 6 (14%)
Development and signalling 2 (5%)***
Non-ETP N = 42

Figure 3 | Recurring mutations in T-lineage ALL. a, Data are shown for 106 T-ALL cases, including the 12 cases that were subjected to whole-genome sequencing (arrowed), and 94 recurrence cases (52 ETP ALL and 42 non-ETP T-ALL). Cases have been grouped by ETP status, and cases lacking any mutations are shown to the left, followed by cases with *NRAS* and *FLT3* mutations. Genes identified as novel targets of mutation in T-ALL are labelled in green. Four cases died while in remission and are excluded from outcome analysis. **b**, Frequency of somatic alterations targeting haematopoietic and lymphoid development in ETP and non-ETP T-ALL, showing an increased frequency of lesions in these pathways in ETP ALL. ***$P < 0.0001$.

The mutations observed in T-ALL commonly involve the Runt domain, include frameshift and nonsense mutations, and are predicted to be deleterious. Nine cases (eight ETP) had deletions or sequence mutations of *IKZF1* (IKAROS), which encodes a zinc-finger transcription factor required for the development of all lymphoid lineages that is commonly mutated in high-risk B-progenitor ALL and murine models of T-ALL (Supplementary Fig. 16).

A notable finding was a high frequency of somatic alterations targeting histone modification in ETP ALL. Six WGS cases had alterations in genes encoding components of the polycomb repressor complex 2 (PRC2), including deletions and sequence mutations of *EED*, *EZH2* and *SUZ12* (Table 1, Fig. 2 and Supplementary Fig. 17). EZH2 catalyses trimethylation of histone 3 lysine 27 (H3K27), resulting in transcriptional repression of genes involved in development, stem cell maintenance and differentiation[33]. Twenty-seven (42.2%) of ETP ALL cases harboured a deletion and/or sequence mutation in these genes, compared to five (11.9%) of non-ETP T-ALL cases ($P = 0.001$). Gain-of-function EZH2 Y641 mutations are common

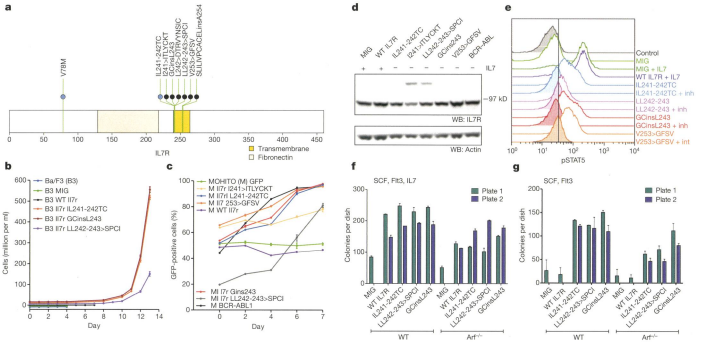

Figure 4 | *IL7R* mutations in T-ALL. **a**, Domain structure of IL7R, showing two hotspots of missense and in-frame insertion-deletion mutations (IL241-242 and VA253-254). The single case with a mutation in the amino-terminal region (V7RM) is accompanied by a transmembrane domain mutation. **b**, **c**, Murine Il7r mutant alleles homologous to the human IL7R mutations were expressed in the murine haematopoietic IL-3-dependent Ba/F3 cell lines (**b**) or the murine IL-7-dependent MOHITO T-ALL cell line (**c**). WT, wild type. Expression of these mutant alleles resulted in transformation to cytokine-independent proliferation. MIG, empty MSCV-IRES-GFP vector. In **b**, growth curves have been offset to permit visualization of each allele. Error bars represent mean ± s.d. for three replicates. In **c**, transformation to cytokine-independent growth is shown as an increasing proportion of Il7r-mutant-expressing cells (or as a positive control, BCR–ABL1), as measured by the percentage of GFP-positive cells. **d**, Western blotting for Il7r in MOHITO cells transduced with wild-type or mutant *Il7r* alleles, showing the formation of Il7r dimers in cells expressing mutant alleles with an unpaired cysteine residue. **e**, Phosphosignalling analysis of MOHITO cells transduced with MIG, WT *Il7r* or four different *Il7r* mutant alleles, showing increased Stat5 phosphorylation in cells stimulated with Il7, or cells expressing mutant *Il7r* alleles in the absence of cytokine. Stat5 phosphorylation was reduced following exposure to Jak inhibitor I (inh) at 3 μM for 1 hour. **f**, **g**, Clonogenic assays of lineage-negative WT or *Arf*$^{-/-}$ murine bone marrow cells expressing mutant *Il7r* alleles show enhanced replating compared to cells transduced with empty vector (**f**), and enhanced replating compared to cells expressing WT Il7r cultured in the absence of Il7 (**g**). Columns show mean of two replicates ± s.e.m.

in lymphoma[34]. In contrast, structural modelling predicts that the mutations observed in T-ALL are likely to disrupt the catalytic SET domain and result in loss of function (Supplementary Results and Supplementary Figs 18 and 19). In addition, case SJTALL192 harboured a focal homozygous deletion of *SETD2* which encodes a H3K36 trimethylase, and an additional four cases had loss-of-function mutations of this gene (Supplementary Fig. 20). Three cases had predicted loss-of-function mutations of the histone acetyltransferase gene *EP300* (p300). Together, 31 ETP and 5 non-ETP cases had mutations affecting epigenetic regulation, which were biallelic or involved multiple genes in 10 cases (9 ETP and 1 non-ETP).

Novel recurrent somatic mutations

Recurring mutations were also identified in genes not previously known to be involved in lymphoid development or oncogenesis. *DNM2* was mutated in 17 cases (13 ETP, 4 non-ETP), including two cases with biallelic mutations (Fig. 2). *DNM2* encodes dynamin 2, a member of a family of large GTPases, and is involved in a wide range of cellular functions, including endocytosis, phagosome formation, intracellular trafficking, interaction with the actin and microtubule networks, and promotion of apoptosis[35]. Inherited *DNM2* mutations result in the degenerative neurologic diseases Charcot–Marie–Tooth peripheral neuropathy and autosomal dominant centronuclear myopathy[35]. As in these diseases, the mutations in T-ALL are located throughout the gene in each functional domain, and include missense, nonsense, splice site and frameshift mutations, and are therefore likely to result in loss of DNM2 function. The role of DNM2 in lymphoid development and tumorigenesis is unknown, although it is expressed in leukaemic lymphoblasts (Supplementary Fig. 22).

Eight cases had missense, nonsense or splice site mutations in *ECT2L* (epithelial cell transforming sequence 2 oncogene gene like). Four cases had non-synonymous mutations in *RELN*, which encodes reelin, a large secreted extracellular matrix protein involved in the regulation of neuronal migration, and which is mutated in the neurodevelopmental disorder autosomal recessive lissencephaly with cerebellar hypoplasia[36]. Notably, several cases had inherited mutations in these two genes that are predicted to be deleterious. Sequence mutations were also found in 12 regulatory RNA genes including one microRNA gene (*MIR1297*).

Mutations in multiple pathways in ETP ALL

Recurring mutations targeting genes regulating haematopoietic development ('type II lesions', for example, *GATA3*, *RUNX1*, *ETV6*, *IKZF1* and *EP300*) and cytokine receptor and RAS signalling ('type I lesions') were present in 7 out of 12 WGS cases, with an additional three cases having either type I or type II lesions, indicating that these events are central to the pathogenesis of ETP ALL. Consistent with this, pathway analysis incorporating both sequence and structural mutations demonstrated enrichment for lesions in these pathways in the 12 WGS cases (Supplementary Table 23). Across the entire cohort, 52 out of 64 (81.3%) ETP cases harboured mutations in these pathways, compared to 13 out of 42 (31%) non-ETP T-ALL cases ($P < 0.0001$; Fig. 3b and Supplementary Table 20). Forty-eight per cent of ETP cases had mutations in the PRC2 genes sequenced, *SETD2* and *EP300*, compared to 12% of non-ETP ALL ($P = 0.0001$). This is

probably an underestimate of the frequency of mutations perturbing chromatin modification, as not all PRC2 and histone-modifying genes have been sequenced. Pathway analysis of the gene expression profile of ETP ALL (Supplementary Table 24 and Supplementary Figs 23–25) demonstrated significant positive enrichment for genes mediating JAK-STAT signalling, and negative enrichment for T-cell receptor signalling genes in ETP ALL. In addition, flow cytometric intracellular phosphosignalling analysis of primary leukaemic cells demonstrated activation of RAS and JAK-STAT signalling pathways in ETP ALL cases (Supplementary Fig. 26). Furthermore, reconstruction of the transcriptional network of ETP ALL using ARACNE[37] identified 30 gene networks ('regulons') with *RUNX1* and *IKZF1* observed to be hub genes of several of these regulons. Thus, alterations of these haematopoietic transcription factors are key determinants of the transcriptional profile of ETP ALL (Supplementary Table 25).

ETP ALL is a stem-cell leukaemia

The immunophenotype and gene expression of ETP ALL are similar to the murine early T-cell precursor[5]. However, detailed comparison of the gene expression profiles of ETP ALL and normal human haematopoietic progenitors has not been performed. Comparison of the gene expression profile of ETP ALL with those of purified normal[38,39] and myeloid leukaemic[40] haematopoietic stem cell and progenitor cell populations demonstrated marked negative enrichment of the gene expression profile of normal human early T-cell precursors (Supplementary Fig. 27). In contrast, the ETP ALL signature showed significant positive enrichment of the gene expression profile of normal human haematopoietic stem cells and granulocyte macrophage precursors. In addition, the ETP ALL signature demonstrated enrichment for a leukaemic stem-cell signature associated with poor outcome in acute myeloid leukaemia[40], and a signature of poor outcome in *IKZF1*-mutated high-risk B-progenitor ALL[41]. Together, these data are compatible with the notion that the genetic alterations identified here result in gross maturational arrest and an aggressive poorly differentiated stem-cell-like leukaemia.

Discussion

Although the striking uniformity of clinical features, immunophenotype and transcriptional profile suggests a common underlying genetic alteration in ETP ALL, we identified a remarkable diversity of novel recurrent genetic alterations. Despite this diversity, the prevalence of mutations in genes involving cytokine receptor and RAS signalling, haematopoietic development and histone modification suggests a common pathogenesis for the establishment of the ETP leukaemic clone. Mutations known or predicted to result in activated cytokine receptor and RAS signalling are present in two-thirds of ETP cases, but only 19% of non-ETP T-ALL. This includes mutations in genes with known roles in leukaemogenesis as well as novel targets of mutation (*JAK3*, *IL7R*, *IFNR1* and *BRAF*). The ability of the identified IL7R activating mutations to induce factor-independent growth of haematopoietic cells coupled with the known function of the other identified signalling mutations strongly supports a direct role for these alterations in leukaemic cell transformation. The high frequency of deleterious mutations in PRC2 genes suggests that disruption of PRC2-mediated gene silencing is a key event in the pathogenesis of this primitive leukaemia, but not more differentiated T-ALL cases. Several of the genes recurrently mutated in ETP are also mutated in inherited disorders (*DNM2*, *EP300*, *GATA3*, *NRAS*, *KRAS*, *PHF6*, *RELN* and *RUNX1*), and the mutational spectrum in several of these genes is similar between the inherited disorders and T-ALL. Thus, sequencing of additional T-ALL cases and other leukaemia genomes will be of great interest to fully examine the relationship of inherited and acquired lesions in leukaemogenesis.

Mutation of genes regulating cytokine receptor and/or RAS signalling pathway and epigenetic modification is a common feature of acute myeloid leukaemia but is less common in T- or B-lineage ALL (Supplementary Table 28)[42]. Although the gene expression profile of ETP ALL is similar to that of the murine ETP, it shows strong similarity to that of normal and myeloid leukaemic haematopoietic stem cells. This indicates that ETP ALL is distinct from non-ETP T-ALL, and in fact represents a neoplasm of a less mature haematopoietic progenitor or stem cell, with arrest at a very early maturational stage that retains the capacity for myeloid differentiation. This observation raises the possibility that treatment regimens used to treat acute myeloid leukaemia, such as those incorporating high dose cytarabine, and/or targeted therapies that inhibit cytokine receptor and JAK signalling may be beneficial in ETP ALL.

METHODS SUMMARY

Whole-genome sequencing was performed for tumour and normal DNA from 12 children with ETP ALL treated at St Jude Children's Research Hospital. All cases fulfilled pathologic and immunophenotypic criteria for ETP ALL[5]. Tumour samples were obtained from diagnostic bone marrow aspirates or peripheral blood, and comprised at least 90% tumour cells. Matched non-tumour samples were obtained from remission blood or bone marrow aspirates with less than 1% leukaemic cells. Recurrence testing was performed using a cohort of 94 childhood T-ALL cases, comprising 52 ETP ALL cases from St Jude, the Children's Oncology Group and the Associazione Italiana Ematologia de Oncologia Pediatrica (AIEOP), and 42 non-ETP T-ALL cases from St Jude. Whole-genome DNA sequencing was performed using a paired-end sequencing strategy as described in detail in the Supplementary Information. The frequency of the identified mutations in the recurrence cohort was determined using PCR amplification and Sanger sequencing and analysis of single-nucleotide polymorphism microarray data. The study was approved by the Institutional Review Boards of St Jude Children's Research Hospital and Washington University.

Received 2 May; accepted 18 November 2011.

1. Pui, C. H., Robison, L. L. & Look, A. T. Acute lymphoblastic leukaemia. *Lancet* **371,** 1030–1043 (2008).
2. Coustan-Smith, E. *et al.* Early T-cell precursor leukaemia: a subtype of very high-risk acute lymphoblastic leukaemia. *Lancet Oncol.* **10,** 147–156 (2009).
3. Rothenberg, E. V., Moore, J. E. & Yui, M. A. Launching the T-cell-lineage developmental programme. *Nature Rev. Immunol.* **8,** 9–21 (2008).
4. Wada, H. *et al.* Adult T-cell progenitors retain myeloid potential. *Nature* **452,** 768–772 (2008).
5. Wang, J. *et al.* CREST maps somatic structural variation in cancer genomes with base-pair resolution. *Nature Methods* **8,** 652–654 (2011).
6. Stephens, P. J. *et al.* Massive genomic rearrangement acquired in a single catastrophic event during cancer development. *Cell* **144,** 27–40 (2011).
7. Bohlander, S. K. ETV6: a versatile player in leukemogenesis. *Semin. Cancer Biol.* **15,** 162–174 (2005).
8. Shurtleff, S. A. *et al.* TEL/AML1 fusion resulting from a cryptic t(12;21) is the most common genetic lesion in pediatric ALL and defines a subgroup of patients with an excellent prognosis. *Leukemia* **9,** 1985–1989 (1995).
9. Barjesteh van Waalwijk van Doorn-Khosrovani, S. *et al.* Somatic heterozygous mutations in ETV6 (TEL) and frequent absence of ETV6 protein in acute myeloid leukemia. *Oncogene* **24,** 4129–4137 (2005).
10. Yokota, S. *et al.* Mutational analysis of the N-ras gene in acute lymphoblastic leukemia: a study of 125 Japanese pediatric cases. *Int. J. Hematol.* **67,** 379–387 (1998).
11. Kawamura, M. *et al.* Alterations of the p53, p21, p16, p15 and Ras genes in childhood T-cell acute lymphoblastic leukemia. *Leuk. Res.* **23,** 115–126 (1999).
12. Flex, E. *et al.* Somatically acquired *JAK1* mutations in adult acute lymphoblastic leukemia. *J. Exp. Med.* **205,** 751–758 (2008).
13. Weng, A. P. *et al.* Activating mutations of *NOTCH1* in human T cell acute lymphoblastic leukemia. *Science* **306,** 269–271 (2004).
14. Paietta, E. *et al.* Activating *FLT3* mutations in CD117/KIT$^+$ T-cell acute lymphoblastic leukemias. *Blood* **104,** 558–560 (2004).
15. Van Vlierberghe, P. *et al.* Activating *FLT3* mutations in CD4$^+$/CD8$^+$ pediatric T-cell acute lymphoblastic leukemias. *Blood* **106,** 4414–4415 (2005).
16. Neumann, M. *et al.* High rate of *FLT3* mutations in adult ETP-ALL. *ASH Annu. Meet. Abstr.* **116,** 1031 (2010).
17. Van Vlierberghe, P. *et al. PHF6* mutations in T-cell acute lymphoblastic leukemia. *Nature Genet.* **42,** 338–342 (2010).
18. Tosello, V. *et al. WT1* mutations in T-ALL. *Blood* **114,** 1038–1045 (2009).
19. Yamashita, Y. *et al.* Array-based genomic resequencing of human leukemia. *Oncogene* **29,** 3723–3731 (2010).
20. Malinge, S. *et al.* Activating mutations in human acute megakaryoblastic leukemia. *Blood* **112,** 4220–4226 (2008).
21. Ziegler, S. F. & Liu, Y. J. Thymic stromal lymphopoietin in normal and pathogenic T cell development and function. *Nature Immunol.* **7,** 709–714 (2006).
22. Russell, L. J. *et al.* Deregulated expression of cytokine receptor gene, *CRLF2*, is involved in lymphoid transformation in B-cell precursor acute lymphoblastic leukemia. *Blood* **114,** 2688–2698 (2009).

23. Mullighan, C. G. *et al.* Rearrangement of *CRLF2* in B-progenitor- and Down syndrome-associated acute lymphoblastic leukemia. *Nature Genet.* **41,** 1243–1246 (2009).
24. Shochat, C. *et al.* Gain-of-function mutations in *interleukin-7 receptor-α (IL7R)* in childhood acute lymphoblastic leukemias. *J. Exp. Med.* **208,** 901–908 (2011).
25. Kleppe, M., Mentens, N., Tousseyn, T., Wlodarska, I. & Cools, J. MOHITO, a novel mouse cytokine-dependent T-cell line, enables studies of oncogenic signaling in the T-cell context. *Haematologica* **96,** 779–783 (2011).
26. Hosoya, T., Maillard, I. & Engel, J. D. From the cradle to the grave: activities of GATA-3 throughout T-cell development and differentiation. *Immunol. Rev.* **238,** 110–125 (2010).
27. Zahirieh, A. *et al.* Functional analysis of a novel *GATA3* mutation in a family with the hypoparathyroidism, deafness, and renal dysplasia syndrome. *J. Clin. Endocrinol. Metab.* **90,** 2445–2450 (2005).
28. Okuda, T., van Deursen, J., Hiebert, S. W., Grosveld, G. & Downing, J. R. AML1, the target of multiple chromosomal translocations in human leukemia, is essential for normal fetal liver hematopoiesis. *Cell* **84,** 321–330 (1996).
29. Downing, J. R. *et al.* An *AML1/ETO* fusion transcript is consistently detected by RNA-based polymerase chain reaction in acute myelogenous leukemia containing the (8;21)(q22;q22) translocation. *Blood* **81,** 2860–2865 (1993).
30. Dicker, F. *et al.* Mutation analysis for *RUNX1*, *MLL-PTD*, *FLT3-ITD*, *NPM1* and *NRAS* in 269 patients with MDS or secondary AML. *Leukemia* **24,** 1528–1532 (2010).
31. Gaidzik, V. I. *et al. RUNX1* mutations in acute myeloid leukemia: results from a comprehensive genetic and clinical analysis from the AML study group. *J. Clin. Oncol.* **29,** 1364–1372 (2011).
32. Gelsi-Boyer, V. *et al.* Genome profiling of chronic myelomonocytic leukemia: frequent alterations of *RAS* and *RUNX1* genes. *BMC Cancer* **8,** 299 (2008).
33. Margueron, R. & Reinberg, D. The Polycomb complex PRC2 and its mark in life. *Nature* **469,** 343–349 (2011).
34. Morin, R. D. *et al.* Somatic mutations altering *EZH2* (Tyr641) in follicular and diffuse large B-cell lymphomas of germinal-center origin. *Nature Genet.* **42,** 181–185 (2010).
35. Durieux, A. C., Prudhon, B., Guicheney, P. & Bitoun, M. Dynamin 2 and human diseases. *J. Mol. Med.* **88,** 339–350 (2010).
36. Hong, S. E. *et al.* Autosomal recessive lissencephaly with cerebellar hypoplasia is associated with human *RELN* mutations. *Nature Genet.* **26,** 93–96 (2000).
37. Margolin, A. A. *et al.* Reverse engineering cellular networks. *Nature Protocols* **1,** 662–671 (2006).
38. Novershtern, N. *et al.* Densely interconnected transcriptional circuits control cell states in human hematopoiesis. *Cell* **144,** 296–309 (2011).
39. Notta, F. *et al.* Isolation of single human hematopoietic stem cells capable of long-term multilineage engraftment. *Science* **333,** 218–221 (2011).
40. Eppert, K. *et al.* Stem cell gene expression programs influence clinical outcome in human leukemia. *Nature Med.* **17,** 1086–1093 (2011).
41. Mullighan, C. G. *et al.* Deletion of *IKZF1* and prognosis in acute lymphoblastic leukemia. *N. Engl. J. Med.* **360,** 470–480 (2009).
42. Gilliland, D. G. Molecular genetics of human leukemias: new insights into therapy. *Semin. Hematol.* **39,** 6–11 (2002).
43. Krzywinski, M. *et al.* Circos: an information aesthetic for comparative genomics. *Genome Res.* **19,** 1639–1645 (2009).

Supplementary Information is linked to the online version of the paper at www.nature.com/nature.

Acknowledgements We thank the many members of St Jude Children's Research Hospital and The Genome Institute and Siteman Cancer Center at Washington University in St Louis for support. We thank H. Mulder for project sample management, M. Stine for assistance with data deposition, B. Pappas and S. Malone for information technology infrastructure, J. Morris, E. Walker, A. Merriman and G. Neale for performing single-nucleotide polymorphism and gene expression microarrays, W. Yang for assistance with analysis of genomic data, and J. Stokes for artwork. We thank the Tissue Resources Laboratory, the Flow Cytometry and Cell Sorting Core, and the Clinical Applications of Core Technology Laboratories of the Hartwell Center for Bioinformatics and Biotechnology of St Jude Children's Research Hospital. We thank S. Kehoe of Beckman Coulter Genomics for assistance with Sanger sequencing. This work was funded by The St Jude Children's Research Hospital – Washington University Pediatric Cancer Genome Project, ALSAC of St Jude Children's Research Hospital, Cancer Center support grant P30 CA021765, NIH U01 GM92666—PAAR4Kids, grants to R.K.W. from Washington University in St Louis and the National Human Genome Research Institute (NHGRI U54 HG003079), grants to the Children's Oncology Group (NCI CA98543, CA98413, CA114766), and grants from Alex's Lemonade Stand and St. Baldrick's Foundation (to M.L.H.). S.L.H. was supported by a Haematology Society of Australasia and New Zealand New Investigator Scholarship. S.P.H. is the Ergen Family Chair in Pediatric Cancer. C.G.M. is a Pew Scholar in the Biomedical Sciences and a St. Baldrick's Scholar.

Author Contributions C.G.M., J.R.D., T.J.L., E.R.M. and R.K.W. designed the experiments. J.Z., L.D. and C.L. led data analysis. C.G.M., L.H., S.L.H., D.P.-T., J.R.C.-U., prepared patient samples and performed laboratory assays. R.S.F. and L.L.F. supervised whole genome sequencing data generation. K.C.B. managed data transfer. D.J.D. supervised the automated analysis pipeline. C.W.N. supervised computing infrastructure. J.E. performed transcriptome sequencing. J.R.C.-U., M.K. and J.C. performed IL7R mutation assays. K.A.S., M.L.H. and K.G.R performed phosphosignalling analyses. K.G.R. performed colony assays. X.C., M.R., J.W., G.W., J.B., D.M., J.M., D.Z., L.W., X.H., K.J.J. and C.C.H. performed sequence analysis. L.H., C.G.M. and J.M. analysed single-nucleotide polymorphism array data. M.P. performed telomere analysis. S.C.R. reviewed cytogenetic data. P.G. prepared Circos plots. D.A. and S.E. managed data. S.-C.C., J.M. and G.S. analysed gene expression microarray data. S.D., K.E., E.L., F.N. and J.E.D. collected and analysed gene expression data from normal and leukaemic stem and progenitor cells. S.B.P. developed the GRIN model and performed genomic pathway analyses. D.P. and C.C. performed association analyses between clinical and genetic variables and outcome. R.H. and R.W.K. performed EZH2 structural modelling. S.-C.C. performed pathway analysis. A.U. performed ARACNE analyses. D.C., E.C.-S., G.B., S.P.H., M.L.L., M.D., W.E.E., B.W., S.W., K.P.D., and C.-H.P. provided clinical samples and data. C.G.M., J.R.D and J.Z. wrote the manuscript. J.Z., L.D., L.H., G.W., S.L.H., D.P.-T., J.E., X.C., J.W., M.R., C.L., S.-C.C., L.W., J.M., K.G.R., S.B.P., A.U., J.B., P.G., R.H., R.W.K., M.P., D.J.M., D.Z., D.A., S.E., K.C.B., G.S., S.R., M.I.B., S.A.S., K.P.D., R.S.F., L.L.F., X.H., C.C.H., D.J.D., K.O., K.I.J., J.C.O., W.E.E., C.-H.P., C.W.N., T.J.L., E.R.M., R.K.W., J.R.D. and C.G.M. are part of the St Jude Children's Research Hospital – Washington University Pediatric Cancer Genome Project.

Author Information The sequence data and single nucleotide polymorphism microarray data have been deposited in the dbGaP database (http://www.ncbi.nlm.nih.gov/gap) under the accession number phs000340.v1.p1. Affymetrix U133A gene expression data have been deposited in the NCBI gene expression omnibus under GSE33315, and Affymetrix U133 Plus 2.0 PM gene expression data under accession GSE28703. The nucleotide sequence for the full-length *ETV-INO80D* transcript has been deposited in GenBank under accession JF736506. A public data portal for results from the St Jude – Washington University Pediatric Cancer Genome Project is available at http://explore.pediatriccancergenomeproject.org/. Reprints and permissions information is available at www.nature.com/reprints. This paper is distributed under the terms of the Creative Commons Attribution-Non-Commercial-Share Alike licence, and is freely available to all readers at www.nature.com/nature. The authors declare no competing financial interests. Readers are welcome to comment on the online version of this article at www.nature.com/nature. Correspondence and requests for materials should be addressed to J.R.D. (james.downing@stjude.org) and C.G.M. (charles.mullighan@stjude.org).

LETTER

doi:10.1038/nature10692

An absence of ex-companion stars in the type Ia supernova remnant SNR 0509−67.5

Bradley E. Schaefer[1] & Ashley Pagnotta[1]

A type Ia supernova is thought to begin with the explosion of a white dwarf star[1]. The explosion could be triggered by the merger of two white dwarfs[2,3] (a 'double-degenerate' origin), or by mass transfer from a companion star[4,5] (the 'single-degenerate' path). The identity of the progenitor is still controversial; for example, a recent argument against the single-degenerate origin[6] has been widely rejected[7–11]. One way to distinguish between the double- and single-degenerate progenitors is to look at the centre of a known type Ia supernova remnant to see whether any former companion star is present[12,13]. A likely ex-companion star for the progenitor of the supernova observed by Tycho Brahe has been identified[14], but that claim is still controversial[15–18]. Here we report that the central region of the supernova remnant SNR 0509−67.5 (the site of a type Ia supernova 400 ± 50 years ago, based on its light echo[19,20]) in the Large Magellanic Cloud contains no ex-companion star to a visual magnitude limit of 26.9 (an absolute magnitude of $M_V = +8.4$) within a region of radius 1.43 arcseconds. (This corresponds to the 3σ maximum distance to which a companion could have been 'kicked' by the explosion.) This lack of any ex-companion star to deep limits rules out all published single-degenerate models for this supernova. The only remaining possibility is that the progenitor of this particular type Ia supernova was a double-degenerate system.

The progenitor of any type Ia supernova has never been identified. Various candidate classes have been proposed (see Table 1 and Supplementary Information section 1), although arguments and counter-arguments have resulted in no decisive solution. It is possible that the observed type Ia supernovae might have two comparable-sized progenitor classes[21]. In double-degenerate systems, the two white dwarfs will both be completely destroyed by the supernova explosion. In single-degenerate systems, the mass-donor star (orbiting the doomed white dwarf) will survive the explosion, and shine at near its pre-explosion brightness from the middle of the expanding supernova remnant. (During the explosion, portions of the outer envelope of the companion star will be stripped off[22,23], but its location on the colour–magnitude diagram will not change greatly[24].) An observational programme to distinguish between the progenitor models by looking for an ex-companion star inside a known type Ia supernova remnant has been attempted only once[14], for Tycho's supernova of 1572. A particular G-type subgiant star has been identified as being the ex-companion: if this is correct, it would point to a recurrent nova as the progenitor for Tycho's supernova[14]. Several concerns have been raised[15,17] about this identification, and these have been answered[18], although the case remains unresolved.

To break this impasse, we have looked at a supernova remnant in the nearest galaxy to our own, the Large Magellanic Cloud (LMC). We consider the case of SNR 0509−67.5, which was an type Ia supernova (of the SN 1991T class) 400 ± 50 years ago[19,20,23,26]. SNR 0509−67.5 has excellent images in the public domain that were taken by the Hubble Space Telescope (HST). All of the stars in the field have been measured for B, V and I magnitude with standard IRAF aperture photometry and converted to Vega magnitudes with the standard calibration (see Table 2). The faintest visible star (at the 5σ detection level) is at $V = 26.9$ mag.

If any ex-companion still exists after the explosion ~400 years ago, then it must be located near the centre of the remnant. We have measured the geometric centre of the shell with three independent methods (see Supplementary Information section 2): using the edge of the Hα shell, the edge of the X-ray shell, and the minimum of the Hα light in the interior of the remnant. Each of these three derived centres are from different gas masses and regions, so they are independent and provide a measure of the statistical and systematic uncertainties in the centre position. Our combined geometric centre is at right ascension 05 h 09 min 31.208 s, declination −67° 31′ 17.48″ (J2000), with 1σ uncertainties of 0.14″ along the short axis (roughly ENE to WSW) and 0.20″ along the long axis (tilted 18° ± 3° to the west of north).

The position of any ex-companion star will be offset from the estimated geometric centre of the shell, owing to proper motion of the star, asymmetries in the shell, and measurement errors of the centre position. We now consider these factors in order. First, the proper motion of the star will depend on its orbital velocity and the kick onto the star from the supernova explosion. This distribution of the offsets from the centre resulting from the proper motion of the

Table 1 | Candidate progenitor classes

Candidate class	P_{orb} (d)	$v_{ex\text{-}comp}$ (km s^{-1})	Surviving companion	M_V (mag)	V range in LMC (mag)
Double-degenerate	NA	NA	None	NA	NA
Recurrent nova	0.6–520	50–350	Red giant or subgiant	−2.5 to +3.5	16–22
Symbiotic star	245–5,700	50–250	Red giant	−2.5 to +0.5	16–19
Supersoft source	0.14–4.0	170–390	Subgiant or >1.16 $M_\odot$ MS	+0.5 to +4.2	19–22.7
Helium star donor	0.04–160	50–350	Red giant or subgiant core	−0.5 to +2.0	18–20.5
Spin-up/spin-down	245–5,700	50–250	Red giant or subgiant core	−0.5 to +2.0	18–20.5

This table gives the basic classes proposed for progenitors; other possibilities have been exhaustively examined and rejected (Supplementary Information section 1). The orbital periods, P_{orb}, in days, give an indication of the size of the companion star, and hence some indication of its brightness in isolation. The velocity of the ex-companion star, $v_{ex\text{-}comp}$, in km s^{-1}, includes the orbital velocity of the companion with respect to the white dwarf plus the kick velocity, and indicates the maximum proper motion that the companion star can have. The fourth column indicates the type of the ex-companion star for each candidate class, with 'MS' indicating a main sequence star. The absolute V-band magnitude (M_V) is that of the ex-companion star after the explosion. The visual magnitude (V) range for the ex-companion stars is for a distance modulus of 18.50 mag. A main point of this table is that the various classes of single-degenerate models all predict ex-companion star brightnesses that are 4.2 mag or more above our limit, and this is too large a gap to overcome by fading cores or stripped envelopes. We note that the single-degenerate candidate classes mix together somewhat, with recurrent novae being temporary supersoft sources, some symbiotic systems appearing as supersoft sources, some recurrent novae being also technically symbiotic systems, and models showing that the long term evolution of a supersoft source is to become a recurrent nova before exploding as an type Ia supernova. The 'supersoft source' progenitor class is perhaps misnamed, as these nuclear burning white dwarfs can be emitting supersoft X-rays with large or small luminosity either episodically or persistently. NA, not applicable.

[1]Department of Physics and Astronomy, Louisiana State University, Baton Rouge, Louisiana 70803, USA.

Table 2 | Objects near the centre of SNR 0509−67.5

Star	RA (h min s), dec. (° ′ ″)	θ (″)	V (mag)	I (mag)	Comments
A	05 09 30.960, −67 31 16.28	1.7	26.08 ± 0.11	24.50 ± 0.08	Nearest to error circle
B	05 09 30.701, −67 31 18.75	1.7	24.82 ± 0.04	23.61 ± 0.04	...
C	05 09 30.753, −67 31 16.63	1.9	26.30 ± 0.13	24.77 ± 0.09	...
D	05 09 30.916, −67 31 19.91	2.0	24.02 ± 0.03	22.98 ± 0.03	...
E	05 09 30.660, −67 31 19.07	2.1	23.99 ± 0.02	23.05 ± 0.03	...
F	05 09 30.824, −67 31 16.03	2.1	23.30 ± 0.02	22.53 ± 0.02	...
G	05 09 31.212, −67 31 16.30	2.2	25.36 ± 0.06	23.76 ± 0.04	...
H	05 09 30.712, −67 31 16.01	2.5	22.87 ± 0.01	22.06 ± 0.02	...
I	05 09 30.581, −67 31 16.74	2.6	26.57 ± 0.15	24.72 ± 0.08	...
J	05 09 31.454, −67 31 17.21	2.9	25.84 ± 0.09	24.43 ± 0.07	...
K	05 09 30.824, −67 31 15.20	2.9	22.55 ± 0.01	21.86 ± 0.01	Nearest $V < 22.7$
L	05 09 31.299, −67 31 15.72	2.9	20.56 ± 0.01	20.07 ± 0.01	...
M	05 09 31.837, −67 31 19.61	5.2	24.26 ± 0.03	21.00 ± 0.01	Very red star
N	05 09 31.604, −67 31 22.54	5.8	20.92 ± 0.01	19.87 ± 0.01	Nearest subgiant
O	05 09 31.586, −67 31 11.49	7.4	18.75 ± 0.01	17.68 ± 0.01	Nearest red giant

The first column lists a letter name for each star for identification. The stars are labelled in Fig. 1 with the letter placed to the immediate right of the star. The ordering is based on radial distance from the centre of the error circle. The second column gives the position for each star; RA, right ascension; dec., declination (J2000). The third column gives the angular distance, θ, from the centre of the error circle to the star. All stars with $\theta < 3.0''$ are included, for the limiting magnitude of $V = 26.9$ mag. Importantly, there are no stars within the extreme 99.73% error ellipse ($\theta < 1.43''$). Three additional stars of interest with $\theta > 3.0''$ are added. The next two columns are the V and I magnitudes (with 1σ uncertainties), followed by a column for comments.

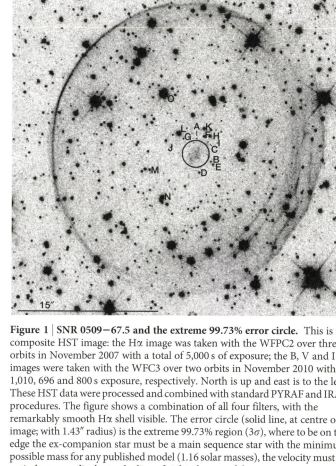

Figure 1 | SNR 0509−67.5 and the extreme 99.73% error circle. This is a composite HST image: the Hα image was taken with the WFPC2 over three orbits in November 2007 with a total of 5,000 s of exposure; the B, V and I images were taken with the WFC3 over two orbits in November 2010 with 1,010, 696 and 800 s exposure, respectively. North is up and east is to the left. These HST data were processed and combined with standard PYRAF and IRAF procedures. The figure shows a combination of all four filters, with the remarkably smooth Hα shell visible. The error circle (solid line, at centre of image; with 1.43″ radius) is the extreme 99.73% region (3σ), where to be on the edge the ex-companion star must be a main sequence star with the minimum possible mass for any published model (1.16 solar masses), the velocity must be entirely perpendicular to the line of sight, the age of the supernova remnant must be pushed to the 3σ highest possible value (550 years), and the measurement error for the remnant's geometric centre must be pushed to the 3σ extreme. The only source inside the error circle is a nebulous object that looks like a background galaxy, however the location of this object at the centre suggests it might be related to the supernova event (see Supplementary Information section 4). There are no stars within the extreme error circle to $V = 26.9$ mag, which corresponds to an absolute magnitude of $M_V = +8.4$ mag in the LMC. All published models for single-degenerate progenitors have the ex-companion star appearing more luminous than $M_V = +4.2$ mag ($V = 22.7$ mag in the LMC). In all, our extreme 99.73% error circle is very conservative, and there is no point source to limits 4.2 mag deeper than possible for any published model of single-degenerate systems.

star does not have a Gaussian profile, so we express the allowed positions as ellipses with a 99.73% probability (that is, 3σ) of containing the position of the ex-companion star. As the proper motion depends on the nature of the companion, we report ellipses for red giants, subgiants and main-sequence stars. Second, for SNR 0509−67.5 in particular, the shell expansion is uniform in all directions except for one quadrant where the interstellar medium is more dense (as shown by the excess 24-μm emission seen in the Spitzer image[27] from pre-existing dust swept up by the shell) and so the expansion has recently slowed down[28]. This slowing in only one quadrant accounts for the small observed ellipticity of the shell, from which we can derive the apparent offset (1.39″ ± 0.14″ along a line 18° ± 3° south of west) between the observed geometric centre of the shell and the site of the supernova explosion. Last, our derived best estimate for the site of the explosion is right ascension 05 h 09 min 30.976 s, declination −67° 31′ 17.90″ (J2000). The error ellipse is nearly circular, with a conservative radius of 1.43″ for a maximal proper motion (390 km s^{-1}), a maximal age for the remnant (550 years) and for 99.73% (3σ) containment. (See Supplementary Information section 3 for details.)

The error circle is completely empty of all visible point sources down to the deep limits of HST. Importantly, there are no red giant or subgiant stars in or near the circle. (Red giants and subgiants can be confidently recognized by their position above the main sequence in the colour–magnitude diagram.) The nearest red giant (star O in Fig. 1) is 7.4″ from the centre, while the nearest subgiant star (star N) is 5.8″ from the centre. The nearest star brighter than $V = 22.7$ mag (star K), that is, the nearest possible ex-companion of any type, is 2.9″ from the centre. The only source in the circle is an extended faint nebula, and the excellent angular resolution of the HST allows us to see that no point source is hidden within the nebula. (This nebula is probably an irregular galaxy of moderate redshift, but the coincidence of this nebula with the site of the supernova suggests that its origin might be associated with the explosion, as discussed in Supplementary Information section 4.) The error circle is empty of point sources to a limiting magnitude of $V = 26.9$ mag (at the 5σ level). This requires that any ex-companion be less luminous than $M_V = +8.4$ mag.

Our new limit can be compared to the expected presence of ex-companion stars for the various single-degenerate models (see Table 1). There is no red giant star in or near the error circle, and this is strongly inconsistent with the symbiotic progenitor model. There is no red giant or sub-giant star in or near the error circle, and this is strongly inconsistent with the recurrent nova, helium star and spin-up/spin-down progenitor models. There is no star brighter than $V = 22.7$ mag in or near the error circle, and this is strongly inconsistent with the supersoft source progenitor model. The lack of any possible ex-companion star to $M_V = +8.4$ mag rules out all published single-degenerate progenitor models. With all single-degenerate models eliminated, the only remaining progenitor model for SNR 0509−67.5 is the double-degenerate model.

Received 29 June; accepted 31 October 2011.

1. Branch, D., Livio, M., Yungelson, L. R., Boffi, F. R. & Baron, E. In search of the progenitors of type Ia supernova. *Publ. Astron. Soc. Pacif.* **107,** 1019–1029 (1995).
2. Webbink, R. F. Double white dwarfs as progenitors of R Coronae Borealis stars and type I supernovae. *Astrophys. J.* **277,** 355–360 (1984).
3. van Kerkwijk, M. H., Chang, P. & Justham, S. Sub-Chandrasekhar white dwarf mergers as the progenitors of type Ia supernovae. *Astrophys. J.* **722,** L157–L161 (2010).
4. Iben, I. & Tutukov, A. V. Supernovae of type I as end products of the evolution of binaries with components of moderate initial mass ($M \leq 9M_{\odot}$). *Astrophys. J. Suppl. Ser.* **54,** 335–372 (1984).
5. Whelan, J. & Iben, I. Binaries and supernovae of type I. *Astrophys. J.* **186,** 1007–1014 (1973).
6. Gilfanov, M. & Bogdan, A. An upper limit on the contribution of accreting white dwarfs to the type Ia supernova rate. *Nature* **463,** 924–925 (2010).
7. Meng, X.-C. & Yang, W.-M. Binary population synthesis study of the supersoft X-ray phase of single degenerate type Ia supernova progenitors. *Res. Astron. Astrophys.* **11,** 965–973 (2011).
8. Di Stefano, R. The progenitors of type Ia supernovae. II. Are they double-degenerate binaries? The symbiotic channel. *Astrophys. J.* **719,** 474–482 (2010).
9. Hachisu, I., Kato, M. & Nomoto, K. Supersoft X-ray phase of single degenerate type Ia supernova progenitors in early-type galaxies. *Astrophys. J.* **724,** L212–L216 (2010).
10. Lipunov, V. M., Panchenko, I. E. & Pruzhinskaya, M. V. The mechanism of supernova Ia explosions in elliptical galaxies. *N. Astron.* **16,** 250–252 (2011).
11. Orio, M., Nelson, T., Bianchini, A., Di Mille, F. & Harbeck, D. A census of the supersoft X-ray sources in M31. *Astrophys. J.* **717,** 739–765 (2010).
12. Ruiz-Lapuente, P. The quest for a supernova companion. *Science* **276,** 1813–1814 (1997).
13. Canal, R., Mendez, J. & Ruiz-Lapuente, P. Identification of the companion stars of type Ia supernovae. *Astrophys. J.* **550,** L53–L56 (2001).
14. Ruiz-Lapuente, P. *et al.* The binary progenitor of Tycho Brahe's 1572 supernova. *Nature* **431,** 1069–1072 (2004).
15. Kerzendorf, W. E. *et al.* Subaru high-resolution spectroscopy of star G in the Tycho supernova remnant. *Astrophys. J.* **701,** 1665–1672 (2009).
16. Ozaki, J. & Shigeyama, T. A method to identify the companion stars of type Ia supernovae in young supernova remnants. *Astrophys. J.* **644,** 954–958 (2006).
17. Ihara, Y. *et al.* Searching for a companion star of Tycho's type Ia supernova with optical spectroscopic observations. *Publ. Astron. Soc. Jpn* **59,** 811–826 (2007).
18. Gonzalez Hernandez, J. I. *et al.* The chemical abundances of Tycho G in supernova remnant 1572. *Astrophys. J.* **691,** 1–15 (2009).
19. Rest, A. *et al.* Light echoes from ancient supernovae in the Large Magellanic Cloud. *Nature* **438,** 1132–1134 (2005).
20. Rest, A. *et al.* Spectral identification of an ancient supernova using light echoes in the Large Magellanic Cloud. *Astrophys. J.* **680,** 1137–1148 (2008).
21. Mannucci, F., Della Valle, M. & Panagia, N. Two populations of progenitors for type Ia supernovae? *Mon. Not. R. Astron. Soc.* **370,** 773–783 (2006).
22. Marietta, E., Burrows, A. & Fryxell, B. Type Ia supernova explosions in binary systems: the impact on the secondary star and its consequences. *Astrophys. J. Suppl. Ser.* **128,** 615–650 (2000).
23. Pan, K.-C., Ricker, P. & Taam, R. E. Impact of type Ia supernova ejecta on a helium-star binary companion. *Astrophys. J.* **715,** 78–85 (2010).
24. Podsiadlowski, P. On the evolution and appearance of a surviving companion after a type Ia supernova explosions. Preprint at (http://arXiv.org/abs/astro-ph/0303660) (2003).
25. Hughes, J. P. *et al.* ASCA observations of the Large Magellanic Cloud supernova remnant sample: typing supernovae from their remnants. *Astrophys. J.* **444,** L81–L84 (1995).
26. Badenes, C., Harris, J., Zaritsky, D. & Prieto, J. L. The stellar ancestry of supernovae in the Magellanic Clouds – I. The most recent supernovae in the Large Magellanic Cloud. *Astrophys. J.* **700,** 727–740 (2009).
27. Borkowski, K. J. *et al.* Dust destruction in type Ia supernovae remnants in the Large Magellanic Cloud. *Astrophys. J.* **642,** L141–L144 (2006).
28. Helder, E. A., Kosenko, D. & Vink, J. Cosmic-ray acceleration efficiency versus temperature equilibration: the case of SNR 0509–67.5. *Astrophys. J.* **719,** L140–L144 (2010).

Supplementary Information is linked to the online version of the paper at www.nature.com/nature.

Acknowledgements The HST images were taken as part of two programmes with Principal Investigators J. P. Hughes and K. Noll. This work was supported by the National Science Foundation.

Author Contributions The authors shared the ideas, the data analysis, and the writing of this paper.

Author Information HST images comprising Fig. 1 are in the public domain (http://heritage.stsci.edu/2010/27/index.html, http://apod.nasa.gov/apod/ap110125.html). Reprints and permissions information is available at www.nature.com/reprints. The authors declare no competing financial interests. Readers are welcome to comment on the online version of this article at www.nature.com/nature. Correspondence and requests for materials should be addressed to B.E.S. (schaefer@lsu.edu).

LETTER

doi:10.1038/nature10684

One or more bound planets per Milky Way star from microlensing observations

A. Cassan[1,2,3], D. Kubas[1,2,4], J.-P. Beaulieu[1,2,25], M. Dominik[1,5], K. Horne[1,5], J. Greenhill[1,6], J. Wambsganss[1,3], J. Menzies[1,7], A. Williams[1,8], U. G. Jørgensen[1,9], A. Udalski[10,11], D. P. Bennett[1,12], M. D. Albrow[1,13], V. Batista[1,2], S. Brillant[1,4], J. A. R. Caldwell[1,14], A. Cole[1,6], Ch. Coutures[1,2], K. H. Cook[1,15], S. Dieters[1,6], D. Dominis Prester[1,16], J. Donatowicz[1,17], P. Fouque[1,18], K. Hill[1,6], N. Kains[1,19], S. Kane[1,20], J.-B. Marquette[1,2], R. Martin[1,8], K. R. Pollard[1,13], K. C. Sahu[1,14], C. Vinter[1,9], D. Warren[1,6], B. Watson[1,6], M. Zub[1,3], T. Sumi[21,22], M. K. Szymański[10,11], M. Kubiak[10,11], R. Poleski[10,11], I. Soszyński[10,11], K. Ulaczyk[10,11], G. Pietrzyński[10,11,23] & Ł. Wyrzykowski[10,11,24]

Most known extrasolar planets (exoplanets) have been discovered using the radial velocity[1,2] or transit[3] methods. Both are biased towards planets that are relatively close to their parent stars, and studies find that around 17–30% (refs 4, 5) of solar-like stars host a planet. Gravitational microlensing[6–9], on the other hand, probes planets that are further away from their stars. Recently, a population of planets that are unbound or very far from their stars was discovered by microlensing[10]. These planets are at least as numerous as the stars in the Milky Way[10]. Here we report a statistical analysis of microlensing data (gathered in 2002–07) that reveals the fraction of bound planets 0.5–10 AU (Sun–Earth distance) from their stars. We find that 17^{+6}_{-9}% of stars host Jupiter-mass planets (0.3–10 M_J, where $M_J \approx 318\,M_\oplus$ and $M_\oplus$ is Earth's mass). Cool Neptunes (10–30 $M_\oplus$) and super-Earths (5–10 $M_\oplus$) are even more common: their respective abundances per star are 52^{+22}_{-29}% and 62^{+35}_{-35}%. We conclude that stars are orbited by planets as a rule, rather than the exception.

Gravitational microlensing is very rare: fewer than one star per million undergoes a microlensing effect at any time. Until now, the planet-search strategy[7] has been mainly split into two levels. First, wide-field survey campaigns such as the Optical Gravitational Lensing Experiment (OGLE; ref. 11) and Microlensing Observations in Astrophysics (MOA; ref. 12) cover millions of stars every clear night to identify and alert the community to newly discovered stellar microlensing events as early as possible. Then, follow-up collaborations such as the Probing Lensing Anomalies Network (PLANET; ref. 13) and the Microlensing Follow-Up Network (μFUN; refs 14, 15) monitor selected candidates at a very high rate to search for very short-lived light curve anomalies, using global networks of telescopes.

To ease the detection-efficiency calculation, the observing strategy should remain homogeneous for the time span considered in the analysis. As detailed in the Supplementary Information, this condition is fulfilled for microlensing events identified by OGLE and followed up by PLANET in the six-year time span 2002−07. Although a number of microlensing planets were detected by the various collaborations between 2002 and 2007 (Fig. 1), only a subset of them are consistent with the PLANET 2002–07 strategy. This leaves us with three compatible detections: OGLE 2005-BLG-071Lb (refs 16, 17) a Jupiter-like planet of mass $M \approx 3.8\,M_J$ and semi-major axis $a \approx 3.6$ AU; OGLE 2007-BLG-349Lb (ref. 18), a Neptune-like planet ($M \approx 0.2\,M_J$, $a \approx 3$ AU); and the

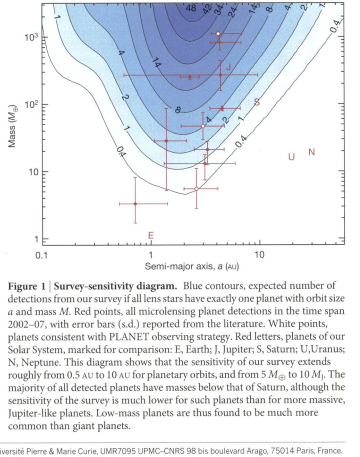

Figure 1 | Survey-sensitivity diagram. Blue contours, expected number of detections from our survey if all lens stars have exactly one planet with orbit size a and mass M. Red points, all microlensing planet detections in the time span 2002–07, with error bars (s.d.) reported from the literature. White points, planets consistent with PLANET observing strategy. Red letters, planets of our Solar System, marked for comparison: E, Earth; J, Jupiter; S, Saturn; U,Uranus; N, Neptune. This diagram shows that the sensitivity of our survey extends roughly from 0.5 AU to 10 AU for planetary orbits, and from 5 $M_\oplus$ to 10 M_J. The majority of all detected planets have masses below that of Saturn, although the sensitivity of the survey is much lower for such planets than for more massive, Jupiter-like planets. Low-mass planets are thus found to be much more common than giant planets.

[1]Probing Lensing Anomalies Network (PLANET) Collaboration, Institut d'Astrophysique de Paris, Université Pierre & Marie Curie, UMR7095 UPMC–CNRS 98 bis boulevard Arago, 75014 Paris, France. [2]Institut d'Astrophysique de Paris, Université Pierre & Marie Curie, UMR7095 UPMC–CNRS 98 bis boulevard Arago, 75014 Paris, France. [3]Astronomischen Rechen-Instituts (ARI), Zentrum für Astronomie, Heidelberg University, Mönchhofstrasse 12–14, 69120 Heidelberg, Germany. [4]European Southern Observatory, Alonso de Cordoba 3107, Vitacura, Casilla 19001, Santiago, Chile. [5]Scottish Universities Physics Alliance (SUPA), University of St Andrews, School of Physics & Astronomy, North Haugh, St Andrews, KY16 9SS, UK. [6]University of Tasmania, School of Maths and Physics, Private bag 37, GPO Hobart, Tasmania 7001, Australia. [7]South African Astronomical Observatory, PO Box 9 Observatory 7935, South Africa. [8]Perth Observatory, Walnut Road, Bickley, Perth 6076, Australia. [9]Niels Bohr Institute and Centre for Star and Planet Formation, Juliane Mariesvej 30, 2100 Copenhagen, Denmark. [10]Optical Gravitational Lensing Experiment (OGLE) Collaboration, Warsaw University Observatory, Al. Ujazdowskie 4, 00-478 Warszawa, Poland. [11]Warsaw University Observatory, Al. Ujazdowskie 4, 00-478 Warszawa, Poland. [12]University of Notre Dame, Physics Department, 225 Nieuwland Science Hall, Notre Dame, Indiana 46530, USA. [13]University of Canterbury, Department of Physics & Astronomy, Private Bag 4800, Christchurch 8140, New Zealand. [14]Space Telescope Science Institute, 3700 San Martin Drive, Baltimore, Maryland 21218, USA. [15]Institute of Geophysics and Planetary Physics, Lawrence Livermore National Laboratory, PO Box 808, California 94550, USA. [16]Department of Physics, University of Rijeka, Omladinska 14, 51000 Rijeka, Croatia. [17]Technical University of Vienna, Department of Computing, Wiedner Hauptstrasse 10, 1040 Vienna, Austria. [18]Laboratoire Astrophysique de Toulouse (LATT), Université de Toulouse, CNRS, 31400 Toulouse, France. [19]European Southern Observatory Headquarters, Karl-Schwarzschild-Strasse 2, 85748 Garching, Germany. [20]NASA Exoplanet Science Institute, Caltech, MS 100-22, 770 South Wilson Avenue, Pasadena, California 91125, USA. [21]Microlensing Observations in Astrophysics (MOA) Collaboration, Department of Earth and Space Science, Osaka University, Osaka 560-0043, Japan. [22]Department of Earth and Space Science, Osaka University, Osaka 560-0043, Japan. [23]Universidad de Concepción, Departamento de Fisica, Casilla 160-C, Concepción, Chile. [24]Institute of Astronomy, University of Cambridge, Madingley Road, Cambridge CB3 0HA, UK. [25]Department of Physics and Astronomy, University College London, Gower Street, London WC1E 6BT, UK.

super-Earth planet OGLE 2005-BLG-390Lb (refs 19, 20; $M \approx 5.5\,M_{\oplus}$, $a \approx 2.6$ AU).

To compute the detection efficiency for the 2002–07 PLANET seasons, we selected a catalogue of unperturbed (that is, single-lens-like) microlensing events using a standard procedure[21], as explained in the Supplementary Information. For each light curve, we defined the planet-detection efficiency $\varepsilon(\log d,\log q)$ as the probability that a detectable planet signal would arise if the lens star had one companion planet, with mass ratio q and projected orbital separation d (in Einstein-ring radius units; ref. 22). The efficiency was then transformed[23] to $\varepsilon(\log a,\log M)$. The survey sensitivity $S(\log a,\log M)$ was obtained by summing the detection efficiencies over all individual microlensing events. It provided the number of planets that our survey would expect to detect if all lens stars had exactly one planet of mass M and semi-major axis a.

We used 2004 as a representative season from the PLANET survey. Among the 98 events monitored, 43 met our quality-control criteria and were processed[24]. Most of the efficiency comes from the 26 most densely covered light curves, which provide a representative and reliable sub-sample of events. We then computed the survey sensitivity for the whole time span 2002–07 by weighting each observing season relative to 2004, according to the number of events observed by PLANET for different ranges of peak magnification. This is described in the Supplementary Information, and illustrated in Supplementary Fig. 2. The resulting planet sensitivity is plotted in blue in Fig. 1, where the labelled contours show the corresponding expected number of detections. The figure shows that the core sensitivity covers 0.5−10 AU for masses between those of Uranus/Neptune and ten times the mass of Jupiter, and extends (with limited sensitivity) down to about $5\,M_{\oplus}$. As inherent to the microlensing technique, our sample of event-host stars probes the natural mass distribution of stars in the Milky Way (K–M dwarfs), in the typical mass range of $0.14-1.0\,M_{\odot}$ (see Supplementary Fig. 3).

To derive the actual abundance of exoplanets from our survey, we proceeded as follows. Let the planetary mass function, $f(\log a,\log M) \equiv dN/(d\log a \times d\log M)$, where N is the average number of planets per star. We then integrate the product $f(\log a,\log M)\,S(\log a,\log M)$ over $\log a$ and $\log M$. This gives $E(f)$, the number of detections we can expect from our survey. For k (fractional) detections, the model then predicts a Poisson probability distribution $P(k|E) = e^{-E}E^k/k!$. A Bayesian analysis assuming an uninformative uniform prior $P(\log f) \equiv 1$ finally yields the probability distribution $P(\log f|k)$ that is used to constrain the planetary mass function.

Although our derived planet-detection sensitivity extends over almost three orders of magnitude of planet masses (roughly $5\,M_{\oplus}$ to $10\,M_{\mathrm{J}}$), it covers fewer than 1.5 orders of magnitude in orbit sizes (0.5−10 AU), thus providing little information about the dependence of f on a. Within these limits, however, we find that the mass function is approximately consistent with a flat distribution in $\log a$ (that is, f does not explicitly depend on a). The planet-detection sensitivity integrated over $\log a$, or $S(\log M)$, is displayed in Fig. 2b. The distribution probabilities of the mass for the three detections (computed according to the mass-error bars reported in the literature) are plotted in Fig. 2c (black curves), as is their sum (red curve).

To study the dependence of f on mass, we assume that to the first order, f is well-approximated by a power-law model: $f = f_0\,(M/M_0)^{\alpha}$, where f_0 (the normalization factor) and α (the slope of the power-law) are the parameters to be derived and M_0 a fiducial mass (in practice, the pivot point of the mass function). Previous works[18,25–27] on planet frequency have demonstrated that a power law provides a fair description of the global behaviour of f with planetary mass. Apart from the constraint based on our PLANET data, we also made use in our analysis of the previous constraints obtained by microlensing: an estimate of the normalization[18] f_0 (0.36 ± 0.15) and an estimate of the slope[25] α (-0.68 ± 0.2), displayed respectively as the blue point and the blue lines in Fig. 2. The new constraint presented here therefore relies on

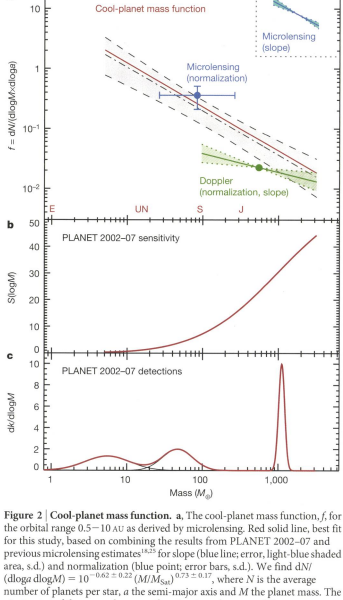

Figure 2 | Cool-planet mass function. a, The cool-planet mass function, f, for the orbital range 0.5−10 AU as derived by microlensing. Red solid line, best fit for this study, based on combining the results from PLANET 2002–07 and previous microlensing estimates[18,25] for slope (blue line; error, light-blue shaded area, s.d.) and normalization (blue point; error bars, s.d.). We find $dN/(d\log a\,d\log M) = 10^{-0.62\,\pm\,0.22}\,(M/M_{\mathrm{Sat}})^{-0.73\,\pm\,0.17}$, where N is the average number of planets per star, a the semi-major axis and M the planet mass. The pivot point of the power-law mass function is at the mass of Saturn ($M_{\mathrm{Sat}} = 95\,M_{\oplus}$). The grey shaded area is the 68% confidence interval around the median (dash-dotted black line). For comparison, the constraint from Doppler measurements[27] (green line and point; error, green shaded area, s.d.) is also displayed. Differences can arise because the Doppler technique focuses mostly on solar-like stars, whereas microlensing a priori probes all types of host stars. Moreover, microlensing planets are located further away from their stars and are cooler than Doppler planets. These two populations of planets may then follow a rather different mass function. **b**, PLANET 2002–07 sensitivity, S: the expected number of detections if all stars had exactly one planet, regardless of its orbit. **c**, PLANET 2002–07 detections, k. Thin black curves, distribution probabilities of the mass for the three detections contained in the PLANET sample; red line, the sum of these distributions.

10 planet detections. We obtained $f = 10^{-0.62\,\pm\,0.22}\,(M/M_{\oplus})^{-0.73\,\pm\,0.17}$ (red line in Fig. 2a) with a pivot point at $M_0 \approx 95\,M_{\oplus}$; that is, at Saturn's mass. The median of f and the 68% confidence interval around the median are marked by the dashed lines and the grey area.

Hence, microlensing delivers a determination of the full planetary mass function of cool planets in the separation range 0.5−10 AU. Our measurements confirm that low-mass planets are very common, and that the number of planets increases with decreasing planet mass, in agreement with the predictions of the core-accretion theory of planet formation[28]. The first microlensing study of the abundances of cool gas

giants[21] found that fewer than 33% of M dwarfs have a Jupiter-like planet between 1.5–4 AU, and even lower limits of 18% have been reported[29,30]. These limits are compatible with our measurement of 5^{+2}_{-2}% for masses ranging from Saturn to 10 times Jupiter, in the same orbit range.

From our derived planetary mass function, we estimate that within 0.5–10 AU (that is, for a wider range of orbital separations than previous studies), on average 17^{+6}_{-9}% of stars host a 'Jupiter' ($0.3-10\ M_{\rm J}$) and 52^{+22}_{-29}% of stars host Neptune-like planets ($10-30\ M_{\oplus}$). Taking the full range of planets that our survey can detect ($0.5-10$ AU, $5\ M_{\oplus}$ to $10\ M_{\rm J}$), we find that on average every star has $1.6^{+0.72}_{-0.89}$ planets. This result is consistent with every star of the Milky Way hosting (on average) one planet or more in an orbital-distance range of 0.5–10 AU. Planets around stars in our Galaxy thus seem to be the rule rather than the exception.

Received 19 January; accepted 28 October 2011.

1. Mayor, M. & Queloz, D. A. Jupiter-mass companion to a solar-type star. *Nature* **378,** 355–359 (1995).
2. Marcy, G. W. & Butler, R. P. A planetary companion to 70 Virginis. *Astrophys. J.* **464,** L147–L151 (1996).
3. Charbonneau, D., Brown, T. M., Latham, D. W. & Mayor, M. Detection of planetary transits across a Sun-like star. *Astrophys. J.* **529,** L45–L48 (2000).
4. Howard, A. *et al.* Planet occurrence within 0.25 AU of Solar-type stars from Kepler. *Astrophys. J.* (submitted); preprint at http://arxiv.org/abs/1103.2541 (2011).
5. Mayor, M. *et al.* The HARPS search for southern extra-solar planets XXXIV. Occurrence, mass distribution and orbital properties of super-Earths and Neptune-mass planets. *Astron. Astrophys.* (submitted); preprint at http://arxiv.org/abs/1109.2497 (2011).
6. Mao, S. & Paczynski, B. Gravitational microlensing by double stars and planetary systems. *Astrophys. J.* **374,** L37–L40 (1991).
7. Gould, A. & Loeb, A. Discovering planetary systems through gravitational microlenses. *Astrophys. J.* **396,** 104–114 (1992).
8. Bennett, D. P. & Rhie, S. H. Detecting Earth-mass planets with gravitational microlensing. *Astrophys. J.* **472,** 660–664 (1996).
9. Wambsganss, J. Discovering Galactic planets by gravitational microlensing: magnification patterns and light curves. *Mon. Not. R. Astron. Soc.* **284,** 172–188 (1997).
10. Sumi, T. *et al.* Unbound or distant planetary mass population detected by gravitational microlensing. *Nature* **473,** 349–352 (2011).
11. Udalski, A. The Optical Gravitational Lensing Experiment. Real time data analysis systems in the OGLE-III survey. *Acta Astronaut.* **53,** 291–305 (2003).
12. Bond, I. A. *et al.* Real-time difference imaging analysis of MOA Galactic bulge observations during 2000. *Mon. Not. R. Astron. Soc.* **327,** 868–880 (2001).
13. Albrow, M. *et al.* The 1995 pilot campaign of PLANET: searching for microlensing anomalies through precise, rapid, round-the-clock monitoring. *Astrophys. J.* **509,** 687–702 (1998).
14. Gould, A. *et al.* Microlens OGLE-2005-BLG-169 implies that cool Neptune-like planets are common. *Astrophys. J.* **644,** L37–L40 (2006).
15. Gaudi, B. S. *et al.* Discovery of a Jupiter/Saturn analog with gravitational microlensing. *Science* **319,** 927–930 (2008).
16. Udalski, A. *et al.* A Jovian-mass planet in microlensing event OGLE-2005-BLG-071. *Astrophys. J.* **628,** L109–L112 (2005).
17. Dong, S. *et al.* OGLE-2005-BLG-071Lb, the most massive M dwarf planetary companion? *Astrophys. J.* **695,** 970–987 (2009).
18. Gould, A. *et al.* Frequency of solar-like systems and of ice and gas giants beyond the snow line from high-magnification microlensing events in 2005–2008. *Astrophys. J.* **720,** 1073–1089 (2010).
19. Beaulieu, J.-P. *et al.* Discovery of a cool planet of 5.5 Earth masses through gravitational microlensing. *Nature* **439,** 437–440 (2006).
20. Kubas, D. *et al.* Limits on additional planetary companions to OGLE 2005-BLG-390L. *Astron. Astrophys.* **483,** 317–324 (2008).
21. Gaudi, B. S. *et al.* Microlensing constraints on the frequency of Jupiter-mass companions: analysis of 5 years of PLANET photometry. *Astrophys. J.* **566,** 463–499 (2002).
22. Einstein, A. Lens-like action of a star by the deviation of light in the gravitational field. *Science* **84,** 506–507 (1936).
23. Dominik, M. Stochastic distributions of lens and source properties for observed galactic microlensing events. *Mon. Not. R. Astron. Soc.* **367,** 669–692 (2006).
24. Cassan, A. An alternative parameterisation for binary-lens caustic-crossing events. *Astron. Astrophys.* **491,** 587–595 (2008).
25. Sumi, T. *et al.* A cold Neptune-mass planet OGLE-2007-BLG-368Lb: cold Neptunes are common. *Astrophys. J.* **710,** 1641–1653 (2010).
26. Howard, A. W. *et al.* The occurrence and mass distribution of close-in super-Earths, Neptunes, and Jupiters. *Science* **330,** 653–655 (2010).
27. Cumming, A. *et al.* The Keck Planet Search: Detectability and the minimum mass and orbital period distribution of extrasolar planets. *Publ. Astron. Soc. Pacif.* **120,** 531–554 (2008).
28. Pollack, J. B. *et al.* Formation of the giant planets by concurrent accretion of solids and gas. *Icarus* **124,** 62–85 (1996).
29. Tsapras, Y. *et al.* Microlensing limits on numbers and orbits of extrasolar planets from the 1998–2000 OGLE events. *Mon. Not. R. Astron. Soc.* **343,** 1131–1144 (2003).
30. Snodgrass, C. *et al.* The abundance of Galactic planets from OGLE-III 2002 microlensing data. *Mon. Not. R. Astron. Soc.* **351,** 967–975 (2004).

Supplementary Information is linked to the online version of the paper at www.nature.com/nature.

Acknowledgements Support for the PLANET project was provided by the HOLMES grant from the French Agence Nationale de la Recherche (ANR), the French National Centre for Scientific Research (CNRS), NASA, the US National Science Foundation, the Lawrence Livermore National Laboratory/National Nuclear Security Administration/Department of Energy, the French National Programme of Planetology, the Program of International Cooperation in Science France–Australia, D. Warren, the German Research Foundation, the Instrument Center for Danish Astronomy and the Danish Natural Science Research Council. The OGLE collaboration is grateful for funding from the European Research Council Advanced Grants Program. K.Ho. acknowledges support from the Qatar National Research Fund. M.D. is a Royal Society University Research Fellow.

Author Contributions A.Ca. led the analysis and conducted the modelling and statistical analyses. A.Ca. and D.K. selected light curves from 2002–07 PLANET/OGLE microlensing seasons, analysed the data and wrote the Letter and Supplement. D.K. computed the magnification maps used for the detection-efficiency calculations. J.-P.B. and Ch.C. wrote the software for online data reduction at the telescopes. J.-P.B. led the PLANET collaboration, with M.D., J.G., J.M. and A.W.; P.F. and M.D.A. contributed to online and offline data reduction. M.D. contributed to the conversion of the detection efficiencies to physical parameter space and developed the PLANET real-time display system with A.W., M.D.A. and Ch.C.; K.Ho. and A.Ca. developed and tested the Bayesian formulation for fitting the two-parameter power-law mass function. J.G. edited the manuscript, conducted the main data cleaning and managed telescope operations at Mount Canopus (1 m) in Hobart. J.W. wrote the original magnification maps software, discussed the main implications and edited the manuscript. J.M., A.W. and U.G.J. respectively managed telescope operations in South Africa (South African Astronomical Observatory 1 m), Australia (Perth 0.61 m) and La Silla (Danish 1.54 m). A.U. led the OGLE campaign and provided the final OGLE photometry. D.P.B, V.B., S.B., J.A.R.C., A.Co., K.H.C., S.D., D.D.P., J.D., P.F., K.Hi., N.K., S.K., J.-B.M., R.M., K.R.P., K.C.S., C.V., D.W., B.W. and M.Z. were involved in the PLANET observing strategy and/or PLANET data acquisition, reduction, real-time analysis and/or commented on the manuscript. T.S. commented on the manuscript. M.K.S., M.K., R.P., I.S., K.U., G.P. and Ł.W. contributed to OGLE data.

Author Information Reprints and permissions information is available at www.nature.com/reprints. The authors declare no competing financial interests. Readers are welcome to comment on the online version of this article at www.nature.com/nature. Correspondence and requests for materials should be addressed to A.C. (cassan@iap.fr).

LETTER

doi:10.1038/nature10713

Implementation of a Toffoli gate with superconducting circuits

A. Fedorov[1], L. Steffen[1], M. Baur[1], M. P. da Silva[2,3] & A. Wallraff[1]

The Toffoli gate is a three-quantum-bit (three-qubit) operation that inverts the state of a target qubit conditioned on the state of two control qubits. It makes universal reversible classical computation[1] possible and, together with a Hadamard gate[2], forms a universal set of gates in quantum computation. It is also a key element in quantum error correction schemes[3–7]. The Toffoli gate has been implemented in nuclear magnetic resonance[3], linear optics[8] and ion trap systems[9]. Experiments with superconducting qubits have also shown significant progress recently: two-qubit algorithms[10] and two-qubit process tomography have been implemented[11], three-qubit entangled states have been prepared[12,13], first steps towards quantum teleportation have been taken[14] and work on quantum computing architectures has been done[15]. Implementation of the Toffoli gate with only single- and two-qubit gates requires six controlled-NOT gates and ten single-qubit operations[16], and has not been realized in any system owing to current limits on coherence. Here we implement a Toffoli gate with three superconducting transmon qubits coupled to a microwave resonator. By exploiting the third energy level of the transmon qubits, we have significantly reduced the number of elementary gates needed for the implementation of the Toffoli gate, relative to that required in theoretical proposals using only two-level systems. Using full process tomography and Monte Carlo process certification, we completely characterize the Toffoli gate acting on three independent qubits, measuring a fidelity of 68.5 ± 0.5 per cent. A similar approach[15] to realizing characteristic features of a Toffoli-class gate has been demonstrated with two qubits and a resonator and achieved a limited characterization considering only the phase fidelity. Our results reinforce the potential of macroscopic superconducting qubits for the implementation of complex quantum operations with the possibility of quantum error correction[17].

We have implemented a Toffoli gate with three transmon qubits (A, B and C) dispersively coupled to a microwave transmission-line resonator, in a sample that is identical to the one used in ref. 14. The resonator is used for joint three-qubit read-out by measuring its transmission[18]. At the same time, it serves as a coupling bus for the qubits[19]. The qubits have a ladder-type energy level structure with sufficient anharmonicity to allow individual microwave addressing of different transitions. We use the first two energy levels as the computational qubit states, $|0\rangle$ and $|1\rangle$, and use the second excited state, $|2\rangle$, to perform two-qubit and qubit–qutrit operations (a qutrit is a quantum ternary digit). From spectroscopy, we deduce a bare resonator frequency $\nu_r = 8.625$ GHz with a quality factor of 3,300; maximum qubit transition frequencies $\nu_A^{max} = 6.714$ GHz, $\nu_B^{max} = 6.050$ GHz and $\nu_C^{max} = 4.999$ GHz; and respective charging energies $E_c/h = 0.264$, 0.296 and 0.307 GHz (h, Planck's constant) and qubit–resonator coupling strengths $g/2\pi = 0.36$, 0.30 and 0.34 GHz for qubits A, B and C. At the maximum transition frequencies, we find respective qubit energy relaxation times of $T_1 = 0.55$, 0.70 and 1.10 μs and phase coherence times of $T_2^* = 0.45$, 0.6 and 0.65 μs for qubits A, B and C.

In the conventional realization of the Toffoli gate, a NOT operation is applied to the target qubit (C) if the control qubits (A and B) are in the state $|11\rangle$. In our set-up, it is more natural to construct a variation of the Toffoli gate shown in Fig. 1a, in which the state of the target qubit is inverted if the control qubits are in $|01\rangle$. This gate can easily be transformed to the conventional Toffoli gate by a redefinition of the computational basis states of qubit A or by applying two π-pulses on qubit A.

The Toffoli gate can be constructed from a 'controlled-controlled-phase' (CCPHASE) gate sandwiched between two Hadamard gates

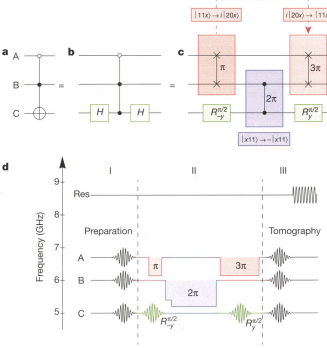

Figure 1 | Circuit diagram of the Toffoli gate. a, A NOT operation (⊕) is applied to qubit C if the control qubits (A and B) are in the ground (○) and excited states (●), respectively. **b**, The Toffoli gate can be decomposed into a CCPHASE gate sandwiched between Hadamard gates (H) applied to qubit C. **c**, The CCPHASE gate is implemented as a sequence of a qubit–qutrit gate, a two-qubit gate and a second qubit–qutrit gate. Each of these gates is realized by tuning the $|11\rangle$ state into resonance with $|20\rangle$ for a $[\pi, 2\pi, 3\pi]$ coherent rotation, respectively. For the Toffoli gate, the Hadamard gates are replaced with $\pm\pi/2$ rotations about the y axis (represented by $R_y^{\pm\pi/2}$). **d**, Pulse sequence used for the implementation of the Toffoli gate. During the preparation (I), resonant microwave pulses are applied to the qubits on the corresponding gate lines. The Toffoli gate (II) is implemented with three flux pulses and resonant microwave pulses (colour coded as in **c**). The measurement (III) consists of microwave pulses that turn the qubit states to the desired measurement axis, and a subsequent microwave pulse applied to the resonator is used to perform a joint dispersive read-out.

[1]Department of Physics, ETH Zurich, CH-8093 Zurich, Switzerland, [2]Disruptive Information Processing Technologies Group, Raytheon BBN Technologies, 10 Moulton Street, Cambridge, Massachusetts 02138, USA. [3]Département de Physique, Université de Sherbrooke, Sherbrooke, Québec J1K 2R1, Canada.

acting on the target qubit as shown in Fig. 1b. A CCPHASE gate leads to a phase shift of π for state $|1\rangle$ of the target qubit if and only if the control qubits are in state $|01\rangle$. In other words, this corresponds to a sign change of only one of the eight computational three-qubit basis states: $|011\rangle \leftrightarrow -|011\rangle$.

The basic idea of 'hiding' states by transforming them into non-computational states to simplify the implementation of a Toffoli gate was theoretically proposed in refs. 20, 21 and has been experimentally implemented for linear optics and ion trap systems[8,9]. The implementation of the scheme of ref. 20 in our set-up would require three controlled-phase (CPHASE) gates, six single-qubit operations and two single-qutrit operations. Instead, we construct the CCPHASE gate from a single two-qubit CPHASE gate and two qubit–qutrit gates. The latter gates are called π-SWAP and 3π-SWAP, respectively (Fig. 1c, red frames). The application of a single CPHASE gate to qubits B and C (Fig. 1c, blue frame) inverts the sign of both $|111\rangle$ and $|011\rangle$. To create the CCPHASE operation, the computational basis state $|111\rangle$ is transferred to the non-computational state $i|201\rangle$ by the π-SWAP gate, effectively hiding it from the CPHASE operation acting on qubits B and C. After the CPHASE operation, $|111\rangle$ is recovered from the non-computational level $i|201\rangle$ by the 3π-SWAP gate. Alternative approaches using optimal control of individual qubits for implementing a Toffoli gate in a single step have been proposed[22] and recently analysed in the context of the circuit quantum electrodynamics architecture[23].

All three-qubit basis states show three distinct evolution paths through our CCPHASE gate (Table 1). Only input state $|011\rangle$ is affected by the CPHASE gate acting on qubits B and C, which transfers $|011\rangle$ to the desired state, $-|011\rangle$. The states $|11x\rangle$ with $x \in \{0, 1\}$ are transferred by the π-SWAP gate to the states $i|20x\rangle$. The subsequent CPHASE gate therefore has no influence on the state. The last gate (3π-SWAP) transfers $i|20x\rangle$ back to $|11x\rangle$. Together the two SWAP gates realize a rotation by 4π, such that the state $|11x\rangle$ does not acquire any extra phase relative to the other states. The states of the last group ($|010\rangle$ and $|x0y\rangle$ with $y \in \{0, 1\}$) do not change during the CCPHASE gate sequence.

The actual experimental implementation of the Toffoli gate consists of a sequence of microwave and flux pulses applied to the qubit local control lines (Fig. 1d). The arbitrary rotations about the x and y axes[24] are realized with resonant microwave pulses applied to the open transmission line at each qubit. We use 8-ns-long, Gaussian-shaped DRAG-pulses[24,25] to prevent population of the third level and phase errors during the single-qubit operations. Few-nanosecond-long current pulses passing through the transmission lines next to the superconducting loops of the respective qubits control the qubit transition frequency realizing z-axis rotations. All two-qubit or qubit–qutrit gates are implemented by tuning a qutrit non-adiabatically to the avoided crossing between the states $|11x\rangle$ and $|20x\rangle$ or, respectively, that between $|x11\rangle$ and $|x20\rangle$ (refs 12, 26, 27). During this time, the system oscillates between these pairs of states with respective frequencies $2J_{11,20}^{AB}$ and $2J_{11,20}^{BC}$. With interaction times $\pi/2J_{11,20}^{AB} = 7$, $3\pi/2J_{11,20}^{AB} = 21$ and $\pi/2J_{11,20}^{BC} = 23$ ns, we realize a π-SWAP and a 3π-SWAP between qubits A and B and a CPHASE gate between qubits B and C, respectively. Our use of qubit–qutrit instead of single-qutrit operations allows for a more efficient construction of the Toffoli gate. Direct realization of the scheme proposed in ref. 20 in our system would require eight additional microwave pulses (used to implement six single-qubit and two single-qutrit gates) with a twofold increase in overall duration of the pulse sequence with respect to our scheme.

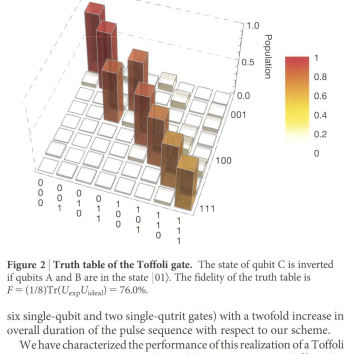

Figure 2 | Truth table of the Toffoli gate. The state of qubit C is inverted if qubits A and B are in the state $|01\rangle$. The fidelity of the truth table is $F = (1/8)\mathrm{Tr}(U_{\mathrm{exp}}U_{\mathrm{ideal}}) = 76.0\%$.

We have characterized the performance of this realization of a Toffoli gate by measuring the truth table, by full process tomography[28] and by Monte Carlo process certification[29,30]. The truth table depicted (Fig. 2) shows the population of all computational basis states after applying the Toffoli gate to each of the computational basis states. It reveals the characteristic properties of the Toffoli gate, namely that a NOT operation is applied on the target qubit (C) if the control qubits (A and B) are in the state $|01\rangle$. The fidelities of the output states show a significant dependence on qubit lifetime. In particular, input states with qubit A (with the shortest lifetime) in the excited state generally have the lowest fidelity, indicating that the protocol is mainly limited by the qubit lifetime. The fidelity of the measured truth table, U_{exp}, with respect to the ideal one, U_{ideal}, namely $F = (1/8)\mathrm{Tr}(U_{\mathrm{exp}}U_{\mathrm{ideal}}) = 76.0\%$, shows the average performance of our gate when acting on the eight basis states.

As an essential addition to the classical characterization of the gate by the truth table, we have performed full, three-qubit process tomography and reconstructed the process matrix, χ_{exp}, to characterize the quantum features of the Toffoli gate completely, overcoming the limited characterization provided by measurements of the phase fidelity only[15]. For this purpose, we prepared a complete set of 64 distinct input states by applying all combinations of single-qubit operations chosen from the set $\{\mathrm{id}, \pi/2_x, \pi/2_y, \pi_x\}$ for each qubit, and performed state tomography on the respective output states. The process matrix reconstructed directly from the data has a fidelity of $F = \mathrm{Tr}(\chi_{\mathrm{exp}}\chi_{\mathrm{ideal}}) = 70 \pm 3\%$ (the error represents a 90% confidence interval), where χ_{ideal} is the ideal process matrix. Using a maximum-likelihood procedure[31] to correct for unphysical properties of χ_{exp}, we find that the obtained process matrix, $\chi_{\mathrm{exp}}^{\mathrm{ML}}$, has a fidelity of $F = \mathrm{Tr}(\chi_{\mathrm{exp}}^{\mathrm{ML}}\chi_{\mathrm{ideal}}) = 69\%$ with expected errors at the level of 3%. In Fig. 3a, χ_{exp} shows the same key features as χ_{ideal} (Fig. 3b).

To gain an accurate alternative estimate of the process fidelity without resorting to a maximum-likelihood procedure, we implemented Monte Carlo process certification following the steps described in ref. 29. First we define a Pauli observable as $\hat{P}_n = \prod_{j=1,\ldots,6}^{\otimes} \hat{P}_{n,j}$, a product of six single-qubit operators chosen from the set of the identity and the Pauli operators ($\hat{p}_{n,j} \in \{1, \sigma_x, \sigma_y, \sigma_z\}$). Then we determine the 232 observables with non-vanishing expectation values $P_n = \mathrm{Tr}(\hat{p}_T \hat{P}_n) \neq 0$, where $\hat{p}_T$ is the Choi matrix of the Toffoli process. For each $\hat{P}_n$, we prepare all ($2^3 = 8$) eigenstates of the product of the first three operators comprising $\hat{P}_n$, apply the Toffoli operation to this state and measure the expectation value of the product of the last three operators in $\hat{P}_n$. Averaging over the results obtained with all eigenstates provides an estimate of P_n.

Table 1 | List of states after each step of the CCPHASE gate

Initial state	After π-SWAP	After CPHASE	After 3π-SWAP
$\|011\rangle$	$\|011\rangle$	$-\|011\rangle$	$-\|011\rangle$
$\|11x\rangle$	$i\|20x\rangle$	$i\|20x\rangle$	$\|11x\rangle$
$\|x0y\rangle$	$\|x0y\rangle$	$\|x0y\rangle$	$\|x0y\rangle$
$\|010\rangle$	$\|010\rangle$	$\|010\rangle$	$\|010\rangle$

The state $|011\rangle$ acquires a phase shift of π during the CPHASE pulse; the states $|11x\rangle$ are transferred to $i|20x\rangle$, 'hiding' them from the CPHASE gate; and the initial states $|x0y\rangle$ and $|010\rangle$ do not change during the sequence.

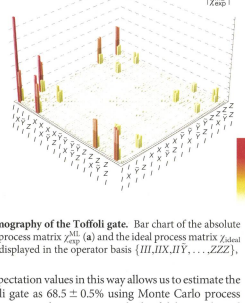

Figure 3 | Process tomography of the Toffoli gate. Bar chart of the absolute value of the measured process matrix χ^{ML}_{exp} (**a**) and the ideal process matrix χ_{ideal} (**b**). The elements are displayed in the operator basis $\{III, IIX, IIY, \ldots, ZZZ\}$,

Extracting all 232 expectation values in this way allows us to estimate the fidelity of the Toffoli gate as $68.5 \pm 0.5\%$ using Monte Carlo process certification, which is in good agreement with the fidelity evaluated using process tomography.

The scheme that we use to implement the Toffoli gate is generic and can readily be applied to other systems because the majority of the quantum systems used as qubits have additional energy levels at their disposal. Reduction of the total gate time by use of qubit–qutrit gates together with the recent advances in the extension of the coherence times of the superconducting circuits[32,33] indicates a path towards the realization of practical quantum error correction.

Received 28 August; accepted 15 November 2011.
Published online 14 December 2011.

1. Toffoli, T. *Reversible Computing* (Lect. Notes Computer Sci. 85, Springer, 1980).
2. Shi, Y. Both Toffoli and controlled-NOT need little help to do universal quantum computation. *Quantum Inf. Comput.* **3,** 84–92 (2003).
3. Cory, D. G. *et al.* Experimental quantum error correction. *Phys. Rev. Lett.* **81,** 2152–2155 (1998).
4. Knill, E., Laflamme, R., Martinez, R. & Negrevergne, C. Benchmarking quantum computers: the five-qubit error correcting code. *Phys. Rev. Lett.* **86,** 5811–5814 (2001).
5. Chiaverini, J. *et al.* Realization of quantum error correction. *Nature* **432,** 602–605 (2004).
6. Pittman, T. B., Jacobs, B. C. & Franson, J. D. Demonstration of quantum error correction using linear optics. *Phys. Rev. A* **71,** 052332 (2005).
7. Aoki, T. *et al.* Quantum error correction beyond qubits. *Nature Phys.* **5,** 541–546 (2009).
8. Lanyon, B. P. *et al.* Simplifying quantum logic using higher-dimensional Hilbert spaces. *Nature Phys.* **5,** 134–140 (2009).
9. Monz, T. *et al.* Realization of the quantum Toffoli gate with trapped ions. *Phys. Rev. Lett.* **102,** 040501 (2009).
10. DiCarlo, L. *et al.* Demonstration of two-qubit algorithms with a superconducting quantum processor. *Nature* **460,** 240–244 (2009).
11. Yamamoto, T. *et al.* Quantum process tomography of two-qubit controlled-z and controlled-not gates using superconducting phase qubits. *Phys. Rev. B* **82,** 184515 (2010).
12. DiCarlo, L. *et al.* Preparation and measurement of three-qubit entanglement in a superconducting circuit. *Nature* **467,** 574–578 (2010).
13. Neeley, M. *et al.* Generation of three-qubit entangled states using superconducting phase qubits. *Nature* **467,** 570–573 (2010).
14. Baur, M. *et al.* Benchmarking a teleportation protocol realized in superconducting circuits. Preprint at (http://arxiv.org/abs/1107.4774) (2011).
15. Mariantoni, M. *et al.* Implementing the quantum Von Neumann architecture with superconducting circuits. *Science* **334,** 61–65 (2011).
16. Barenco, A. *et al.* Elementary gates for quantum computation. *Phys. Rev. A* **52,** 3457–3467 (1995).
17. Reed, M. D. *et al.* Realization of three-qubit quantum error correction with superconducting circuits. Preprint at (http://arxiv.org/abs/1109.4948) (2011).
18. Filipp, S. *et al.* Two-qubit state tomography using a joint dispersive readout. *Phys. Rev. Lett.* **102,** 200402 (2009).
19. Majer, J. *et al.* Coupling superconducting qubits via a cavity bus. *Nature* **449,** 443–447 (2007).
20. Ralph, T. C., Resch, K. J. & Gilchrist, A. Efficient Toffoli gates using qudits. *Phys. Rev. A* **75,** 022313 (2007).
21. Borrelli, M., Mazzola, L., Paternostro, M. & Maniscalco, S. Simple trapped-ion architecture for high-fidelity Toffoli gates. *Phys. Rev. A* **84,** 012314 (2011).
22. Spörl, A. *et al.* Optimal control of coupled Josephson qubits. *Phys. Rev. A* **75,** 012302 (2007).
23. Stojanovic, V. M., Fedorov, A., Bruder, C. & Wallraff, A. Quantum-control approach to realizing a Toffoli gate in circuit QED. Preprint at (http://arxiv.org/abs/1108.3442) (2011).
24. Gambetta, J. M., Motzoi, F., Merkel, S. T. & Wilhelm, F. K. Analytic control methods for high-fidelity unitary operations in a weakly nonlinear oscillator. *Phys. Rev. A* **83,** 012308 (2011).
25. Motzoi, F., Gambetta, J. M., Rebentrost, P. & Wilhelm, F. K. Simple pulses for elimination of leakage in weakly nonlinear qubits. *Phys. Rev. Lett.* **103,** 110501 (2009).
26. Strauch, F. W. *et al.* Quantum logic gates for coupled superconducting phase qubits. *Phys. Rev. Lett.* **91,** 167005 (2003).
27. Haack, G., Helmer, F., Mariantoni, M., Marquardt, F. & Solano, E. Resonant quantum gates in circuit quantum electrodynamics. *Phys. Rev. B* **82,** 024514 (2010).
28. Chuang, I. L. & Nielsen, M. A. Prescription for experimental determination of the dynamics of a quantum black box. *J. Mod. Opt.* **44,** 2455–2467 (1997).
29. da Silva, M. P., Landon-Cardinal, O. & Poulin, D. Practical characterization of quantum devices without tomography. *Phys. Rev. Lett.* **107,** 210404 (2011).
30. Flammia, S. T. & Liu, Y.-K. Direct fidelity estimation from few Pauli measurements. *Phys. Rev. Lett.* **106,** 230501 (2011).
31. Ježek, M., Fiurášek, J., Hradil, Z. & v.. Quantum inference of states and processes. *Phys. Rev. A* **68,** 012305 (2003).
32. Bylander, J. *et al.* Noise spectroscopy through dynamical decoupling with a superconducting flux qubit. *Nature Phys.* **7,** 565–570 (2011).
33. Paik, H. *et al.* How coherent are Josephson junctions? Preprint at (http://arxiv.org/abs/1105.4652v1) (2011).

Acknowledgements We thank S. Filipp, A. Blais for useful discussions and K. Pakrouski for his contributions in early stages of the experimental work. This work was supported by the Swiss National Science Foundation, the EU IP SOLID and ETH Zurich.

Author Contributions A.F. developed the scheme to realize the Toffoli gate. L.S., A.F. and M.B. carried out the experiments and analysed the data. L.S. designed and fabricated the superconducting resonator. A.F. and M.B. designed and fabricated the qubits. M.P.d.S. provided general theoretical support and specific advice on using Monte Carlo process certification. A.F., L.S., M.B. and A.W. contributed to setting up and maintaining the experiment. A.F., A.W. and L.S. wrote the manuscript. All authors commented on the manuscript. A.W. supervised the project.

Author Information Reprints and permissions information is available at www.nature.com/reprints. The authors declare no competing financial interests. Readers are welcome to comment on the online version of this article at www.nature.com/nature. Correspondence and requests for materials should be addressed to A.F. (fedoroar@phys.ethz.ch) or A.W. (andreas.wallraff@phys.ethz.ch).

LETTER

doi:10.1038/nature10704

Charge order and three-site distortions in the Verwey structure of magnetite

Mark S. Senn[1], Jon P. Wright[2] & J. Paul Attfield[1]

The mineral magnetite (Fe_3O_4) undergoes a complex structural distortion and becomes electrically insulating at temperatures less than 125 kelvin. Verwey proposed in 1939 that this transition is driven by a charge ordering of Fe^{2+} and Fe^{3+} ions[1], but the ground state of the low-temperature phase has remained contentious[2,3] because twinning of crystal domains hampers diffraction studies of the structure[4]. Recent powder diffraction refinements[5–7] and resonant X-ray studies[8–12] have led to proposals of a variety of charge-ordered and bond-dimerized ground-state models[13–19]. Here we report the full low-temperature superstructure of magnetite, determined by high-energy X-ray diffraction from an almost single-domain, 40-micrometre grain, and identify the emergent order. The acentric structure is described by a superposition of 168 atomic displacement waves (frozen phonon modes), all with amplitudes of less than 0.24 ångströms. Distortions of the FeO_6 octahedra show that Verwey's hypothesis is correct to a first approximation and that the charge and Fe^{2+} orbital order are consistent with a recent prediction[17]. However, anomalous shortening of some Fe–Fe distances suggests that the localized electrons are distributed over linear three-Fe-site units, which we call 'trimerons'. The charge order and three-site distortions induce substantial off-centre atomic displacements and couple the resulting large electrical polarization to the magnetization. Trimerons may be important quasiparticles in magnetite above the Verwey transition and in other transition metal oxides.

The cubic spinel type structure of magnetite distorts to a monoclinic superstructure with *Cc* space group symmetry below the $T_V \approx 125$ K Verwey transition[4,20]. *Cc* domains[21] ~1 μm in size are formed in up to 24 orientations within magnetite crystals, and microtwinning of these domains severely hampers diffraction studies. We have investigated the use of small magnetite grains as potential single-domain crystals for high-energy X-ray structure analysis (Fig. 1). In the smallest and least-twinned grain of many that we investigated, 89% of the scattering was from a single orientation and 11% was from a secondary domain (Fig. 1a). The *Cc* crystal structure was determined using 91,433 symmetry-unique Bragg reflections from this 40-μm grain (see Methods Summary and Supplementary Information for details of the structure and derived quantities used below). No further superstructure or lowering of space group symmetry below *Cc* was evident in the diffraction data.

The low-temperature *Cc* crystal structure of magnetite has 168 variable (x, y, z) atomic coordinates, of which 166 are independent and two are constrained to fix the cell origin. The coordinates are equivalently described by the same number of amplitudes of frozen displacement waves (phonons), all with values $q < 0.24$ Å, as shown graphically in Fig. 2. Only one of these (an O-site Γ-mode) is present in the high-temperature cubic structure and the remainder all freeze at the Verwey transition. The three largest-amplitude modes have Δ_5 symmetry and are acentric, heralding the large off-centre structural distortions described later, but the smoothly varying distribution of amplitudes shows that many centric and acentric Δ, X and W modes contribute significantly. Hence, the superstructure is not approximated well by a few frozen phonons, and even attempts to describe the important features with up to 100 lattice modes were unsuccessful.

Magnetite has an AB_2O_4 spinel structure in which Fe^{3+} occupies the tetrahedrally coordinated A cation sites, and a 1:1 order of Fe^{2+} and Fe^{3+} is expected over the 16 inequivalent octahedral B sites of the *Cc* superstructure in the Verwey hypothesis. Each B-site FeO_6 octahedron has an irregular distortion from which the amplitudes of radial expansion (breathing) local modes (Q_{Rad}) and tetragonal Jahn–Teller (Q_{JT}) local modes were extracted because these are sensitive to charge-ordering and associated orbital-ordering displacements. For Q_{JT} we find a bimodal Verwey-type distribution (Fig. 3a) in which eight near-zero values are consistent with Fe^{3+}, which is Jahn–Teller inactive as the high-spin $3d^5$ electron configuration is non-degenerate. The other eight Q_{JT} values are negative as expected for $3d^6$ Fe^{2+}, where tetragonal Jahn–Teller compression removes the degeneracy created by the extra electron occupying one of the three t_{2g} symmetry d orbitals (d_{xy}, d_{xz} or d_{yz}). In addition, the plot of Q_{Rad} (the increase in octahedral average Fe–O bond distance) against Q_{JT} shows that the eight Jahn–Teller-distorted B sites are also the eight most expanded, consistent with Fe^{2+}, and that the eight undistorted sites are the least expanded, as expected for Fe^{3+}. The bimodal distribution of tetragonal distortions and their correlation with the radial amplitudes demonstrate experimentally that Verwey's Fe^{2+}–Fe^{3+} ordering hypothesis is correct to a useful first approximation. However, the distribution of Q_{Rad} and

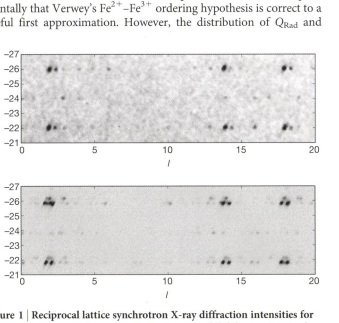

Figure 1 | Reciprocal lattice synchrotron X-ray diffraction intensities for magnetite microcrystal grains at 90 K. Sections of $(h\ k\ l)$ intensities in the $h = 50$ plane are shown. **a**, Intensities for an approximately spherical grain of diameter 40 μm, which was used to determine the crystal structure. The microcrystal is almost single domain; faint spots to the right of the main intensities reveal the secondary twin. **b**, Intensities from an irregular grain of dimension ~100 μm showing multiple twin domains.

[1]Centre for Science at Extreme Conditions and School of Chemistry, University of Edinburgh, West Mains Road, Edinburgh EH9 3JZ, UK. [2]European Synchrotron Radiation Facility, 6 rue Jules Horowitz, BP 220, 38043 Grenoble Cedex 9, France.

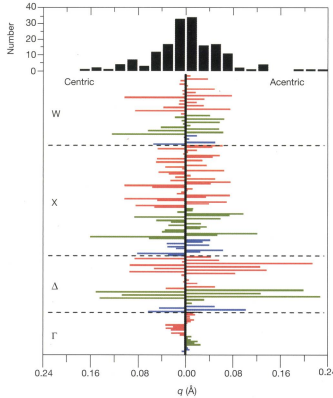

Figure 2 | The 168 displacement amplitudes of the low-temperature *Cc* magnetite structure. Main panel: centric and acentric mode amplitudes, q, which have estimated standard deviations <0.003 Å. Top panel: distribution of amplitudes. A, B and O atom modes of the cubic *Fd*$\bar{3}$*m* AB_2O_4 spinel type structure are coloured blue, green and red, respectively. The displacement waves have periodicities corresponding to the Γ (0, 0, 0), Δ (0, 1/2, 0), X (0, 1, 0) and W (1/2, 1, 0) points in the Brillouin zone of the cubic structure. Many acentric and centric Δ, X and W modes involving the B and O sites contribute significantly to the overall superstructure, but the Γ modes are less important.

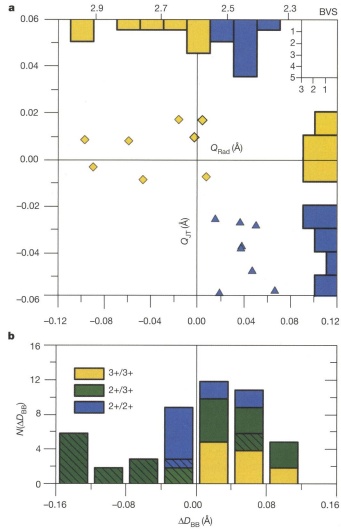

Figure 3 | Local distortion distributions that reveal electronic order in the low-temperature magnetite structure. **a**, Plot of local distortions for the 16 distinct FeO_6 octahedra. Q_{Rad} and Q_{IT} are the amplitudes of the radial (breathing) and tetragonal Jahn–Teller distortions. Their estimated standard deviations of <0.002 Å are smaller than the symbols shown. Q_{Rad} is the difference between the average Fe–O bond distance in an FeO_6 octahedron and the average over all octahedra. The points fall into two groups describing characteristic local distortions for Fe^{2+} and Fe^{3+} (blue and yellow bars and symbols, respectively). The distributions of the two modes (inside top and right edges of plot, with scales top right) show that there is bimodal segregation of the Q_{IT} amplitudes but that the Q_{Rad} dispersion is more continuous. BVS estimates of formal Fe charge are shown above the Q_{Rad} distribution. **b**, Distribution of the 48 distinct Fe–Fe distances between neighbouring B sites, relative to the average D_{BB} (= 2.967 Å), coloured according to the Fe charge states. The 16 distances from the eight Fe^{2+} sites to their two neighbours perpendicular to the local orbital ordering axis (Fe^{2+} in 15 cases and Fe^{2+} once) are hatched. The anomalous shortening of most of these distances indicates the linear three-site (trimeron) distortions as shown in Fig. 4c.

equivalent bond valence sum (BVS) estimates of formal Fe charge (Fig. 3a) does not seem bimodal, indicating the more complex electronic order described later.

The average BVS formal oxidation states for the eight Fe^{2+}- and Fe^{3+}-like B sites in the *Cc* magnetite structure are 2.47 and 2.75, respectively, consistent with an earlier partial refinement[5,6] and structural results for other charge-ordered transition metal oxides[22]. The Fe^{2+}–Fe^{3+} arrangement (Fig. 4a) differs from the original prediction of Verwey[23], but the charge and Fe^{2+} orbital ordering (Fig. 4b) are in agreement with a recent model based on electronic structure calculations[17]. The arrangement is close to a centric structure in which the Fe^{2+} states form chains of corner-linked $(Fe^{2+})_3$ triangles, but with a neighbouring Fe^{2+}–Fe^{3+} pair exchanged at every fourth triangle as shown (Fig. 4a). Anderson's condition[24] that each tetrahedron of four neighbouring B sites should contain two Fe^{2+} ions is only satisfied in a quarter of the tetrahedra. The complexity of the charge and orbital ordering may be explained in part by the distribution of Jahn–Teller distortions. The octahedral compressions of the 16 Fe^{2+} sites in the basic cell act parallel to the a, b, and c axes of the high-temperature cubic lattice in a 5:5:6 ratio that minimizes strain in the highly connected spinel lattice. More-symmetric charge and orbital orderings tend to have less equal ratios. The small anisotropy arising from excess distortion in the c direction may account for the change in magnetic easy-axis from cubic [111] to [001] at temperatures less than T_V.

Edge sharing of FeO_6 octahedra allows direct B–B electronic interactions within linear chains that extend in six directions. The nearest-neighbour B–B distances, D_{BB}, are all equivalent in the cubic magnetite structure, but $D_{BB}(Fe^{2+}–Fe^{3+})$, the nearest-neighbour Fe^{2+}–Fe^{3+} distance, in particular shows a wide distribution in the Verwey phase (Fig. 3b). Electrostatic repulsions tend to disperse the distance values such that $D_{BB}(Fe^{2+}–Fe^{2+}) < D_{BB}(Fe^{2+}–Fe^{3+}) < D_{BB}(Fe^{3+}–Fe^{3+})$, so the observed tail of anomalously short Fe^{2+}–Fe^{3+} distances is not expected in a Verwey model and indicates magnetically driven B–B bonding by the additional t_{2g} electrons. (The five parallel unpaired d-electron spins at all B sites are ferromagnetically ordered below the Curie temperature (858 K), so only the additional electron from each $3d^6$ Fe^{2+} state has an opposed, minority, spin and may be delocalized between B sites through bonding.)

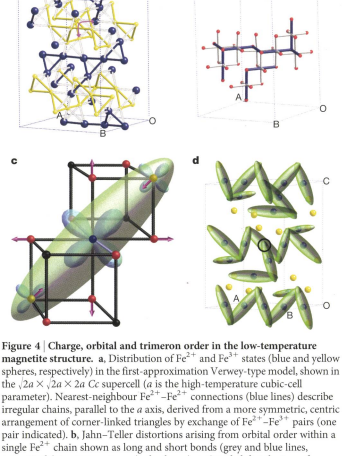

Figure 4 | Charge, orbital and trimeron order in the low-temperature magnetite structure. **a**, Distribution of Fe^{2+} and Fe^{3+} states (blue and yellow spheres, respectively) in the first-approximation Verwey-type model, shown in the $\sqrt{2}a \times \sqrt{2}a \times 2a$ *Cc* supercell (*a* is the high-temperature cubic-cell parameter). Nearest-neighbour Fe^{2+}–Fe^{2+} connections (blue lines) describe irregular chains, parallel to the *a* axis, derived from a more symmetric, centric arrangement of corner-linked triangles by exchange of Fe^{2+}–Fe^{3+} pairs (one pair indicated). **b**, Jahn–Teller distortions arising from orbital order within a single Fe^{2+} chain shown as long and short bonds (grey and blue lines, respectively) to oxygen atoms (red spheres). **c**, Coupled distribution of a minority-spin electron (with approximate atomic populations indicated by the sizes of blue t_{2g} orbitals) and associated atomic displacements (purple arrows) within a linear three-Fe-site (trimeron) unit. Orbital order at the central Fe^{2+} site (blue) localizes the minority-spin electron in one of the t_{2g} orbitals and elongates the four Fe–O bonds perpendicular to the local Jahn–Teller axis. Weak bonding interactions transfer minority-spin density into coplanar t_{2g} orbitals at two neighbouring B sites (shown as yellow Fe^{2+}) and shorten the Fe–Fe distances. The minority-spin electron density is approximated by a scalene ellipsoid encompassing the three Fe sites. Other B-site Fe^{2+} or Fe^{3+} neighbours (black spheres) do not participate. **d**, Trimeron distribution in the low-temperature magnetite structure, following the experimentally observed distortions, with Fe^{2+} and Fe^{3+} states shown as blue and yellow spheres, respectively, and trimeron ellipsoids as in **c**. The trimerons are mainly end-linked through Fe^{3+} ions, but one trimeron is terminated by an Fe^{2+} ion (circled). Some Fe^{3+} sites do not participate in any trimerons.

Chains of alternating short and long B–B distances are predicted in bond-dimerized models[13,16,19], but are not observed in our structure. Instead, the two B–B distances perpendicular to the local orbital-ordering axis at each of the eight Fe^{2+} positions both tend to be shortened: this is the case for 14 of these 16 distances (Fig. 3b, hatched). This suggests that minority-spin t_{2g} electron density is significantly delocalized from an Fe^{2+} donor onto two adjacent B-site acceptors, which are usually Fe^{3+} sites. This single charge, delocalized over three B sites with associated displacements of the two acceptor B sites and surrounding oxygen atoms (Fig. 4c), corresponds to a highly structured small polaron that may be described as a 'trimeron', by analogy with dimeron quasiparticles in $La_{1-x}Ca_xMnO_3$ (ref. 25). Fifteen of the 16 trimeron acceptor sites are Fe^{3+} ions, but one Fe^{2+} (Fig. 4d, circled) accepts into a t_{2g} orbital that is orthogonal to its own trimeron. Trimeron distortions are intrinsically symmetric (having $D_{BB} = 2.832$ and 2.848 Å in the most regular environment of the *Cc* structure, where $D_{BB} = 2.967$ Å on average), but asymmetric connectivity leads to off-centre distortions and long B–B bonds in 2 of 16 cases.

The linear three-site (trimeron) distortions (Fig. 4d) significantly perturb charge order in the *Cc* magnetite structure and couple the magnetism to the complex overall distortion. Only two B ions are available per minority-spin electron, so trimeron units are constrained to share sites. End-sharing connections with angles of 60°, 120° and 180° are possible, but 180° linkages are apparently avoided to maximize charge transfer because two or three different t_{2g} orbitals are used by an Fe^{3+} ion participating in two or three trimerons. This is analogous to the formation of two or three short *cis*-bonds in some d^0 transition metal oxides and oxynitrides[26], and creates off-centre Fe^{3+} displacements that contribute strongly to the acentric lattice modes and electric polarization. High connectivity seems favourable because four of the eight Fe^{3+} sites participate in the maximum of three trimerons. The orderings of linear three-site, one-electron units along the infinite B chains correspond to charge density waves with wavevector magnitude $q_c = 1/N$ for a repeat sequence of one trimeron for every *N* B sites. The structural average is $q_c = 1/6$ but only chains with $q_c = 0$, 1/8 and 1/4 are present, in a 1:6:5 ratio. The unique $q_c = 0$ chain contains only Fe^{2+} ions (Fig. 4a, b) but their three-site distortions are always within other chains.

The linear three-site distortions we attribute to trimerons also account for the non-Verwey distribution of radial amplitudes (Q_{Rad}) and BVS values for the B-site FeO_6 octahedra (Fig. 3a). Each Fe^{2+} ion donates minority-spin t_{2g} electron density to two B-site acceptors within a trimeron (Fig. 4c), so the eight Fe^{2+}-like sites have a narrow Q_{Rad} distribution and BVS ≈ 2.4. However, Fe^{3+} ions are acceptors in varying numbers of trimerons. Two Fe^{3+} sites do not participate in any trimerons and so have the two lowest Q_{Rad} values and the highest B-site BVS values, ~3.0 (Fig. 3a). The other six Fe^{3+} sites are acceptors for one to three trimerons and thus have a spread of higher Q_{Rad} values and lower valences with BVS ≈ 2.6–2.8. Charge transfer within trimerons tends to equalize the electron density across B sites: in the limit of maximum donor-to-acceptor transfers (of 0.2*e*, where *e* is the electron charge), an Fe^{3+} ion participating in three trimerons has the same formal charge, +2.4*e*, as the Fe^{2+} donor sites. However, the two states are still distinguished by their minority-spin t_{2g} distributions, as the former site has populations $d_{xy}^{0.2}d_{xz}^{0.2}d_{yz}^{0.2}$ that preserve the high symmetry of Fe^{3+}, whereas the latter has a distribution such as $d_{xy}^{0.6}d_{xz}^{0}d_{yz}^{0}$, retaining the orbital order of Fe^{2+}. This justifies the use of formal valence states to describe charge-ordered structures even when the apparent charge separations are small, as here in magnetite.

The discovery of multiferroism in charge-ordered $LuFe_2O_4$ (ref. 27) has led to recent interest in the coupling of magnetism and the ferroelectric polarization expected in the acentric *Cc* magnetite superstructure[16,17]. Measured electric polarization values of $P = 0.05\,C\,m^{-2}$ for magnetite crystals and thin films agree with estimates from previous structural models[17], but an $Fe^{2.5+}$–Fe^{3+}–O^{2-} point-charge calculation for our structure gives a polarization larger by an order of magnitude ($P_a = 0.118\,C\,m^{-2}$, $P_c = 0.405\,C\,m^{-2}$; $P = 0.422\,C\,m^{-2}$; where P_a and P_c are the respective magnitudes of the polarization vector components parallel to the crystallographic *a* and *c* axes and *P* is the magnitude of the resultant polarisation vector). The same calculation with average $Fe^{2.5+}$ B-site charges gives similar results ($P_a = 0.080\,C\,m^{-2}$, $P_c = 0.346\,C\,m^{-2}$; $P = 0.355\,C\,m^{-2}$), showing that atomic displacements resulting from charge order and three-site distortions are responsible for most of the polarization, with exchange of Fe^{2+}–Fe^{3+} pairs (Fig. 4a) contributing only 16% of the total. The large P_c component, parallel to the magnetic easy axis, shows that a substantial magnetoelectric coupling is expected in single magnetite domains.

Lattice effects in the cubic phase of magnetite are indicated by diffuse scattering above the Verwey transition[12,28] and a continuous increase in the electrical conductivity up to a maximum at ~$3T_V$. Hence, trimeron fluctuations may be important quasiparticles in the

cubic phase. The expected entropy change at the Verwey transition is conventionally assumed to be $R\ln(4) = 1.4R$ (where R is the molar gas constant) for full disorder of Fe^{2+} and Fe^{3+} charges, but our structure shows that this change should be $R\ln(12) = 2.5R$ for additional randomization of the triply degenerate Fe^{2+} orbital states. Hence, the observed entropy change of ~0.7R corresponds to only 30% of the possible disorder at T_V (ref. 29). Previous estimates have used Anderson's condition or other charge configurations within tetrahedra of four B sites, but trimeron-based models may provide alternative predictions. An approximate calculation based on the above local connectivity of Fe^{2+} sites reduces the predicted transition entropy from 2.5R to 2.1R (or from 1.4R to 1.0R if orbital states are neglected), but these estimates are still greater than the observed value and suggest that trimeron or other correlations persist at temperatures greater than T_V.

This investigation shows that single domains of the Verwey phase may be accessible in ~10–50-μm grains for future low-temperature studies of magnetite. Self-organization of the charge and orbital states couples the spin order of this eponymous magnetic material to the complex Verwey distortion. Trimerons may be important quasiparticles above the Verwey transition and may also be relevant to other transition metal oxides such as superconducting $LiTi_2O_4$ spinel. Finally, we note that a full *ab initio* simulation of the low-temperature magnetite structure starting from calculations on the cubic state presents a future challenge to improve understanding of the Verwey phase, now that the experimental structure has been determined.

METHODS SUMMARY

Grains from a highly stoichiometric powder used in previous studies[6,8,8] were placed in a 100-μm, focused monochromatic beam (wavelength, 0.16653(1) Å; estimated standard deviation shown in parenthesis) on the ID11 diffractometer at ESRF, Grenoble. Multiple scattering and extinction problems were reduced by using small crystallites and a high X-ray energy (74 keV), which also gave access to an abundance of diffraction peaks at very high momentum transfer and reduced absorption effects. Crystals were aligned and de-twinned using a permanent magnet (producing a field of approximately 0.1 T at the sample), and were verified as being cubic single domains at 130 K before cooling through the Verwey transition to 90 K.

The grain used for structure determination was approximately spherical with diameter ~40 μm. We used ω-scans with varying exposure times to increase the dynamic range of the data from the charge-coupled-device detector (Frelon2K camera) and these were performed at azimuthal angles ϕ and $\phi + 180°$ to improve data redundancy and test for multiple scattering. Reciprocal lattice sections (Fig. 1a) were reconstructed using local software. Small-box integrations were used to identify the orientation of the two observed domains, and large-box integration was performed to encompass intensity from both domains and allow structure refinement as a pseudo-merohedral twin.

Two thousand starting models were generated by applying random atomic displacements to the high-temperature structure and were optimized by least-squares refinement. A global minimum at residual $R[F^2 > 4\sigma] = 4.99\%$ (where F and σ are the observed magnitude and standard deviation of a structure factor) was observed most frequently (292 times), in addition to local refinement minima ($R[F^2 > 4\sigma] \cong 5.88\%$). The final refinement of the global minimum model used independent anisotropic thermal parameters for all atoms and all data to a resolution of $d \cong 0.3$ Å, giving R values $R[F^2 > 4\sigma] = 3.40\%$, $R[F^2] = 5.18\%$ and weighted residual $wR_2 = 6.96\%$. Full crystallographic information and details of the analysis software are given in Supplementary Information.

Received 1 June; accepted 8 November 2011.
Published online 21 December 2011.

1. Verwey, E. J. W. Electronic conduction of magnetite (Fe_3O_4) and its transition point at low temperatures. *Nature* **144,** 327–328 (1939).
2. Walz, F. The Verwey transition: a topical review. *J. Phys. Condens. Matter* **14,** R285–R340 (2002).
3. Coey, M. Condensed-matter physics: charge-ordering in oxides. *Nature* **430,** 155–157 (2004).
4. Iizumi, M. *et al.* Structure of magnetite (Fe_3O_4) below the Verwey transition-temperature. *Acta Crystallogr. B* **38,** 2121–2133 (1982).
5. Wright, J. P., Attfield, J. P. & Radaelli, P. G. Long range charge ordering in magnetite below the Verwey transition. *Phys. Rev. Lett.* **87,** 266401 (2001).
6. Wright, J. P., Attfield, J. P. & Radaelli, P. G. Charge ordered structure of magnetite Fe_3O_4 below the Verwey transition. *Phys. Rev. B* **66,** 214422 (2002).
7. Blasco, J., Garcia, J. & Subias, G. Structural transformation in magnetite below the Verwey transition. *Phys. Rev. B* **83,** 104105 (2011).
8. Goff, R. J., Wright, J. P., Attfield, J. P. & Radaelli, P. G. Resonant X-ray diffraction study of the charge ordering in magnetite. *J. Phys. Condens. Matter* **17,** 7633–7642 (2005).
9. Nazarenko, E. *et al.* Resonant X-ray diffraction studies on the charge ordering in magnetite. *Phys. Rev. Lett.* **97,** 056403 (2006).
10. Joly, Y. *et al.* Low-temperature structure of magnetite studied using resonant X-ray scattering. *Phys. Rev. B* **78,** 134110 (2008).
11. Bland, S. R. *et al.* Full polarization analysis of resonant superlattice and forbidden X-ray reflections in magnetite. *J. Phys. Condens. Matter* **21,** 485601 (2009).
12. Lorenzo, J. E. *et al.* Charge and orbital correlations at and above the Verwey phase transition in magnetite. *Phys. Rev. Lett.* **101,** 226401 (2008).
13. Seo, H., Ogata, M. & Fukuyama, H. Aspects of the Verwey transition in magnetite. *Phys. Rev. B* **65,** 085107 (2002).
14. Jeng, H. T., Guo, G. Y. & Huang, D. J. Charge-orbital ordering and Verwey transition in magnetite. *Phys. Rev. Lett.* **93,** 156403 (2004).
15. Jeng, H. T., Guo, G. Y. & Huang, D. J. Charge-orbital ordering in low-temperature structures of magnetite: GGA+U investigations. *Phys. Rev. B* **74,** 195115 (2006).
16. van den Brink, J. & Khomskii, D. I. Multiferroicity due to charge ordering. *J. Phys. Condens. Matter* **20,** 434217 (2008).
17. Yamauchi, K., Fukushima, T. & Picozzi, S. Ferroelectricity in multiferroic magnetite Fe_3O_4 driven by noncentrosymmetric Fe^{2+}/Fe^{3+} charge-ordering: first-principles study. *Phys. Rev. B* **79,** 212404 (2009).
18. Zhou, F. & Ceder, G. First-principles determination of charge and orbital interactions in Fe_3O_4. *Phys. Rev. B* **81,** 205113 (2010).
19. Fukushima, T., Yamauchi, K. & Picozzi, S. Ab initio investigations of Fe^{2+}/Fe^{3+} bond dimerization and ferroelectricity induced by intermediate site/bond-centered charge ordering in magnetite. *J. Phys. Soc. Jpn* **80,** 014709 (2011).
20. Yoshida, J. & Iida, S. X-ray-diffraction study on low-temperature phase of magnetite. *J. Phys. Soc. Jpn.* **42,** 230–237 (1977).
21. Kasama, T., Church, N. S., Feinberg, J. M., Dunin-Borkowski, R. E. & Harrison, R. J. Direct observation of ferrimagnetic/ferroelastic domain interactions in magnetite below the Verwey transition. *Earth Planet. Sci. Lett.* **297,** 10–17 (2010).
22. Attfield, J. P. Charge ordering in transition metal oxides. *Solid State Sci.* **8,** 861–867 (2006).
23. Verwey, E. J. W. & Heilmann, E. L. Physical properties and cation arrangement of oxides with spinel structures. I. Cation arrangement in spinels. *J. Chem. Phys.* **15,** 174–180 (1947).
24. Anderson, P. W. Ordering and antiferromagnetism in ferrites. *Phys. Rev.* **102,** 1008–1013 (1956).
25. Downward, L. *et al.* Universal relationship between magnetization and changes in the local structure of $La_{1-x}Ca_xMnO_3$: evidence for magnetic dimers. *Phys. Rev. Lett.* **95,** 106401 (2005).
26. Yang, M. H. *et al.* Anion order in perovskite oxynitrides. *Nat. Chem.* **3,** 47–52 (2011).
27. Ikeda, N. *et al.* Ferroelectricity from iron valence ordering in the charge-frustrated system $LuFe_2O_4$. *Nature* **436,** 1136–1138 (2005).
28. Yamada, Y., Wakabayashi, N. & Nicklow, R. M. Neutron diffuse-scattering in magnetite due to molecular polarons. *Phys. Rev. B* **21,** 4642–4648 (1980).
29. Shepherd, J. P., Koenitzer, J. W., Aragon, R., Sandberg, C. J. & Honig, J. M. Heat-capacity studies on single-crystal annealed Fe_3O_4. *Phys. Rev. B* **31,** 1107–1113 (1985).

Supplementary Information is linked to the online version of the paper at www.nature.com/nature.

Acknowledgements We thank C. Morrison for supplying code for electrical polarization calculations, J. Honig for provision of the magnetite sample, the Leverhulme Trust for financial support, and EPSRC and STFC for financial support and provision of continuing access to ESRF.

Author Contributions J.P.A. and J.P.W. designed the study, data were collected and analysed by M.S.S. and J.P.W., and J.P.A. wrote the paper with contributions from M.S.S. and J.P.W.

Author Information Reprints and permissions information is available at www.nature.com/reprints. The authors declare no competing financial interests. Readers are welcome to comment on the online version of this article at www.nature.com/nature. Correspondence and requests for materials should be addressed to J.P.A. (j.p.attfield@ed.ac.uk) or J.P.W. (wright@esrf.fr).

LETTER

doi:10.1038/nature10687

Modelling the rheology of MgO under Earth's mantle pressure, temperature and strain rates

Patrick Cordier[1], Jonathan Amodeo[1] & Philippe Carrez[1]

Plate tectonics, which shapes the surface of Earth, is the result of solid-state convection in Earth's mantle over billions of years. Simply driven by buoyancy forces, mantle convection is complicated by the nature of the convecting materials, which are not fluids but polycrystalline rocks. Crystalline materials can flow as the result of the motion of defects—point defects, dislocations, grain boundaries and so on. Reproducing in the laboratory the extreme deformation conditions of the mantle is extremely challenging. In particular, experimental strain rates are at least six orders of magnitude larger than in nature[1]. Here we show that the rheology of MgO at the pressure, temperature and strain rates of the mantle is accessible by multiscale numerical modelling starting from first principles and with no adjustable parameters. Our results demonstrate that extremely low strain rates counteract the influence of pressure. In the mantle, MgO deforms in the athermal regime and this leads to a very weak phase. It is only in the lowermost lower mantle that the pressure effect could dominate and that, under the influence of lattice friction, a viscosity of the order of 10^{21}–10^{22} pascal seconds can be defined for MgO.

So far, experimental studies have dominated the contribution of mineral physics to the study of mantle rheology. Experiments are usually designed to describe how a solid deforms under a constant load (creep tests) or how stress evolves with strain at a constant strain rate. The current challenge is to perform such experiments under pressures (P) representative of the mantle (that is, up to ~135 GPa), and several studies have achieved this[2]. The simultaneous determination of the strain rate ($\dot{\varepsilon}$) and of the deviatoric stress (σ) is necessary to parameterize semi-empirical constitutive flow laws, $\dot{\varepsilon}=f(\sigma,T,P)$ (often of power-law form[3,4]), which are used for extrapolation to natural conditions (here T is temperature). A major difficulty is that strain rates available in the laboratory are of the order of 10^{-6}–$10^{-3}\,s^{-1}$, very different from natural strain rates (10^{-12}–$10^{-16}\,s^{-1}$). Although this issue was recognized early on[1,5], it has received very little attention, if any, in recent years. Here we propose a physically based model able to describe the rheology of MgO (the magnesium end-member of the second most abundant phase of the lower mantle, ferropericlase (Mg, Fe)O) under very low strain rates representative of mantle convection.

For all crystalline materials, the critical resolved shear stress (CRSS) for plastic yielding follows the same general evolution with temperature (Fig. 1). At 0 K, dislocations move under the influence of stress only. This stress is called the Peierls stress. It measures the intrinsic lattice friction opposed to plastic shear[6]. At finite temperature, dislocation motion is assisted by thermal activation and by stress[7]. A strongly thermally activated regime is observed (Fig. 1) when plastic shear is governed by the intrinsic mobility of dislocations. A microscopic constitutive equation, called the Orowan equation, describes flow in this regime:

$$\dot{\varepsilon}=\rho b v \tag{1}$$

Here ρ is the mobile dislocation density, b is the Burgers vector modulus and v is the average dislocation velocity. Above a critical temperature, T_a (called the athermal temperature), thermal activation is sufficient to overcome lattice friction and plastic shear is essentially athermal, only constrained by the interactions between dislocations. These fundamental features are the basis of our model for the rheology of MgO.

In materials science, multiscale modelling has been developed to link our understanding of a few elementary mechanisms (usually at the

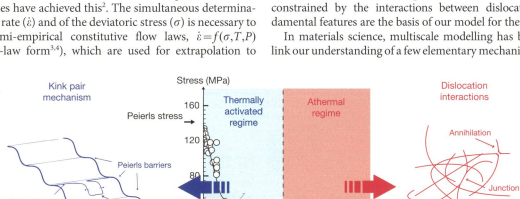

Figure 1 | Evolution of the critical resolved shear stress (CRSS) with temperature. Centre panel, CRSS versus temperature for ½<110>{110} glide in MgO at ambient pressure; symbols show experimental data (see Supplementary Information for more details), and the line corresponds to our model[12]. As the temperature is increased from 0 K (at which the CRSS is the Peierls stress), the CRSS is strongly temperature dependent until the athermal temperature, T_a, is reached. Below T_a, lattice friction dominates (blue area, 'thermally activated regime') and plastic flow is controlled by the mobility of dislocations governed by the kink-pair mechanism (left panel). Above T_a, plastic flow is essentially athermal (pink area, 'athermal regime', line reaches a plateau) and dislocation interactions dominate (right panel).

[1]Université Lille 1, Unité Matériaux et Transformations, UMR CNRS 8207, F-59650 Villeneuve d'Ascq, France.

microscopic scale) with behaviour observed at the macroscopic scale, which might be well characterized but which remains poorly understood[8–10]. For plastic deformation, the absence of a global theory results from the range of length scales and timescales spanned. Crystalline plasticity results from the motion of crystal defects: point defects, linear defects (dislocations) or two-dimensional defects (grain boundaries, twin boundaries). The motion of dislocations generally represents the most efficient strain-producing mechanism. Recent calculations[11] have shown that very small grain sizes (100 μm–1 mm) would be required for point defect diffusion to dominate the rheology of the lower mantle. Moreover, mantle temperatures reach only 40–50% of the melting temperature of MgO, which is a very refractory oxide. In the present study, we focus on the contribution of dislocation glide to the rheology of MgO.

We have recently proposed a multiscale model of plasticity that combines three modelling ingredients in a logical chain[12]. As described in Methods, our approach starts with atomistic calculations of dislocation cores, which have a paramount influence on dislocation mobility[13]. This mobility is then modelled in the thermally activated regime using the kink-pairs formalism[14,15] (see below). Finally, above the athermal temperature, T_a, plastic flow is described within realistic dislocation dynamics (DD) simulations[16]. This multiscale approach has been applied to MgO and has shown its efficiency in reproducing the evolution with temperature of the CRSS observed experimentally (Fig. 1). This model is also able to describe the influence of pressure on the plasticity of MgO (ref. 17). In the range of conditions relevant to Earth's mantle, pressure affects the electronic structure and bonding of MgO and has a strong influence on the core structure and mobility of dislocations. This results in an inversion of slip systems from ½<110>{110} to ½<110>{100} under the influence of pressure. Another effect of pressure is to shift T_a towards higher temperatures. At high pressure (and laboratory strain rates), MgO becomes a material characterized by a large lattice friction.

Our physically based description of the mobility of dislocations gives us the capability of modelling the influence of strain rate on the rheology of MgO. Overcoming the Peierls energy barrier requires nucleation of a critical bowing-out (called a kink-pair) of the dislocation line by thermal fluctuations. Rapid lateral motion of the kinks brings the dislocation line into the next low-energy position (Fig. 1). The nucleation rate of kink-pairs is thus generally assumed to limit

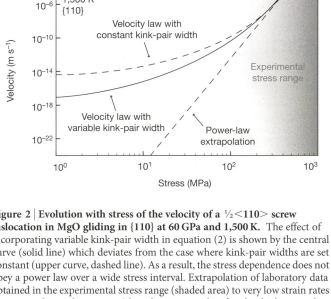

Figure 2 | Evolution with stress of the velocity of a ½<110> screw dislocation in MgO gliding in {110} at 60 GPa and 1,500 K. The effect of incorporating variable kink-pair width in equation (2) is shown by the central curve (solid line) which deviates from the case where kink-pair widths are set constant (upper curve, dashed line). As a result, the stress dependence does not obey a power law over a wide stress interval. Extrapolation of laboratory data obtained in the experimental stress range (shaded area) to very low strain rates (corresponding to low stresses) based on a power law fitted to high-stress data (straight dashed line) is thus invalid.

the dislocation velocity[18]. As a result of this mechanism, the average velocity of a moving dislocation (of length L) over a Peierls barrier of width a' can be written as[19]

$$v(\tau,T)=\frac{\nu_D a' bL}{w^2}\exp\left(\frac{-\Delta H_0}{kT}\right)\sinh\left(\frac{\Delta H_0-\Delta H(\tau)}{kT}\right) \qquad (2)$$

where $\nu_D b/w$ is the vibration frequency for a thermal fluctuation of width w on the dislocation of Burgers vector modulus b (ν_D is the Debye frequency), L/w is twice the number of nucleation sites, $\Delta H(\tau)$ is the activation enthalpy of the kink-pair mechanism under an applied stress τ (ΔH_0 corresponds to the case where $\tau = 0$) and k is Boltzmann's constant. This formalism satisfactorily reproduces dislocation dynamics in the thermally activated regime[12,20,21]. To extend this formalism to a very low stress (or strain-rate) regime we (1) explicitly incorporate the stress dependence of the kink-pair width,

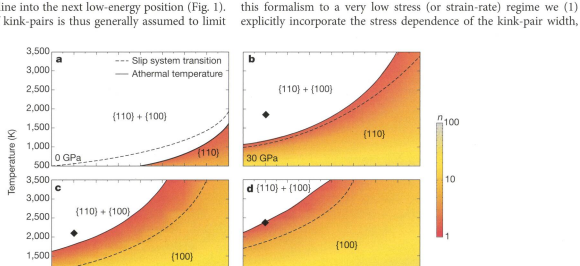

Figure 3 | Influence of the strain rate and of temperature on the deformation mechanisms of MgO at four pressures. a, 0 GPa; **b**, 30 GPa; **c**, 60 GPa; and **d**, 100 GPa. The line between the white and coloured regions corresponds to the athermal temperature, T_a. The domain shown white corresponds to the athermal regime. In the thermally activated domain (coloured regions), we have calculated and represented an apparent stress exponent, n (following the colour scale on the right). The dashed line separates domains where different slip systems dominate. The dominant glide planes are given. The filled diamond symbol represents average mantle conditions corresponding to these pressures[22].

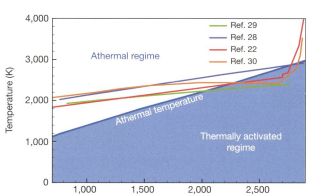

Figure 4 | Deformation mechanisms of MgO under mantle conditions, and a typical mantle strain rate of 10^{-16} s^{-1}. The athermal temperature is compared to several geotherms[22,28–30]. The exact interval where MgO deforms in the thermally activated regime depends on the thermal state of the mantle and, given lateral thermal heterogeneities[30], can vary significantly from place to place.

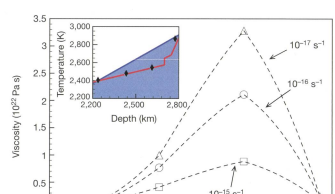

Figure 5 | MgO viscosity profile in the layer (shown in the inset) governed by the thermally activated deformation regime. Main panel, viscosity versus depth; dashed lines are a guide for the eye. We note that because decreasing the strain rate by an order of magnitude results in a very small variation of the stress, the viscosity increases when the strain rate decreases. The more the temperature departs from T_a within the thermally activated regime (blue area in the inset), the more pronounced this nonlinearity becomes. Inset, the depth interval between 2,200 and 2,800 km corresponding to the geotherm of ref. 22 within Fig. 4. The symbols along the geotherm (in red) correspond to the viscosity calculations.

$w(\tau)$, and of $\Delta H(\tau)$ as calculated from kink-pair theory (Supplementary Information), and (2) take into account possible backward and forward jumps of the kink-pair through the sinh function. Figure 2 shows that dislocation velocity curves bend significantly with decreasing stress (that is, decreasing strain rates). A power-law-based extrapolation (obtained from a linear approximation on a short stress interval in the high-stress regime) to low strain rates would underestimate the actual velocities.

The rheology of MgO in the thermally activated regime can be inferred from a combination of equations (1) and (2). The evolution with temperature of the CRSS (Supplementary Fig. 4) allows the determination of the athermal temperature, T_a, at which thermal activation overcomes lattice friction. Figure 3 shows that decreasing pressure, like decreasing strain rate, tends to shift T_a to lower values. At a given temperature and pressure, laboratory and natural strain rates may induce very different deformation mechanisms. For instance, at 60 GPa and 2,000 K, at laboratory strain rates, MgO deforms on $\frac{1}{2}\langle 110\rangle\{100\}$, under a CRSS of 215 MPa (due to lattice friction) and with a very nonlinear rheology (apparent stress exponent, $n = 13$). Decreasing the strain rate results in a decrease of the stress and of the stress exponent. The second slip system becomes active at 10^{-8} s^{-1} under a stress of 100 MPa. When a strain rate of $\sim 10^{-14}$ s^{-1} is reached, the rheology becomes linear. Below this strain rate, MgO deforms in the athermal regime; it becomes very plastic and insensitive to temperature and to strain rate.

The rheology of MgO as a function of temperature and strain rate, at four different pressures[22], is shown in Fig. 3. It appears that in most cases, the flow corresponds to deformation in the athermal regime, which can only be reached at very high temperatures at laboratory strain rates. All through the lower mantle, both slip systems, $\frac{1}{2}\langle 110\rangle\{110\}$ and $\frac{1}{2}\langle 110\rangle\{100\}$, are activated simultaneously. Figure 4 describes the evolution of the rheology of MgO with mantle depth. At depths less than ~2,000 km, MgO deforms in the athermal regime. In this regime, the flow stress is governed only by the dislocation microstructure, it is independent of strain rate and a viscosity cannot be defined[23]. In this athermal regime, MgO seems to be very weak (CRSS below 1 MPa for a dislocation density of 10^8 m^{-2}) and should be much weaker than Mg-silicate perovskite in similar conditions. Deeper than ~2,000 km, MgO enters a thermally activated regime. Only there can a viscosity be defined from the Orowan law. We find it to be of the order of 10^{21}–10^{22} Pa s, with a depth dependence shown in Fig. 5. In the vicinity of T_a, the rheology is close to linear and the viscosity is minimum. When the temperature departs from T_a, the viscosity increases and becomes more dependent on strain rate. Just above the core–mantle boundary, MgO can again enter a very weak, athermal regime. The depth and extent of this layer, characterized by a thermally activated regime, will depend on the thermal state of the lower mantle, as illustrated by Fig. 4, which displays several temperature profiles. The actual situation is probably even more complex, as large thermal heterogeneities (of the order of 1,000 K) are likely to be superimposed on these average temperature profiles[23].

Changes of the deformation mechanism of MgO could thus account for strong radial and lateral rheology heterogeneities inferred in the lowermost mantle[24], even in the absence of significant chemical heterogeneities. However, knowledge of the single-crystal rheology of both MgO and Mg-silicate perovskite will not on its own be enough to define the rheology of the mantle. Some form of even larger-scale modelling will be required, which can form a bridge between the scale of a mineral grain and the scale of a convection cell in a general circulation model of lower-mantle dynamics.

METHODS SUMMARY

In this study, we use the hierarchical multiscale approach developed in ref. 12 to model the plasticity of MgO single crystals. Atomistic dislocation core structures are modelled with a Peierls–Nabarro–Galerkin (PNG) approach[25]. The electronic structure is explicitly taken into account through γ-surfaces calculated *ab initio* using VASP[26]. The dislocation mobility, governed by equation (2), is controlled by kink-pair nucleation. The nucleation enthalpy of kink-pairs, $\Delta H(\tau)$, and the kink-pair geometry are evaluated using the elastic interaction method[27]. Low-stress effects are explicitly taken into account in equation (2) by considering the formal geometry of possible backward and forward kink-pairs. Mesoscopic-scale simulations of MgO deformation processes are performed by dislocation dynamics simulations[16] incorporating dislocation mobilities described by equation (2). The accuracy of such a multiscale model has been validated against room-pressure experimental data[12]. An extended description of the techniques is available in the online-only Methods section.

Full Methods and any associated references are available in the online version of the paper at www.nature.com/nature.

Received 3 June; accepted 25 October 2011.

1. Paterson, M. S. Problems in the extrapolation of laboratory rheological data. *Tectonophysics* **133,** 33–43 (1987).
2. Raterron, P. & Merkel, S. *In situ* rheological measurements at extreme pressure and temperature using synchrotron X-ray diffraction and radiography. *J. Synchrotron Radiat.* **16,** 748–756 (2009).
3. Poirier, J. P. *Creep of Crystals* (Cambridge Univ. Press, 1985).
4. Karato, S. *Deformation of Earth Materials: An Introduction to the Rheology of Solid Earth* (Cambridge Univ. Press, 2008).

5. Heard, H. C. Effect of large changes in strain rate in the experimental deformation of Yule marble. *J. Geol.* **71,** 162–195 (1963).
6. Peierls, R. The size of a dislocation. *Proc. Phys. Soc. Lond.* **52,** 34–37 (1940).
7. Caillard, D. & Martin, J. L. *Thermally Activated Mechanisms in Crystal Plasticity* (Pergamon, 2003).
8. Bulatov, V. V. & Kubin, L. P. Dislocation modelling at atomistic and mesoscopic scales. *Curr. Opin. Solid State Mater. Sci.* **3,** 558–561 (1998).
9. Needleman, A. Computational mechanics at the mesoscale. *Acta Mater.* **48,** 105–124 (2000).
10. de la Rubia, T. D. & Bulatov, V. V. Materials research by means of multiscale computer simulations. *Mater. Res. Soc. Bull.* **26,** 169–175 (2001).
11. Ammann, M. W., Brodholt, J. P., Wookey, J. & Dobson, D. P. First-principles constraints on diffusion in lower-mantle minerals and a weak D'' layer. *Nature* **465,** 462–465 (2010).
12. Amodeo, J., Carrez, P., Devincre, B. & Cordier, P. Multiscale modelling of MgO plasticity. *Acta Mater.* **59,** 2291–2301 (2011).
13. Cai, W., Bulatov, V. V., Chang, J., Li, J. & Yip, S. in *Dislocations in Solids* Vol. 12 (eds Nabarro, F. N. R. & Hirth, J. P.) 1–80 (Elsevier, 2004).
14. Seeger, A. & Schiller, P. Bildung und Diffusion von Kinken als Grundprozess der Versetzungsbewegung bei der Messung der inneren Reibung. *Acta Metall.* **10,** 348–357 (1962).
15. Guyot, P. & Dorn, J. E. A critical review of Peierls mechanism. *Can. J. Phys.* **45,** 983–1016 (1967).
16. Devincre, B., Kubin, L. P., Lemarchand, C. & Madec, R. Mesoscopic simulations of plastic deformation. *Mater. Sci. Eng. A* **309–310,** 211–219 (2001).
17. Amodeo, J., Carrez, P. & Cordier, P. Modelling the effect of pressure on the critical shear stress of MgO single crystals. *Phil. Mag.* (in the press).
18. Frost, H. J. & Ashby, M. F. *Deformation-Mechanism Maps: The Plasticity and Creep of Metals and Ceramics* (Pergamon, 1982).
19. Nabarro, F. R. N. One-dimensional models of thermal activation under shear stress. *Phil. Mag.* **83,** 3047–3054 (2003).
20. Tang, M., Kubin, L. P. & Canova, G. R. Dislocation mobility and the mechanical response of bcc crystals: a mesoscopic approach. *Acta Mater.* **46,** 3221–3235 (1998).
21. Monnet, G., Devincre, B. & Kubin, L. P. Dislocation study of prismatic slip systems and their interactions in hexagonal close packed metals: application to zirconium. *Acta Mater.* **52,** 4317–4328 (2004).
22. Ono, S. Experimental constraints on the temperature profile in the lower mantle. *Phys. Earth Planet. Inter.* **170,** 267–273 (2008).
23. Paterson, M. S. Relating experimental and geological rheology. *Int. J. Earth Sci.* **90,** 157–167 (2001).
24. Forte, A. M. & Mitrovica, J. X. Deep-mantle high-viscosity flow and thermochemical structure inferred from seismic and geodynamic data. *Nature* **410,** 1049–1056 (2001).
25. Denoual, C. Dynamic dislocation modeling by combining Peierls Nabarro and Galerkin methods. *Phys. Rev. B* **70,** 024106 (2004).
26. Kresse, G. & Hafner, J. Ab initio molecular-dynamics for liquid-metals. *Phys. Rev. B* **47,** 558–561 (1993).
27. Kozumi, H., Kirchner, H. O. K. & Suzuki, T. Kink pair nucleation and critical shear-stress. *Acta Metall. Mater.* **41,** 3483–3493 (1993).
28. Anderson, O. L. The Earth's core and the phase diagram of iron. *Phil. Trans. R. Soc. Lond. A* **306,** 21–35 (1982).
29. Brown, J. M. & Shankland, T. J. Thermodynamic parameters in the Earth as determined from seismic profiles. *Geophys. J. R. Astron. Soc.* **66,** 579–596 (1981).
30. Schuberth, B. S. A., Bunge, H.-P., Steinle-Neumann, G., Moder, C. & Oeser, J. Thermal versus elastic heterogeneity in high-resolution mantle circulation models with pyrolite composition: high plume excess temperatures in the lowermost mantle. *Geochem. Geophys. Geosyst.* **10,** Q01W01 (2009).

Supplementary Information is linked to the online version of the paper at www.nature.com/nature.

Acknowledgements This work was supported by ANR (Diup project).

Author Contributions P.C. conceived the project. P.C. and Ph.C. designed the work. J.A. and Ph.C. performed numerical simulations. All authors discussed and interpreted the results. P.C. wrote the paper with feedback and contributions from all co-authors.

Author Information Reprints and permissions information is available at www.nature.com/reprints. The authors declare no competing financial interests. Readers are welcome to comment on the online version of this article at www.nature.com/nature. Correspondence and requests for materials should be addressed to P.C. (Patrick.Cordier@univ-lille1.fr).

LETTER

doi:10.1038/nature10710

Tail-assisted pitch control in lizards, robots and dinosaurs

Thomas Libby[1], Talia Y. Moore[2], Evan Chang-Siu[3], Deborah Li[2], Daniel J. Cohen[4], Ardian Jusufi[2] & Robert J. Full[2]

In 1969, a palaeontologist proposed[1] that theropod dinosaurs used their tails as dynamic stabilizers during rapid or irregular movements, contributing to their depiction as active and agile predators. Since then the inertia of swinging appendages has been implicated in stabilizing human walking[2,3], aiding acrobatic manoeuvres by primates[4–8] and rodents[9], and enabling cats to balance on branches[10]. Recent studies on geckos[11–13] suggest that active tail stabilization occurs during climbing, righting and gliding. By contrast, studies on the effect of lizard tail loss show evidence of a decrease, an increase or no change in performance[14,15]. Application of a control-theoretic framework could advance our general understanding of inertial appendage use in locomotion. Here we report that lizards control the swing of their tails in a measured manner to redirect angular momentum from their bodies to their tails, stabilizing body attitude in the sagittal plane. We video-recorded Red-Headed Agama lizards (*Agama agama*) leaping towards a vertical surface by first vaulting onto an obstacle with variable traction to induce a range of perturbations in body angular momentum. To examine a known controlled tail response, we built a lizard-sized robot with an active tail that used sensory feedback to stabilize pitch as it drove off a ramp. Our dynamics model revealed that a body swinging its tail experienced less rotation than a body with a rigid tail, a passively compliant tail or no tail. To compare a range of tails, we calculated tail effectiveness as the amount of tailless body rotation a tail could stabilize. A model *Velociraptor mongoliensis* supported the initial tail stabilization hypothesis[1], showing as it did a greater tail effectiveness than the Agama lizards. Leaping lizards show that inertial control of body attitude can advance our understanding of appendage evolution and provide biological inspiration for the next generation of manoeuvrable search-and-rescue robots.

Agama lizards (average mass, 66.96 ± 2.93 g) ran within an acrylic track and rapidly transitional to a vertical wall with a shelter on top. To stimulate a leap with a long aerial phase, we directed the animals over a small box that acted as a vault (Fig. 1a, b). To induce perturbations during the transition, we varied the traction available on top of the vault. We proposed that a sandpaper-covered vault would allow the lizard sufficient traction to closely direct its ground reaction force vector through its centre of mass (COM) and thereby minimize body rotation in the aerial phase (Fig. 1a and Supplementary Movie 1). Covering the vault with smooth card stock (Fig. 1b and Supplementary Movie 2) would cause feet to slip, misaligning the ground reaction force vector and imparting a rotational impulse during this critical phase when lizards redirect horizontal momentum upwards. We recorded body and tail motion with a high-speed digital camera.

To quantify the possible effect a tail has on maintaining attitude stability in the pitch axis during the leap, we determined the angle through which a tailless body would rotate after a given perturbation at take-off. We measured the perturbation magnitude at take-off for each trial by estimating the mean total angular momentum (H) over the duration of the leap. We computed H using the lizard's kinematic data during the aerial phase by fitting a two-link (body and tail), planar dynamic model constructed from morphometric data from five Agama lizard cadavers (Supplementary Table 1). Assuming aerodynamic forces to be negligible[8,12,13], we took the computed H to be the perturbation applied during take-off. The variable surface vault produced a broad range in aerial-phase angular momentum, $\pm 1.5 \times 10^{-3}\,\mathrm{kg\,m^2\,s^{-1}}$. To better compare the magnitude of the perturbation among individuals, we normalized H by body moment of inertia (I_b) about its COM and by leap duration (t). The normalized perturbation magnitude, $(H/I_b)t$ (Fig. 2, abscissa), represents the angle through which an individual's body would rotate without its tail, given the observed angular momentum and trial duration. Because the duration of foot slippage was brief, take-off angle was not affected by the perturbation (coefficient of determination, $r^2 = 0.13$). Hence, we proposed that a constant body angle was maintained after the perturbation.

We reasoned that defining inertial appendage control over a range of perturbations could benefit from a physical model with a known control mechanism. We built an Agama-sized, tailed robot that used proportional–derivative (PD) feedback control (Fig. 1c, d) to stabilize body angle[16]. Inertial stabilization of robotic locomotion has been modelled before[17], and simple air-righting accomplished[18], but our robot is the first with a specialized tail-like appendage for continuous inertial stabilization. Previous investigations of tails in mobile robots have focused on substrate interaction and passive stability[19,20]. Our wheeled robot swung an aluminium rod tail in the sagittal plane in response to sensing using a microelectromechanical systems gyroscope. A ski-jump-like ramp launched the robot at the same take-off angle that the lizards selected. The unbalanced gravitational moment as the front wheels left the ramp applied a similar rotational perturbation to that induced on the lizards by the low-friction vault. We launched the robot in two situations: with the controller off and the tail rigidly held parallel to the body (Fig. 1c and Supplementary Movie 3) and with the PD feedback controller on and the reference angle set to the take-off angle of the ramp (Fig. 1d and Supplementary Movie 4). Varying the perturbation on the robot by changing the speed with which it left the ramp altered the imparted angular momentum. As the perturbation increased, the robot with PD feedback tail control maintained a nearly constant body angle by swinging its tail upward and incurred 72% less rotation after a perturbation than did the robot without tail control (Fig. 2b).

Lizards swung their tails during leaps in a manner consistent with the control of body pitch observed in the robot. Tail swinging was not an all-or-none behaviour, but was proportional to perturbation magnitude. The change in tail angle relative to the body during the aerial phase correlated with the normalized perturbation magnitude ($r = 0.79$, $P < 0.001$). A larger perturbation at take-off resulted in a correspondingly greater tail swing. Attenuation of body pitch was not unidirectional: lizards swung their tails upwards to compensate for nose-down perturbations and downwards in response to nose-up perturbations (Fig. 2a and Supplementary Movie 5). By rotating their

[1]Center for Interdisciplinary Bio-Inspiration in Education and Research, University of California, Berkeley, California 94720-3140, USA. [2]Department of Integrative Biology, University of California, Berkeley, California 94720-3140, USA. [3]Department of Mechanical Engineering, University of California, Berkeley, California 94720-1740, USA. [4]Department of Bioengineering, University of California, Berkeley, California 94720-1762, USA.

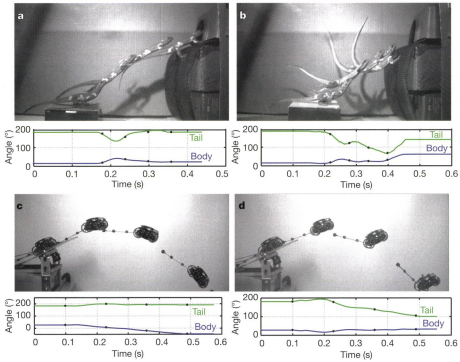

Figure 1 | Pitch stabilization using a tail in a lizard and robot. Tail angle (green) relative to body axis and body angle (blue) relative to ground. **a**, **b**, Agama lizards ran along a track and vaulted off an obstacle to a vertical wall with a shelter on top. Overlain images are separated by 60 ms. **a**, A high-traction vault surface produced small perturbations in body angular momentum, allowing tail and body angles to remain constant (Supplementary Movie 1). **b**, A low-traction vault surface produced slipping that generated an angular momentum perturbation. By swinging their tails upwards, lizards redirected angular momentum from the body to the tail to maintain body angle (Supplementary Movie 2). **c**, **d**, A wheeled robot drove off a ramp, producing a nose-down perturbation in body angular momentum. Overlain images are separated by 130 ms. **c**, Without PD feedback control, the robot body and tail rotated as a rigid body (Supplementary Movie 3). **d**, With PD feedback control, the tail swung upwards as the controller applied torque to stabilize the body, keeping the body angle constant (Supplementary Movie 4).

tails with respect to the body in the sagittal plane, the lizards transferred angular momentum from the body to tail, thereby reducing body angular velocity and the effect of perturbation on body rotation (Fig. 2a).

We characterized the sensitivity to pitch perturbations by regressing experimentally observed rotations against the normalized perturbation, yielding a dimensionless metric (S, the slope of the lines in Fig. 2a) representing the observed body rotation due to a perturbation relative to the rotation a tailless body would undergo. A sensitivity value, or slope, of one would indicate that the individual stabilized itself no better than would a tailless body. A value less than one signifies that the animal or robot attenuated the effect of the perturbation on its body rotation. A

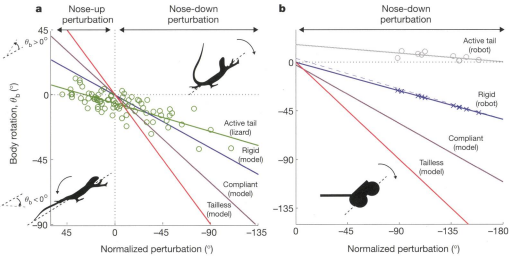

Figure 2 | Sensitivity of body rotation to a perturbation in a lizard and robot. Body rotation (θ_b) as a function of perturbation, defined as the angle through which the body would rotate without a tail. The slope of the lines represents sensitivity to perturbations. **a**, Lizards (green circles and line) controlled body rotation by swinging their tails downwards to correct a nose-up pitch (normalized perturbation, $>0°$) and upwards to correct a nose-down pitch (normalized perturbation, $<0°$). Lizards were less sensitive to perturbations than were tailless (red), compliant-tail (purple) or rigid-tail (blue) Agama models. **b**, Robots (grey circles and line) controlled body rotation by swinging their tails upwards to correct a nose-down pitch (normalized perturbation, $<0°$) more effectively than lizards. Robots were far less sensitive to perturbations than were tailless (red) and compliant-tail (purple) models or robots with rigid tails (blue crosses and line).

value of zero shows perfect compensation (Fig. 2a, b, horizontal dashed line). Supporting the hypothesis of tail-facilitated control, we found the measured sensitivity of Agama lizards to a rotational perturbation to be very low, $S = 0.22 \pm 0.02$, relative to the tailless model value, $S = 1$, although not as low as that of our PD-feedback-controlled tailed robot ($S = 0.090 \pm 0.035$; Supplementary Table 2).

We compared the lizard's effectiveness in controlling body pitch using an active tail with those of our robot and three mathematical models: a tailless animal (single body link), a rigid-tailed animal (body and tail links with a rigid joint), and a compliant tailed animal (both links with a torque-free pin joint). We used a morphologically averaged Agama model to generate a prediction of perturbation sensitivity for each passive tail condition, and calculated the difference with respect to the experimentally measured value (Supplementary Table 2). Adding a compliant or rigid tail to the tailless model Agama decreased its sensitivity by 36% ($S = 0.64$) or 58% ($S = 0.42$), respectively, indicating that passive tails can improve aerial stability. The actual Agamas actively controlling their tails were significantly less sensitive to perturbations than either passive tail model ($P < 0.001$; Supplementary Table 2). Our model results showed that animals received 48% less rotation after a perturbation than they would if they had held their tails rigid during the aerial phase, 66% less rotation than if they had left the tail compliant and 78% less rotation than if they had no tail at all. By comparing the average proportion of angular momentum in each segment with the expected value for a rigidly linked model, we found that the lizards had 41.000 ± 0.043% less angular momentum in their bodies than the rigid model, and a corresponding increase in tail momentum, indicating active momentum transfer.

The PD-feedback-controlled robot incurred 72% less rotation after a perturbation than it would if it had held its tail rigid during the aerial phase, 85% less rotation than if it had left the tail compliant and 91% less rotation than if it had no tail at all (Supplementary Table 2). The experimental control (that is, with PD feedback controller off) was not significantly different from the model case in which the tail was rigidly connected to the body (Fig. 2b, blue line and crosses; $t = -5.0$, $P < 0.001$). We found that the tail contained 31.00 ± 0.04% more angular momentum than if it was rotating rigidly with the body, and that the body contained 40.00 ± 0.08% less. With the PD feedback controller off, the passive-tail robot's links did not contain significantly different momentum than did the rigid model (analysis of variance, $F = 0.32$, $P = 0.58$). Hence, the effect of the PD feedback controller on regulating body angle was to redirect angular momentum from the body to the tail, supporting our hypotheses for lizards.

Our mathematical model allows us to predict the effectiveness of different tails in preventing body rotation. Assuming that total angular momentum is conserved after a perturbation, the tail must rotate for the body's orientation to remain stable. The amount of rotation required depends on tail morphology[12,13]. We define tail effectiveness as the amount of tailless body rotation a tail could stabilize per degree of tail rotation (that is, the absolute value of the reciprocal slope from Fig. 3 linearized around a tail rotation of $\phi_t = 0^\circ$). For a tail effectiveness of one, a perturbation rotating a tailless animal by 45° could be completely stabilized by rotating the tail through the same angle. Less effective tails would require more tail rotation to stabilize the same perturbation. Because tails are limited in range of motion, effectiveness limits the size of perturbation a tail can completely stabilize. After modelling each lizard in our study, we found their average tail effectiveness to be 0.79: for the typical maximum tail stroke of 100°, the lizards could completely stabilize a perturbation that would rotate a tailless lizard by almost 80° (Fig. 3; range shown by green shaded area). When our robot's body–tail length ratio was similar to those of the Agama lizards, it was over twice as effective (1.84; Fig. 3, dashed line, bottom grey shaded area). This resulted from concentrating mass at the tip (Supplementary Table 1), rather than at the base as in lizards. We modelled a range of possible tail configurations in the robot, from a small tail (5% body mass, 50% body length) to a large tail (10% body mass, 200% body length). The smallest-tail model was far less effective than in lizards (Fig. 3, upper bound of grey area), whereas the largest-tail model (Fig. 3, lower bound of grey shaded area) was considerably more effective than even our actual robot.

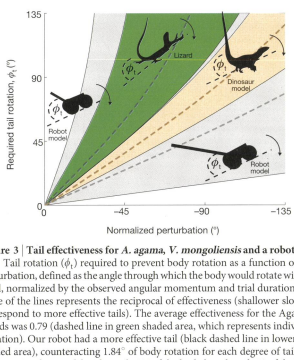

Figure 3 | Tail effectiveness for *A. agama*, *V. mongoliensis* and a robot with tail. Tail rotation (ϕ_t) required to prevent body rotation as a function of perturbation, defined as the angle through which the body would rotate without a tail, normalized by the observed angular momentum and trial duration. The slope of the lines represents the reciprocal of effectiveness (shallower slopes correspond to more effective tails). The average effectiveness for the Agama lizards was 0.79 (dashed line in green shaded area, which represents individual variation). Our robot had a more effective tail (black dashed line in lower grey shaded area), counteracting 1.84° of body rotation for each degree of tail rotation. A robot model with a tail 50% of the body length and 5% of the body mass was least effective (upper bound of grey shaded area), whereas a tail 200% of body length and 10% of the body mass was greater than three times more effective (lower bound of grey shaded area) than our robot. The *Velociraptor* model had a more effective tail than the most effective Agama lizard (slope, 1.23; dashed line in tan area, which represents 15% variation in model body and tail moment of inertia).

Finally, we tested the original tail stabilization hypothesis[1] with regard to tail use in theropods. By using our model with a conservative morphometric reconstruction[21], we found that *Velociraptor mongoliensis*[22], an agile, 20-kg, 1.5-m-tall biped, with a tail effectiveness of 1.23 (Fig. 3, tan shaded area) given sufficient muscular capacity, could have outperformed even the most tail-effective Agama lizard. Although the distal portion of dromeosaur tails was bony and possibly stiff[9], the proximal tail base could bend by up to 90° (ref. 23). Such a range of motion would enable *Velociraptor* to sustain a perturbation that would rotate a tailless animal by 110°, or to adjust its body angle by up to 45° in an unperturbed leap. Despite previously proposed limitations of passive tails[24], small theropods like *Velociraptor* with active tails might have been capable of aerial acrobatics beyond even those displayed by present-day arboreal lizards[11–15].

METHODS SUMMARY

Dynamic models. For simple characterization of the underlying dynamics of tail-assisted manoeuvres, we derived a planar, two-link, rigid-body model. By taking the derivative of the total angular momentum of each link and solving for the model's orientation and velocities with respect to actuation torque, we obtained a set of nonlinear, coupled ordinary differential equations realized in state-space form. We initialized the model with links oriented 180° apart. We set angular velocity of the tail link to zero and that of the body link such that the total angular momentum was as desired. We averaged the morphometrics of all animals to create the Agama model used in simulations. Simulations using morphometric models of individual Agama lizards did not yield significantly different perturbation sensitivities from those of the averaged Agama model. We performed numerical simulations in MATLAB.

Kinematics. To estimate the angular momentum of the animal or robot from kinematics, we treated the body and tail as rigid bodies with a hinge at the base of the tail (1 cm posterior to the vent in lizards). We used video tracking software (Xcitex PROANALYST) to capture kinematics, and calculated positions and velocities of

COMs in MATLAB. We estimated H from the two-link, rigid-body model for each video frame and averaged over the leap.

Statistics. We used multiple regression analysis in MATLAB to compare sensitivities (linear fits) of the experimental data to model hypotheses (t-test of slope). Sensitivities of individual animals were not significantly different from one another (analysis of variance, $F = 2.1$, $P = 0.073$).

***Velociraptor* model.** To model the tail stabilization performance of an extinct theropod, we estimated mass properties from a two-dimensional reconstruction (Supplementary Table 1). We represented the head, trunk and lung capacity as ellipsoids, the neck as an elliptical cylinder, the limbs as point masses, and the tail as a truncated cone by digitizing points on the dorsal and sagittal views of the reconstruction. Estimates of combined trunk–tail moment of inertia agreed well with ref. 25.

Full Methods and any associated references are available in the online version of the paper at www.nature.com/nature.

Received 11 August; accepted 10 November 2011.
Published online 4 January 2012.

1. Ostrom, J. H. Osteology of *Deinonychus antirrhopus*, an unusual theropod from the Lower Cretaceous of Montana. *Bull. Peabody Mus. Nat. Hist. (Paris)* **30,** 68–80, 144 (1969).
2. Pijnappels, M. *et al.* Armed against falls: the contribution of arm movements to balance recovery after tripping. *Exp. Brain Res.* **201,** 689–699 (2010).
3. Roos, P. E. *et al.* The role of arm movement in early trip recovery in younger and older adults. *Gait Posture* **27,** 352–356 (2008).
4. Dunbar, D. C. Aerial maneuvers of leaping lemurs: the physics of whole-body rotations while airborne. *Am. J. Primatol.* **16,** 291–303 (1988).
5. Larson, S. G. & Stern, J. T. Maintenance of above-branch balance during primate arboreal quadrupedalism: coordinated use of forearm rotators and tail motion. *Am. J. Phys. Anthropol.* **129,** 71–81 (2006).
6. Günther, M. M., Ishida, H., Kumakura, H. & Nakano, Y. The jump as a fast mode of locomotion in arboreal and terrestrial biotopes. *Z. Morphol. Anthropol.* **78,** 341–372 (1991).
7. Demes, B. *et al.* Body size and leaping kinematics in Malagasy vertical clingers and leapers. *J. Hum. Evol.* **31,** 367–388 (1996).
8. Peters, A. & Preuschoft, H. in *Biology of Tarsiers* (ed. Niemitz, C.) 227–255 (Fischer, 1984).
9. Bartholomew, G. A. & Caswell, H. H. Locomotion in kangaroo rats and its adaptive significance. *J. Mamm.* **32,** 155–169 (1951).
10. Walker, C. *et al.* Balance in the cat: role of the tail and effects of sacrocaudal transection. *Behav. Brain Res.* **91,** 41–47 (1998).
11. Jusufi, A., Goldman, D. I., Revzen, S. & Full, R. J. Active tails enhance arboreal acrobatics in geckos. *Proc. Natl Acad. Sci. USA* **105,** 4215–4219 (2008).
12. Jusufi, A., Kawano, D. T., Libby, T. & Full, R. J. Righting and turning in mid-air using appendage inertia: reptile tails, analytical models and bio-inspired robots. *Bioinspir. Biomim.* **5,** 045001 (2010).
13. Jusufi, A., Zeng, Y., Full, R. J. & Dudley, R. Aerial righting reflexes in flightless animals. *Integr. Comp. Biol.* **51,** 937–943 (2011).
14. Bateman, P. W. & Fleming, P. A. To cut a long tail short: a review of lizard caudal autotomy studies carried out over the last 20 years. *J. Zool. (Lond.)* **277,** 1–14 (2009).
15. Gillis, G. B., Bonvini, L. A. & Irschick, D. J. Losing stability: tail loss and jumping in the arboreal lizard *Anolis carolinensis*. *J. Exp. Biol.* **212,** 604–609 (2009).
16. Chang-Siu, E., Libby, T., Tomizuka, M. & Full, R. J. in *IEEE/RSJ Internat. Conf. Intelligent Robots Systems 2011* 1887–1894 (IEEE, 2011).
17. Berkemeier, M. D. & Fearing, R. S. Control of a two-link robot to achieve sliding and hopping gaits. *IEEE Trans. Robot. Autom.* **1,** 286–291 (1992).
18. Mather, T. W. & Yim, M. in *IEEE/RSJ Internat. Conf. Intelligent Robots Systems 2009* 5905–5910 (IEEE, 2009).
19. Hyun Soo, P. *et al.* in *IEEE Internat. Conf. Robotics Automation 2009* 2655–2660 (IEEE, 2009).
20. Saunders, A. *et al.* The RiSE climbing robot: body and leg design. *Proc. SPIE* **6230,** 623017 (2006).
21. Alexander, R. M. Dinosaur biomechanics. *Proc. R. Soc. B* **273,** 1849–1855 (2006).
22. Paul, G. S. *The Princeton Field Guide to Dinosaurs* 137 (Princeton Univ. Press, 2010).
23. Paul, G. S. *Dinosaurs of the Air: the Evolution and Loss of Flight in Dinosaurs and Birds* 45 (Johns Hopkins Univ. Press, 2002).
24. Carrier, D. R. *et al.* Influence of rotational inertia on turning performance of theropod dinosaurs: clues from humans with increased rotational inertia. *J. Exp. Biol.* **204,** 3917–3926 (2001).
25. Sellers, W. I. & Manning, P. L. Estimating dinosaur maximum running speeds using evolutionary robotics. *Proc. R. Soc. B* **274,** 2711–2716 (2007).

Supplementary Information is linked to the online version of the paper at www.nature.com/nature.

Acknowledgements We thank P. Jennings for video editing and figure production, T. Full for digitizing the lizard video and K. Padian for his advice on the dinosaur reconstruction and capability. We thank O. O'Reilly, S. Sponberg and N. Sapir for advice on analysis. This work was supported by a US NSF FIBR grant to R.J.F., a MAST CTA grant to R.J.F, an NSF IGERT under award DGE-0903711 and a Swiss NSF Fellowship to A.J.

Author Contributions T.L. designed the study and robot, carried out experiments, analysed data and wrote initial drafts of the manuscripts. T.Y.M. designed the study, carried out animal experiments and worked out kinematics. E.C.-S. designed and constructed the robot, carried out experiments and derived the analytical model. D.L. carried out experiments and worked out kinematics. D.J.C. designed experiments and collected and analysed animal kinematic data. A.J. designed and performed experiments and analysed data. R.J.F. directed the project, defined the analysis and wrote the final version of the manuscript.

Author Information Reprints and permissions information is available at www.nature.com/reprints. The authors declare no competing financial interests. Readers are welcome to comment on the online version of this article at www.nature.com/nature. Correspondence and requests for materials should be addressed to R.J.F. (rjfull@berkeley.edu).

LETTER

doi:10.1038/nature10726

Topoisomerase inhibitors unsilence the dormant allele of *Ube3a* in neurons

Hsien-Sung Huang[1]*, John A. Allen[2]*, Angela M. Mabb[1], Ian F. King[1], Jayalakshmi Miriyala[1], Bonnie Taylor-Blake[1], Noah Sciaky[2], J. Walter Dutton Jr[1], Hyeong-Min Lee[2], Xin Chen[3], Jian Jin[3], Arlene S. Bridges[4], Mark J. Zylka[1,5,6], Bryan L. Roth[2,5,6,7,8] & Benjamin D. Philpot[1,5,6]

Angelman syndrome is a severe neurodevelopmental disorder caused by deletion or mutation of the maternal allele of the ubiquitin protein ligase E3A (*UBE3A*)[1–3]. In neurons, the paternal allele of *UBE3A* is intact but epigenetically silenced[4–6], raising the possibility that Angelman syndrome could be treated by activating this silenced allele to restore functional UBE3A protein[7,8]. Using an unbiased, high-content screen in primary cortical neurons from mice, we identify twelve topoisomerase I inhibitors and four topoisomerase II inhibitors that unsilence the paternal *Ube3a* allele. These drugs included topotecan, irinotecan, etoposide and dexrazoxane (ICRF-187). At nanomolar concentrations, topotecan upregulated catalytically active UBE3A in neurons from maternal *Ube3a*-null mice. Topotecan concomitantly downregulated expression of the *Ube3a* antisense transcript that overlaps the paternal copy of *Ube3a*[9–11]. These results indicate that topotecan unsilences *Ube3a* in *cis* by reducing transcription of an imprinted antisense RNA. When administered *in vivo*, topotecan unsilenced the paternal *Ube3a* allele in several regions of the nervous system, including neurons in the hippocampus, neocortex, striatum, cerebellum and spinal cord. Paternal expression of *Ube3a* remained elevated in a subset of spinal cord neurons for at least 12 weeks after cessation of topotecan treatment, indicating that transient topoisomerase inhibition can have enduring effects on gene expression. Although potential off-target effects remain to be investigated, our findings suggest a therapeutic strategy for reactivating the functional but dormant allele of *Ube3a* in patients with Angelman syndrome.

No effective therapies exist for Angelman syndrome—an imprinting disorder caused by mutations or deletions in the maternal allele of *UBE3A*[1–3]. *Ube3a* is biallelically expressed in most tissues of the body; however, in rodents and humans, most neurons express *Ube3a* only from the maternally-inherited allele[4,12–14]. This unique epigenetic pattern of regulation suggested that it might be possible to unsilence the dormant paternal *Ube3a* allele in neurons[7,8].

To test this possibility, we developed a 384-well high-content screen using primary mouse cortical neurons from *Ube3a*–yellow fluorescent protein (*Ube3a–YFP*) knock-in mice[15], and searched for drug-like molecules that could unsilence the paternal *Ube3a–YFP* allele (Fig. 1a). This screen was based on our observation that the imprinting of *Ube3a–YFP* was maintained *in vitro* in cultured embryonic cortical neurons. Notably, *Ube3a–YFP* expression was undetectable (silenced) in cultured neurons when *Ube3a–YFP* was paternally inherited ($Ube3a^{m+/pYFP}$), but was expressed when *Ube3a–YFP* was maternally inherited ($Ube3a^{mYFP/p+}$) (Fig. 1b), with expression increasing from 4 to 10 days *in vitro* (DIV) (Fig. 1c). This significant difference between maternal and paternal UBE3A–YFP protein levels provided a large screening window and a Z'-factor score of 0.58 (determined by statistically comparing antibody-enhanced fluorescence intensities and variations between maternal and paternal UBE3A–YFP signals at DIV10), making our high-content platform suitable for unbiased screening.

To perform the screen, we cultured $Ube3a^{m+/pYFP}$ neurons for 7 days and then treated these neurons with compounds (10 μM for 72 h) from several small-molecule libraries (Fig. 1d and Supplementary Fig. 1). In total, we screened 2,306 small molecules in quadruplicate, normalizing values to vehicle-treatment (0.2% dimethyl sulphoxide (DMSO)) (for full methods see Supplementary Methods; for list of all compounds tested see Supplementary Table 1). Although methylation and other epigenetic marks are thought to control imprinting of $Ube3a$[9,16–18], to our surprise, none of the commonly used compounds that target the epigenome, including chromatin-remodelling drugs and DNA methyltransferase inhibitors, unsilenced the paternal *Ube3a–YFP* allele. A number of compounds were identified as false positives (grey compounds in Fig. 1d) due to their intrinsic fluorescence (Supplementary Fig. 2). Our initial screen identified one compound—irinotecan, an FDA-approved topoisomerase type I inhibitor. Irinotecan lacked intrinsic fluorescence and upregulated UBE3A–YFP fluorescence (Fig. 1d, e and Supplementary Fig. 3). Irinotecan (10 μM) also upregulated paternal UBE3A–YFP protein (Fig. 1f) and endogenous UBE3A protein (Fig. 1g) in neuronal cultures from $Ube3a^{m+/pYFP}$ and $Ube3a^{m-/p+}$ mice (Angelman syndrome model mice[13]), respectively.

Many topoisomerase I inhibitors, including irinotecan and the related FDA-approved drug topotecan, are derived from the natural product camptothecin (CPT)[19]. To explore structure activity relationships, we tested CPT analogues and other topoisomerase inhibitors (Fig. 2a and Supplementary Figs 4–10). The analogues we tested all lack inherent fluorescence (Supplementary Fig. 3). We found that irinotecan and topotecan upregulated paternal UBE3A–YFP in a dose- and time-dependent manner in cultured neurons, with topotecan being 20 times more potent than irinotecan (Fig. 2a, b and Supplementary Fig. 11). In contrast, an inactive analogue of CPT (lactam E ring-CPT) that does not inhibit topoisomerases[20] failed to unsilence the paternal *Ube3a–YFP* allele (Fig. 2a and Supplementary Fig. 4). Ten additional topoisomerase I inhibitors unsilenced *Ube3a–YFP* in a dose-dependent manner, including CPT analogues and structurally distinct indenoisoquinolines (Table 1 and Supplementary Figs 4–7). Furthermore, four structurally distinct topoisomerase II inhibitors (etoposide, dexrazoxane, ICRF-193 and amsacrine) also unsilenced the paternal *Ube3a–YFP* allele (Table 1 and Supplementary Figs 8–10). Thus, our data with 16 topoisomerase inhibitors and one inactive analogue strongly suggest that inhibition of topoisomerase I or II can unsilence the paternal *Ube3a* allele.

[1]Department of Cell and Molecular Physiology, University of North Carolina School of Medicine, Chapel Hill, North Carolina 27599, USA. [2]Department of Pharmacology, University of North Carolina School of Medicine, Chapel Hill, North Carolina 27599, USA. [3]Center for Integrative Chemical Biology and Drug Discovery, Division of Chemical Biology and Medicinal Chemistry, University of North Carolina Eshelman School of Pharmacy, Chapel Hill, North Carolina 27599, USA. [4]Department of Pathology and Laboratory Medicine, University of North Carolina School of Medicine, Chapel Hill, North Carolina 27599, USA. [5]Carolina Institute for Developmental Disabilities, University of North Carolina, Chapel Hill, North Carolina 27599, USA. [6]University of North Carolina Neuroscience Center, Chapel Hill, North Carolina 27599, USA. [7]Division of Chemical Biology and Medicinal Chemistry, University of North Carolina Eshelman School of Pharmacy, Chapel Hill, North Carolina 27599, USA. [8]National Institute of Mental Health, Psychoactive Drug Screening Program, Department of Pharmacology, University of North Carolina School of Medicine, Chapel Hill, North Carolina 27599, USA.
*These authors contributed equally to this work.

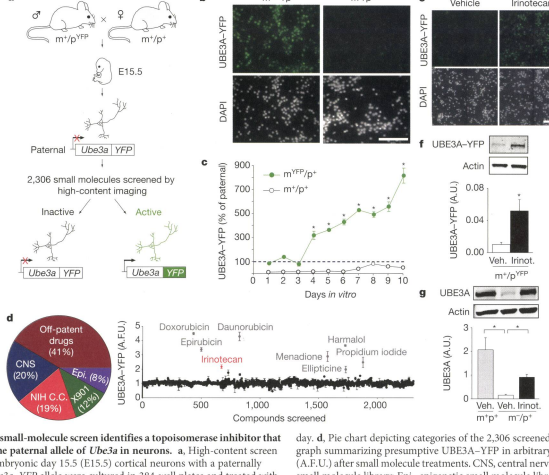

Figure 1 | A small-molecule screen identifies a topoisomerase inhibitor that unsilences the paternal allele of *Ube3a* in neurons. **a**, High-content screen flowchart. Embryonic day 15.5 (E15.5) cortical neurons with a paternally inherited *Ube3a–YFP* allele were cultured in 384-well plates and treated with small molecules from DIV7–DIV10. Active compounds that unsilence the paternal *Ube3a–YFP* allele were detected with antibody-enhanced fluorescence and high-content imaging. **b**, High-content imaging of DIV7 neurons that inherited *Ube3a–YFP* maternally (m^{YFP}/p^{+}) or paternally (m^{+}/p^{YFP}). Nuclei were stained with 4′,6-diamidino-2-phenylindole (DAPI). Scale bar, 50 μm. **c**, Mean ± s.e.m. levels of UBE3A–YFP fluorescence in neurons cultured from maternal *Ube3a–YFP* (m^{YFP}/p^{+}) or wild-type (m^{+}/p^{+}) mice, normalized to levels in age-matched neurons cultured from paternal *Ube3a–YFP* mice (m^{+}/p^{YFP}). Two-way analysis of variance (ANOVA) revealed main effects of genotype, duration and a genotype–duration interaction ($P < 0.001$); Bonferroni post hoc test examined comparisons between maternal and paternal *Ube3a–YFP* mice from DIV4 to DIV10, $^{*}P < 0.001$; $n = 2$–6 culture wells per day. **d**, Pie chart depicting categories of the 2,306 screened compounds and graph summarizing presumptive UBE3A–YFP in arbitrary fluorescence units (A.F.U.) after small molecule treatments. CNS, central nervous system selective small molecule library; Epi., epigenetic small molecule library; NIH C.C., NIH Clinical Collection; X901, NIMH X-901 small molecule library. Small molecules that were subsequently found to be autofluorescent (Supplementary Fig. 2) are depicted in grey. The initial screen identified one active compound, irinotecan (red). **e**, High-magnification view of wells treated with vehicle (0.2% DMSO) or 10 μM irinotecan for 72 h. Neuron density and health is similar in vehicle- and irinotecan-treated cells as evidenced by counterstaining with the nuclear marker DAPI. Scale bar, 100 μm. **f**, **g**, Western blots of cultured cortical neurons probed with GFP or UBE3A antibodies, respectively, with or without irinotecan (10 μM for 72 h). Irinot., irinotecan; Veh., vehicle. **f**, $^{*}P < 0.05$; two-tailed *t*-test, $n = 3$ per group. **g**, $^{*}P < 0.001$, one-way ANOVA with Bonferroni post hoc, $n = 7$–8 per group. All data are presented as means ± s.e.m.

We focused our remaining studies on the topoisomerase I inhibitor topotecan because it is approved for use in humans, it unsilenced *Ube3a* in the low nanomolar range, and topotecan (300 nM, 72 h) restored UBE3A protein to wild-type levels in cultured neurons from $Ube3a^{m-/p+}$ mice (Fig. 2c).

Many topoisomerase inhibitors, including topotecan, covalently link topoisomerases to DNA, forming stable DNA–enzyme complexes that are separable from free topoisomerase enzymes[19]. Because topotecan inhibits topoisomerase I (TOP1) and *Top1* is expressed at high levels in the developing and adult brain[19,21], we focused our subsequent analysis on this enzyme. We found that topotecan (300 nM, 72 h) significantly reduced the amount of free TOP1 (Fig. 2d) in cultured neurons, indicating that topotecan engages its known molecular target at doses that unsilence the paternal *Ube3a* allele.

UBE3A is a HECT (homology to E6 carboxyl terminus) domain E3 ligase that forms a thioester-ubiquitin intermediate in the presence of E1 and E2 enzymes[22]. This thioester-ubiquitin intermediate is required for HECT domain E3 ligases to mono- and polyubiquitinate their substrates[23]. Interestingly, we noticed that topotecan (300 nM, 72 h) upregulated UBE3A protein in $Ube3a^{m-/p+}$ cultures along with a higher molecular weight form (resolved after running gels for longer times; Fig. 2e). This high molecular weight band was also seen in wild-type ($Ube3a^{m+/p+}$) cultures and was lost upon addition of the reducing agent dithiothreitol (DTT) (Fig. 2e). These data indicate that the unsilenced paternal copy of UBE3A is catalytically active and competent to form a thioester-ubiquitin intermediate, just like wild-type, maternal-derived UBE3A.

To demonstrate further that UBE3A was catalytically active, we immunoprecipitated UBE3A from cultured wild-type and $Ube3a^{m-/p+}$ neurons (with or without topotecan), then tested these samples using a gel-mobility shift assay in the presence or absence of the ubiquitin E2 UBCH7 (ref. 24). Both wild-type (maternal-derived) and topotecan-unsilenced (paternal-derived) UBE3A underwent mobility shifts in the presence of UBCH7 plus free ubiquitin that were abolished by addition of DTT (Fig. 2f). This observation indicates that the mobility shift was due to addition of covalent ubiquitin, and demonstrates that topotecan can upregulate a functional UBE3A enzyme.

Table 1 | Efficacies and potencies of topoisomerase inhibitors for unsilencing the paternal allele of *Ube3a–YFP* in cultured neurons

Compound	Potency (half-maximum effective concentration EC_{50}, nM)	Efficacy E_{max} (fold over vehicle)
Camptothecin derivatives		
7-ethyl-camptothecin (7-ethyl-CPT)	7.2 ± 2.3	1.70 ± 0.04
7-ethyl-10-hydroxy-CPT	11 ± 3.2	1.99 ± 0.06
10-hydroxy-CPT	14 ± 5.7	1.82 ± 0.08
Belotecan (CKD602)	19 ± 4.4	1.88 ± 0.05
Camptothecin (CPT)	21 ± 3.8	2.11 ± 0.05
Topotecan*	54 ± 3.4	2.25 ± 0.04
Rubitecan (9-nitro-CPT)	62 ± 18	2.09 ± 0.09
Irinotecan*	994 ± 13	2.17 ± 0.05
Silatecan (DB67)	2,244 ± 171	1.65 ± 0.05
Lactam E ring-CPT (inactive)	inactive	inactive
Indenoisoquinoline derivatives		
NSC725776	10 ± 1.6	1.76 ± 0.03
NSC706744	11 ± 3.2	1.84 ± 0.07
NSC724998	14 ± 2.2	1.69 ± 0.03
Podophyllotoxin derivative		
Etoposide*	1,600 ± 980	1.68 ± 0.04
Bis-dioxopiperazine derivatives		
ICRF-193	205 ± 70	2.21 ± 0.09
Dexrazoxane (ICRF-187)*	20,470 ± 1,450	1.82 ± 0.05
Aminoacridine derivative		
Amsacrine	27 ± 5.2	1.74 ± 0.06

*FDA-approved compounds.

Ube3a is repressed in *cis* by a large antisense transcript (*Ube3a–ATS*) that overlaps the paternal allele of *Ube3a* (Fig. 2g)[9–11]. *Ube3a–ATS* is expressed exclusively from the paternal allele as a result of allele-specific methylation of an imprinting centre that overlaps the *Ube3a–ATS* and *Snurf/Snrpn* transcription start site[25]. We next sought to determine if topotecan regulated *Ube3a* expression through changes in *Ube3a–ATS* expression or altered methylation at the imprinting centre. We found that topotecan upregulated expression of *Ube3a* in cultured neurons from $Ube3a^{m-/p+}$ mice while concomitantly downregulating expression of *Ube3a–ATS* and *Snurf/Snrpn* (Fig. 2h). However, topotecan did not alter methylation at the imprinting centre (Fig. 2i and Supplementary Fig. 12). Taken together, these data indicate that topotecan unsilences paternal *Ube3a* by reducing transcription of a regulatory antisense RNA without appreciably affecting genomic methylation at the imprinting centre.

We then sought to determine if topotecan could unsilence the paternal *Ube3a* allele *in vivo*. We first identified a dose that was well tolerated, meaning there were no significant decreases in body weight between the beginning and end of the drug treatments (Supplementary Fig. 13). We then administered topotecan ($3.74\ \mu g\ h^{-1}$) unilaterally into the lateral ventricle of $Ube3a^{m+/pYFP}$ or $Ube3a^{m-/p+}$ mice by intracerebroventricular (i.c.v.) infusion for 2 weeks and then killed the mice

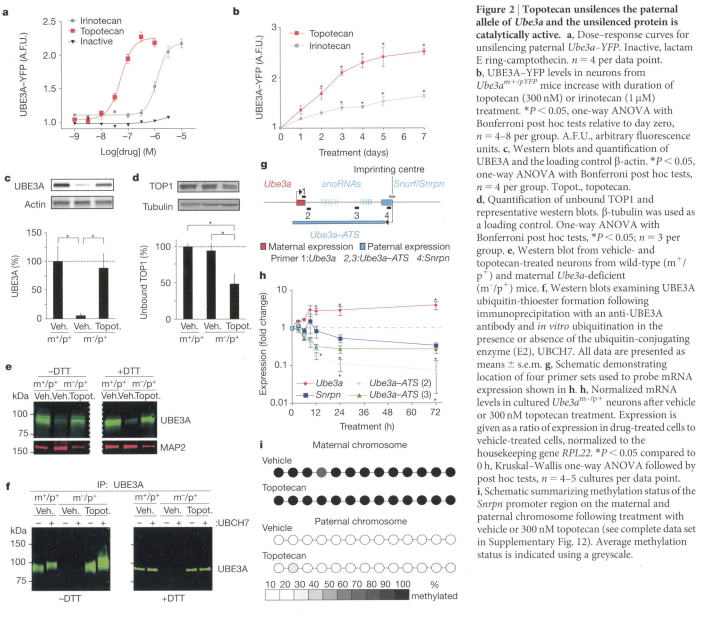

Figure 2 | Topotecan unsilences the paternal allele of *Ube3a* and the unsilenced protein is catalytically active. **a**, Dose–response curves for unsilencing paternal *Ube3a–YFP*. Inactive, lactam E ring-camptothecin. $n = 4$ per data point. **b**, UBE3A–YFP levels in neurons from $Ube3a^{m-/pYFP}$ mice increase with duration of topotecan (300 nM) or irinotecan (1 μM) treatment. $*P < 0.05$, one-way ANOVA with Bonferroni post hoc tests relative to day zero, $n = 4$–8 per group. A.F.U., arbitrary fluorescence units. **c**, Western blots and quantification of UBE3A and the loading control β-actin. $*P < 0.05$, one-way ANOVA with Bonferroni post hoc tests, $n = 4$ per group. Topot., topotecan. **d**, Quantification of unbound TOP1 and representative western blots. β-tubulin was used as a loading control. One-way ANOVA with Bonferroni post hoc tests, $*P < 0.05$; $n = 3$ per group. **e**, Western blot from vehicle- and topotecan-treated neurons from wild-type (m^+/p^+) and maternal *Ube3a*-deficient (m^-/p^+) mice. **f**, Western blots examining UBE3A ubiquitin-thioester formation following immunoprecipitation with an anti-UBE3A antibody and *in vitro* ubiquitination in the presence or absence of the ubiquitin-conjugating enzyme (E2), UBCH7. All data are presented as means ± s.e.m. **g**, Schematic demonstrating location of four primer sets used to probe mRNA expression shown in **h**. **h**, Normalized mRNA levels in cultured $Ube3a^{m-/p+}$ neurons after vehicle or 300 nM topotecan treatment. Expression is given as a ratio of expression in drug-treated cells to vehicle-treated cells, normalized to the housekeeping gene *RPL22*. $*P < 0.05$ compared to 0 h, Kruskal–Wallis one-way ANOVA followed by post hoc tests, $n = 4$–5 cultures per data point. **i**, Schematic summarizing methylation status of the *Snrpn* promoter region on the maternal and paternal chromosome following treatment with vehicle or 300 nM topotecan (see complete data set in Supplementary Fig. 12). Average methylation status is indicated using a greyscale.

either immediately or 5 h after drug cessation. Strikingly, topotecan unsilenced paternal *Ube3a* in the hippocampus, striatum and cerebral cortex of the infused hemisphere, but had only a modest effect on the contralateral (non-infused) hemisphere with no effect in the cerebellum (Fig. 3a–e and Supplementary Figs 14–15). Pharmacokinetic analyses demonstrated that a significant amount of topotecan was detectable in the infused hemisphere immediately after treatment, whereas low levels were present in the contralateral (non-infused) hemisphere and in cerebellum (Fig. 3a and Supplementary Fig. 14). However, a higher dose of topotecan (21.6 μg h^{-1} for 5 days) did unsilence the paternal allele of *Ube3a* in Purkinje neurons of the cerebellum (Supplementary Fig. 16). No significant difference in topotecan levels was detected in blood between drug- and vehicle-treated mice (data not shown). Topotecan concentrations significantly declined five hours after cessation of i.c.v. drug delivery (Fig. 3a), indicating that topotecan does not persist and is rapidly removed/metabolized in the brain. Taken together, these pharmacokinetic and pharmacodynamic data indicate that the degree to which topotecan unsilences the paternal *Ube3a* allele is directly correlated with drug concentrations in the brain. Moreover, our data indicate topotecan has the potential to unsilence the paternal *Ube3a* allele throughout the nervous system.

Genomic imprinting is thought to be established only during prescribed germline and embryonic periods of development and imprinted genes typically remain epigenetically regulated throughout life[26]. Thus, we next sought to determine if topotecan had transient or long-lasting effects on paternal *Ube3a* expression. To test this possibility, we turned to an intrathecal (i.t.) delivery protocol (Fig. 3f) because topotecan (Fig. 3g) and irinotecan (not shown) unsilenced paternal *Ube3a* in a sparse population of lumbar spinal neurons, allowing us to quantify all UBE3A–YFP-positive neurons. Moreover, i.t. delivery has been used to deliver topotecan to the brain in humans[27]. We found that topotecan (50 nmol in 5 μl; i.t. once daily, for 10 out of 14 days) was well tolerated (Supplementary Fig. 13) and significantly increased the number of paternal UBE3A–YFP-positive cells in the lumbar spinal cord of mice (Fig. 3g, h and Supplementary Fig. 17a). The vast majority (>93%) of these UBE3A–YFP-positive cells were $NeuN^+$ neurons (Supplementary Fig. 17a, b), indicating topotecan primarily unsilences *Ube3a* in neurons *in vivo*. Moreover, the unsilenced paternal UBE3A–YFP protein was expressed at levels comparable to maternal UBE3A–YFP controls (Supplementary Fig. 17c). Remarkably, the number of UBE3A–YFP-positive spinal cord neurons remained elevated 12 weeks after cessation of drug treatment (Fig. 3g, h), much longer than the elimination of topotecan from tissue (Fig. 3a). These results indicate that topotecan can enduringly unsilence paternal *Ube3a* in a subset of spinal neurons and indicate that a single course of drug treatment has the capacity to permanently modify expression of *Ube3a*.

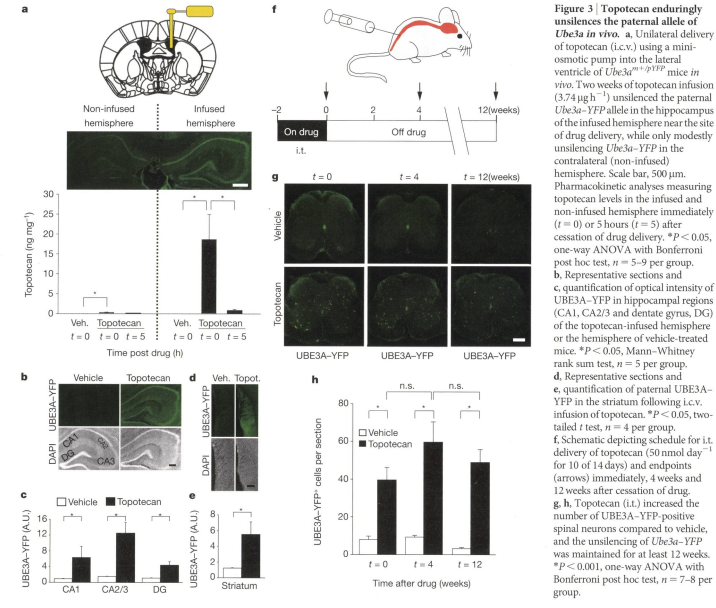

Figure 3 | Topotecan enduringly unsilences the paternal allele of *Ube3a in vivo*. **a**, Unilateral delivery of topotecan (i.c.v.) using a mini-osmotic pump into the lateral ventricle of $Ube3a^{m+/pYFP}$ mice *in vivo*. Two weeks of topotecan infusion (3.74 μg h^{-1}) unsilenced the paternal *Ube3a–YFP* allele in the hippocampus of the infused hemisphere near the site of drug delivery, while only modestly unsilencing *Ube3a–YFP* in the contralateral (non-infused) hemisphere. Scale bar, 500 μm. Pharmacokinetic analyses measuring topotecan levels in the infused and non-infused hemisphere immediately ($t = 0$) or 5 hours ($t = 5$) after cessation of drug delivery. *$P < 0.05$, one-way ANOVA with Bonferroni post hoc test, $n = 5$–9 per group. **b**, Representative sections and **c**, quantification of optical intensity of UBE3A–YFP in hippocampal regions (CA1, CA2/3 and dentate gyrus, DG) of the topotecan-infused hemisphere or the hemisphere of vehicle-treated mice. *$P < 0.05$, Mann–Whitney rank sum test, $n = 5$ per group. **d**, Representative sections and **e**, quantification of paternal UBE3A–YFP in the striatum following i.c.v. infusion of topotecan. *$P < 0.05$, two-tailed t test, $n = 4$ per group. **f**, Schematic depicting schedule for i.t. delivery of topotecan (50 nmol day^{-1} for 10 of 14 days) and endpoints (arrows) immediately, 4 weeks and 12 weeks after cessation of drug. **g**, **h**, Topotecan (i.t.) increased the number of UBE3A–YFP-positive spinal neurons compared to vehicle, and the unsilencing of *Ube3a–YFP* was maintained for at least 12 weeks. *$P < 0.001$, one-way ANOVA with Bonferroni post hoc test, $n = 7$–8 per group.

In conclusion, we found that topoisomerase inhibitors can unsilence the paternal allele of *Ube3a* and that the paternally-derived protein is functional. These findings suggest that topoisomerase inhibitors have the potential to rescue the molecular, cellular and behavioural deficits associated with loss of UBE3A[7,13,28]. *Ube3a* expression is modestly upregulated in the brain of *Top2b* knockout mice[29], providing genetic support that topoisomerases regulate *Ube3a* expression. We also found that topotecan reduced expression of paternal *Snrpn* and *Ipw*, a genomic region whose deletion is associated with Prader–Willi syndrome[7,17]. To what extent topotecan regulates expression of other genes in the brain, including *Igf2r*-, *Kcnq1*- and *Gnas*-imprinted gene clusters, and whether long-term treatments with topoisomerase inhibitors produce a Prader–Willi-like condition are unknown. However, topotecan and irinotecan are approved for use in patients with cancer, penetrate into the central nervous system, and are well-tolerated when administered chronically to both adult and paediatric patients[27,30]. As well, patients treated with topoisomerase inhibitors do not display symptoms associated with Prader–Willi syndrome. Ultimately, our study indicates that topoisomerase inhibitors regulate gene expression through a transcriptional mechanism and could be used to treat symptoms associated with Angelman syndrome.

METHODS SUMMARY

All animal procedures were approved by the University of North Carolina at Chapel Hill Animal Care and Use Committee. We used male and female *Ube3a–YFP* knock-in mice^{13}, $Ube3a^{m-/p+}$ mice[13] and their age-matched, wild-type controls. High-content screening was performed on a BD Pathway 855 system. UBE3A–YFP was detected for drug screening with an anti-GFP antibody (Novus Biologicals, NB600-308; 1:1,000) because intrinsic YFP fluorescence levels were low in cultured neurons and tissue sections. All data are presented as mean ± s.e.m., with sample sizes (n) shown in figures or stated in the text. Statistical analyses were performed using SigmaPlot 11 (Systat Software). Normality tests (Shapiro–Wilk) and equal variance tests were run and passed ($P > 0.05$) before parametric statistical analyses were run.

Full Methods and any associated references are available in the online version of the paper at www.nature.com/nature.

Received 28 June; accepted 22 November 2011.
Published online 21 December 2011.

1. Kishino, T., Lalande, M. & Wagstaff, J. UBE3A/E6-AP mutations cause Angelman syndrome. *Nature Genet.* **15,** 70–73 (1997).
2. Matsuura, T. *et al.* *De novo* truncating mutations in E6-AP ubiquitin-protein ligase gene (*UBE3A*) in Angelman syndrome. *Nature Genet.* **15,** 74–77 (1997).
3. Sutcliffe, J. S. *et al.* The E6-Ap ubiquitin-protein ligase (*UBE3A*) gene is localized within a narrowed Angelman syndrome critical region. *Genome Res.* **7,** 368–377 (1997).
4. Albrecht, U. *et al.* Imprinted expression of the murine Angelman syndrome gene, *Ube3a*, in hippocampal and Purkinje neurons. *Nature Genet.* **17,** 75–78 (1997).
5. Rougeulle, C., Glatt, H. & Lalande, M. The Angelman syndrome candidate gene, *UBE3A/E6-AP*, is imprinted in brain. *Nature Genet.* **17,** 14–15 (1997).
6. Vu, T. H. & Hoffman, A. R. Imprinting of the Angelman syndrome gene, *UBE3A*, is restricted to brain. *Nature Genet.* **17,** 12–13 (1997).
7. Mabb, A. M., Judson, M. C., Zylka, M. J. & Philpot, B. D. Angelman syndrome: insights into genomic imprinting and neurodevelopmental phenotypes. *Trends Neurosci.* **34,** 293–303 (2011).
8. Peters, S. U. *et al.* Double-blind therapeutic trial in Angelman syndrome using betaine and folic acid. *Am. J. Med. Genet.* **152A,** 1994–2001 (2010).
9. Chamberlain, S. J. & Brannan, C. I. The Prader–Willi syndrome imprinting center activates the paternally expressed murine *Ube3a* antisense transcript but represses paternal *Ube3a*. *Genomics* **73,** 316–322 (2001).
10. Landers, M. *et al.* Regulation of the large (approximately 1000 kb) imprinted murine *Ube3a* antisense transcript by alternative exons upstream of *Snurf/Snrpn*. *Nucleic Acids Res.* **32,** 3480–3492 (2004).
11. Numata, K., Kohama, C., Abe, K. & Kiyosawa, H. Highly parallel SNP genotyping reveals high-resolution landscape of mono-allelic *Ube3a* expression associated with locus-wide antisense transcription. *Nucleic Acids Res.* **39,** 2649–2657 (2011).
12. Nakatani, J. *et al.* Abnormal behavior in a chromosome-engineered mouse model for human 15q11-13 duplication seen in autism. *Cell* **137,** 1235–1246 (2009).
13. Jiang, Y. H. *et al.* Mutation of the Angelman ubiquitin ligase in mice causes increased cytoplasmic p53 and deficits of contextual learning and long-term potentiation. *Neuron* **21,** 799–811 (1998).
14. Miura, K. *et al.* Neurobehavioral and electroencephalographic abnormalities in *Ube3a* maternal-deficient mice. *Neurobiol. Dis.* **9,** 149–159 (2002).
15. Dindot, S. V., Antalffy, B. A., Bhattacharjee, M. B. & Beaudet, A. L. The Angelman syndrome ubiquitin ligase localizes to the synapse and nucleus, and maternal deficiency results in abnormal dendritic spine morphology. *Hum. Mol. Genet.* **17,** 111–118 (2008).
16. Rougeulle, C., Cardoso, C., Fontes, M., Colleaux, L. & Lalande, M. An imprinted antisense RNA overlaps UBE3A and a second maternally expressed transcript. *Nature Genet.* **19,** 15–16 (1998).
17. Runte, M. *et al.* The IC-*SNURF–SNRPN* transcript serves as a host for multiple small nucleolar RNA species and as an antisense RNA for *UBE3A*. *Hum. Mol. Genet.* **10,** 2687–2700 (2001).
18. Watanabe, Y. *et al.* Genome-wide analysis of expression modes and DNA methylation status at sense-antisense transcript loci in mouse. *Genomics* **96,** 333–341 (2010).
19. Pommier, Y. Topoisomerase I inhibitors: camptothecins and beyond. *Nature Rev. Cancer* **6,** 789–802 (2006).
20. Hertzberg, R. P. *et al.* Modification of the hydroxy lactone ring of camptothecin: inhibition of mammalian topoisomerase I and biological activity. *J. Med. Chem.* **32,** 715–720 (1989).
21. Plaschkes, I., Silverman, F. W. & Priel, E. DNA topoisomerase I in the mouse central nervous system: age and sex dependence. *J. Comp. Neurol.* **493,** 357–369 (2005).
22. Scheffner, M., Nuber, U. & Huibregtse, J. M. Protein ubiquitination involving an E1–E2–E3 enzyme ubiquitin thioester cascade. *Nature* **373,** 81–83 (1995).
23. Beaudenon, S., Dastur, A. & Huibregtse, J. M. Expression and assay of HECT domain ligases. *Methods Enzymol.* **398,** 112–125 (2005).
24. Kumar, S., Kao, W. H. & Howley, P. M. Physical interaction between specific E2 and Hect E3 enzymes determines functional cooperativity. *J. Biol. Chem.* **272,** 13548–13554 (1997).
25. Bressler, J. *et al.* The SNRPN promoter is not required for genomic imprinting of the Prader-Willi/Angelman domain in mice. *Nature Genet.* **28,** 232–240 (2001).
26. Reik, W. Stability and flexibility of epigenetic gene regulation in mammalian development. *Nature* **447,** 425–432 (2007).
27. Gammon, D. C. *et al.* Intrathecal topotecan in adult patients with neoplastic meningitis. *Am. J. Health Syst. Pharm.* **63,** 2083–2086 (2006).
28. Greer, P. L. *et al.* The Angelman syndrome protein Ube3A regulates synapse development by ubiquitinating arc. *Cell* **140,** 704–716 (2010).
29. Lyu, Y. L. *et al.* Role of topoisomerase IIβ in the expression of developmentally regulated genes. *Mol. Cell. Biol.* **26,** 7929–7941 (2006).
30. Bomgaars, L., Berg, S. L. & Blaney, S. M. The development of camptothecin analogs in childhood cancers. *Oncologist* **6,** 506–516 (2001).

Supplementary Information is linked to the online version of the paper at www.nature.com/nature.

Acknowledgements We thank A. Beaudet and Y.-h. Jiang for providing *Ube3a–YFP* and $Ube3a^{m-/p+}$ mice; T. Ricay and J. E. Han for assistance in i.c.v. mini-osmotic pump infusion; A. Burns for assistance in maintaining mouse colonies; V. Gukassyan for help with the Surveyor and confocal imaging systems; K. McNaughton for help with tissue sectioning; W. Zamboni for providing belotecan, rubitecan and silatecan; and W. Janzen and the Center of Integrative Chemical Biology and Drug Discovery for providing the epigenetic library. B.D.P., M.J.Z. and B.L.K. were supported by the Simons Foundation Autism Research Initiative (SFARI) and by the Angelman Syndrome Foundation. B.D.P. and M.J.Z. were supported by the National Institute of Mental Health (NIMH) (R01MH093372). B.D.P. was supported by the National Eye Institute (R01EY021833) and NC TraCS (10KR20016). M.J.Z. was supported by the National Institute of Neurological Disorders and Stroke (NINDS) (R01NS060725, R01NS067688). B.L.K. was supported by national Institutes of Health (NIH) HHSN-271-2008-00025-C, the NIMH Psychoactive Drug Screening Program, the Michael Hooker Distinguished Chair of Pharmacology, and grants from NIMH and the National Institute on Drug Abuse (NIDA). H.-S.H. was supported by a NARSAD grant from the Brain and Behavior Research Foundation Young Investigator Award and NC TraCS (10KR20910). J.A.A. was supported by NIH T32HD040127-07, the University of North Carolina-Carolina Institute for Developmental Disabilities, and an Autism Concept Award AR093464 from the US Department of Defense. A.M.M. was supported by a National Research Service Award from NINDS (5F32NS067712). I.F.K. was supported by a Joseph E. Wagstaff Postdoctoral Research Fellowship from the Angelman Syndrome Foundation. Assay development costs were partially supported by NINDS (5P30NS045892). Confocal and montage imaging was performed at the University of North Carolina at Chapel Hill Confocal and Multiphoton Imaging Facility, which is co-funded by grants from NINDS (5P30NS045892) and the National Institute of Child Health and Human Development (NICHD) (P30HD03110).

Author Contributions H.-S.H., J.A.A., A.M.M., I.F.K., M.J.Z., B.L.R. and B.D.P. conceived and designed experiments, and wrote the manuscript. All authors reviewed and edited the manuscript. H.-S.H., J.A.A., J.M. and H.-M.L. performed drug screens and validations. H.-S.H., B.T.-B., J.M. and J.W.D. performed *in vivo* studies and immunofluorescence. H.-S.H. and A.S.B. performed pharmacokinetic analyses. A.M.M. performed tests of UBE3A functionality. I.F.K. performed quantitative PCR with reverse transcription and methylation analyses. N.S. oversaw high content screening instrumentation and implemented image processing algorithms. X.C. and J.J. synthesized the lactam E ring inactive camptothecin analogue and the three indenoisoquinoline derivatives. The laboratories of M.J.Z., B.L.R. and B.D.P. contributed equally to this work.

Author Information Reprints and permissions information is available at www.nature.com/reprints. The authors declare no competing financial interests. Readers are welcome to comment on the online version of this article at www.nature.com/nature. Correspondence and requests for materials should be addressed to M.J.Z. (zylka@med.unc.edu), B.L.R. (bryan_roth@med.unc.edu) or B.D.P. (bphilpot@med.unc.edu).

LETTER

doi:10.1038/nature10661

A microRNA regulon that mediates endothelial recruitment and metastasis by cancer cells

Kim J. Png[1]*, Nils Halberg[1]*, Mitsukuni Yoshida[1] & Sohail F. Tavazoie[1]

Metastatic progression of cancer is a complex and clinically daunting process[1–4]. We previously identified a set of human microRNAs (miRNAs) that robustly suppress breast cancer metastasis to lung and bone[5,6] and which display expression levels that predict human metastasis. Although these findings revealed miRNAs as suppressors of cell-autonomous metastatic phenotypes, the roles of non-coding RNAs in non-cell-autonomous cancer progression processes remain unknown. Here we reveal that endogenous miR-126, an miRNA silenced in a variety of common human cancers[7,8], non-cell-autonomously regulates endothelial cell recruitment to metastatic breast cancer cells, *in vitro* and *in vivo*. It suppresses metastatic endothelial recruitment, metastatic angiogenesis and metastatic colonization through coordinate targeting of *IGFBP2*, *PITPNC1* and *MERTK*—novel pro-angiogenic genes and biomarkers of human metastasis. Insulin-like growth factor binding protein 2 (IGFBP2) secreted by metastatic cells recruits endothelia by modulating IGF1-mediated activation of the IGF type-1 receptor on endothelial cells; whereas c-Mer tyrosine kinase (MERTK) receptor cleaved from metastatic cells promotes endothelial recruitment by competitively antagonizing the binding of its ligand GAS6 to endothelial MERTK receptors. Co-injection of endothelial cells with breast cancer cells non-cell-autonomously rescues their miR-126-induced metastatic defect, revealing a novel and important role for endothelial interactions in metastatic initiation. Through loss-of-function and epistasis experiments, we delineate an miRNA regulatory network's individual components as novel and cell-extrinsic regulators of endothelial recruitment, angiogenesis and metastatic colonization. We also identify the IGFBP2/IGF1/IGF1R and GAS6/MERTK signalling pathways as regulators of cancer-mediated endothelial recruitment. Our work further reveals endothelial recruitment and endothelial interactions in the tumour microenvironment to be critical features of metastatic breast cancer.

To determine the role of endogenous miR-126 in metastatic progression, stable miR-126 and control knockdown cells were generated (Supplementary Fig. 1), injected into immunodeficient mice and evaluated for metastatic colonization capacity in tail-vein, intracardiac and portal circulation colonization assays. miR-126 silencing in parental MDA-231 breast cancer cells significantly increased lung metastatic colonization (Fig. 1a and Supplementary Fig. 2), systemic metastatic colonization to multiple organs such as brain and bone (Fig. 1b, c) and hepatic metastatic colonization (Fig. 1d). miR-126 inhibition did not significantly enhance proliferation *in vitro* and resulted in a modest increase in mammary tumour volume (39.4%; Supplementary Fig. 3), which was an order of magnitude smaller than its effect on metastasis enhancement. This indicates that the effect of miR-126 on metastasis was not simply a result of its effect on tumour growth suppression. Histological quantification revealed a significant increase in the total number of metastatic nodules (small and large) in miR-126 knockdown lungs (13.6 ± 3.2 compared with 4.9 ± 1.8 in controls, $P < 0.03$; Fig. 1e). Importantly, the increase in nodule

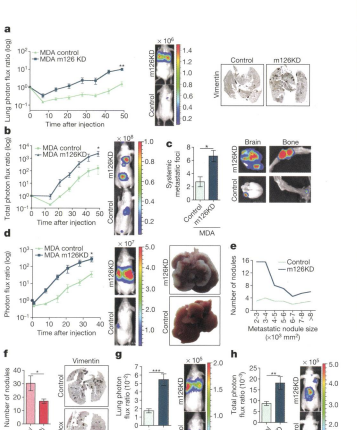

Figure 1 | Endogenous miR-126 suppresses metastatic colonization. **a**, Bioluminescence imaging plot of lung metastasis by 4×10^4 MDA-MB-231 breast cancer cells expressing a hairpin (miR-Zip) targeting miR-126 (MDA/miR-126KD (KD, knockdown)) or a control hairpin (MDA/control); $n = 5$. Lungs were extracted at D49 and stained for vimentin. **b**, Bioluminescence quantification of systemic metastasis by 4×10^4 MDA/miR-126KD or MDA/control cells; $n = 6$. **c**, Total number of metastatic foci in mice from **b** were counted. Representative images of brain and bone metastatic nodules shown. **d**, Bioluminescence quantification of liver metastasis by 5×10^5 MDA/miR-126KD or MDA/control cells; $n = 6$. **e**, Sizes of metastatic nodules in lungs extracted from **a** were measured using ImageJ. **f**, 4×10^4 Lm2 cells expressing doxycycline-inducible pre-miR-126 were injected at day 0. At day 3, doxycycline ($2\ \mathrm{mg\ ml^{-1}}$) was added to the drinking water. At D49, the lungs were removed and stained for vimentin (right). Total number of nodules/lung shown. **g**, Bioluminescence quantification of lung metastasis by 5×10^5 poorly metastatic CN34 breast cancer cells expressing a hairpin targeting miR-126 (CN34/miR-126KD) or a control hairpin (CN34/control); $n = 7$. **h**, Bioluminescence quantification of systemic metastasis by 1×10^6 CN34/miR-126KD and CN34/control cells; $n = 6$. Error bars, s.e.m.; all P values are based on one-sided Student's t-tests. $^*P < 0.05$; $^{**}P < 0.001$; $^{***}P < 0.0001$.

[1]Laboratory of Systems Cancer Biology, Rockefeller University, 1230 York Avenue, New York, New York 10065, USA.
*These authors contributed equally to this work.

number was more pronounced for smaller nodule sizes than larger ones, consistent primarily with an increase in the initiation of metastases rather than an increase in the growth of established metastases. Consistent with a role for miR-126 in metastatic initiation in the niche, conditionally restoring miR-126 expression to metastatic LM2 cells after extravasation in the lung (day 3 (ref. 9)) significantly reduced metastatic colonization (Fig. 1f). Finally, miR-126 knockdown enhanced lung and systemic metastatic colonization by an independent poorly metastatic CN34 line (Fig. 1g, h). These findings reveal endogenous miR-126 to be a suppressor of metastatic initiation and metastatic colonization.

While considering the basis of the selective advantage provided by miR-126 silencing, we noted that miR-126 knockdown metastases displayed higher vessel densities on microscopic visualization of lung tissue sections stained with haematoxylin and eosin. Image analysis and quantification revealed metastases derived from miR-126 knockdown cells to have significantly higher endothelial densities than control cells (Fig. 2a and Supplementary Fig. 4). Lectin injection and cytochemistry revealed miR-126 knockdown metastases to contain increased functional blood vessel densities (Fig. 2b), whereas dextran injection revealed increased perfusion to miR-126 knockdown metastases (Supplementary Fig. 5). Thus, these independent and complementary methods reveal that miR-126 suppresses metastatic endothelial density, functional metastatic angiogenesis and perfusion; consequently, its inhibition provides metastatic cells with a selective advantage in endothelial interactions and angiogenic progression.

We next sought to determine the cellular basis for the miR-126-dependent angiogenesis phenotype observed. miR-126 did not suppress adhesion of metastatic cells to endothelial cells, endothelial proliferation or tube formation as assessed by automated quantification of branch points (Supplementary Fig. 6). We speculated that miR-126 might regulate the recruitment of endothelial cells to metastatic cells. Interestingly, metastatic LM2 cells, which display silencing of miR-126, placed in the bottom of a Boyden chamber strongly recruited human umbilical vein endothelial cells (HUVECS) through a porous trans-well insert and recruited significantly more endothelia than their less metastatic parental line (Fig. 2c). Endothelial recruitment was strongly inhibited by miR-126 overexpression (Fig. 2d). Conversely, miR-126 knockdown through miR-Zip (Fig. 2d and Supplementary Fig. 7) or LNA approaches (Supplementary Fig. 8a) significantly increased endothelial recruitment. The CN34-LM1A metastatic derivative also displayed significantly enhanced endothelial recruitment capacity relative to its poorly metastatic parental line (Supplementary Fig. 8b). miR-126 significantly suppressed endothelial recruitment by the CN34 cell population and the HER2-positive SkBr3 line (Fig. 2e), and suppressed recruitment of HMVEC endothelial cells (Supplementary Fig. 8c). These findings reveal enhanced endothelial recruitment capacity to be a key feature of metastatic breast cancer populations and identify endogenous miR-126 as a major regulator of this process.

We next asked whether endogenous miR-126 can selectively regulate endothelial recruitment to breast cancer cells independent of their location. Endothelial recruitment to metastatic cells injected in the mammary fat-pad was specifically inhibited by miR-126 expression and enhanced by miR-126 suppression (Supplementary Fig. 9a–c), whereas miR-126 silencing did not increase leukocyte (Supplementary Fig. 9d) or macrophage densities (Supplementary Fig. 9e). These findings reveal miR-126 to regulate endothelial recruitment to breast cancer cells selectively, independent of their anatomical location, and they provide a non-cell-autonomous mechanism for the enhanced primary tumour-size phenotype seen with miR-126 silencing.

To identify the targets of miR-126, we used an integrative transcriptomic approach and identified a set of eight genes that were suppressed by endogenous miR-126 (Fig. 2f, Supplementary Fig. 10 and Supplementary Table 1). Interestingly, patients whose primary breast cancers displayed overexpression of these genes were significantly

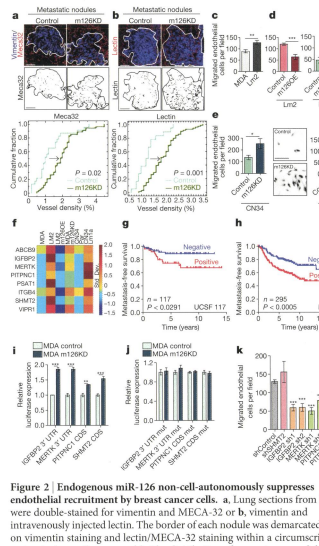

Figure 2 | Endogenous miR-126 non-cell-autonomously suppresses endothelial recruitment by breast cancer cells. **a**, Lung sections from Fig. 1a were double-stained for vimentin and MECA-32 or **b**, vimentin and intravenously injected lectin. The border of each nodule was demarcated based on vimentin staining and lectin/MECA-32 staining within a circumscribed region is shown (lower panels). The distribution of percentage vessel density (area positive for lectin/MECA-32 staining per area) is shown in a cumulative fraction plot; $n = 8$ (18 and 68 nodules in control and miR-126 knockdown groups, respectively). P value is based on the Kolmogorov–Smirnov test. **c**, Trans-well recruitment of 5×10^4 HUVEC cells by 2.5×10^5 MDA and LM2 cells was assessed by counting the number of HUVEC cells that migrated to the basal side of the trans-well inserts; $n = 4$. **d**, LM2/miR-126OE or LM2/control and MDA/miR-126KD or MDA/control cells were subjected to the HUVEC recruitment assay; $n = 4$. **e**, CN34/miR-126KD or CN34/control and SkBr3 breast cancer cells transfected with control or miR-126-targeting LNAs were subjected to the HUVEC recruitment assay; $n = 5$. Representative images are shown. Scale bar, 100 μm. **f**, The miR-126 metastasis signature comprises eight genes overexpressed in metastatic cells, downregulated by miR-126OE and upregulated by miR-126KD. The heat map represents variance-normalized expression levels based on microarray and quantitative PCR (qPCR) analyses. The colour map corresponds to standard deviation change from the mean. **g**, **h**, Kaplan–Meier curves for the UCSF breast cancer cohort ($n = 117$) and NKI cohort ($n = 295$) depicting metastasis-free-survival of patients as a function of their primary tumours' miR-126 signature status. An aggregate expression score (sum of the expression values of the eight genes) greater or lower than the mean of the entire population is classified as miR-126 positive or negative, respectively. P values are based on a Mantel–Cox log-rank test. **i**, Luciferase reporter assays of miR-126 target genes in MDA/miR-126KD or MDA/control cells; $n = 4$. UTR, untranslated region; CDS, coding sequence. **j**, The miR-126 complementary regions were mutated and the luciferase reporter assays repeated; $n = 4$. **k**, LM2 cells expressing hairpins targeting *IGFBP2*, *MERTK*, *PITPNC1*, *SHMT2* or a control hairpin were subjected to the HUVEC recruitment assay; $n = 4$. Error bars, s.e.m.; P values were obtained using one-sided Student's t-tests (**c**–**e**, **i**–**k**).

more likely to develop distal metastases and experienced shorter metastasis-free survival in multiple cohorts than those whose cancers did not (Fig. 2g, h). The prognostic power of this signature was subtype independent and performed robustly in the combined MSK/NKI/UCSF (Memorial Sloan-Kettering Cancer Center/Nederlands Kanker Instituut/University of California, San Francisco) cohorts ($n = 494$; $P < 0.0004$; Supplementary Fig. 11). Thus, miR-126 suppresses the expression of a set of eight genes that are positively and strongly correlated with human metastatic relapse.

Luciferase reporter assays and subsequent mutagenesis of the 3′ untranslated regions and coding sequences of this entire set revealed endogenous miR-126 to interact with *IGFBP2* and receptor kinase *MERTK* 3′ untranslated regions, and the coding regions of the phosphatidylinositol transfer protein *PITPNC1* and the hydroxymethyltransferase *SHMT2* (Fig. 2i, j and Supplementary Fig. 12). We next asked if any of the miR-126 target genes regulate the recruitment of endothelial cells by cancer cells. Of these four genes, knockdown of *IGFBP2*, *MERTK* or *PITPNC1* significantly suppressed the ability of metastatic LM2 and CN34-LM1A cells to recruit endothelial cells (Fig. 2k and Supplementary Fig. 13h), whereas their overexpression in MDA-231 and CN34-Par cells enhanced endothelial recruitment (Supplementary Fig. 13l). Importantly, knockdown of these genes did not significantly decrease cancer cell proliferation (Supplementary Fig. 14). Given the requirement of each of these genes for endothelial recruitment, we wondered if each of these genes individually correlates with human metastatic relapse. Interestingly, expression levels of *IGFBP2*, *MERTK* and *PITPNC1* were individually and significantly increased in patients with stage III and IV primary tumours relative to those with stage I and II tumours in an additional cohort of 96 patients (Fig. 3a and Supplementary Table 2). We next assessed the requirement of these genes for metastasis and *in vivo* endothelial recruitment. Knockdown of *IGFBP2* using independent short hairpins significantly suppressed metastatic colonization to the lung (sh_1, tenfold; sh_2, 6.25-fold; Fig. 3b), whereas knockdown of *PITPNC1* and *MERTK* also strongly inhibited metastatic colonization (*PITPNC1*sh_1, 7.69-fold; *PITPNC1*sh_2, 4.55-fold, Fig. 3c; *MERTK*sh_1, 3.91-fold; *MERTK*sh_2, 3.08-fold, Fig. 3d). Additionally, shRNA inhibition of *IGFPB2*, *PITPNC1* or *MERTK* using independent hairpins significantly reduced metastatic endothelial density (Fig. 3e) and functional vessel content (Supplementary Fig. 15). Epistasis experiments revealed that knockdown of *IGFBP2*, *MERTK* or *PITPNC1* in miR-126 knockdown cells significantly suppressed endothelial recruitment (Fig. 3f) and metastatic colonization (Fig. 3h and Supplementary Fig. 16) normally seen with miR-126 knockdown. Conversely, *IGFBP2*, *MERTK* or *PITPNC1* overexpression in miR-126-overexpressing cells rescued the ability of cancer cells to recruit endothelia (Fig. 3g). These findings reveal that the miR-126 direct target genes *IGFBP2*, *PITPNC1* and *MERTK* are individually required for endothelial recruitment and metastatic colonization, are downstream of miR-126 and individually correlate in expression with human metastatic progression.

We next sought to determine the mechanisms by which these miR-126 target genes mediate endothelial recruitment and metastasis. Of the miR-126 targets, IGFBP2 is secreted and thus poised to mediate extracellular effects. Consistent with this, enzyme-linked immunosorbent assay (ELISA) analysis revealed metastatic LM2 cells to secrete 2.1-fold higher levels of this factor than less metastatic parental MDA-231 cells, whereas miR-126 knockdown enhanced IGFBP2 levels (2.75-fold; Fig. 4a) and had no effect on vascular endothelial growth factor (VEGF) levels (Supplementary Fig. 17). Antibody-mediated inhibition of IGFBP2 in a trans-well recruitment assay significantly inhibited metastatic-cell endothelial recruitment and prevented miR-126-dependent recruitment in MDA and CN34 Par cells (Fig. 4b and Supplementary Fig. 18a, b). Finally, recombinant IGFBP2 protein rescued the endothelial recruitment defect of miR-126-overexpressing cells (Fig. 4c). *IGFBP2* is a member of a large family known to bind IGF1 and/or IGF2 in the extracellular space to modulate their signalling

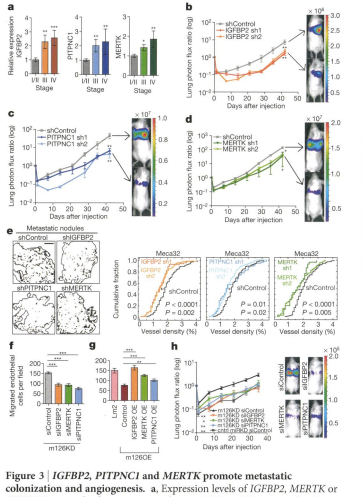

Figure 3 | *IGFBP2*, *PITPNC1* and *MERTK* promote metastatic colonization and angiogenesis. **a**, Expression levels of *IGFBP2*, *MERTK* or *PITPNC1* in samples from patients with stage I/II ($n = 53$) compared with stage III ($n = 29$) or stage IV ($n = 9$) breast tumours. **b**–**d**, Bioluminescence quantification of lung metastasis by LM2 cells expressing the control hairpin or hairpins targeting *IGFBP2* (**b**), *PITPNC1* (**c**) or *MERTK* (**d**); $n = 5$. **e**, Lung sections were double stained for vimentin and MECA-32. The metastatic MECA-32 signal is shown in black. Distributions of percentage vessel densities are shown in cumulative fraction plots; $n = 4$. *P* values are based on the Kolmogorov–Smirnov test. **f**, MDA/miR126 knockdown cells were transfected with short interfering RNAs (siRNAs) targeting *IGFBP2*, *MERTK* and *PITPNC1* or control siRNA and subjected to HUVEC recruitment assays; $n = 9$. **g**, Coding regions of *IGFBP2*, *MERTK* and *PITPNC1* were overexpressed in LM2/miR-126-overexpressing cells that were subjected to HUVEC recruitment assays; $n = 6$. **h**, Bioluminescence imaging of lung metastasis by MDA/miR-126 knockdown cells transfected with siRNAs targeting *IGFBP2*, *MERTK* and *PITPNC1* or control siRNA; $n = 5$. Error bars, s.e.m., *P* values were obtained using a one-sided Student's *t*-test (**a**–**d**, **f**, **h**).

activity[10]. To determine which IGF mediates miR-126-dependent endothelial recruitment, we treated cells with specific blocking antibodies and found that antibody-mediated inhibition of IGF1, which is present in endothelial media, but not IGF2, significantly reduced endothelial recruitment resulting from miR-126 knockdown (Fig. 4d). Next, inhibition of IGF type-1 receptor (IGF1R) with a blocking antibody, but not IGF2R, on endothelial cells significantly reduced endothelial recruitment resulting from miR-126 knockdown (Fig. 4e and Supplementary Fig. 18c, d). Finally, both recombinant IGFBP2 and conditioned media from miR-126 knockdown cells activated IGF1R on endothelial cells as assessed by western blot (Fig. 4f and Supplementary Fig. 19a), whereas recombinant IGFBP2 protein was sufficient, in a dose-dependent manner, to promote endothelial chemotaxis (Fig. 4g) and migration (Supplementary Fig. 19b) in an IGF1R-dependent manner. These findings suggest that the miR-126/IGFBP2/IGF1 pathway

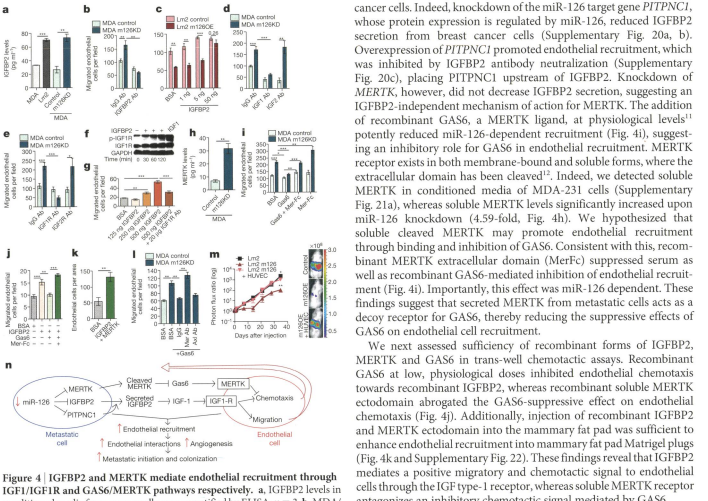

Figure 4 | IGFBP2 and MERTK mediate endothelial recruitment through IGF1/IGF1R and GAS6/MERTK pathways respectively. **a**, IGFBP2 levels in conditioned media from cancer cells were quantified by ELISA; $n = 3$. **b**, MDA/miR-126KD and MDA/control cells were subjected to the HUVEC recruitment assay in the presence of 50 ng ml^{-1} IGFBP2 Ab or 50 ng ml^{-1} control IgG Ab; $n = 4$. **c**, LM2/miR-126OE and LM2/control cells were subjected to the HUVEC recruitment assay with 1, 5 or 50 ng ml^{-1} rhIGFBP2 or 50 ng ml^{-1} BSA; $n = 4$. **d**, **e**, MDA/miR-126KD and MDA/control cells were subjected to the HUVEC recruitment assay in the presence IGF-1, IGF-2 or IgG Ab (**d**) and IGF1R, IGF2R or IgG Ab (**e**); $n = 4$. **f**, HUVEC cells were treated with 520 ng ml^{-1} rhIGFBP2 or 50 ng ml^{-1} rhIGF-1 and analysed by western blot. **g**, Chemotaxis of HUVECs towards an IGFBP2 source across trans-well inserts was assessed; $n = 4$. **h**, Soluble MERTK levels in conditioned media from cancer cells was quantified by ELISA; $n = 4$; i, MDA/miR-126KD and MDA/control cells were subjected to the HUVEC recruitment assay in the presence of 1 ng ml^{-1} GAS6 and/or 10 μg ml^{-1} MerFc; $n = 4$. **j**, Chemotaxis of HUVECs towards an IGFBP2 source was assessed in the presence of Gas6 (5 ng ml^{-1}) and MerFc (10 μg ml^{-1}) protein; $n = 4$. **k**, Endothelial recruitment to mammary fat pads was analysed *in vivo* using Matrigel plugs containing either recombinant IGFBP2 (1 μg ml^{-1}) and MERTK (10 μg ml^{-1}) or BSA (11 μg ml^{-1}). $n = 5$. Error bars, s.e.m. *P* values were obtained using a one-sided Mann–Whitney test. **l**, HUVEC cells were pre-treated with 10 μg ml^{-1} MERTK blocking Ab, 20 μg ml^{-1} AXL blocking Ab or 20 μg ml^{-1} IgG Ab for 1 h before HUVEC recruitment capacity in the presence of 1 ng ml^{-1} GAS6 was assessed; $n = 4$. **m**, Bioluminescence imaging of liver metastasis by LM2/control cancer cells, LM2/miR-126OE cells as well as LM2/miR-126OE cells co-injected with HUVEC cells; $n = 4$. **n**, Schematic of miR-126 regulation of endothelial recruitment and metastatic colonization through *IGFBP2*, *PITPNC1* and *MERTK* targeting. Error bars, s.e.m. *P* values were obtained using a one-sided Student's *t*-test (**a**–**e**, **g**–**l**).

activates IGF1R on endothelial cells, resulting in enhanced endothelial migration towards metastatic cells.

Given our identification of IGFBP2 as a secreted miR-126-dependent factor that mediates endothelial recruitment and metastasis, we asked whether PITPNC1 or MERTK regulate the secretion of this factor from cancer cells. Indeed, knockdown of the miR-126 target gene *PITPNC1*, whose protein expression is regulated by miR-126, reduced IGFBP2 secretion from breast cancer cells (Supplementary Fig. 20a, b). Overexpression of *PITPNC1* promoted endothelial recruitment, which was inhibited by IGFBP2 antibody neutralization (Supplementary Fig. 20c), placing PITPNC1 upstream of IGFBP2. Knockdown of *MERTK*, however, did not decrease IGFBP2 secretion, suggesting an IGFBP2-independent mechanism of action for MERTK. The addition of recombinant GAS6, a MERTK ligand, at physiological levels[11] potently reduced miR-126-dependent recruitment (Fig. 4i), suggesting an inhibitory role for GAS6 in endothelial recruitment. MERTK receptor exists in both membrane-bound and soluble forms, where the extracellular domain has been cleaved[12]. Indeed, we detected soluble MERTK in conditioned media of MDA-231 cells (Supplementary Fig. 21a), whereas soluble MERTK levels significantly increased upon miR-126 knockdown (4.59-fold, Fig. 4h). We hypothesized that soluble cleaved MERTK may promote endothelial recruitment through binding and inhibition of GAS6. Consistent with this, recombinant MERTK extracellular domain (MerFc) suppressed serum as well as recombinant GAS6-mediated inhibition of endothelial recruitment (Fig. 4i). Importantly, this effect was miR-126 dependent. These findings suggest that secreted MERTK from metastatic cells acts as a decoy receptor for GAS6, thereby reducing the suppressive effects of GAS6 on endothelial cell recruitment.

We next assessed sufficiency of recombinant forms of IGFBP2, MERTK and GAS6 in trans-well chemotactic assays. Recombinant GAS6 at low, physiological doses inhibited endothelial chemotaxis towards recombinant IGFBP2, whereas recombinant soluble MERTK ectodomain abrogated the GAS6-suppressive effect on endothelial chemotaxis (Fig. 4j). Additionally, injection of recombinant IGFBP2 and MERTK ectodomain into the mammary fat pad was sufficient to enhance endothelial recruitment into mammary fat pad Matrigel plugs (Fig. 4k and Supplementary Fig. 22). These findings reveal that IGFBP2 mediates a positive migratory and chemotactic signal to endothelial cells through the IGF type-1 receptor, whereas soluble MERTK receptor antagonizes an inhibitory chemotactic signal mediated by GAS6.

We then sought to identify the endothelial receptor that mediates the GAS6-suppressive effect on endothelial recruitment. To this end, we inhibited endothelial MERTK and AXL, two GAS6 receptors that are highly expressed by endothelial cells, with neutralizing antibodies as well as RNAi. We found that MERTK inhibition on endothelial cells occluded GAS6-induced suppression of endothelial recruitment. These findings indicate endothelial MERTK receptor as the mediator of the GAS6 phenotype (Fig. 4l and Supplementary Fig. 21b).

Finally, we reasoned that if the suppressive effect of miR-126 on metastasis is indeed secondary to compromised endothelial recruitment and is non-cell autonomous, it should be rescued upon the addition of endothelial cells. To this end, we injected metastatic LM2 cells as well as LM2 cells overexpressing miR-126 into the portal circulation. miR-126 overexpression strongly suppressed hepatic metastatic colonization. Interestingly, co-injection of endothelial cells along with miR-126-overexpressing cells in colonization assays completely rescued their metastatic colonization defect (Fig. 4m and Supplementary Fig. 23). These dramatic findings reveal endothelial recruitment capacity to be the key metastatic phenotype regulated by miR-126 and reveal a major role for cancer–endothelial interactions in metastatic initiation leading to colonization. Metastatic cells displaying silencing of this miRNA and the resulting induction of its targets *IGFBP2*, *MERTK* and *PITPNC1* are able to establish more readily the endothelial and blood vessel interactions required for metastatic initiation and colonization (Supplementary Discussion). Our findings establish a key required role for cancer–endothelial interactions and cooperation in metastatic initiation leading to colonization. We propose that endothelial cells provide incipient metastases a key signal that promotes metastatic initiation efficiency. This novel non-canonical role for endothelial cells in metastatic initiation results

in enhanced metastatic colonization. Our systematic analysis and focus on metastasis and metastatic angiogenesis has led to the identification of several molecules, including secreted IGFBP2, the transfer protein PITPNC1 and the kinase MERTK, as well as their respective pathways IGFBP2/IGF1/IGF1R and cleaved MERTK/GAS6/MERTK as necessary and sufficient for mediating metastatic cell endothelial recruitment (Fig. 4n). The combined modulation of these endothelial-convergent signalling pathways by cancer cells empowers these cells with enhanced endothelial recruitment capacity and metastatic efficiency. It also reveals novel cooperative molecular targets for therapeutic inhibition with the potential for preventing metastatic breast cancer in the adjuvant setting.

METHODS SUMMARY

See Methods for additional information on cell culture, endothelial assays, luciferase assays, microarray analyses, ELISA, western blotting, histology, survival analyses, statistical methods and animal studies, as well as generation of lentivirus, retrovirus, knockdown and overexpressing cells.

Full Methods and any associated references are available in the online version of the paper at www.nature.com/nature.

Received 23 January; accepted 21 October 2011.
Published online 14 December 2011.

1. Chiang, A. C. & Massague, J. Molecular basis of metastasis. *N. Engl. J. Med.* **359,** 2814–2823 (2008).
2. Talmadge, J. E. & Fidler, I. J. AACR centennial series: the biology of cancer metastasis: historical perspective. *Cancer Res.* **70,** 5649–5669 (2010).
3. Hanahan, D. & Weinberg, R. A. Hallmarks of cancer: the next generation. *Cell* **144,** 646–674 (2011).
4. Valastyan, S. & Weinberg, R. A. MicroRNAs: crucial multi-tasking components in the complex circuitry of tumor metastasis. *Cell Cycle* **8,** 3506–3512 (2009).
5. Tavazoie, S. F. *et al.* Endogenous human microRNAs that suppress breast cancer metastasis. *Nature* **451,** 147–152 (2008).
6. Png, K. J. *et al.* MicroRNA-335 inhibits tumor reinitiation and is silenced through genetic and epigenetic mechanisms in human breast cancer. *Genes Dev.* **25,** 226–231 (2011).
7. Guo, C. *et al.* The noncoding RNA, miR-126, suppresses the growth of neoplastic cells by targeting phosphatidylinositol 3-kinase signaling and is frequently lost in colon cancers. *Genes Chromosom. Cancer* **47,** 939–946 (2008).
8. Feng, R. *et al.* miR-126 functions as a tumour suppressor in human gastric cancer. *Cancer Lett.* **298,** 50–63 (2010).
9. Gupta, G. P. *et al.* Mediators of vascular remodelling co-opted for sequential steps in lung metastasis. *Nature* **446,** 765–770 (2007).
10. Jones, J. I. & Clemmons, D. R. Insulin-like growth factors and their binding proteins: biological actions. *Endocr. Rev.* **16,** 3–34 (1995).
11. Balogh, I. *et al.* Analysis of Gas6 in human platelets and plasma. *Arterioscler. Thromb. Vasc. Biol.* **25,** 1280–1286 (2005).
12. Sather, S. *et al.* A soluble form of the Mer receptor tyrosine kinase inhibits macrophage clearance of apoptotic cells and platelet aggregation. *Blood* **109,** 1026–1033 (2007).

Supplementary Information is linked to the online version of the paper at www.nature.com/nature.

Acknowledgements We thank the members of the Tavazoie laboratory, Saeed Tavazoie, M. Tavazoie, S. Kurdistani, C. Alarcon and E. Mandel for comments on previous versions of this manuscript. We thank V. Gueorguiev and the Memorial Sloan-Kettering Cancer Center's Molecular Cytology Core Facility for help. We thank the Memorial Sloan-Kettering Cancer Center's High-Throughput Screening Core Facility for providing the shRNAs. We thank H. Lee for cloning assistance. K.J.P. is an A*STAR National Science Scholar. S.F.T. is a Department of Defense Era of Hope Scholar and the Leon Hess Head of the Elizabeth and Vincent Mayer Laboratory at Rockefeller University.

Author Contributions S.F.T. conceived the project and supervised all research. K.J.P., N.H. and S.F.T. wrote the manuscript. K.J.P., N.H. and S.F.T. designed the experiments. K.J.P., N.H. and M.Y. performed the experiments.

Author Information The data from miR-126-overexpressing and MDA/LM2 microarrays are deposited in Gene Expression Omnibus under accession numbers GSE 23905 and 23904 respectively. Reprints and permissions information is available at www.nature.com/reprints. The authors declare no competing financial interests. Readers are welcome to comment on the online version of this article at www.nature.com/nature. Correspondence and requests for materials should be addressed to S.F.T. (stavazoie@mail.rockefeller.edu).

LETTER

doi:10.1038/nature10712

Ars2 maintains neural stem–cell identity through direct transcriptional activation of *Sox2*

Celia Andreu-Agullo[1], Thomas Maurin[1], Craig B. Thompson[2] & Eric C. Lai[1]

Fundamental questions remain unanswered about the transcriptional networks that control the identity and self-renewal of neural stem cells (NSCs), a specialized subset of astroglial cells that are endowed with stem properties and neurogenic capacity. Here we report that the zinc finger protein Ars2 (arsenite-resistance protein 2; also known as Srrt) is expressed by adult NSCs from the subventricular zone (SVZ) of mice, and that selective knockdown of *Ars2* in cells expressing glial fibrillary acidic protein within the adult SVZ depletes the number of NSCs and their neurogenic capacity. These phenotypes are recapitulated in the postnatal SVZ of *hGFAP-cre*::*Ars2*$^{fl/fl}$ conditional knockout mice, but are more severe. *Ex vivo* assays show that Ars2 is necessary and sufficient to promote NSC self-renewal, and that it does so by positively regulating the expression of *Sox2*. Although plant[1–3] and animal[4,5] orthologues of Ars2 are known for their conserved roles in microRNA biogenesis, we unexpectedly observed that Ars2 retains its capacity to promote self-renewal in *Drosha* and *Dicer1* knockout NSCs. Instead, chromatin immunoprecipitation revealed that Ars2 binds a specific region within the 6-kilobase NSC enhancer of *Sox2*. This association is RNA-independent, and the region that is bound is required for Ars2-mediated activation of *Sox2*. We used gel-shift analysis to refine the Sox2 region bound by Ars2 to a specific conserved DNA sequence. The importance of *Sox2* as a critical downstream effector is shown by its ability to restore the self-renewal and multipotency defects of *Ars2* knockout NSCs. Our findings reveal Ars2 as a new transcription factor that controls the multipotent progenitor state of NSCs through direct activation of the pluripotency factor *Sox2*.

Stem cells reside in most mammalian tissues throughout adult life, and contribute to normal homeostasis and repair after injury[6]. They are defined by their capacity to both self-renew and differentiate, thus perpetuating themselves while generating more committed daughter cells. Two major stem-cell niches exist in the adult brain, and these are found within the hippocampus and within the SVZ. Relatively quiescent NSCs give rise to actively proliferating transit-amplifying progenitors, which generate oligodendrocytes that are destined for the corpus callosum[7] and neuroblasts that migrate rostrally and differentiate into local interneurons in the olfactory bulb[8,9]. Much remains to be understood about the mechanisms and factors that control NSC self-renewal and multipotency[10].

Mammalian Ars2 was reported to be essential for cell proliferation, to be downregulated in quiescent cells, and to be required for the accumulation of several microRNAs (miRNAs) that are implicated in cellular transformation[4]. Unexpectedly, we observed that Ars2 expression in the adult SVZ did not correlate with proliferation, as 95 ± 2% of Ars2$^+$-positive (Ars2$^+$) cells lacked the proliferative marker Ki67. Moreover, Ars2 was present in only 7 ± 2% of Mash1$^+$ transit-amplifying progenitors (Supplementary Fig. 1b) and was absent from doublecortin (DCX)-positive (DCX$^+$) neuroblasts (Fig. 1a); these comprise the most highly proliferative cells in the SVZ. Ars2 was also absent from GFAP$^+$Nestin$^+$Sox2$^+$ astroglial cells and S100β$^+$ mature astrocytes (Supplementary Fig. 1). Instead, Ars2 was

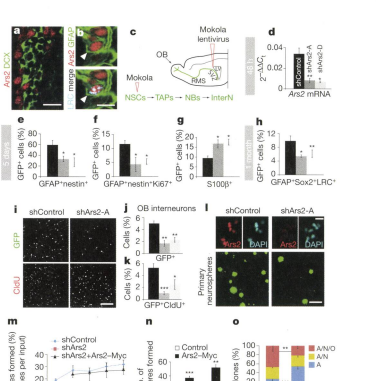

Figure 1 | Ars2 maintains neural stem cells in the adult SVZ. a, **b**, In the adult SVZ, Ars2 (red) is not expressed by DCX$^+$ (green) neuroblasts (**a**) but colocalizes with GFAP$^+$ (green), CldU-retaining (blue) NSCs (**b**). **c**, **d**, Experimental protocol (**c**) and validation of *Ars2* knockdown ($n = 3$ animals per condition) (**d**). **e**–**g**, *Ars2* knockdown in the SVZ exhibited reduced GFAP$^+$Nestin$^+$NSCs (**e**), reduced NSC proliferation (**f**) and increased S100β$^+$ mature astrocytes (**g**); $n = 3$ animals per condition. **h**, *Ars2* knockdown reduced LRCs ($n = 3$–7 animals per condition). **i**, Olfactory bulb sections double-stained for green fluorescent protein (GFP) and CldU. **j**, Percentage of GFP$^+$ cells per olfactory bulb slice ($n = 7$–11 animals per condition). **k**, Reduced newly generated neurons after *Ars2* knockdown ($n = 7$–11 animals per condition). **l**, Immunocytochemistry for Ars2 (red) and DAPI (4′,6-diamidino-2-phenylindole; blue) (top) and GFP$^+$ transduced primary neurospheres (green; bottom). **m**, Long-term self-renewal assay ($n = 4$ cultures per condition). **n**, *In vivo* Ars2 overexpression increased neurosphere formation ($n = 4$ cultures per condition). **o**, Ars2 deficiency reduced NSC multipotency ($n = 4$ cultures per condition). A, astrocytes; InterN, interneuron; LV, lateral ventricle; N, neurons; NBs, neuroblasts; O, oligodendrocytes; OB, olfactory bulb; RMS, rostral migratory stream; TAPs, transit-amplifying progenitors. $*P < 0.05$; $**P < 0.01$; $***P < 0.005$. Scale bars: **a**, **b**, 10 μm; **i**, 100 μm; **l**, 200 μm. Errors bars represent s.e.m. Supplementary Table 2 provides details of numbers of scored cells.

[1]Department of Developmental Biology, Sloan-Kettering Institute, 1275 York Avenue, Box 252, New York, New York 10065, USA. [2]Department of Cancer Biology and Genetics, Sloan-Kettering Institute, 1275 York Avenue, Box 252, New York, New York 10065, USA.

expressed by niche astrocytes, ependymal cells and GFAP$^+$CD133$^+$ stem cells[11] (Supplementary Fig. 1). A hallmark of NSCs is their quiescence, which is reflected in their ability to retain S-phase labels such as 5-chlorodeoxyuridine (CldU) for extended periods (that is, label-retaining cells (LRCs))[12,13]. We observed expression of Ars2 in 87 ± 3% of LRCs that were marked 1 month earlier (Fig. 1b), demonstrating the presence of Ars2 in this slow dividing population *in vivo*.

To assay the roles of Ars2 in NSCs *in vivo*, we used short hairpin RNAs (shRNAs) that suppressed endogenous Ars2 (Supplementary Fig. 2c). We packaged these into GFP-expressing Mokola lentivirus, which specifically transduces astroglial cells[14] (Supplementary Fig. 3). We used a defective lentivirus which is pseudotyped with a lyssavirus envelope of the Mokola virus. We injected these viruses into the adult SVZ and killed the mice 48 h, 5 days or 1 month later (Fig. 1c). At 48 h after infection, shArs2-GFP$^+$ cells exhibited an 80% reduction in *Ars2* messenger RNA relative to control shRNA cells (Fig. 1d). Apoptosis was unaffected by shArs2, and the number of GFP$^+$ Ki67$^+$ cells and the levels of cyclin D1 or cyclin E transcripts were also unchanged (Supplementary Figs 3, 4b and 5b). However, 5 days after infection, shArs2 SVZs exhibited a 50% reduction in the number and the proliferation rate of the GFAP$^+$Nestin$^+$NSCs (Fig. 1e, f), but apoptosis was unaffected (Supplementary Fig. 5b). Loss of NSC potential has been linked to an increase in mature astrocytes[15–17]. Consistent with this, we observed a 50% increase in the number of GFP$^+$S100b$^+$ cells (Fig. 1g).

To assess the number of LRCs, shRNA-infected mice were injected with CldU and killed 1 month later. Notably, we observed a decrease of ~50% in transduced LRCs in shArs2 SVZs (Fig. 1h), suggesting that Ars2 maintains the NSC pool. If this is true, we would expect it to have downstream effects on neurogenesis. Indeed, 5 days after infection, we observed a decrease in DCX$^+$ neuroblasts (Supplementary Fig. 6). LRCs also label post-mitotic cells that incorporate CldU just before cell cycle exit (such as differentiated cells and newly generated olfactory bulb interneurons). One month after infection, the population of shArs2-GFP$^+$, newly formed CldU$^+$ olfactory bulb interneurons was strongly reduced (Fig. 1i–k).

We performed additional analysis using neurospheres derived from shRNA-infected SVZ. Long-term self-renewal assays revealed that depletion of Ars2 rapidly extinguished neurosphere cultures, indicating a defect in self-renewing divisions (Fig. 1l, m). This defect was fully restored by an shRNA-resistant form of Ars2 (Fig. 1m and Supplementary Fig. 2d). Reciprocally, *in vivo* overexpression of Ars2 in wild-type mice increased neurosphere formation (Fig. 1n). Multipotency of Ars2-deficient neurospheres was also affected, as the frequency of clones that generated βIII-tubulin$^+$ neurons and O4$^+$ oligodendrocytes was decreased in favour of unipotent GFAP$^+$ clones (Fig. 1o). We conclude that Ars2 is required to maintain NSCs in a self-renewing and multipotent state.

We sought to confirm these shRNA results by breeding the conditional knockout allele of *Ars2* (*Ars2*$^{fl/fl}$) with *hGFAP-cre* (ref.[18]). *hGFAP-cre*::*Ars2*$^{fl/fl}$ mice (*Ars2*$^{Δ/Δ}$ mice) (Supplementary Fig. 7d) were born at the expected Mendelian ratios relative to wild-type and *hGFAP-cre*::*Ars2*$^{fl/+}$ littermates (used as controls). However, by postnatal day 15 (P15), *Ars2*$^{Δ/Δ}$ mice showed progressive growth retardation, hydrocephalus and ataxia, resulting in death between P20 and P25. Further analysis of P15 *Ars2*$^{Δ/Δ}$ mice revealed enlarged ventricles and smaller olfactory bulbs (Fig. 2a, b), suggestive of a requirement of Ars2 during postnatal neurogenesis. The expression pattern of Ars2 in P15 wild-type SVZ was analogous to the adult SVZ (Supplementary Fig. 7a,b), and analysis of the conditional knockout confirmed essentially complete absence of Ars2 in the SVZ (Supplementary Fig. 7c). Notably, the number of NSCs (marked by expression of nestin, Sox2, LeX (also known as Fut4) and GFAP) was reduced by 80% in *Ars2*$^{Δ/Δ}$ SVZ, and their proliferation rate decreased twofold (Fig. 2c, d, f). Caspase 3 staining showed that this was not due to cell death (Supplementary Fig. 8a, b). Conversely, assessment by GFAP and S100β staining showed that there was marked astrogliosis in *Ars2*$^{Δ/Δ}$ mice (Fig. 2e, f).

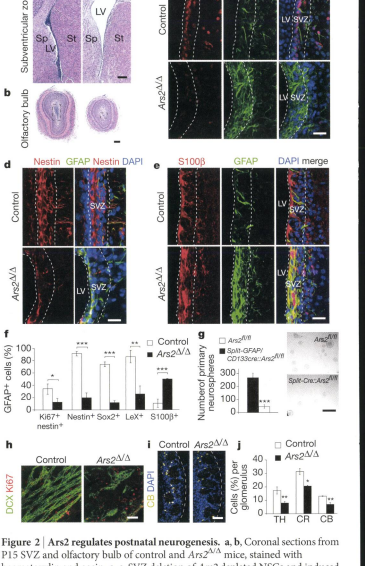

Figure 2 | Ars2 regulates postnatal neurogenesis. a, **b**, Coronal sections from P15 SVZ and olfactory bulb of control and *Ars2*$^{Δ/Δ}$ mice, stained with haematoxylin and eosin. **c**–**e**, SVZ deletion of *Ars2* depleted NSCs and induced astrogliosis, as shown by loss of Sox2$^+$ (red) and accumulation of GFAP$^+$ (green) cells (**c**), loss of nestin$^+$ (red) cells (**d**), and increased S100β$^+$ (red) cells (**e**); DAPI is in blue. **f**, **g**, Reduced number and proliferation of NSCs and elevation of mature astrocytes in *Ars2*$^{Δ/Δ}$ mice (**f**), and strong reduction of primary neurospheres from *GFAP/CD133-cre*::*Ars2*$^{fl/fl}$ electroporated pups (**g**). **h**, Whole-mount immunostaining for DCX (green) and Ki67 (red). **i**, Olfactory bulb coronal sections immunostained for calbindin (CB; yellow) and DAPI (blue). **j**, Quantification of interneuron reduction in control and *Ars2*$^{Δ/Δ}$ mice. CB, calbindin; CR, calretinin; TH, tyrosine hydroxylase. $*P < 0.05$; $**P < 0.01$; $***P < 0.005$. Scale bars: **a**, **b**, 100 μm; **c**–**e**, 30 μm; **g**–**i**, 50 μm. Error bars represent s.e.m from six animals per genotype or condition.

As Ars2 is expressed in niche astrocytes and ependymal cells, in addition to NSCs, we wished to demonstrate an autonomous function of Ars2 in NSCs. We co-injected GFP$^+$ and Split-Cre plasmids that specifically drive excision in GFAP$^+$CD133$^+$ NSCs[11] into the SVZ of P0–1 *Ars2*$^{fl/fl}$ pups, and introduced these plasmids using electroporation. Five days later, we isolated GFP$^+$ cells and plated for self-renewal assay. GFAP$^+$CD133$^+$ NSCs deleted for *Ars2* were strongly compromised for neurosphere generation, demonstrating a cell-autonomous requirement of Ars2 in this population (Fig. 2g and Supplementary Fig. 9). Consistent with a decrease in the number of NSCs, *Ars2*$^{Δ/Δ}$ mice had approximately 2.5-fold fewer DCX$^+$ neuroblasts (Fig. 2h) relative to control mice, although their proliferation rate was not affected (data not shown).

In the olfactory bulb, the frequency of tyrosine hydroxylase$^+$, calbindin$^+$ and calretinin$^+$ interneurons per glomerulus was also deeply reduced in *Ars2*$^{\Delta/\Delta}$ (Fig. 2i, j and Supplementary Fig. 10). In summary, the severe defects of the postnatal SVZ in which *Ars2* has been deleted solidified the requirement of Ars2 to maintain NSC identity.

As Ars2 functions in miRNA biogenesis[2–5], we tested whether the ability of Ars2 to promote NSC self-renewal was mediated by miRNAs. This was not the case, as overexpression of Ars2 in *Dicer1*$^{\Delta/\Delta}$ and *Drosha*$^{\Delta/\Delta}$ cells increased neurosphere yield (Fig. 3a,b). We sought to investigate this further by examining transcription factors that are known to have substantial roles in NSC self-renewal, including Hes1, Hes5 and Sox2 (refs 19–21). *Sox2* mRNA, but not *Hes1* mRNA, was significantly reduced 48 h after *Ars2* knockdown *in vivo* (Fig. 3c). One month after induction, *in vivo* knockdown of *Ars2* decreased *Hes1* and *Hes5* mRNA levels by ~30%, but resulted in a more substantial 70% reduction in *Sox2* (Fig. 3d). Reciprocally, *Sox2* levels increased by ~60% in neurospheres overexpressing Ars2 (Fig. 3e). These effects seemed to be transcriptional in nature, as Ars2 activated a 6-kilobase (kb) *Sox2-luc* reporter containing *cis*-regulatory sequences responsible for *Sox2* expression within adult neurogenic zones[23] (Fig. 3f). This was not simply due to the cancelling effects of overexpressing any self-renewal gene, because *in vitro* overexpression of Sox2 (Fig. 3g), but not Hes5 (Fig. 3h), rescued the Ars2-dependent loss in self-renewal capacity of shArs2 cells. Reciprocally, *in vitro* knockdown of *Sox2* (Supplementary Fig. 11a) caused rapid depletion of self-renewing neurospheres[23] (Fig. 3i) and compromised multipotency (Supplementary Fig. 11b), similar to the effects of *Ars2* knockdown (Fig. 1m, o). Together, these data indicated that Sox2 is a critical downstream effector of Ars2 in NSCs.

To evaluate whether the ability of Ars2 to activate *Sox2* expression might reflect a transcriptional role for this nuclear protein, we performed chromatin immunoprecipitation (ChIP) of Ars2 in NSCs, querying across the 6-kb *Sox2* promoter and the *Sox2* transcription unit. Interestingly, Ars2 associated not only with its 5′ untranslated region (UTR) and 3′ UTR but was highly enriched in region 8 (−2 to −2.5 kb) of the *Sox2* promoter (Fig. 4a); we validated this binding pattern using an independent antibody (Supplementary Fig. 12a). RNase treatment of chromatin samples eliminated UTR-associated Ars2 ChIP signals, and this is consistent with CBC-mediated association with capped transcripts[4]. However, binding of Ars2 to promoter region 8 was maintained, suggesting a more direct association of Ars2 with chromatin (Fig. 4b). No binding was found to the *Sox2* coding region (Fig. 4a) or to the promoters of *Hes1*, *Hes5* (ref. [24]), *K14* and *Myod1* (Supplementary Fig. 12b–e). Chromatin association of Ars2 was cell-type-dependent, as Ars2 did not bind the *Sox2* enhancer in NIH3T3 cells (Fig. 4a), which express high levels of Ars2 (Supplementary Fig. 2a).

Simple binding of Ars2 to the *Sox2* enhancer might not necessarily be of functional consequence. We prepared two deletions of the 6-kb *Sox2-luc* reporter, removing region 8 that was bound by Ars2 or region 5 as a

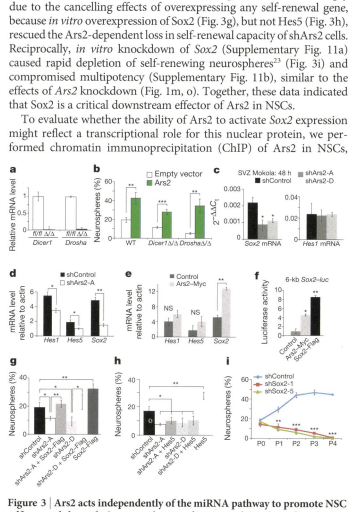

Figure 3 | Ars2 acts independently of the miRNA pathway to promote NSC self-renewal through *Sox2*. **a**, Absence of *Dicer1* and *Drosha* in floxed NSC cultures after Cre treatment ($n = 2$ experiments per condition). **b**, Ectopic Ars2 promoted NSC self-renewal in *Dicer1*- and *Drosha*-deleted NSCs ($n = 3$ experiments per condition). **c**, qPCR measurements from purified GFP$^+$ cells 48 h after infection ($n = 3$). **d**, qPCR measurements of self-renewal genes from primary infected GFP$^+$ NSCs ($n = 3$). **e**, Overexpression of Ars2 increased *Sox2* mRNA ($n = 3$). **f**, Both Ars2 and Sox2 activate a Sox2 transcriptional reporter ($n = 3$). **g**, **h**, Percentage of neurospheres formed from NSCs infected with the indicated constructs ($n = 3$). **i**, Long-term self-renewal assay shows that Sox2 is required for NSC self-renewing divisions ($n = 4$). *$P < 0.05$; **$P < 0.01$; ***$P < 0.005$. Error bars represent s.e.m; NS, not significant; WT, wildtype.

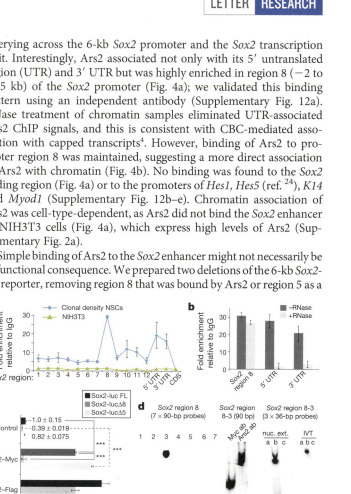

Figure 4 | Ars2 directly activates transcription of *Sox2* to mediate NSC self-renewal and multipotency. **a**, ChIP of Ars2 to the *Sox2* locus ($n = 4$ independent experiments). **b**, Ars2 binding to *Sox2* promoter region 8 is RNA independent ($n = 2$). **c**, Ars2 requires region 8 to activate *Sox2-luc* ($n = 4$). **d**, Gel shifts of the Ars2 binding site in the *Sox2* promoter using nuclear extract or *in vitro*-translated Ars2. **e**, Conservation of the Ars2-binding site in *Sox2*. **f**, Long-term self-renewal assay from NSCs isolated from control and *Ars2*$^{\Delta/\Delta}$ mice electroporated *in vivo* with the indicated constructs ($n = 6$ animals per condition). **g**, *Ars2*$^{\Delta/\Delta}$ defect in multipotency can be rescued by *in vivo* expression of Sox2 ($n = 6$ animals per condition). **h**–**k**, Differentiated NSC colonies stained for GFAP (blue), mouse anti-β-tubulin (Tuj1, yellow) and O4 (pink). Ab, antibody; bp, base pairs; CDS, coding sequence; EMSA, electrophoretic mobility shift assay; FL, full length; IVT, *in vitro*-translated; Luc, luciferase; Nuc. ext, nuclear extract; UTR, untranslated region; *$P < 0.05$; ***$P < 0.005$. Error bars represent s.e.m. Scale bars: **h**–**k**, 50 μm.

control deletion. Loss of region 8 strongly reduced *Sox2-luc* expression relative to the control deletion, whereas reciprocally, ectopic Ars2 activated the control deletion but not the version lacking the Ars2 binding site (Fig. 4c). Therefore, Ars2 activates *Sox2* through promoter region 8. We then incubated NSC nuclear extract with a series of overlapping 90-bp radiolabelled probes covering the ~500 base pairs (bp) of *Sox2* region 8, and observed a specific gel shift of subregion 8-3 (Fig. 4d). This band was completely super-shifted by inclusion of Ars2 antibody, but not Myc antibody (Fig. 4d). We defined the Ars2 binding site more precisely, revealing that Ars2 bound specifically to the central portion of *Sox2* region 8-3 (Fig. 4d). This reflected direct DNA binding activity of Ars2, as *in vitro* translated Ars2 recapitulated specific binding to *Sox2* probe 8-3b (Fig. 4d). This identified a sequence that is highly constrained across mammalian genomes (Fig. 4e and Supplementary Fig. 13).

To determine whether Sox2 mediates Ars2 function *in vivo*, we electroporated *Sox2* expression construct into $Ars2^{\Delta/\Delta}$ postnatal SVZ. Notably, Sox2 rescued the self-renewal and multipotency defects of $Ars2^{\Delta/\Delta}$ knockout cells (Fig. 4f–j). By contrast, NSCs derived from $Ars2^{\Delta/\Delta}$ SVZ electroporated with cyclin D1 lacked self-renewal capacity (Fig. 4f) and multipotency (Fig. 4g,k). This confirmed that *Ars2* knockout cells cannot be rescued by driving proliferation. Instead, Ars2 confers NSC identity as a self-renewing cell type by activating *Sox2*.

A central goal of stem-cell biology is to understand the molecular mechanisms that regulate stem-cell self-renewal and multipotency. We show that Ars2 is specifically expressed by NSCs, and not by transit-amplifying progenitors and neuroblasts, and that it maintains the self-renewal and multipotency capacity of postnatal and adult NSCs. In this setting, Ars2 is not required for cell viability, but is instead essential for maintaining core NSC properties. *Ars2* depletion or knockout decreased the NSC pool, decreased neurogenesis and strongly increased non-neurogenic astrocytes. We have assigned a new molecular function for the conserved RNA factor Ars2 as a sequence-specific DNA binding protein, and a critical direct activator of *Sox2* during *in vivo* NSC self-renewal and multipotency. More generally, in light of the interest surrounding the role of Sox2 as a core pluripotency factor in embryonic stem cells and induced pluripotent stem cells, Ars2 may regulate stem-cell self-renewal in these settings as well. This possibility is bolstered by the early embryonic arrest of *Ars2* knockout mice[25], which strongly resembles embryonic arrest in *Sox2* knockout mice[26].

METHODS SUMMARY

All procedures using mice were performed in accordance with the Institutional Animal Care and Use Committee (IACUC). For analysis of adult cells, we injected GFP-expressing Mokola lentivirus (shControl or shAs2) into two different locations of the SVZ using stereotaxic control, and processed brain sections for immunohistochemistry. In addition, we dissected infected SVZs, purified GFP^+ cells and assayed them for self-renewal and multipotency capacity, as described[27]. For conditional knockout analysis, we crossed mice carrying the *Ars2* conditional allele[4] with *hGFAP-Cre* mice. For intraventricular electroporation assays using Split-Cre[11], we used neonatal and P1 $Ars2^{f/f}$ pups and killed them 5 days later for self-renewal and multipotency assays. $Dicer1^{\Delta/\Delta}$ and $Drosha^{\Delta/\Delta}$ NSC cultures were generated by transfection with 5 μg of pMSCV-GFP-Cre, and resulting GFP^+ cells were isolated and cultured for 2 weeks before analysis. For chromatin immunoprecipitation, three million NSCs were crosslinked in 1% paraformaldehyde (PFA) and incubated with nuclear lysate and Ars2 antibody. Binding of nuclear extract or in vitro translated Ars2 to radiolabelled Sox2 probes was assayed in 4% tris-borate-EDTA (TBE) gels. All primers used for cloning, ChIP followed by quantitative PCR (ChIP–qPCR) and gel shifts are listed in Supplementary Tables 1–6.

Full Methods and any associated references are available in the online version of the paper at www.nature.com/nature.

Received 2 March; accepted 14 November 2011.
Published online 25 December 2011.

1. Laubinger, S. *et al.* Dual roles of the nuclear cap-binding complex and SERRATE in pre-mRNA splicing and microRNA processing in *Arabidopsis thaliana*. *Proc. Natl Acad. Sci. USA* **105,** 8795–8800 (2008).
2. Lobbes, D., Rallapalli, G., Schmidt, D. D., Martin, C. & Clarke, J. SERRATE: a new player on the plant microRNA scene. *EMBO Rep.* **7,** 1052–1058 (2006).
3. Yang, L., Liu, Z., Lu, F., Dong, A. & Huang, H. SERRATE is a novel nuclear regulator in primary microRNA processing in *Arabidopsis*. *Plant J.* **47,** 841–850 (2006).
4. Gruber, J. J. *et al.* Ars2 links the nuclear cap-binding complex to RNA interference and cell proliferation. *Cell* **138,** 328–339 (2009).
5. Sabin, L. R. *et al.* Ars2 regulates both miRNA- and siRNA-dependent silencing and suppresses RNA virus infection in *Drosophila*. *Cell* **138,** 340–351 (2009).
6. Fuchs, E., Tumbar, T. & Guasch, G. Socializing with the neighbors: stem cells and their niche. *Cell* **116,** 769–778 (2004).
7. Menn, B. *et al.* Origin of oligodendrocytes in the subventricular zone of the adult brain. *J. Neurosci.* **26,** 7907–7918 (2006).
8. Kriegstein, A. & Alvarez-Buylla, A. The glial nature of embryonic and adult neural stem cells. *Annu. Rev. Neurosci.* **32,** 149–184 (2009).
9. Lledo, P. M., Merkle, F. T. & Alvarez-Buylla, A. Origin and function of olfactory bulb interneuron diversity. *Trends Neurosci.* **31,** 392–400 (2008).
10. Shi, Y., Sun, G., Zhao, C. & Stewart, R. Neural stem cell self-renewal. *Crit. Rev. Oncol. Hematol.* **65,** 43–53 (2008).
11. Beckervordersandforth, R. *et al.* *In vivo* fate mapping and expression analysis reveals molecular hallmarks of prospectively isolated adult neural stem cells. *Cell Stem Cell* **7,** 744–758 (2010).
12. Potten, C. S. Stem cells in gastrointestinal epithelium: numbers, characteristics and death. *Phil. Trans. R. Soc. Lond. B* **353,** 821–830 (1998).
13. Cotsarelis, G., Sun, T. T. & Lavker, R. M. Label-retaining cells reside in the bulge area of pilosebaceous unit: implications for follicular stem cells, hair cycle, and skin carcinogenesis. *Cell* **61,** 1329–1337 (1990).
14. Alonso, M. *et al.* Turning astrocytes from the rostral migratory stream into neurons: a role for the olfactory sensory organ. *J. Neurosci.* **28,** 11089–11102 (2008).
15. Raponi, E. *et al.* S100B expression defines a state in which GFAP-expressing cells lose their neural stem cell potential and acquire a more mature developmental stage. *Glia* **55,** 165–177 (2007).
16. Shi, Y. *et al.* Expression and function of orphan nuclear receptor TLX in adult neural stem cells. *Nature* **427,** 78–83 (2004).
17. Zencak, D. *et al. Bmi1* loss produces an increase in astroglial cells and a decrease in neural stem cell population and proliferation. *J. Neurosci.* **25,** 5774–5783 (2005).
18. Zhuo, L. *et al.* hGFAP-cre transgenic mice for manipulation of glial and neuronal function *in vivo*. *Genesis* **31,** 85–94 (2001).
19. Ohtsuka, T., Sakamoto, M., Guillemot, F. & Kageyama, R. Roles of the basic helix-loop-helix genes *Hes1* and *Hes5* in expansion of neural stem cells of the developing brain. *J. Biol. Chem.* **276,** 30467–30474 (2001).
20. Hitoshi, S. *et al.* Notch pathway molecules are essential for the maintenance, but not the generation, of mammalian neural stem cells. *Genes Dev.* **16,** 846–858 (2002).
21. Ferri, A. L. *et al. Sox2* deficiency causes neurodegeneration and impaired neurogenesis in the adult mouse brain. *Development* **131,** 3805–3819 (2004).
22. Suh, H. *et al.* In vivo fate analysis reveals the multipotent and self-renewal capacities of $Sox2^+$ neural stem cells in the adult hippocampus. *Cell Stem Cell* **1,** 515–528 (2007).
23. Favaro, R. *et al.* Hippocampal development and neural stem cell maintenance require *Sox2*-dependent regulation of *Shh*. *Nature Neurosci.* **12,** 1248–1256 (2009).
24. Ohtsuka, T. *et al.* Visualization of embryonic neural stem cells using Hes promoters in transgenic mice. *Mol. Cell. Neurosci.* **31,** 109–122 (2006).
25. Wilson, M. D. *et al. ARS2* is a conserved eukaryotic gene essential for early mammalian development. *Mol. Cell. Biol.* **28,** 1503–1514 (2008).
26. Avilion, A. A. *et al.* Multipotent cell lineages in early mouse development depend on SOX2 function. *Genes Dev.* **17,** 126–140 (2003).
27. Andreu-Agulló, C., Morante-Redolat, J. M., Delgado, A. C. & Farinas, I. Vascular niche factor PEDF modulates Notch-dependent stemness in the adult subependymal zone. *Nature Neurosci.* **12,** 1514–1523 (2009).

Supplementary Information is linked to the online version of the paper at www.nature.com/nature.

Acknowledgements We thank X. Lu, M. Götz, A. Rizzino, P. M. LLedo, P. Charneau, M. Segura, P. L. Howard and S. Olejniczak for reagents. We are grateful to K. Hadjantonakis, A. Ferrer-Vaquer, J. Zhang and Y. Ganat for assistance. U. Ruthishauser, V. Tabar and the Molecular Cytology Core Facility at the Memorial Sloan-Kettering Cancer Center shared equipment. S. R. Ferron, H. Mira, A. Joyner, H. Duan, Q. Dai, I. Farinas and S. Shi provided critical comments. Work in E.C.L.'s group was supported by the Burroughs Wellcome Fund, the Starr Cancer Consortium (13-A-139) and the NIH (R01-GM083300). C.A.-A. was funded by a EMBO Long-Term Fellowship (ALTF 718-2008) and a NYSTEM Fellowship.

Author Contributions C.A.-A. performed and designed all of the experiments, T.M. performed *in vivo* lentivirus injections and C.B.T. provided reagents. C.A.-A. and E.C.L. conceived the project, interpreted the results and wrote the manuscript.

Author Information Reprints and permissions information is available at www.nature.com/reprints. The authors declare no competing financial interests. Readers are welcome to comment on the online version of this article at www.nature.com/nature. Correspondence and requests for materials should be addressed to C.A.-A. (andreuac@mskcc.org) or E.C.L. (laie@mskcc.org).

LETTER

doi:10.1038/nature10698

Acquisition of a multifunctional IgA$^+$ plasma cell phenotype in the gut

Jörg H. Fritz[1,4]*, Olga Lucia Rojas[1]*, Nathalie Simard[1,2], Douglas D. McCarthy[1], Siegfried Hapfelmeier[3]†, Stephen Rubino[4], Susan J. Robertson[1], Mani Larijani[1]†, Jean Gosselin[5], Ivaylo I. Ivanov[6], Alberto Martin[1], Rafael Casellas[7], Dana J. Philpott[1], Stephen E. Girardin[4], Kathy D. McCoy[3], Andrew J. Macpherson[3], Christopher J. Paige[1,2] & Jennifer L. Gommerman[1]

The largest mucosal surface in the body is in the gastrointestinal tract, a location that is heavily colonized by microbes that are normally harmless. A key mechanism required for maintaining a homeostatic balance between this microbial burden and the lymphocytes that densely populate the gastrointestinal tract is the production and transepithelial transport of poly-reactive IgA (ref. 1). Within the mucosal tissues, B cells respond to cytokines, sometimes in the absence of T-cell help, undergo class switch recombination of their immunoglobulin receptor to IgA, and differentiate to become plasma cells[2]. However, IgA-secreting plasma cells probably have additional attributes that are needed for coping with the tremendous bacterial load in the gastrointestinal tract. Here we report that mouse IgA$^+$ plasma cells also produce the antimicrobial mediators tumour-necrosis factor-α (TNF-α) and inducible nitric oxide synthase (iNOS), and express many molecules that are commonly associated with monocyte/granulocyte cell types. The development of iNOS-producing IgA$^+$ plasma cells can be recapitulated *in vitro* in the presence of gut stroma, and the acquisition of this multifunctional phenotype *in vivo* and *in vitro* relies on microbial co-stimulation. Deletion of TNF-α and iNOS in B-lineage cells resulted in a reduction in IgA production, altered diversification of the gut microbiota and poor clearance of a gut-tropic pathogen. These findings reveal a novel adaptation to maintaining homeostasis in the gut, and extend the repertoire of protective responses exhibited by some B-lineage cells.

Most class switch recombination (CSR) to IgA takes place in the Peyer's patches and requires encounters between B cells and cytokine-secreting T cells within germinal centres. However, IgA CSR can also take place outside of Peyer's patches within isolated lymphoid follicles of the lamina propria[2]. Local production of nitric oxide (NO) via the inducible nitric oxide synthase (NOS2 or iNOS) has been shown to be a critical mediator of CSR to IgA within the small intestinal lamina propria of mice[3,4]. Because lymphotoxin-deficient mice have a significant, unexplained IgA defect[5], we hypothesized that this could be due to a lack of iNOS in the gut. Indeed, we identified a population of CD11c^{hi}iNOS$^+$ cells by flow cytometric analysis of intestinal lamina propria cell preparations, and these CD11c^{hi}iNOS$^+$ cells were decreased in both lymphotoxin-β-deficient and lymphotoxin-β-receptor-deficient mice (*Ltb*$^{-/-}$ and *Ltbr*$^{-/-}$, respectively; Fig. 1a and Supplementary Table 1), confirming a relationship between iNOS and the generation/maintenance of IgA$^+$ plasma cells[4].

The absence of iNOS-expressing cells in lymphotoxin-deficient mice prompted us to ask whether B-lineage cells could influence the expression of iNOS within the gut, as lymphotoxin-deficient mice lack some B-cell subsets in the small intestinal lamina propria[5]. Accordingly, we examined B-cell-deficient mice for evidence of iNOS expression in the gut and found that CD11c^{hi}iNOS$^+$ cells were absent in *Jh*$^{-/-}$ mice, *Rag2*$^{-/-}$ mice and strongly reduced in μMt mice (Fig. 1b, Supplementary Table 1 and Supplementary Fig. 1a). Because lymphotoxin-deficient mice also lack IgA$^+$ plasma cells, and iNOS-expressing cells are strongly reduced in B-cell-deficient and lymphotoxin-deficient mice, we examined the possibility that IgA$^+$ plasma cells may have the capacity to produce iNOS. Indeed, when we gated on iNOS$^+$ cells, we found that they expressed IgA (Fig. 1a) and low levels of B220 (not shown), indicating that IgA-producing cells may account for significant iNOS expression within the gut in the steady state. In agreement with this result, we found that purified CD11c^{hi}iNOS$^+$ cells exhibited evidence of a rearranged V-D-J*H*4 product (Supplementary Fig. 1b).

We next asked what proportion of IgA$^+$ cells express iNOS. Compared to knockout controls, a subset of IgA$^+$ plasma cells expresses iNOS and TNF-α, the expression of which has also been described in monocyte-derived cells[6] (see Fig. 1c and Supplementary Table 2 for relative frequencies of each population and Fig. 1e for immunofluorescence microscopy). We further confirmed these observations by performing cytospins on small intestinal lamina-propria-derived cells (Supplementary Figs 2 and 3). Collectively, these data indicate that gut-resident B-lineage cells contribute towards iNOS and TNF-α expression within the small intestinal lamina propria.

To determine better which B-lineage cells were expressing TNF-α/iNOS, we examined whether previous expression of activation induced cytidine deaminase (AID), an enzyme that is required for both CSR and somatic hypermutation in B cells[7], correlated with iNOS and TNF-α expression. Using AID-Cre × YFP mice[8], we observed three populations of cells in the small intestinal lamina propria: (1) YFP$^-$IgA$^-$ cells, that is, any lamina-propria-derived cells that have not undergone CSR nor somatic hypermutation, such as a dendritic cells or naive B cells; (2) YFP$^+$IgA$^-$ cells, that is, B cells that have undertaken somatic hypermutation or have undergone CSR to a class of immunoglobulin other than IgA; and (3) YFP$^+$IgA$^+$ cells, that is, B cells that have undergone CSR to IgA (Fig. 1d and Supplementary Table 3 for relative frequencies of each population). Confirming that YFP$^+$IgA$^+$ cells probably represent IgA$^+$ plasma cells, YFP$^+$IgA$^+$ cells also expressed low levels of the plasma cell marker syndecan-1 (CD138) and were CD19^{low} (compare YFP$^+$IgA$^+$ (red trace) with YFP$^+$IgA$^-$ B cells (blue trace), which are CD138$^-$CD19^{hi}; Fig. 1d). Using this approach, we found that some YFP$^+$IgA$^+$ cells (red box) expressed iNOS as well as TNF-α (Fig. 1d and Supplementary Table 4 for the relative expression of TNF-α/iNOS for each population). Furthermore, YFP$^+$IgA$^+$ cells also expressed leukocyte surface markers commonly associated

[1]Department of Immunology, University of Toronto, Toronto M5S 1A8, Canada. [2]Ontario Cancer Institute, Princess Margaret Hospital, University Health Network, Toronto M5G 2M9, Canada. [3]University of Bern, Department Klinische Forschung (Gastroenterologie), Mutenstrasse 35, 3010 Bern, Switzerland. [4]Department of Laboratory Medicine and Pathobiology, University of Toronto, Toronto M5S 1A8, Canada. [5]Department of Molecular Medicine, University of Laval, Quebec G1V 4G2, Canada. [6]Department of Microbiology and Immunology, Columbia University Medical Center, College of Physicians and Surgeons, New York, New York 10032, USA. [7]Genomics and Immunity, National Institute of Arthritis and Musculoskeletal and Skin Diseases, National Institutes of Health, Bethesda, Maryland 20892, USA. †Present addresses: Complex Traits Group, Department of Microbiology and Immunology, McGill University, Montreal H3G 0B1, Canada (J.H.F.); University of Bern, Institute of Infectious Disease, Friedbühlstrasse 51, 3010 Bern, Switzerland (S.H.); Division of Biomedical Sciences, Faculty of Medicine, Memorial University of Newfoundland, St John's A1B 3V6, Canada (M.L.).
*These authors contributed equally to this work.

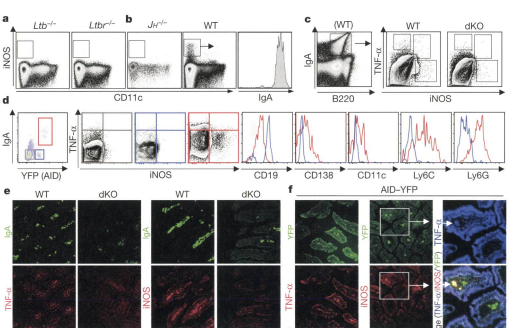

Figure 1 | IgA$^+$ plasma cells in the small intestinal lamina propria can produce iNOS and TNF-α. **a**, **b**, Small intestinal lamina propria cells from *Ltb*$^{-/-}$, *Ltbr*$^{-/-}$, *Jh*$^{-/-}$ and wild-type (WT) mice were isolated and viable cells were analysed for CD11c and iNOS expression by flow cytometry. (See also Supplementary Table 1.) iNOS$^+$ cells were gated and analysed for IgA expression ($n = 5$ for knockout mice and $n = 20$ for wild-type mice). **c**, Small intestinal lamina propria cells were isolated from wild-type and *Tnfa*$^{-/-}$*iNOS*$^{-/-}$ double-deficient mice and analysed for IgA, TNF-α and iNOS expression (note a wild-type example here for IgA/B220 staining is shown; although IgA-expressing cells are reduced in double knockout mice (*Tnfa*$^{-/-}$*iNOS*$^{-/-}$ or dKO) mice as per Fig. 3c, it is possible to still gate on IgA-expressing cells within the lamina propria of double knockout mice) ($n = 10$–14, see also Supplementary Table 2). **d**, Intestinal lamina propria cells from AID–YFP animals were isolated and viable cells were analysed for their expression of IgA and YFP. YFP$^-$IgA$^-$, grey rectangle; YFP$^+$IgA$^+$, blue rectangle; YFP$^+$IgA$^+$, red rectangle. (See also Supplementary Table 3.) These gated populations were further analysed for their expression of iNOS and TNF-α (note that cross-hairs were added based on isotype control staining; see also Supplementary Table 4). Expression of other lineage-specific markers for each of the three populations are denoted as histograms (YFP$^-$IgA$^-$, grey trace; YFP$^+$IgA$^-$, blue trace; YFP$^+$IgA$^+$, red trace). Note that for CD11c expression, YFP$^-$IgA$^-$ dendritic cells were used as a positive control (grey trace). Representative plots are shown from $n = 8$ mice. **e**, **f**, Sections of small intestines from wild-type versus double knockout mice (**e**) and AID$^+$YFP$^+$ mice (**f**) were stained with specific fluorochrome-tagged antibodies for iNOS, TNF-α and IgA (or visualized for YFP) as indicated. Stained sections were then analysed by fluorescence microscopy at ×200. Representative pictures are shown from at least three separate experiments. Arrows denote areas of co-localization and the rectangle indicates a villus that was enlarged to visualize simultaneous expression of each iNOS, TNF-α and YFP (×630).

with monocytic and granulocytic cells, including Ly6C and Ly6G[9] and low levels of CD11c (Fig. 1d, for CD11c, dendritic cells (grey trace) were used as a comparator). By immunofluorescence microscopy, we found that YFP expression co-localizes with IgA expression as expected (Supplementary Fig. 4), and using these AID–YFP tissues we detected the expression of iNOS and TNF-α in some, but not all, YFP$^+$ cells in the small intestinal lamina propria tissue (Fig. 1f), and occasional co-expression of both iNOS and TNF-α was observed in YFP$^+$ cells, consistent with our flow cytometry data (Fig. 1f; see boxed insert). Taken together, we have found that a proportion of IgA$^+$ cells within the small intestinal lamina propria express the antimicrobial mediators TNF-α and iNOS. Although we do not detect significant expression of these molecules in other lamina propria cells (YFP$^+$IgA$^-$ B cells, YFP$^-$ populations), it is possible that our detection methods are not sufficiently sensitive to pick up low levels of protein expression of TNF-α and iNOS in these cell types, or that expression of TNF-α and iNOS in these cells is induced during particular microbial encounters, as has been observed in non-mucosal tissues[6].

Notably, not all IgA$^+$ cells expressed iNOS or TNF-α, or co-expressed both iNOS and TNF-α simultaneously (Fig. 1c, d and Supplementary Tables 2 and 4), which would make sense given the pro-inflammatory nature of these molecules. Indeed, cytospin analysis of IgA$^+$ cells that express iNOS and/or TNF-α revealed a different morphology and cellular IgA localization than IgA$^+$iNOS$^-$TNF-α$^-$ cells, suggesting that acquisition of iNOS and TNF-α expression may be accompanied by additional activation steps beyond IgA CSR (Supplementary Figs 2 and 3). To understand further the necessary signals required for the induction of these two antimicrobial mediators in IgA$^+$ plasma cells, we assessed the expression of iNOS by IgA$^+$ plasma cells in germ-free mice. Although greatly reduced in number, IgA$^+$ cells in the lamina propria of germ-free mice did not express iNOS; however, the expression of iNOS could be recovered if germ-free mice were reconstituted with a limited microbiota (Fig. 2a). Even 'reversible colonization' of germ-free mice with a single species of *Escherichia coli* (HA107)[10] was sufficient to restore iNOS expression in IgA$^+$ cells. Therefore, microbial colonization of the gut is necessary for the expression of iNOS by IgA$^+$ plasma cells, and a single species of bacteria is sufficient.

To recapitulate what we observed *in vivo*, we assessed whether the acquisition of iNOS expression in IgA$^+$ cells could be supported by gut-derived support/stromal cells (see Methods where we describe the generation of stromal cell monolayers) compared with a bone-marrow-derived S17 stromal cell line or *ex vivo* preparations of bone marrow stroma[11]. In the presence of a combination of pro-IgA CSR factors, both bone marrow and gut stroma could support the development of YFP$^+$IgA$^+$ cells from B220$^+$ bone marrow cells derived from

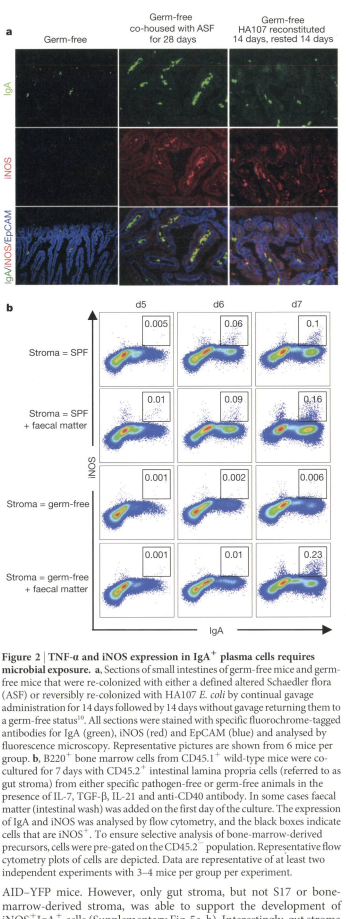

Figure 2 | TNF-α and iNOS expression in IgA$^+$ plasma cells requires microbial exposure. a, Sections of small intestines of germ-free mice and germ-free mice that were re-colonized with either a defined altered Schaedler flora (ASF) or reversibly re-colonized with HA107 *E. coli* by continual gavage administration for 14 days followed by 14 days without gavage returning them to a germ-free status[10]. All sections were stained with specific fluorochrome-tagged antibodies for IgA (green), iNOS (red) and EpCAM (blue) and analysed by fluorescence microscopy. Representative pictures are shown from 6 mice per group. **b**, B220$^+$ bone marrow cells from CD45.1$^+$ wild-type mice were co-cultured for 7 days with CD45.2$^+$ intestinal lamina propria cells (referred to as gut stroma) from either specific pathogen-free or germ-free animals in the presence of IL-7, TGF-β, IL-21 and anti-CD40 antibody. In some cases faecal matter (intestinal wash) was added on the first day of the culture. The expression of IgA and iNOS was analysed by flow cytometry, and the black boxes indicate cells that are iNOS$^+$. To ensure selective analysis of bone-marrow-derived precursors, cells were pre-gated on the CD45.2$^+$ population. Representative flow cytometry plots of cells are depicted. Data are representative of at least two independent experiments with 3–4 mice per group per experiment.

AID–YFP mice. However, only gut stroma, but not S17 or bone-marrow-derived stroma, was able to support the development of iNOS$^+$IgA$^+$ cells (Supplementary Fig. 5a, b). Interestingly, gut stroma from *Ltbr*$^{-/-}$ mice was likewise able to support the development of iNOS$^+$IgA$^+$ cells in the presence of pro-IgA CSR factors, indicating that the defective CSR observed in *Ltbr*$^{-/-}$ mice can be overcome *in vitro* in the presence of exogenous cytokines and CD40 ligation (Supplementary Fig. 5b). Not unlike the *in vivo* scenario, microbes are required for *in vitro* development of iNOS$^+$IgA$^+$ cells, as preparations of gut stroma from specific pathogen-free but not germ-free mice supports the development of iNOS$^+$IgA$^+$ cells (Fig. 2b). Furthermore, co-incubation of germ-free gut stroma with faecal matter derived from specific pathogen-free mice restores the development of iNOS$^+$IgA$^+$ cells (Fig. 2b). Thus, our *in vivo* and *in vitro* results suggest that the gut microenvironment, influenced by the local microbiota, supports the development of multifunctional B cells that express IgA and iNOS.

To examine the functional relevance of TNF-α/iNOS expression in IgA$^+$ cells, we created TNF-α/iNOS double knockout mice (*Tnfa*$^{-/-}$*iNOS*$^{-/-}$ mice). *Tnfa*$^{-/-}$*iNOS*$^{-/-}$ mice exhibited reduced levels of serum IgA (Fig. 3a), and this reduction was more marked than what we observed for *iNOS*$^{-/-}$ single knockout mice, which, in agreement with previous findings[4], also exhibited decreased levels of serum IgA (data not shown). Bone marrow from double knockout mice, in combination with B-cell-deficient *Jh*$^{-/-}$ bone marrow, was used to reconstitute B-cell-deficient, lethally irradiated recipients, thus creating mixed bone marrow chimaeras in which B cells are unable to produce TNF-α/iNOS (see Supplementary Fig. 6). *Jh*$^{-/-}$ plus double knockout mixed chimaeric mice exhibited a normal complement of immune cells in the periphery, although we did note some changes in splenic microarchitecture (Supplementary Fig. 7), in agreement with the effects of B-cell-derived TNF-α on splenic stromal cell biology[12]. Consistent with a role for TNF-α/iNOS in the regulation of CSR to IgA (ref. 4), *Jh*$^{-/-}$ plus double knockout mixed bone marrow chimaeric mice exhibited a significant drop in serum IgA but not IgG1 when compared with two groups of control mixed bone marrow chimaeric mice (double knockout plus wild type and *Jh*$^{-/-}$ plus wild type mixed bone marrow chimaeric mice) (Fig. 3a, b), and this decrease in serum IgA tracked with significant reductions in IgA$^+$ cells within the lamina propria as quantified by immunofluorescence microscopy (Fig. 3c, d). Although all mixed bone marrow recipients were generated using the same cohort of recipient mice, we observed changes in the composition of the commensal bacterial community in the small intestine of *Jh*$^{-/-}$ plus wild type versus *Jh*$^{-/-}$ plus double knockout reconstituted mixed bone marrow chimaeric mice (Fig. 3e). Focusing on microbial populations that are known to influence immune cell function[13], we noted that segmented filamentous bacteria were nearly absent from *Jh*$^{-/-}$ plus double knockout mixed bone marrow chimaeras in small intestinal tissue ($P < 0.05$), as well as in small intestinal 'scrapes' enriched for epithelial cells (not shown). In contrast, *Clostridium leptum* and *Bacillus* were increased in small intestinal tissue of *Jh*$^{-/-}$ plus double knockout mixed chimaeras, and this may possibly account for the reduced frequency of segmented filamentous bacteria. The altered composition of commensal microbiota probably reflects the deficiency in TNF-α/iNOS rather than a reduction in IgA, as mice that are completely IgA-deficient exhibit excessive outgrowth of segmented filamentous bacteria[14]. Therefore, although our data do not eliminate the possibility that complete deletion of TNF-α/iNOS in all monocytes/dendritic cells would have an impact on IgA production, these results show that the expression of TNF-α/iNOS in B-lineage cells is essential for the homeostatic production of IgA and the maintenance of an appropriate representation of different commensal microbes within the small intestine.

We next assessed the impact of TNF-α/iNOS deletion in B cells on clearance of the mouse pathogen *Citrobacter rodentium*, which colonizes the caecum and large intestine following infection. First, using AID–YFP mice, we found that *C. rodentium* infection results in a significant accumulation of YFP$^+$IgA$^+$ cells as well as YFP$^+$CD11c$^+$ cells (but not IgA$^-$ B cells) in the caecum and large intestine as early as 36 h after infection (Fig. 4a–c). With these kinetics established, we infected *Jh*$^{-/-}$ plus wild type versus *Jh*$^{-/-}$ plus double knockout mixed bone marrow chimaeras with *C. rodentium*. Interestingly, *C.*

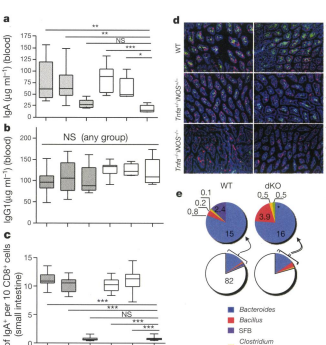

Figure 3 | Reduced IgA production and altered commensal flora composition in iNOS/TNF-α double-deficient mixed chimaeric mice. **a**, **b**, Steady-state serum IgA, but not IgG1, levels are markedly decreased in double knockout and double knockout mixed chimaeras. Serum IgA and IgG1 levels were measured by ELISA in wild-type ($n = 15$), *Tnfa*$^{+/-}$ *iNOS*$^{+/-}$ ($n = 12$) and *Tnfa*$^{-/-}$ *iNOS*$^{-/-}$ (dKO, $n = 7$) non-chimaeric mice as well as in wild-type plus double knockout ($n = 8$), *Jh*$^{-/-}$ plus wild-type ($n = 5$) and *Jh*$^{-/-}$ plus double knockout ($n = 6$) mixed chimaeric mice. Similar results were obtained with two additional batches of mixed bone marrow chimaeric mice (not shown). Data represent median, quartiles and range values. **c**, The numbers of small intestinal lamina propria IgA$^+$ plasma cells and CD8α$^+$ cells were quantified from immunofluorescence microscopy images using ImageJ. A total of five different sections from 6 mice ($n = 6$) per group was analysed. **d**, Representative images of frozen small intestinal tissue sections derived from the groups described in **a**–**c** stained for CD8α (red), IgA (green) and DAPI (blue). A total of five different sections from 6 mice per group were analysed. **e**, Seven weeks after bone-marrow reconstitution, the small intestines of wild-type and double knockout mixed chimaeras ($n = 4$ for each group) were analysed for their commensal bacteria composition by quantitative real-time PCR amplification of 16S rRNA isolated from small intestinal preparations. Coloured pie graphs represent the percentages of the indicated bacteria species. A significant difference in the relative representation of segmented filamentous bacteria (SFB) was observed between wild-type and double knockout mice. Similar results for segmented filamentous bacteria were obtained in small intestinal scrapes of the epithelium (data not shown). Data represent means and s.d. values. $***P = 0.001$, $**P = 0.01$, $*P < 0.05$.

rodentium translocation to the spleen, enhanced weight loss and colonic pathology were all noted in *Jh*$^{-/-}$ plus double knockout but not *Jh*$^{-/-}$ plus wild type mixed chimaeric mice (Fig. 4d–f). Similar impaired clearance of *C. rodentium* was observed in *Jh*$^{-/-}$ plus double knockout mixed bone marrow chimaeric mice when they were directly compared with another control group (wild type plus double knockout mixed bone marrow chimaeras; see Supplementary Fig. 8a–c). Because we did not observe an accumulation of IgA$^-$B cells at the site of infection, by inference we conclude that along with other dendritic-cell-mediated immune mechanisms, TNF-α/iNOS production by

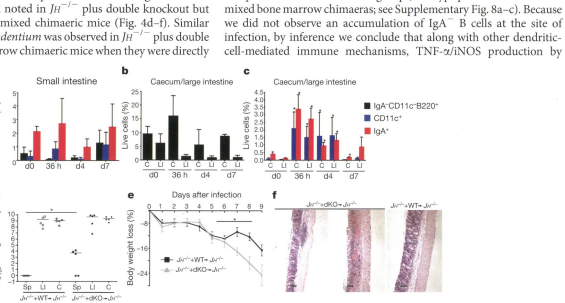

Figure 4 | iNOS/TNF-α double-deficient mixed chimaeras are more susceptible to infection with *C. rodentium*. AID–YFP animals were infected by oral gavage with 1×10^9 colony-forming units (c.f.u.) of a nalidixic-acid-resistant strain of *C. rodentium* DBS100. **a**–**c**, The kinetics of accumulation of viable YFP$^+$IgA$^-$CD11c$^-$B220$^+$ (black bars), YFP$^-$CD11c$^+$ (blue bars) and YFP$^+$IgA$^+$ (red bars) cells in the small intestine, the caecum (C) and the large intestine (LI) was analysed by flow cytometry (day 0 (d0), 36 h, day 4 (d4) and day 7 (d7)). The percentages of viable cells as mean and s.e.m. values are shown ($n = 4$). A representative example of two individual experiments is shown. **d**, The colonization by *C. rodentium* was determined 9 days after infection. *C. rodentium* colonization of spleen (Sp) is significantly enhanced in double knockout (dKO) mice at day 9 after infection and at day 4 after infection (data not shown). Data are representative of two individual experiments from at least 5 mice per group in each experiment. Mean values are shown. **e**, The percentage of body weight loss in wild-type plus *Jh*$^{-/-}$→*Rag*$^{-/-}$ and dKO + *Jh*$^{-/-}$→*Rag*$^{-/-}$ mixed chimaeras after *C. rodentium* infection over time is depicted. Significantly increased body weight loss was observed in double knockout mice from day 6 to 9 after infection ($n = 5$–12 per group). Note that double knockout plus *Jh*$^{-/-}$ mixed chimaeric mice were killed 9 days after infection for humane reasons as weight loss exceeded 20% of their original body weight. Mean and s.e.m. values are shown. **f**, Large intestines from wild-type plus *Jh*$^{-/-}$ and double knockout plus *Jh*$^{-/-}$ mixed chimaeric mice were harvested 9 days after infection and the pathological scores were analysed by standard histological staining procedures using haematoxylin and eosin. Large intestines from double knockout plus *Jh*$^{-/-}$ mice show more severe large intestine pathology. Haematoxylin and eosin stainings of two representative double knockout mice with a moderate and a more severe condition, as well as one representative wild-type plus *Jh*$^{-/-}$ chimaeric mouse, are shown ($n = 5$ mice per group). The panel shows the original magnification of ×100. Scale bars represent 100 μm. $*P < 0.05$.

IgA^+ plasma cells is required, either directly or indirectly, for optimal control of *C. rodentium* in the gut, although it cannot be excluded at this stage that TNF-α/iNOS production by other B-lineage cells outside of the gut may have contributed to the observed phenotype. Moreover, we cannot eliminate the possibility that production of TNF-α/iNOS by B-lineage cells may have provoked the expression of TNF-α/iNOS in monocytes/dendritic cells to control the infection. Nevertheless, our findings show that B-cell-associated TNF-α/iNOS production is critical for control of *C. rodentium*, and this may explain why B-cell-deficient mice, but not $IgA^{-/-}$ mice or mice that lack secreted IgM, also fail to control *C. rodentium*[15].

The immune system responds differently to antigens encountered systemically as opposed to at mucosal surfaces[1]. We postulate that in the process of differentiating to become IgA^+ plasma cells, the gut environment may have imprinted IgA^+ cells with more 'monocytic' potential, a phenomenon that has been previously observed *in vitro*[16]. Indeed, there is a precedent for B cells to display non-conventional 'monocyte/dendritic cell' functions in other species[17] and in response to TLR ligation[18], and B cells have emerged as important effector[19] and regulatory cells[20] during innate responses to bacterial infection. Furthermore, B cells and monocytes share common precursors during their development[21,22], and plasma cells have been recently shown to possess antigen-presenting capacity[23]. These results document a novel effector mechanism for IgA^+ plasma cells, which seems to arise in the unique environment of the gut, and may be critical to mount effective responses to microbial assault.

METHODS SUMMARY

Mice. Mice were either purchased from commercial vendors or bred in-house at the University of Toronto. Germ-free wild-type mice were re-derived and maintained in the Germ-free Unit at McMaster University or the University of Bern, Switzerland. Germ-free wild-type mice were re-associated with a low-complexity microbiota, by co-housing with gnotobiotic mice that had been associated with the altered Schaedler flora. Reversible colonization experiments were carried out by gavaging germ-free mice with the *E. coli* K12 triple mutant strain HA107 and subsequently tested germ-free.

Cell purification and flow cytometry. Small intestine (free of Peyer's patches) as well as large intestine and the caecum were dissected, washed and epithelial cells were removed. Remaining tissue was digested with collagenase and the resulting suspension was filtered and analysed by flow cytometry or used for cytospin preparations. For flow cytometry, cells were subjected to aqua dead cell stain, then incubated with Fc-block followed by incubation with pre-determined concentrations of fluorochrome labelled antibodies to cell-surface markers, fixed/permeabilized and incubated with pre-determined concentrations of fluorochrome labelled antibodies to intracellular proteins. Cells were acquired using either a FACS Cailbur or a LSR-II (BD Biosciences). Acquired data were analysed and processed using FlowJo.

Immunofluorescence microscopy. Re-hydrated 5 μm sections of small intestinal tissue were subjected to blocking with serum and Fc-block followed by staining with fluorochrome-labelled antibodies. Slides were then stained with DAPI before being mounted with Gel/Mount and visualized with a Leica DMRA2 microscope accompanied by OpenLab software (Improvision).

Co-culture of stromal cells and bone marrow cells. Bone-marrow- or lamina-propria-derived stromal cells were plated together with bone-marrow-derived $B220^+$ congenically disparate (CD45.1) cells. Co-cultures were supplemented with IgA switch factors including TGF-β, IL-21 and anti-CD40 as well as IL-7. At the indicated times, cells were harvested and analysed by flow cytometry.

Full Methods and any associated references are available in the online version of the paper at www.nature.com/nature.

Received 11 June; accepted 4 November 2011.
Published online 11 December 2011.

1. Hooper, L. V. & Macpherson, A. J. Immune adaptations that maintain homeostasis with the intestinal microbiota. *Nature Rev. Immunol.* **10,** 159–169 (2010).
2. Fagarasan, S., Kawamoto, S., Kanagawa, O. & Suzuki, K. Adaptive immune regulation in the gut: T cell-dependent and T cell-independent IgA synthesis. *Annu. Rev. Immunol.* **28,** 243–273 (2010).
3. Lee, M. R., Seo, G. Y., Kim, Y. M. & Kim, P. H. iNOS potentiates mouse Ig isotype switching through AID expression. *Biochem. Biophys. Res. Commun.* **410,** 602–607 (2011).
4. Tezuka, H. *et al.* Regulation of IgA production by naturally occurring TNF/iNOS-producing dendritic cells. *Nature* **448,** 929–933 (2007).
5. Kang, H. S. *et al.* Signaling via LTβR on the lamina propria stromal cells of the gut is required for IgA production. *Nature Immunol.* **3,** 576–582 (2002).
6. Serbina, N. V., Salazar-Mather, T. P., Biron, C. A., Kuziel, W. A. & Pamer, E. G. TNF/iNOS-producing dendritic cells mediate innate immune defense against bacterial infection. *Immunity* **19,** 59–70 (2003).
7. Muramatsu, M. *et al.* Class switch recombination and hypermutation require activation-induced cytidine deaminase (AID), a potential RNA editing enzyme. *Cell* **102,** 553–563 (2000).
8. Crouch, E. E. *et al.* Regulation of AID expression in the immune response. *J. Exp. Med.* **204,** 1145–1156 (2007).
9. Serbina, N. V. & Pamer, E. G. Monocyte emigration from bone marrow during bacterial infection requires signals mediated by chemokine receptor CCR2. *Nature Immunol.* **7,** 311–317 (2006).
10. Hapfelmeier, S. *et al.* Reversible microbial colonization of germ-free mice reveals the dynamics of IgA immune responses. *Science* **328,** 1705–1709 (2010).
11. Cumano, A., Dorshkind, K., Gillis, S. & Paige, C. J. The influence of S17 stromal cells and interleukin 7 on B cell development. *Eur. J. Immunol.* **20,** 2183–2189 (1990).
12. Tumanov, A. V. *et al.* Cellular source and molecular form of TNF specify its distinct functions in organization of secondary lymphoid organs. *Blood* **116,** 3456–3464 (2010).
13. Ivanov, I. I. & Littman, D. R. Modulation of immune homeostasis by commensal bacteria. *Curr. Opin. Microbiol.* **14,** 106–114 (2011).
14. Suzuki, K. *et al.* Aberrant expansion of segmented filamentous bacteria in IgA-deficient gut. *Proc. Natl Acad. Sci. USA* **101,** 1981–1986 (2004).
15. Maaser, C. *et al.* Clearance of *Citrobacter rodentium* requires B cells but not secretory immunoglobulin A (IgA) or IgM antibodies. *Infect. Immun.* **72,** 3315–3324 (2004).
16. Delogu, A. *et al.* Gene repression by Pax5 in B cells is essential for blood cell homeostasis and is reversed in plasma cells. *Immunity* **24,** 269–281 (2006).
17. Li, J. *et al.* B lymphocytes from early vertebrates have potent phagocytic and microbicidal abilities. *Nature Immunol.* **7,** 1116–1124 (2006).
18. Johnson, B. A. *et al.* B-lymphoid cells with attributes of dendritic cells regulate T cells via indoleamine 2,3-dioxygenase. *Proc. Natl Acad. Sci. USA* **107,** 10644–10648 (2010).
19. Kelly-Scumpia, K. M. *et al.* B cells enhance early innate immune responses during bacterial sepsis. *J. Exp. Med.* **208,** 1673–1682 (2011).
20. Neves, P. *et al.* Signaling via the MyD88 adaptor protein in B cells suppresses protective immunity during *Salmonella typhimurium* infection. *Immunity* **33,** 777–790 (2010).
21. Cumano, A., Paige, C. J., Iscove, N. N. & Brady, G. Bipotential precursors of B cells and macrophages in murine fetal liver. *Nature* **356,** 612–615 (1992).
22. Montecino-Rodriguez, E., Leathers, H. & Dorshkind, K. Bipotential B-macrophage progenitors are present in adult bone marrow. *Nature Immunol.* **2,** 83–88 (2001).
23. Pelletier, N. *et al.* Plasma cells negatively regulate the follicular helper T cell program. *Nature Immunol.* **11,** 1110–1118 (2010).

Supplementary Information is linked to the online version of the paper at www.nature.com/nature.

Acknowledgements We thank D. White in the Faculty of Medicine Flow Cytometry core facility and H. Singh for critical reading of the manuscript. We thank E. Verdu for providing additional germ-free mice at short notice, and we also thank C. Guidos for numerous $Rag2^{-/-}$ mice for mixed bone marrow chimeras. C.J.P. is supported by a CIHR operating grant MOP number 9862. R.C. is supported in part by the Intramural Research Program of the National Institute of Arthritis and Musculoskeletal and Skin Diseases of the National Institutes of Health. I.I.I. is supported by NIH (R00 DK085329-02) and CCFA (CDA #2388). A.M. is supported by a CIHR operating grant MOP number 89783. J.H.F. acknowledges support by an APART-fellowship of the Austrian Academy of Sciences, McGill start-up funds and a CIHR operating grant MOP number 114972. N.S. acknowledges the support of a CIHR Doctoral Award. J.L.G. is funded by the Canadian Institutes of Health Research (CIHR) and acknowledges the support of CIHR operating grant MOP number 67157 as well as infrastructure support from the Ontario Research Fund and that Canadian Foundation for Innovation. All authors have reviewed and agree with the content of the manuscript.

Author Contributions J.H.F. generated data in Figs 1d–f, 3a–d, 4d–f and Supplementary Figs 2–4, 7 and 8. O.L.R. contributed data in Figs 1a–d, 3a, b, 4, Supplementary Figs 7, 8 and Supplementary Tables 1–3. N.S. and C.J.P. contributed data in Fig. 2b and Supplementary Fig. 6. D.D.M. contributed data in Figs 1a, b, 2a and Supplementary Figs 1–3. S.H. contributed data in Fig. 2a. A.M. and M.L. contributed Supplementary Fig. 1b (D.M. did the sort). R.C. provided AID–YFP mice. I.I.I. originally suggested that we examine IgA^+ plasma cells as putative TNF-α/iNOS-producing cells and urged us to do the initial experiments. D.J.P and S.J.R. contributed data in Fig. 3e and provided critical insights. S.E.G. and S.R. helped us set up the *Citrobacter rodentium* experiments and provided critical insights. A.J.M., S.H. and K.D.M. provided intestinal tissues from germ-free and re-colonized mice. J.G. provided gene-deficient mice. J.L.G. wrote the manuscript and obtained funding for the work from the Canadian Institutes of Health Research.

Author Information Reprints and permissions information is available at www.nature.com/reprints. The authors declare no competing financial interests. Readers are welcome to comment on the online version of this article at www.nature.com/nature. Correspondence and requests for materials should be addressed to J.L.G. (jen.gommerman@utoronto.ca).

LETTER

doi:10.1038/nature10690

Cysteine methylation disrupts ubiquitin-chain sensing in NF-κB activation

Li Zhang[1,2], Xiaojun Ding[2], Jixin Cui[2], Hao Xu[2], Jing Chen[2], Yi-Nan Gong[2], Liyan Hu[2], Yan Zhou[2], Jianning Ge[2], Qiuhe Lu[2], Liping Liu[2], She Chen[2] & Feng Shao[2]

NF-κB is crucial for innate immune defence against microbial infection[1,2]. Inhibition of NF-κB signalling has been observed with various bacterial infections[3,4]. The NF-κB pathway critically requires multiple ubiquitin-chain signals of different natures[5,6]. The question of whether ubiquitin-chain signalling and its specificity in NF-κB activation are regulated during infection, and how this regulation takes place, has not been explored. Here we show that human TAB2 and TAB3, ubiquitin-chain sensory proteins involved in NF-κB signalling, are directly inactivated by enteropathogenic *Escherichia coli* NleE, a conserved bacterial type-III-secreted effector responsible for blocking host NF-κB signalling. NleE harboured an unprecedented *S*-adenosyl-L-methionine-dependent methyltransferase activity that specifically modified a zinc-coordinating cysteine in the Npl4 zinc finger (NZF) domains in TAB2 and TAB3. Cysteine-methylated TAB2-NZF and TAB3-NZF (truncated proteins only comprising the NZF domain) lost the zinc ion as well as the ubiquitin-chain binding activity. Ectopically expressed or type-III-secretion-system-delivered NleE methylated TAB2 and TAB3 in host cells and diminished their ubiquitin-chain binding activity. Replacement of the NZF domain of TAB3 with the NleE methylation-insensitive Npl4 NZF domain resulted in NleE-resistant NF-κB activation. Given the prevalence of zinc-finger motifs and activation of cysteine thiol by zinc binding, methylation of zinc-finger cysteine might regulate other eukaryotic pathways in addition to NF-κB signalling.

Bacterial pathogens such as *Salmonella*, *Shigella* and enteropathogenic *E. coli* (EPEC) target the NF-κB pathway to counteract host defence[3,4,7]. Recent genetic studies reveal that EPEC suppression of host NF-κB signalling and NF-κB-dependent pro-inflammatory cytokine production requires a type-III-secreted effector called NleE[8–10] that also has homologues in *Shigella* and certain *Salmonella* species. Consistent with these studies, ectopic expression of NleE in HeLa cells efficiently blocked both IL-1β and TNF-α-induced NF-κB luciferase reporter activation (Fig. 1a) and nuclear translocation of NF-κB p65 subunit (Supplementary Fig. 1). NleE did not affect Ras-activated extracellular signal-activation regulated kinase 1 and 2 (Erk1/2) signalling (Supplementary Fig. 2a). NleE abolished IκBα degradation stimulated by TNF-α in 293T cells and IL-1β in HeLa cells[8,9] (Fig. 1b). The adaptor Myd88 and the ubiquitin ligase TRAF6 are downstream of the IL-1β receptor, whereas TRAF2 and TRAF5 ubiquitin ligases act downstream of the TNF-α receptor[2]. NleE efficiently blocked NF-κB activation stimulated with Myd88, TRAF6 or TRAF2 (Fig. 1c and Supplementary Fig. 2b). The TRAF-downstream TAK1 complex is composed of the kinase subunit TAK1, TAB1 and one of the homologous adaptors TAB2 and TAB3 (refs 11–13). TAB2 and TAB3 (TAB2/3) induce oligomerization-dependent auto-phosphorylation and activation of TAK1. Overexpression of TAK1 and TAB1 could stimulate the NF-κB signalling, but this activation was not inhibited by NleE (Fig. 1c). Thus, NleE alone is sufficient to block host NF-κB signalling by acting downstream of TRAF and upstream of TAK1.

The IL-1β-activated NF-κB pathway can be reconstituted in cell-free extracts by using recombinant TRAF6 protein. Addition of highly purified NleE into the cell extracts or pre-expression of NleE in cells abolished TRAF6-induced IκBα phosphorylation as well as phosphorylation of IKKα/β in the IKK complex (Fig. 1d and Supplementary Fig. 3a, b). In agreement with the luciferase data, purified NleE diminished TRAF6-induced phosphorylation of TAK1 at Thr 187 (ref. 14) in the cell-free extracts (Fig. 1e). A previously identified non-functional NleE variant with deletion of $_{209}$IDSYMK$_{214}$ (NleEΔ6)[9] failed to block NF-κB signalling in all these assays (Fig. 1d, e and Supplementary Fig. 1). These results indicate that NleE directly targets and blocks TRAF-induced TAK1 activation.

NleE did not affect TRAF6-catalysed ubiquitin chain synthesis (Supplementary Fig. 4), which directed our focus to TAK1 complex components. In a yeast two-hybrid assay (Fig. 2a), NleE interacted specifically with TAB3, but not ubiquitin, TAK1 and TAB1. The interaction

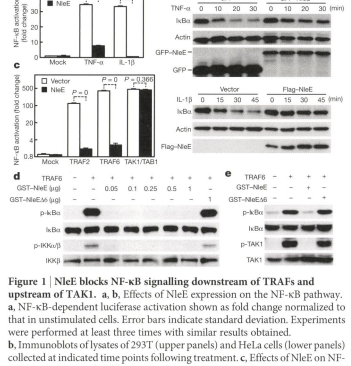

Figure 1 | NleE blocks NF-κB signalling downstream of TRAFs and upstream of TAK1. a, **b**, Effects of NleE expression on the NF-κB pathway. **a**, NF-κB-dependent luciferase activation shown as fold change normalized to that in unstimulated cells. Error bars indicate standard deviation. Experiments were performed at least three times with similar results obtained. **b**, Immunoblots of lysates of 293T (upper panels) and HeLa cells (lower panels) collected at indicated time points following treatment. **c**, Effects of NleE on NF-κB activation stimulated by TRAF2, TRAF6 or TAK1 plus TAB1. *y* axis is a logarithmic scale. Error bars indicate standard deviation. Experiments were performed at least three times with similar results obtained. **d**, **e**, Effects of purified NleE on NF-κB activation reconstituted in cell-free extract system. Recombinant TRAF6 protein together with GST–NleE was added into extracts prepared from MEF (**d**) or J774A.1 (**e**) cells. NleEΔ6 is an NleE variant with a six-residue deletion of $_{209}$IDSYMK$_{214}$.

[1]Graduate Program in Chinese Academy of Medical Sciences and Peking Union Medical College, Beijing 100730, China. [2]National Institute of Biological Sciences, Beijing 102206, China.

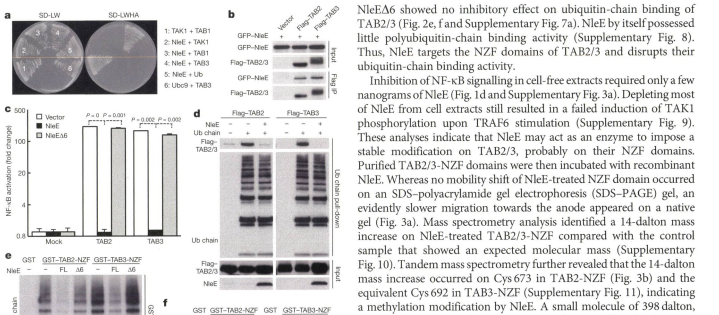

Figure 2 | NleE directly targets TAB2 and TAB3 and impairs their ubiquitin-chain binding activity. **a**, Yeast two-hybrid interaction assay of NleE and TAK1-complex components. Yeast strain was transformed with indicated plasmid combinations (bait plus prey). Activation of the *HIS3* and *ADE2* reporters was assessed by growth on SD-LWHA media. **b**, Co-immunoprecipitation assay of NleE and TAB2/3 interaction in 293T cells. Shown are immunoblots of anti-Flag immunoprecipitates (Flag IP) and total cell lysates (Input). **c**, Luciferase assays of effects of NleE on NF-κB activation stimulated by TAB2/3. *y* axis is shown on the logarithmic scale. Error bars indicate standard deviation. Experiments were performed at least three times with similar results obtained. **d**, Effects of NleE on ubiquitin-chain (Ub chain) binding of TAB2/3. Lysates of 293T cells transfected with Flag–TAB2/3 and NleE were subjected to Lys 63-linked ubiquitin-chain pull-down. Shown are immunoblots of the pull-down (Ub chain pull-down) and total cell lysates (Input). **e**, **f**, Effects of purified NleE on ubiquitin-chain binding of TAB2/3-NZF. Lys 63-linked ubiquitin chains (**e**) or tetra-ubiquitin (**f**) were subjected to pull-down by bacterially purified GST–TAB2/3-NZF in the presence or absence of recombinant NleE. FL, full-length; Δ6, NleEΔ_{209}IDSYMK$_{214}$.

was confirmed by co-immunoprecipitation of NleE with TAB3 as well as TAB2 from 293T cells (Fig. 2b). Consistently, NleE, but not NleEΔ6, completely blocked TAB2/3-stimulated NF-κB activation (Fig. 2c and Supplementary Fig. 5).

The effect of NleE on the integrity of the TAK1 signalling complex was then examined. NleE did not affect co-immunoprecipitation of endogenous TAB1 and TAK1 with TAB2 in both resting and Myd88-stimulated cells (Supplementary Fig. 6). TAB2 and TAB3 perceive the upstream Lys 63-linked polyubiquitin-chain signal for inducing TAK1 activation[15–17]. Lys 63-linked polyubiquitin chains readily precipitated TAB2/3 from 293T cells, which were largely abolished by NleE co-expression (Fig. 2d). Recombinant NleE also blocked precipitation of TAB2/3 by Lys 63-linked polyubiquitin chains from cell extracts (Supplementary Fig. 7a). The linear ubiquitin chain is known to have an important role in NF-κB signalling[18–20]. Linear tetra-ubiquitin could precipitate TAB3 from cell extracts, but much less proficiently than Lys 63-linked chains, and this binding was similarly sensitive to NleE treatment (Supplementary Fig. 7b). The carboxy-terminal conserved Npl4 zinc-finger (NZF) domains in TAB2/3 mediate TAB2/3 binding to polyubiquitin chains. When the NZF domain alone of TAB2 and TAB3 (TAB2/3-NZF) were assayed for Lys 63-linked ubiquitin chain binding, NleE had the same disruptive effect (Fig. 2e, f).

NleEΔ6 showed no inhibitory effect on ubiquitin-chain binding of TAB2/3 (Fig. 2e, f and Supplementary Fig. 7a). NleE by itself possessed little polyubiquitin-chain binding activity (Supplementary Fig. 8). Thus, NleE targets the NZF domains of TAB2/3 and disrupts their ubiquitin-chain binding activity.

Inhibition of NF-κB signalling in cell-free extracts required only a few nanograms of NleE (Fig. 1d and Supplementary Fig. 3a). Depleting most of NleE from cell extracts still resulted in a failed induction of TAK1 phosphorylation upon TRAF6 stimulation (Supplementary Fig. 9). These analyses indicate that NleE may act as an enzyme to impose a stable modification on TAB2/3, probably on their NZF domains. Purified TAB2/3-NZF domains were then incubated with recombinant NleE. Whereas no mobility shift of NleE-treated NZF domain occurred on an SDS–polyacrylamide gel electrophoresis (SDS–PAGE) gel, an evidently slower migration towards the anode appeared on a native gel (Fig. 3a). Mass spectrometry analysis identified a 14-dalton mass increase on NleE-treated TAB2/3-NZF compared with the control sample that showed an expected molecular mass (Supplementary Fig. 10). Tandem mass spectrometry further revealed that the 14-dalton mass increase occurred on Cys 673 in TAB2-NZF (Fig. 3b) and the equivalent Cys 692 in TAB3-NZF (Supplementary Fig. 11), indicating a methylation modification by NleE. A small molecule of 398 dalton, matching the mass of S-adenosyl-L-methionine (SAM), the most commonly used methyl donor by methyltransferases, was identified in bacterially purified NleE (Supplementary Fig. 12), indicating that SAM is co-purified with NleE from the bacteria. Consistently, addition of exogenous SAM decreased the minimal amount of NleE required for complete modification of TAB3-NZF by about 30-fold (Supplementary Fig. 13). NleE efficiently transferred ^{3}H-methyl from radiolabelled SAM onto TAB2/3-NZF domains (Fig. 3c) as well as full-length TAB2 and TAB3 purified from 293T cells *in vitro* (Fig. 3d and Supplementary Fig. 20a). Mass spectrometric analysis was performed to examine NleE

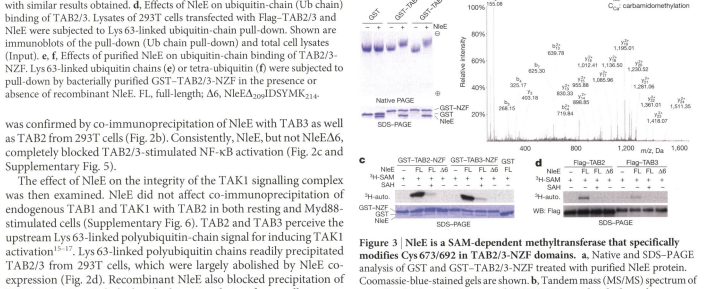

Figure 3 | NleE is a SAM-dependent methyltransferase that specifically modifies Cys 673/692 in TAB2/3-NZF domains. **a**, Native and SDS–PAGE analysis of GST and GST–TAB2/3-NZF treated with purified NleE protein. Coomassie-blue-stained gels are shown. **b**, Tandem mass (MS/MS) spectrum of a quadruply charged NleE-treated TAB2-NZF peptide. The b- and y-type product ions are marked in the spectrum, and also illustrated along the peptide sequence shown on top of the spectrum, which unambiguously identified the second cysteine as the methylated residue. The other three non-methylated cysteine residues were carbamidomethylated due to the iodoacetamide treatment during sample preparation as described in the Methods. **c**, **d**, ^{3}H-SAM labelling of TAB2/3-NZF and full-length TAB2/3 by purified NleE and the effects of S-adenosyl-L-homocysteine (SAH). GST–TAB2/3-NZF (**c**) and Flag–TAB2/3 (**d**) were purified from bacteria and 293T cells, respectively. FL, full-length; Δ6, NleEΔ_{209}IDSYMK$_{214}$. ^{3}H-auto., ^{3}H autoradiography; WB, western blot.

methylation of TAB2/3 in mammalian cells. The extracted ion chromatogram (XIC) identified the unmethylated form but not the methylated form of the Cys 673-containing peptide from Flag–TAB2 purified from vector-transfected cells (Supplementary Fig. 14). In marked contrast, only the methylated form of the corresponding peptide was identified from Flag–TAB2 purified from NleE-expressing cells, suggesting a nearly complete modification of TAB2 by NleE *in vivo*. NleE-catalysed methylation of TAB2/3-NZF domains and full-length TAB2/3 was effectively inhibited by *S*-adenosyl-L-homocysteine (SAH), the methyl transfer reaction product of SAM (Fig. 3c, d). Again, NleEΔ6 induced no mobility shift of TAB2/3-NZF on the native gel (Supplementary Fig. 13) and also failed to transfer ^{3}H-methyl onto TAB2/3 (Fig. 3c, d). NleE shows no sequence homology to any known methyltransferase[21]. The crystal structure of NleE (Q.Y., J.C. and F.S., unpublished data) reveals a new SAM-binding pocket, which involves Y212 (deleted in NleEΔ6) and more critically R107 in NleE. Mutation of either residue abolished NleE methylation of TAB3-NZF (Supplementary Fig. 15a). Thus, NleE is a new SAM-dependent methyltransferase that specifically modifies Cys 673 and Cys 692 in NZF domains of TAB2 and TAB3, respectively.

The approximately 30-residue NZF domain contains a zinc ion coordinated by four conserved cysteine residues[22,23] including the one modified by NleE in TAB2/3. In the TAB2-NZF and Lys 63-linked diubiquitin complex structure[16,17] (Fig. 4a), NleE-modified cysteine is involved in forming a hydrophobic surface that interacts with the Ile 44-centred hydrophobic patch in ubiquitin. In fact, the NleE-methylated NZF completely lost the ubiquitin-chain binding activity (Fig. 4b). Leucine or methionine substitution of Cys 673 in TAB2 (or Cys 692 in TAB3) abolished methylation of the corresponding NZF domain by NleE (Supplementary Fig. 16a), and both mutants were indeed devoid of ubiquitin-chain binding activity (Supplementary Fig. 16b). These mutations are expected to disrupt the zinc binding as leucine and methionine are not zinc ligands. NleE-methylated TAB3-NZF domain also lost the zinc ion, similarly to the effect of EDTA treatment (Supplementary Fig. 17). Thus, NleE methylation of a specific zinc-coordinating cysteine in TAB2/3-NZF domains and the consequent loss of zinc results in disruption of TAB2/3 ubiquitin-chain binding activity.

Mutation of any one of three other zinc-coordinating cysteines in TAB2/3-NZF domains also abolished the methylation by NleE (Supplementary Fig. 15b), indicating that NleE recognizes an intact zinc-finger structure. Notably, deletion of the NZF domain from TAB3 had little effect on NleE- and TAB3-binding in both yeast two-hybrid and co-immunoprecipitation assays (Supplementary Fig. 18a, b), indicating that structural information other than the NZF domain provides an additional docking interaction with NleE. This bipartite interaction mode is likely to be important for specific and highly efficient targeting of TAB2/3 by NleE.

The NZF domain is present in a number of proteins from different organisms, with members of this family being Npl4 and yeast Vps36 (Fig. 4a)[22,23]. NleE showed negligible activity towards Npl4-NZF, but methylated Vps36-NZF efficiently (Fig. 4c), raising the possibility that NleE targets other NZF-domain proteins in addition to TAB2/3. The NZF domain is also present in HOIL-1L, HOIP and Sharpin, the three components of the linear ubiquitin chain assembly complex (LUBAC) functioning in NF-κB signalling[18–20]. However, methylation of NZF domains from HOIL-1L, HOIP and Sharpin was hardly detected despite an excess amount of NleE used (Supplementary Fig. 19a). Linear ubiquitin binding activities of LUBAC-NZF domains were not affected by pre-incubation with excess NleE (Supplementary Fig. 19b). Full-length HOIL-1L, HOIP and Sharpin purified from 293T cells, as well as the active LUBAC complex, were all resistant to methylation by NleE (Supplementary Fig. 20a). The linear ubiquitin-chain synthesis activity of the LUBAC complex was not altered by co-incubation with NleE and SAM (Supplementary Fig. 21). NleE showed little effect on the ability of HOIL-1L, HOIP and Sharpin to bind linear tetra-ubiquitin

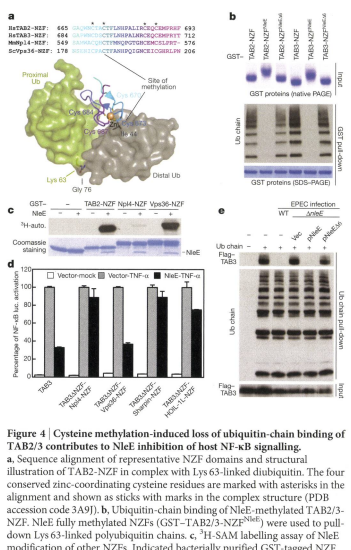

Figure 4 | Cysteine methylation-induced loss of ubiquitin-chain binding of TAB2/3 contributes to NleE inhibition of host NF-κB signalling. **a**, Sequence alignment of representative NZF domains and structural illustration of TAB2-NZF in complex with Lys 63-linked diubiquitin. The four conserved zinc-coordinating cysteine residues are marked with asterisks in the alignment and shown as sticks with marks in the complex structure (PDB accession code 3A9J). **b**, Ubiquitin-chain binding of NleE-methylated TAB2/3-NZF. NleE fully methylated NZFs (GST–TAB2/3-NZF^{NleE}) were used to pull-down Lys 63-linked polyubiquitin chains. **c**, ^{3}H-SAM labelling assay of NleE modification of other NZFs. Indicated bacterially purified GST-tagged NZF domains were incubated with recombinant NleE in the presence of ^{3}H-SAM. The reaction mixtures were loaded on an SDS–PAGE gel. The upper and lower panels are radiograph and Coomassie blue staining of the gel, respectively. **d**, Luciferase (luc.) assays of sensitivities of chimaeric TAB3 to NleE inhibition in TNF-α-induced NF-κB activation. TAB3ΔNZF-Vps36-NZF, TAB3ΔNZF-Npl4-NZF, TAB3ΔNZF-HOIL-1L-NZF and TAB3ΔNZF-Sharpin-NZF are chimaeric constructs with replacement of the NZF domain in TAB3 with that from Vps36, Npl4, HOIL-1L and Sharpin, respectively. Cells were transfected with chimaeric plasmids together with an NleE-expressing plasmid for 24 h and then subjected to a second transfection with NF-κB luciferase reporters. After 12 h, cells were treated with TNF-α for another 6 h before assaying the luciferase activity. Luciferase activation was shown as fold change normalized to that from TNF-α treatment without NleE expression. Error bars denote standard deviation. The *P* values for TAB3 versus TAB3ΔNZF-Npl4-NZF, TAB3ΔNZF-Vps36-NZF, TAB3ΔNZF-HOIL-1L-NZF and TAB3ΔNZF-Sharpin-NZF in TNF-α-treated NleE-expressing cells are 0.015, 0.082, 0 and 0.007, respectively. Experiments were performed at least three times with similar results obtained. **e**, Effects of type-III-delivered NleE on ubiquitin-chain binding of TAB3 during EPEC infection. 293T cells expressing Flag–TAB3 were infected with indicated EPEC strains. Cell lysates were subjected to Lys 63-linked ubiquitin-chain pull-down. WT, wild-type EPEC strain (E2348/69); *ΔnleE*, NleE-deletion strain. pNleE and pNleEΔ6 are rescue plasmids expressing wild-type NleE and the NleEΔ6 mutant, respectively.

(Supplementary Fig. 20b). The inability of NleE to target LUBAC *in vivo* agrees with the fact that NleE did not interact with HOIL-1, HOIP and Sharpin (Supplementary Fig. 18c), probably due to lack of the docking interaction provided by regions outside of the NZF domains in TAB2/3 (Supplementary Fig. 18a, b). Moreover, NleE could not methylate the C-terminal zinc-finger domain of NEMO

(Supplementary Fig. 22) that is also involved in ubiquitin-chain sensing in the NF-κB pathway[24].

A subset of the NZF domains, including those from Npl4, Vps36 and LUBAC, bind the polyubiquitin chain[19,22,23,25]. Npl4-NZF and Vps36-NZF could functionally substitute TAB3-NZF in stimulating NF-κB signalling[15]. Notably, NF-κB activation by the TAB3ΔNZF–Vps36-NZF chimaeric protein showed a similar sensitivity to NleE inhibition as that shown by wild-type TAB3, whereas TAB3ΔNZF–Npl4-NZF was much more resistant to the inhibitory action of NleE on NF-κB activation (Supplementary Fig. 23a). The four LUBAC-NZF domains behaved similarly to Npl4-NZF in this assay (Supplementary Fig. 23b). The ability of TAB3ΔNZF–Vps36-NZF and TAB3 to mediate TNF-α-induced NF-κB activation was sensitive to NleE inhibition; however, the LUBAC-NZF domains behaved similarly to Npl4-NZF and showed resistance to NleE inhibition (Fig. 4d and Supplementary Fig. 24). Furthermore, when the NZF domains in HOIL-1L and Sharpin were replaced with Npl4-NZF, no NleE-resistant effects in TNF-α-induced NF-κB activation were observed (Supplementary Fig. 25). These results agree well with the fact that these NZF domains, except for Vps36-NZF, are poor methylation substrates of NleE and further suggest that NleE-induced methylation of cellular TAB2/3 (Supplementary Fig. 14) is mainly responsible for the inhibition of the NF-κB signalling. Consistently, simultaneous knockdown of TAB2 and TAB3 severely attenuated TNF-induced NF-κB activation[11,15] (Supplementary Fig. 26), and expression of NleE in knockdown cells produced little additional effects (Supplementary Fig. 27). Interestingly, LUBAC-stimulated NF-κB activation is also sensitive to NleE inhibition as well as RNA-interference-mediated knockdown of TAB2/TAB3 expression (Supplementary Fig. 28). This indicates that LUBAC and TAB2/3-mediated ubiquitin-chain signalling might be linked together for full NF-κB activation.

NleE is mainly responsible for EPEC inhibition of host NF-κB signalling, and genetic deletion of NleE from the wild-type EPEC strain resulted in nuclear localization of p65 upon infection[8,9] (Supplementary Fig. 29). Polyubiquitin chains efficiently precipitated TAB3 from uninfected cells, but failed to do so from cells infected with wild-type EPEC (Fig. 4e). Importantly, deletion of NleE from EPEC resulted in efficient polyubiquitin-chain pull-down of TAB3. Complementation of the NleE-deletion strain with wild-type NleE, but not the methyltransferase-inactive NleEΔ6, restored the inhibition of ubiquitin-chain pull-down of TAB3 (Fig. 4e). These data indicate that type-III-secreted NleE can target host TAB2/3 for methylation and inactivation, contributing to disruption of host NF-κB signalling by EPEC infection.

We have discovered a bacterial effector that uses an unprecedented methyltransferase activity to specifically modify a zinc-finger cysteine in host TAB2/3. This modification abolishes ubiquitin-chain binding of the NZF domains in TAB2/3 and thereby disrupts host NF-κB signalling. Methylation modification usually occurs on a lysine or an arginine as extensively exemplified by epigenetic modifications of histone. Our finding represents the first example of enzyme-catalysed cysteine methylation as a mechanism in regulating signal transduction. Two other instances of thiol methylation have been noted previously. The *E. coli* sacrificial DNA repair protein Ada transfers a methyl group from Sp-configurated methyl phosphotriesters in damaged DNA to one of its own cysteines, thereby conferring cellular resistance to genotoxic effects of methylating agents[26,27]. The thiol group in small-molecule homocysteine is methylated by betaine-homocysteine *S*-methyltransferase (BHMT)[28] and methionine synthases[29] in homocysteine metabolism and methionine biosynthesis. In both instances, the methyl acceptor thiol is one of the four zinc-coordinating cysteines (occasionally three cysteines plus a histidine). Chemically, zinc binding can electronically activate the cysteine and generate a thiolate with high nucleophilicity[26]. The zinc thiolate is prone to undergo enzyme-catalysed methylation that usually uses S_N2 nucleophilic attack on the donor methyl group by the substrate[21]. Given the wide presence of zinc-finger proteins and methyltransferase activities in cells, cysteine methylation might be a previously underappreciated mechanism in regulating signal transduction.

METHODS SUMMARY

Reagents and NleE modification of TAB2/3-NZF domains. DNA for NleE was amplified from enteropathogenic *E. coli* E2348/69 strain. For *in vitro* modification, 4 μg of glutathione *S*-transferase-tagged TAB2/3-NZF were incubated with 3 μg of NleE for 30 min at 37 °C in 30 μl of buffer containing 50 mM Tris-HCl, pH 7.5, 150 mM NaCl, 5 mM DTT and 0.1% NP-40. For ^{3}H-SAM labelling, the reaction was supplemented with 0.55 μCi of ^{3}H-SAM (Perkin Elmer) and the amount of NleE was lowered to 0.6 μg. For ^{3}H-SAM labelling of full-length TAB2/TAB3, Flag–TAB2/3 immunopurified from 293T cells was reacted with 0.2 μg of NleE. To assay binding of NleE–methylated NZF to Lys 63 ubiquitin chains, 20 μg of GST–TAB2/3-NZF were incubated with 3 μg of NleE for 30 min at 37 °C in a 40 μl reaction containing 0.8 mM SAM. Part of the reaction mixtures (3/8) were loaded onto a native PAGE gel to confirm the complete modification; the rest of the mixtures were subjected to Lys 63 ubiquitin-chain pull-down.

Full Methods and any associated references are available in the online version of the paper at www.nature.com/nature.

Received 17 April; accepted 28 October 2011.
Published online 11 December 2011.

1. Hayden, M. S. & Ghosh, S. Shared principles in NF-κB signaling. *Cell* **132,** 344–362 (2008).
2. Vallabhapurapu, S. & Karin, M. Regulation and function of NF-κB transcription factors in the immune system. *Annu. Rev. Immunol.* **27,** 693–733 (2009).
3. Bhavsar, A. P., Guttman, J. A. & Finlay, B. B. Manipulation of host-cell pathways by bacterial pathogens. *Nature* **449,** 827–834 (2007).
4. Roy, C. R. & Mocarski, E. S. Pathogen subversion of cell-intrinsic innate immunity. *Nature Immunol.* **8,** 1179–1187 (2007).
5. Terzic, J., Marinovic-Terzic, I., Ikeda, F. & Dikic, I. Ubiquitin signals in the NF-κB pathway. *Biochem. Soc. Trans.* **35,** 942–945 (2007).
6. Skaug, B., Jiang, X. & Chen, Z. J. The role of ubiquitin in NF-κB regulatory pathways. *Annu. Rev. Biochem.* **78,** 769–796 (2009).
7. Cui, J. & Shao, F. Biochemistry and cell signaling taught by bacterial effectors. *Trends Biochem. Sci.* **36,** 532–540 (2011).
8. Nadler, C. *et al.* The type III secretion effector NleE inhibits NF-κB activation. *PLoS Pathog.* **6,** e1000740 (2010).
9. Newton, H. J. *et al.* The type III effectors NleE and NleB from enteropathogenic *E. coli* and OspZ from Shigella block nuclear translocation of NF-κB p65. *PLoS Pathog.* **6,** e1000898 (2010).
10. Vossenkämper, A. *et al.* Inhibition of NF-κB signaling in human dendritic cells by the enteropathogenic *Escherichia coli* effector protein NleE. *J. Immunol.* **185,** 4118–4127 (2010).
11. Ishitani, T. *et al.* Role of the TAB2-related protein TAB3 in IL-1 and TNF signaling. *EMBO J.* **22,** 6277–6288 (2003).
12. Cheung, P. C., Nebreda, A. R. & Cohen, P. TAB3, a new binding partner of the protein kinase TAK1. *Biochem. J.* **378,** 27–34 (2004).
13. Jin, G. *et al.* Identification of a human NF-κB-activating protein, TAB3. *Proc. Natl Acad. Sci. USA* **101,** 2028–2033 (2004).
14. Singhirunnusorn, P., Suzuki, S., Kawasaki, N., Saiki, I. & Sakurai, H. Critical roles of threonine 187 phosphorylation in cellular stress-induced rapid and transient activation of transforming growth factor-β-activated kinase 1 (TAK1) in a signaling complex containing TAK1-binding protein TAB1 and TAB2. *J. Biol. Chem.* **280,** 7359–7368 (2005).
15. Kanayama, A. *et al.* TAB2 and TAB3 activate the NF-κB pathway through binding to polyubiquitin chains. *Mol. Cell* **15,** 535–548 (2004).
16. Kulathu, Y., Akutsu, M., Bremm, A., Hofmann, K. & Komander, D. Two-sided ubiquitin binding explains specificity of the TAB2 NZF domain. *Nature Struct. Mol. Biol.* **16,** 1328–1330 (2009).
17. Sato, Y., Yoshikawa, A., Yamashita, M., Yamagata, A. & Fukai, S. Structural basis for specific recognition of Lys 63-linked polyubiquitin chains by NZF domains of TAB2 and TAB3. *EMBO J.* **28,** 3903–3909 (2009).
18. Gerlach, B. *et al.* Linear ubiquitination prevents inflammation and regulates immune signalling. *Nature* **471,** 591–596 (2011).
19. Ikeda, F. *et al.* SHARPIN forms a linear ubiquitin ligase complex regulating NF-κB activity and apoptosis. *Nature* **471,** 637–641 (2011).
20. Tokunaga, F. *et al.* SHARPIN is a component of the NF-κB-activating linear ubiquitin chain assembly complex. *Nature* **471,** 633–636 (2011).
21. Schubert, H. L., Blumenthal, R. M. & Cheng, X. Many paths to methyltransfer: a chronicle of convergence. *Trends Biochem. Sci.* **28,** 329–335 (2003).
22. Meyer, H. H., Wang, Y. & Warren, G. Direct binding of ubiquitin conjugates by the mammalian p97 adaptor complexes, p47 and Ufd1-Npl4. *EMBO J.* **21,** 5645–5652 (2002).
23. Wang, B. *et al.* Structure and ubiquitin interactions of the conserved zinc finger domain of Npl4. *J. Biol. Chem.* **278,** 20225–20234 (2003).
24. Laplantine, E. *et al.* NEMO specifically recognizes K63-linked poly-ubiquitin chains through a new bipartite ubiquitin-binding domain. *EMBO J.* **28,** 2885–2895 (2009).

25. Alam, S. L. *et al.* Ubiquitin interactions of NZF zinc fingers. *EMBO J.* **23,** 1411–1421 (2004).
26. Sedgwick, B., Robins, P., Totty, N. & Lindahl, T. Functional domains and methyl acceptor sites of the *Escherichia coli* Ada protein. *J. Biol. Chem.* **263,** 4430–4433 (1988).
27. He, C. *et al.* A methylation-dependent electrostatic switch controls DNA repair and transcriptional activation by *E. coli* Ada. *Mol. Cell* **20,** 117–129 (2005).
28. Castro, C. *et al.* Dissecting the catalytic mechanism of betaine-homocysteine *S*-methyltransferase by use of intrinsic tryptophan fluorescence and site-directed mutagenesis. *Biochemistry* **43,** 5341–5351 (2004).
29. Koutmos, M. *et al.* Metal active site elasticity linked to activation of homocysteine in methionine synthases. *Proc. Natl Acad. Sci. USA* **105,** 3286–3291 (2008).
30. Matthews, R. G. & Goulding, C. W. Enzyme-catalyzed methyl transfers to thiols: the role of zinc. *Curr. Opin. Chem. Biol.* **1,** 332–339 (1997).

Supplementary Information is linked to the online version of the paper at www.nature.com/nature.

Acknowledgements We thank I. Rosenshine for providing NleE deletion strains, K. Iwai for the HOIL-1L and HOIP expression plasmids, H. Sakurai for the phospho-TAK1 antibody, Z. Chen for TAB2/3 and Npl4-NZF chimera constructs, and S. Fukai for the NZF expression plasmid. We also thank members of the Shao laboratory for helpful discussions and technical assistance. This work was supported by the National Basic Research Program of China (973 Programs, 2010CB835400 and 2012CB518700).

Author Contributions L.Z. performed the majority of the experiments, assisted by J.C., H.X. and Y.-N.G.; X.D. and S.C. performed mass spectrometry analysis and analysed the data. J.C., L.H., Y. Z., J.G., Q.L. and L.L. generated reagents. L.Z. and F.S. analysed the data and wrote the manuscript. All authors discussed the results and commented on the manuscript.

Author Information Reprints and permissions information is available at www.nature.com/reprints. The authors declare no competing financial interests. Readers are welcome to comment on the online version of this article at www.nature.com/nature. Correspondence and requests for materials should be addressed to F.S. (shaofeng@nibs.ac.cn).

LETTER

doi:10.1038/nature10697

Basic amino-acid side chains regulate transmembrane integrin signalling

Chungho Kim[1]*, Thomas Schmidt[2]*, Eun-Gyung Cho[3], Feng Ye[1], Tobias S. Ulmer[2] & Mark H. Ginsberg[1]

Side chains of Lys/Arg near transmembrane domain (TMD)[1–3] membrane–water interfaces can 'snorkel', placing their positive charge near negatively charged phospholipid head groups[4–6]; however, snorkelling's functional effects are obscure. Integrin β TMDs have such conserved basic amino acids. Here we use NMR spectroscopy[7,8] to show that integrin β_3(Lys 716) helps determine β_3 TMD topography. The $\alpha_{IIb}\beta_3$ TMD structure indicates that precise β_3 TMD crossing angles enable the assembly of outer and inner membrane 'clasps' that hold the αβ TMD together to limit transmembrane signalling". Mutation of β_3(Lys 716) caused dissociation of $\alpha_{IIb}\beta_3$ TMDs and integrin activation. To confirm that altered topography of β_3(Lys 716) mutants activated $\alpha_{IIb}\beta_3$, we used directed evolution of β_3(K716A) to identify substitutions restoring default state. Introduction of Pro(711) at the midpoint of β_3 TMD (A711P) increased $\alpha_{IIb}\beta_3$ TMD association and inactivated integrin $\alpha_{IIb}\beta_3$(A711P,K716A). β_3(Pro 711) introduced a TMD kink of 30 ± 1° precisely at the border of the outer and inner membrane clasps, thereby decoupling the tilt between these segments. Thus, widely occurring snorkelling residues in TMDs can help maintain TMD topography and membrane-embedding, thereby regulating transmembrane signalling.

Integrins are composed of α and β type I transmembrane subunits[10]; association of the α and β TMDs regulates bidirectional transmembrane signal transduction[11]. Most metazoan integrin β subunits contain a positively charged Lys or Arg (Fig. 1a) near the inner TMD boundary that precedes an additional hydrophobic patch, termed the 'membrane proximal region'[12]. The membrane proximal region of integrin β_3 and, in particular, Lys 716, is protected from paramagnetic $Mn^{2+}EDDA^{2-}$ and is therefore membrane-embedded. This region in other integrin β subunits is also embedded[13]; hence, the membrane proximal domain is the carboxy (C)-terminal limb of a long α-helical TMD that is tilted at an angle of approximately 25°, thus enabling the ε-amino group of β_3(Lys 716) to snorkel near phospholipid head groups[7].

To assess the role of β_3(Lys 716) in TMD topography, we mutated it to a Glu residue and assessed embedding in phospholipid bicelles by measuring protection of the backbone amide protons from the electroneutral paramagnetic $Mn^{2+}EDDA^{2-}$ agent[7,8]. Lipid embedding on the extracellular side, defined by the protection pattern of Leu 694–Val 696, was unchanged in β_3(K716E) (Fig. 1b). In contrast, β_3(K716E) reduced protection on the intracellular side by approximately five residues, shifting the membrane border from residue 721 to 716 and decreasing membrane crossing angle. The absence of significant $^{13}C^{\alpha}$ chemical shift changes between β_3 and β_3(K716E) indicated no change in secondary structure as a consequence of the mutation (Supplementary Fig. 1a). At the level of H^N shifts, which are sensitive to surrounding chemical environment, relatively small H^N chemical changes between β_3 and β_3(K716E) indicated limited rearrangements in bicelle structure (Fig. 1c), suggesting that Glu 716 still localized within the lipid–water interface. In analogy to the K716(ε-NH_3^+)-lipid(PO_4^-) snorkelling interaction, glutamate's γ-COO^- group may engage a POPC lipid's choline $N(CH_3)_3^+$ group or a POPS lipid's amino NH_3^+ group within the lipid head group region (Fig. 1d). β_3(K716E) TMD-tail was not aggregated (Supplementary Fig. 1b), indicating that displacement of negatively charged Glu716 from the hydrophobic core shifted Leu(717)–Ile(721) into a more polar environment. Thus, Lys 716 substitutions perturb β_3 TMD membrane embedding and crossing angle.

Disruption of the interaction between integrin α and β TMDs leads to allosteric rearrangements that result in increased ligand-binding affinity of the extracellular domain (integrin activation)[10,11,14] and activation of cytosolic signalling pathways[15]. A stable αβ TMD association, which is crucial in the regulation of and physiological functions of integrins, requires the simultaneous formation of two discrete assemblies, an inner and outer membrane clasp (IMC and OMC), respectively (Fig. 1e)[9]. Because the β_3 TMD forms a continuous α-helix, its crossing angle appears critical for the simultaneous assembly of these clasps[9]. To examine the effect of β_3(Lys 716) mutations on the $\alpha_{IIb}\beta_3$ TMD association in mammalian cell membranes, we used a mini-integrin affinity capture assay[16] and chemical cross-linking. The latter experiments showed that the $\alpha_{IIb}\beta_3$ TMD interaction is primarily a 1:1 heterodimer (Supplementary Fig. 2). For the capture assay, an α_{IIb} mini-integrin bait containing the TMD and cytoplasmic tail of α_{IIb} (Fig. 2a) joined to a C-terminal tandem affinity purification (TAP) tag[16] for rapid efficient purification was expressed with preys comprising the extracellular domain of the Tac (IL-2 receptor α) joined to the TMD and tail of β_3 or β_3-bearing Lys 716 substitutions (Fig. 2a). When the cells were lysed and baits were captured using calmodulin beads, we found that the α_{IIb} bait captured the β_3 prey, as expected; however, neutral (Ala), polar (Cys, Ser), acidic (Glu), or hydrophobic (Leu) substitutions at β_3(Lys 716) blocked the $\alpha_{IIb}\beta_3$ TMD association. In contrast, a basic amino-acid substitution (Arg) did not disrupt the association, consistent with the idea that a snorkelling residue in this position is required to the formation of the $\alpha_{IIb}\beta_3$ TMD complex. To examine the potential effects of β_3(Lys 716) mutations on transmembrane signalling, we assayed their effects on the affinity state of integrin $\alpha_{IIb}\beta_3$ by measuring binding to activation-specific $\alpha_{IIb}\beta_3$ antibody (PAC1)[17] as in Fig. 2b. The results precisely correlated with the effects on αβ TMD interaction; all substitutions with the exception of Arg led to spontaneous integrin activation (Fig. 2c). The importance of this highly conserved Lys seems general because mutation of the paralogous residue in integrin β_{1A} (K732E) activated integrin $\alpha_5\beta_1$ (Supplementary Fig. 3a–d) and inhibited the association of the β1 TMD with either the α_5 or α_V TMD (Supplementary Fig. 3e). Thus, loss of a conserved basic residue in integrin β TMDs leads to disruption of the α–β TMD interaction and spontaneous transmembrane signalling.

The findings that β_3(Lys 716) substitutions that prohibit snorkelling alter TMD embedding, that such mutations dissociate the $\alpha_{IIb}\beta_3$ TMD

[1]Department of Medicine, University of California, San Diego, La Jolla, California 92093, USA. [2]Department of Biochemistry and Molecular Biology, Zilkha Neurogenetic Institute, Keck School of Medicine, University of Southern California, Los Angeles, California 90033, USA. [3]Center for Neuroscience, Aging, and Stem Cell Research, Sanford-Burnham Medical Research Institute, La Jolla, California 92037, USA.
*These authors contributed equally to this work.

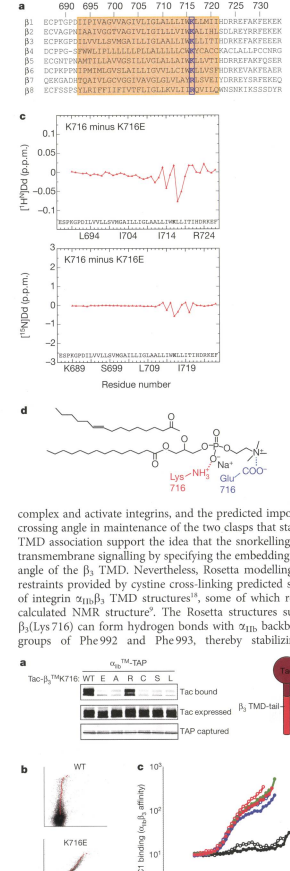

Figure 1 | Loss of snorkelling lysine changes lipid embedding of β_3 TMD. a, Sequence alignment of TMD regions of integrin β subunits indicated with β_3 numbering. Transmembrane domains are highlighted in orange. Conserved positive charged amino acids at position 716 (of β_3) are bolded and boxed with blue line. **b**, Mutation of β_3(Lys 716) changes TMD membrane embedding. The TROSY H–N cross-peak signal intensity of a residue in the presence and absence of 1 mM Mn^{2+}-$EDDA^{2-}$ in the aqueous phase, I/I_0, was measured to express quantitatively protection from the paramagnetic reagent. Experiments were performed in duplicates using independently prepared samples and quote the standard error between data sets. **c**, Chemical shift changes of K716E relative to the wild type. **d**, The predicted interaction of Lys 716 side chain ε-NH_3^+ with a lipid's PO_4^- group (red) and the interaction of glutamate's γ-COO^- with a POPS lipid's amino NH_3^+ group (blue) are illustrated. **e**, NMR structure of integrin $\alpha_{IIb}\beta_3$ TMD (PBD ID 2K9J). Side chains of residues essential to forming the OMC (Gly 972, Gly 976 in α_{IIb} and Gly 708 in β_3) and the IMC (Phe 992, Phe 993, Arg 995 in α_{IIb}, Asp 723 in β_3) are indicated.

complex and activate integrins, and the predicted importance of the crossing angle in maintenance of the two clasps that stabilize the αβ TMD association support the idea that the snorkelling Lys controls transmembrane signalling by specifying the embedding and crossing angle of the β_3 TMD. Nevertheless, Rosetta modelling with sparse restraints provided by cystine cross-linking predicted seven clusters of integrin $\alpha_{IIb}\beta_3$ TMD structures[18], some of which resembled the calculated NMR structure[9]. The Rosetta structures suggested that β_3(Lys 716) can form hydrogen bonds with α_{IIb} backbone carbonyl groups of Phe 992 and Phe 993, thereby stabilizing the α–β interaction[18]; the same paper reported that mutations at β_3(Lys 716) resulted in integrin activation[18], a result we confirmed. However, NMR-based structural restraints[9] preclude β_3(Lys 716/ε-NH_3^+)–α_{IIb}(Phe 993/CO) interactions (Supplementary Fig. 4). Furthermore, the embedding of the isolated β_3 TMD was similar to that observed in the $\alpha_{IIb}\beta_3$ complex[9] and, as shown, loss of the snorkelling β_3(Lys 716) alters β_3 TMD embedding. We therefore sought a positive experimental confirmation that the effects of β_3(Lys 716) mutations on $\alpha_{IIb}\beta_3$ TMD association and on integrin activation were dominated by changes in the β_3 membrane topography.

If β_3(Lys 716) mutations changed topography to prevent the simultaneous formation of the IMC and OMC, thereby leading to integrin activation, we reasoned that compensating mutations within the β_3 TMD might exist that would correct the crossing angle.

Figure 2 | Mutations in the snorkelling lysine induce integrin activation and disrupt α-β TMD interaction. a, Mutations of β_3(Lys 716) disrupt the $\alpha_{IIb}\beta_3$ TMD interaction. CHO cells were co-transfected with α_{IIb} TMD-tail construct fused with C-terminal TAP tag, $\alpha_{IIb}{}^{TM}$-TAP, and β_3 TMD-tail constructs fused with N-terminal Tac extracellular domain, Tac-$\beta_3{}^{TM}$, bearing various mutations at β_3(K716) as indicated. $\alpha_{IIb}{}^{TM}$-TAP proteins were isolated and associated Tac-$\beta_3{}^{TM}$ was detected by western blotting (upper panel). Expressed Tac-$\beta_3{}^{TM}$ proteins (middle panel) and captured $\alpha_{IIb}{}^{TM}$-TAP proteins (bottom panel) are also shown. **b**, β_3(K716E) activates integrin $\alpha_{IIb}\beta_3$. CHO cells stably expressing integrin α_{IIb} (CHO/α_{IIb}) were transiently transfected with wild-type (WT) integrin β_3 or β_3(K716E). Eighteen hours later, surface expression (D57 binding) and affinity of $\alpha_{IIb}\beta_3$ (PAC1 binding) were analysed. Geometric means of PAC1 binding in cells expressing different quantities of $\alpha_{IIb}\beta_3$ were plotted as larger red dots. **c**, Multiple β_3(K716) mutations activate integrin $\alpha_{IIb}\beta_3$. CHO/α_{IIb} cells were transfected with integrin β_3 bearing different mutations in the K716 residue as indicated. The geometric means of PAC1 binding to those CHO/α_{IIb} cells were plotted against D57 binding.

Conversely, if β_3(Lys 716) formed hydrogen bonds with the α_{IIb}, then a compensating mutation might introduce additional basic residues that could form such bonds.

We used random mutagenesis in a window of five residues amino (N)-terminal and 10 residues C-terminal to the β_3(K716) substitution (Fig. 3a and Supplementary Fig. 6a) to identify mutations that would complement the activating effects. We chose β_3(K716A) as the activating mutation; its effects may be less profound than β_3(K716E), thus favouring the discovery of weakly compensating mutations. Lentivirus particles carry two genomes[18], making it possible that a single particle might encode two mutants. To test this possibility, we transfected packaging cells with a mixture of lentiviral plasmids encoding integrin β_3 and β_3(K716A). When CHO cells bearing integrin α_{IIb} were infected with the resulting viruses, we found only populations containing either fully active or fully inactive $\alpha_{IIb}\beta_3$, with no intermediate phenotype (Supplementary Fig. 5). Thus, the packaging cells incorporated two copies of identical genomes into each viral particle. We performed PCR using a primer that was synthesized with 9% contamination of incorrect nucleotides in the randomized windows. The contamination level was predicted by computer simulation to cover most single amino-acid changes within the window (Supplementary Fig. 6b and Supplementary Table 1). We ligated the PCR fragments containing random mutations into a lentiviral vector encoding full-length integrin β_3, to create a randomized β_3 complementary DNA (cDNA) library (Fig. 3b).

CHO/α_{IIb} cells were infected with the mutant β_3 lentiviral particles and the infected cells were analysed for integrin expression (D57 antibody binding) and activation (PAC1 antibody binding) by using flow cytometry (Fig. 3b). In contrast to the β_3(K716A)-infected cells, cells infected with the mutant β_3 library exhibited a population of cells that expressed inactive $\alpha_{IIb}\beta_3$ (R3 region in Fig. 3c). To identify those mutations, we collected approximately 7,000 cells in the R3 region and purified genomic DNAs from those cells and used PCR to isolate the region of integrin β_3 containing the mutagenized window (Fig. 3b). Sequencing of the bulk product revealed that a β_3(A711P) mutation and stop codons at residues 724 and 725 were found in the mutagenized window (Fig. 3d). We performed NheI and BamHI digestion to isolate individual fragments containing the mutations and, after ligation into wild-type integrin β_3, confirmed the compensating effect of the mutations by transient transfection into cells expressing wild-type integrin α_{IIb} and measuring PAC1 binding (Supplementary Fig. 7). The clones that showed a compensating effect were sequenced and fell into three major groups (Fig. 3e): clones containing Pro substitutions at

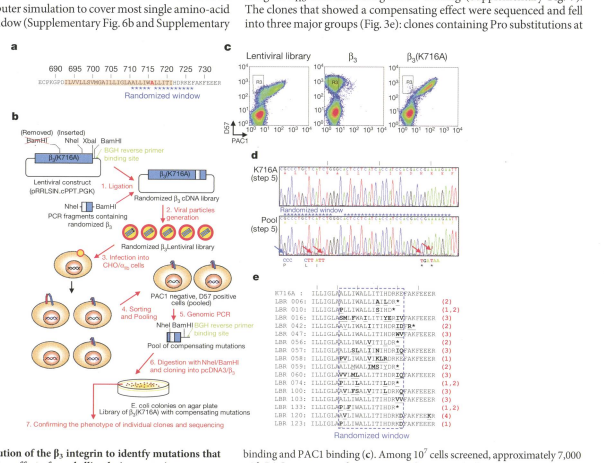

Figure 3 | Directed evolution of the β_3 integrin to identify mutations that complement the activating effect of snorkelling lysine mutation.
a, Mutational window. The randomized amino-acid sequence in integrin β_3(K716A) is indicated by stars. **b**–**e**, Strategy and results of random mutagenesis. After removing BamHI and inserting NheI restriction enzyme sites by silent mutations, integrin β_3(K716A) was cloned into lentiviral vector. TMD-tail fragments of integrin β_3 containing random mutations in the mutational window were produced by performing PCR with randomized forward primer and reverse primer containing a BamHI linker (Supplementary Fig. 6). The lentiviral β_3(K716A) construct and PCR fragments were digested with NheI and BamHI, and ligated to generate a randomized β_3 cDNA library containing 310,000 independent clones. By transfecting the cDNA library into HEK293T cells with packaging vectors, viral particles were generated. CHO/α_{IIb} cells were infected with the lentiviral particles, so that 10% of cells were infected to ensure that single lentiviral particle could be introduced into each cell (Supplementary Fig. 5). Cells infected with the lentiviral library, and cells infected with wild-type integrin β_3 or β_3(K716A) lentivirus, were tested for D57 binding and PAC1 binding (**c**). Among 10^7 cells screened, approximately 7,000 with PAC1-negative and D57-positive phenotypes (cells in R3 in **c**) were sorted and pooled. Their genomic DNAs were prepared and TMD-tail regions of introduced integrin β_3 were amplified by PCR using integrin-β_3-specific forward primer and BGH reverse primer. The genomic PCR products from cells infected with lentiviral library or integrin β_3(K716A) mutant lentivirus were sequenced in bulk (**d**) to identify predominant mutations in the pool of compensating mutations. The genomic PCR products were ligated into integrin β_3 to obtain individual compensating clones. Those individual clones (140 clones) were transiently transfected into CHO/α_{IIb} cells to verify that they exhibited reduced PAC1 binding (Supplementary Fig. 7), and compensating clones were sequenced. Those clones were grouped according to the major mutation present (**e**). Clones were grouped into those that contained A711P mutations (group 1), R724X or K725X mutations (group 2), neutral residue substitutions for E726 (group 3) or spontaneous mutations that did not fall within the target window (group 4). The group number is depicted in red and the mutations are in bold type.

Ala 711 (group 1), stop codons at Arg 724 or Lys 725 (group 2) or a neutral residue substitution at Glu 726 (group 3).

The only compensating mutation consistently observed in the TMD was β_3(A711P) (group 1 in Fig. 3e). This represents an integrin TMD point mutation that inhibits transmembrane signalling. This residue is inaccessible to talin or other cytoplasmic proteins and is unlikely to provide a direct interaction with α_{IIb} because it is not in the α–β TMD binding interface[9]. We confirmed that β_3(A711P) compensates both β_3(K716A) and β_3(K716E) mutations with respect to integrin activation (Fig. 4a and Supplementary Fig. 8b). In addition, β_3(A711P) increased interaction of the β_3(K716A) TMD with that of α_{IIb} (Fig. 4b). In contrast, the two other groups of compensating mutations were in the β_3 cytoplasmic domain. The truncated β_3 caused by β_3(724X or 725X) (group 2) deletes the talin binding site in the β_3 tail[20]. Furthermore, β_3 Glu 726 can contribute to talin binding through electrostatic interactions with Lys 317 and Lys 364 in talin1 (ref. 21).

Thus, we suspected that talin binding might amplify the activating effect of β_3(K716A); to test this idea we examined its effects in conjunction with β_3(Y747A) a mutation that disrupts talin binding[15]. Indeed the $\alpha_{IIb}\beta_3$(K716A,Y747A) mutant was less active than $\alpha_{IIb}\beta_3$(K716A) (Supplementary Fig. 8a). Thus, the only consistent TMD mutation that compensated for β_3(Lys 716) substitutions was the introduction of a Pro at position 711.

The structure of the β_3(A711P,K716A) TMD peptide embedded in phospholipid bicelles was determined. In accordance with the capacity of Pro to introduce kinks in transmembrane helices[22], A711P induced a 30 ± 1° kink between preceding and succeeding helical segments (Fig. 4c) caused by its side-chain geometry and the ensuing disruption of helix-stabilizing hydrogen bonds between Ile 707 and the proline residue and between Gly 708 and Leu 712 (Supplementary Fig. 9). This kink precisely separated the α-helical segments of β_3 that constitute the inner and outer clasps. Moreover, A711P introduced a tilt between

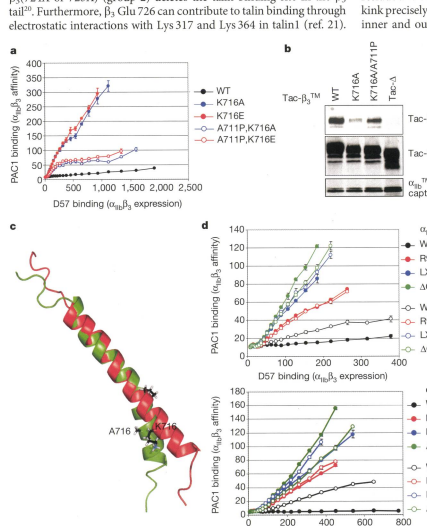

Figure 4 | Proline introduced in the TMD forms a flexible kink that stabilizes the $\alpha_{IIb}\beta_3$(K716A) TMD interaction and reduces integrin activation. a, β_3(A711P) complements β_3(Lys 716) mutations in integrin activation. CHO/α_{IIb} cells were transiently transfected with various integrin β_3 constructs as indicated, and their binding to PAC1 and D57 was analysed as described above. Error bars, s.e.m. ($n = 3$). **b**, β_3(A711P) stabilizes the TMD interactions of $\alpha_{IIb}\beta_3$(K716A). CHO cells were co-transfected with α_{IIb}^{TM}-TAP constructs and wild type, or mutant Tac-β_3^{TM} constructs as indicated, and the interaction between those integrin TMDs were analysed as previously reported[16]. **c**, Structure of the β_3(K716A,A711P) TMD. Structure of the bicelle-embedded integrin β_3(A711P,K716A) TMD segment (shown in green, Protein Data Bank ID 2L91) compared with the wild-type β_3 TMD structure (shown in red)[7]. To illustrate the proline-induced kink, the structures were superimposed on the backbone heavy atom coordinates of Ile 693–Leu 709. Average structures are shown. **d**, The inactive state of $\alpha_{IIb}\beta_3$(A711P,K716A/E) requires formation of both IMC and OMC. Mutations in α_{IIb} that disrupt either the OMC (α_{IIb} G972L,G976L) (LXXXL) or IMC (α_{IIb}R995D or $\alpha_{IIb}(\Delta G^{991}$FFKR) reactivate the $\alpha_{IIb}\beta_3$(K716A,A711P) integrin (upper panel) or $\alpha_{IIb}\beta_3$(K716E,A711P) integrin (lower panel). Error bars, s.e.m. ($n = 3$). **e**, Mechanism of proline-mediated compensation of snorkelling mutations. Snorkelling of positive-charged residue fixes the crossing angle of β_3 TMD (left). Loss of snorkelling changes the crossing angle and preventing simultaneous formation of IMC and OMC, thereby disrupting TMD interaction (middle). The proline-induced kink restores the angle of N-terminal half of the helix (right), enabling reformation of both clasps.

these elements that is independent of the overall membrane β_3 TMD crossing angle. Thus, even if the tilt angle of the inner helix is perturbed, this kink can aid the formation of both inner and outer membrane clasps[8] to stabilize the $\alpha\beta$ dimer. To verify that both clasps still partake in maintaining the inactive state of the integrin, mutations that disrupted either clasp were examined. The OMC involves packing interactions of α_{IIb}(Gly 972 and Gly 976) and β_3(Gly 708)[8,23]. α_{IIb}(G972,976A) substitutions that disrupt the OMC overcame the compensating effect of β_3(A711P) in both K716A and K716E backgrounds (Fig. 4d). Similarly, the α_{IIb}(R995D) mutation or α_{IIb}(ΔGFFKR) deletion, which disrupt the IMC, also overcame compensation (Fig. 4d). Thus, the kink introduced by β_3(A711P) allows the formation of the two membrane clasps required to stabilize the integrin in the off state (Fig. 4e).

In summary, we demonstrated that the loss of a snorkelling residue in integrin β TMDs can change membrane embedding and, thus, membrane-crossing angle, providing direct evidence that snorkelling can specify the topography of TMDs. Furthermore, we showed that snorkelling can affect transmembrane signalling by altering the stability of interactions between integrin TMDs. We have developed an efficient random lentiviral mutagenesis screening method, which was used to discover that a Pro-induced helix kink led to the stabilization of integrin α and β TMDs interaction by facilitating the formation of the inner and outer membrane clasps. Thus, the long-appreciated snorkelling of basic residues in TMDs[1–3] can have an important role in their topography and lateral association and therefore in signal transduction.

METHODS SUMMARY

NMR spectroscopy. Peptides encompassing human integrin β_3(P685–F727), either wild type or K716E mutant, were produced enriched in ^{15}N or $^{2}H/^{13}C/^{15}N$ isotopes as described previously[7]. Defined amounts of freeze-dried peptide were reconstituted in 25 mM HEPES•NaOH, pH 7.4, 6% D_2O, 0.02% w/v NaN_3 solution containing 200 mM 1,2-dihexanoyl-*sn*-glycero-3-phosphocholine (DHPC), 40 mM 1-palmitoyl-2-oleoyl-*sn*-glycero-3-phosphocholine (POPC) and 20 mM 1-palmitoyl-2-oleoyl-*sn*-glycero-3-[phospho-l-serine] (Avanti Polar Lipids). Two-dimensional TROSY H–N experiments were recorded in the absence and presence of 1 mM Mn^{2+}EDDA^{2-} using peptide concentrations of 0.2 mM (ref. 8). K716E assignment was transferred from the wild type using HNCA experiments.

Random β_3 library construction. Integrin β_3(K716A) cDNA was mutated to remove the BamHI site and introduce an NheI site with silent mutations. The cDNA was cloned into lentiviral vector, which was modified from pRRLSIN.cPPT.PGK–IRES–GFP WPRE (Addgene) to have a BamHI site and BGH reverse primer binding site between PGK promoter and internal ribosome entry site/green fluorescent protein (IRES–GFP). The region between the NheI and BamHI sites was cut out and replaced with NheI- and BamHI-restricted mutagenized PCR products by ligation. The mutagenized PCR products were generated using BGH reverse primer and mutagenized forward primer (Supplementary Fig. 6a). A total of approximately 310,000 *Escherichia coli* colonies on plates from the ligation reaction were collected and pooled. Plasmids from those cells were purified to make the mutagenized β_3 cDNA library.

Full Methods and any associated references are available in the online version of the paper at www.nature.com/nature.

Received 14 February; accepted 3 November 2011.
Published online 18 December 2011.

1. Killian, J. A. & von Heijne, G. How proteins adapt to a membrane–water interface. *Trends Biochem. Sci.* **25,** 429–434 (2000).
2. von Heijne, G. Membrane proteins: from sequence to structure. *Annu. Rev. Biophys. Biomol. Struct.* **23,** 167–192 (1994).
3. Sipos, L. & von Heijne, G. Predicting the topology of eukaryotic membrane proteins. *Eur. J. Biochem.* **213,** 1333–1340 (1993).
4. Krishnakumar, S. S. & London, E. The control of transmembrane helix transverse position in membranes by hydrophilic residues. *J. Mol. Biol.* **374,** 1251–1269 (2007).
5. Strandberg, E. & Killian, J. A. Snorkeling of lysine side chains in transmembrane helices: how easy can it get? *FEBS Lett.* **544,** 69–73 (2003).
6. Strandberg, E. *et al.* Lipid dependence of membrane anchoring properties and snorkeling behavior of aromatic and charged residues in transmembrane peptides. *Biochemistry* **41,** 7190–7198 (2002).
7. Lau, T. L., Partridge, A. W., Ginsberg, M. H. & Ulmer, T. S. Structure of the integrin beta3 transmembrane segment in phospholipid bicelles and detergent micelles. *Biochemistry* **47,** 4008–4016 (2008).
8. Lau, T. L., Dua, V. & Ulmer, T. S. Structure of the integrin αIIb transmembrane segment. *J. Biol. Chem.* **283,** 16162–16168 (2008).
9. Lau, T. L., Kim, C., Ginsberg, M. H. & Ulmer, T. S. The structure of the integrin αIIbβ3 transmembrane complex explains integrin transmembrane signalling. *EMBO J.* **28,** 1351–1361 (2009).
10. Arnaout, M. A., Mahalingam, B. & Xiong, J. P. Integrin structure, allostery, and bidirectional signaling. *Annu. Rev. Cell Dev. Biol.* **21,** 381–410 (2005).
11. Shattil, S. J., Kim, C. & Ginsberg, M. H. The final steps of integrin activation: the end game. *Nature Rev. Mol. Cell Biol.* **11,** 288–300 (2010).
12. Ginsberg, M. H., Partridge, A. & Shattil, S. J. Integrin regulation. *Curr. Opin. Cell Biol.* **17,** 509–516 (2005).
13. Stefansson, A., Armulik, A., Nilsson, I., von Heijne, G. & Johansson, S. Determination of N- and C-terminal borders of the transmembrane domain of integrin subunits. *J. Biol. Chem.* **279,** 21200–21205 (2004).
14. Hynes, R. O. Integrins: bidirectional, allosteric signaling machines. *Cell* **110,** 673–687 (2002).
15. Zhu, J. *et al.* Requirement of α and β subunit transmembrane helix separation for integrin outside-in signaling. *Blood* **110,** 2475–2483 (2007).
16. Kim, C., Lau, T. L., Ulmer, T. S. & Ginsberg, M. H. Interactions of platelet integrin αIIb and β3 transmembrane domains in mammalian cell membranes and their role in integrin activation. *Blood* **113,** 4747–4753 (2009).
17. Shattil, S. J., Hoxie, J. A., Cunningham, M. & Brass, L. F. Changes in the platelet membrane glycoprotein IIb.IIIa complex during platelet activation. *J. Biol. Chem.* **260,** 11107–11114 (1985).
18. Zhu, J. *et al.* The structure of a receptor with two associating transmembrane domains on the cell surface: integrin αIIbβ3. *Mol. Cell* **34,** 234–249 (2009).
19. Frankel, A. D. & Young, J. A. HIV-1: fifteen proteins and an RNA. *Annu. Rev. Biochem.* **67,** 1–25 (1998).
20. Tadokoro, S. *et al.* Talin binding to integrin β tails: a final common step in integrin activation. *Science* **302,** 103–106 (2003).
21. Anthis, N. J. *et al.* The structure of an integrin/talin complex reveals the basis of inside-out signal transduction. *EMBO J.* **28,** 3623–3632 (2009).
22. Senes, A., Engel, D. E. & DeGrado, W. F. Folding of helical membrane proteins: the role of polar, GxxxG-like and proline motifs. *Curr. Opin. Struct. Biol.* **14,** 465–479 (2004).
23. Berger, B. W. *et al.* Consensus motif for integrin transmembrane helix association. *Proc. Natl Acad. Sci. USA* **107,** 703–708 (2010).

Supplementary Information is linked to the online version of the paper at www.nature.com/nature.

Acknowledgements This work was supported by grants from the National Institutes of Health of the USA. T.S.U. acknowledges support from the National Institutes of Health (HL089726) and M.H.G. was supported by HL078784, HL579O0 and AR27214. C.K. is a recipient of a postdoctoral fellowship from the American Institute for Cancer Research.

Author Contributions The project was conceived by C.K. and M.H.G. All experiments with the exception of the NMR studies were performed by C.K. The NMR studies were conducted by T.S. under the supervision of T.S.U. E.C. and F.Y. contributed reagents. M.H.G. and C.K. wrote the paper, which was edited by T.S. and T.S.U.

Author Information Reprints and permissions information is available at www.nature.com/reprints. The authors declare no competing financial interests. Readers are welcome to comment on the online version of this article at www.nature.com/nature. Correspondence and requests for materials should be addressed to M.H.G. (mhginsberg@ucsd.edu) or T.S.U. (tulmer@usc.edu).

LETTER

doi:10.1038/nature10699

Subnanometre-resolution structure of the intact *Thermus thermophilus* H^+-driven ATP synthase

Wilson C. Y. Lau[1,2] & John L. Rubinstein[1,2,3]

Ion-translocating rotary ATPases serve either as ATP synthases, using energy from a transmembrane ion motive force to create the cell's supply of ATP, or as transmembrane ion pumps that are powered by ATP hydrolysis[1]. The members of this family of enzymes each contain two rotary motors: one that couples ion translocation to rotation and one that couples rotation to ATP synthesis or hydrolysis. During ATP synthesis, ion translocation through the membrane-bound region of the complex causes rotation of a central rotor that drives conformational changes and ATP synthesis in the catalytic region of the complex. There are no structural models available for the intact membrane region of any ion-translocating rotary ATPase. Here we present a 9.7 Å resolution map of the H^+-driven ATP synthase from *Thermus thermophilus* obtained by electron cryomicroscopy of single particles in ice. The 600-kilodalton complex has an overall subunit composition of $A_3B_3CDE_2FG_2IL_{12}$. The membrane-bound motor consists of a ring of L subunits and the carboxy-terminal region of subunit I, which are equivalent to the c and a subunits of most other rotary ATPases, respectively. The map shows that the ring contains 12 L subunits[2] and that the I subunit has eight transmembrane helices[3]. The L_{12} ring and I subunit have a surprisingly small contact area in the middle of the membrane, with helices from the I subunit making contacts with two different L subunits. The transmembrane helices of subunit I form bundles that could serve as half-channels across the membrane, with the first half-channel conducting protons from the periplasm to the L_{12} ring and the second half-channel conducting protons from the L_{12} ring to the cytoplasm. This structure therefore suggests the mechanism by which a transmembrane proton motive force is converted to rotation in rotary ATPases.

To investigate how the structure of the *T. thermophilus* ATP synthase allows its rotary mechanism, we imaged the detergent-solubilized intact enzyme by electron cryomicroscopy (cryo-EM) and calculated a three-dimensional map to approximately 10 Å resolution (Supplementary Fig. 1). This resolution was sufficient to observe α-helices in the structure. Achieving this resolution required optimization of the specimen preparation and imaging conditions, and development of a new map refinement algorithm (Methods). Figure 1a shows the refined three-dimensional map. Available crystal structures of subunits and subcomplexes of the enzyme were fitted into the map with remarkably good agreement (Fig. 1b, c). A cross-section through the soluble region of the map shows that the α-helices that make up each of the E and G subunits of the two peripheral stalks can be resolved (Fig. 1d, purple and beige arrows, respectively), as can densities that correspond to α-helices in subunits with more complex folds, such as the A subunits (Fig. 1d, for example, circled in yellow). Map segments corresponding to subunits matched available crystal structures with high fidelity (Fig. 1e–g). If the protein particles imaged occupied all possible rotational states of the central rotor, the three-dimensional map would show the average conformation of each A and B subunit and the density corresponding to the DF subcomplex would

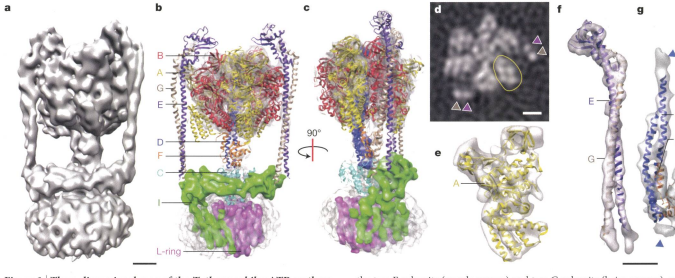

Figure 1 | Three-dimensional map of the *T. thermophilus* ATP synthase. **a**, A surface view of the three-dimensional map. **b**, **c**, The overall map (semi-transparent grey) with fitted crystal structures and segments corresponding to individual subunits. Segments of the cryo-EM map are shown for the L_{12} ring, subunit I and residues of subunit D missing from its crystal structure. **d**, A cross-section through the soluble region of the map shows that α-helices from the two E subunits (purple arrows) and two G subunits (beige arrows) can be resolved. Helices can also be resolved in other subunits, such as the A subunits (example circled in yellow). The map segments agree with crystal structures, such as subunit A (**e**), the EG subcomplex (**f**) and the DF subcomplex (**g**). Density corresponding to missing residues from the crystal structure of the D subunit is indicated with blue arrows. Scale bars, 25 Å.

[1]Molecular Structure and Function Program, The Hospital for Sick Children Research Institute, 555 University Avenue, Toronto, Ontario M5G 1X8, Canada. [2]Department of Biochemistry, The University of Toronto, Ontario M5S 1A8, Canada. [3]Department of Medical Biophysics, The University of Toronto, Ontario M5G 2M9, Canada.

appear as a rotational average of the structure of these subunits. However, docking an A_3B_3DF crystal structure[4] into the map (Fig. 1b, c and Supplementary Fig. 2) and fitting the DF-rotor subcomplex into its corresponding map segment (Fig. 1g) revealed that the enzyme was arrested in a single rotational state[3]. This homogeneity explains why we were able to extract nanometre-resolution information when averaging many different particles to calculate the map. The crystal structure of the A_3B_3DF subcomplex showed that two of the AB subunit pairs took on similar closed or narrow conformations, designated A_NB_N and $A_{N'}B_{N'}$, whereas the third adopted an open or wide conformation, designated A_WB_W[4]. From the position of the D and F subunits in the cryo-EM map, it is apparent that the A_NB_N pair, which corresponds to the $\beta_{TP}\alpha_{TP}$ pair in mitochondrial F_1-ATPase[6], is positioned at the A/B interface between the two peripheral stalks (Supplementary Fig. 2). Because we did not take any measures to stop the rotor in one rotational state, the existence of this unique position suggests that in the intact complex the observed state has a lower energy than other positions of the rotor. For the membrane-bound subunits I and L, where no crystal structures are available, segmented densities are shown in Fig. 1b, c.

The extramembranous portion of the map contains a wealth of information on how the different subunits interact in the intact enzyme. The two peripheral stalks of the complex have the same structures in the intact assembly, both adopting conformations that match the available crystal structure[7]. Contacts between the catalytic A_3B_3 hexamer and the peripheral stalks exclusively involve the B subunits and E subunits of the stalks, and are mostly between the amino-terminal β-barrel domains of the B subunits and the C-terminal α/β-domains of the E subunits. The N-terminal region of both subunits E and G in both of the peripheral stalks interact with the N-terminal region of subunit I. The funnel-shaped C subunit, which links the DF portion of the central rotor to the L_{12} ring and has been crystallized in isolation[8], is significantly more open in the intact enzyme than in the crystal structure so that it can accept the DF subunits into its central cavity (Fig. 2). The three pseudo-symmetric domains of the C subunit can be differentiated in the map showing that interaction of the C subunit and the L_{12} ring strongly involves the N-terminal α-helix of the first domain of subunit C. The C subunit sits asymmetrically on the L_{12} ring and does not penetrate significantly into the central pore of the ring. The cryo-EM map shows that the N-terminal region of subunit I consists of an elongated helical bundle flanked by two domains, consistent with a crystal structure of a homologous protein that was published after submission of this manuscript[9] (Supplementary Fig. 3).

The map provides the first detailed insight into how the I subunit and L_{12} ring fit together to allow the generation of rotation (Fig. 3a). Cross-sections through the detergent-embedded region of the map show two concentric rings of densities, with the outer ring consisting of 12 well-resolved densities (Fig. 3b–e). These 12 densities undoubtedly correspond to the outer helices of the L_{12} ring, where each L subunit consists of a helical hairpin. The N-terminal inner helices of the L_{12} ring could not be resolved and appear as a nearly continuous density. Our ability to resolve the outer helices is consistent with the loose packing and gaps seen between the outer helices in crystal structures of related ring subcomplexes[10–15]. Although composed of similarly sized residues as the outer helices, the crystallographic studies suggest that the inner helices are more tightly packed and resolving them would require a resolution better than 9.7 Å. As shown previously[5], the detergent used to keep the enzyme soluble, dodecylmaltoside, has a density higher than that of ice and is visible surrounding the transmembrane region of the complex (Fig. 3b, left panel, white bars). Features in the detergent micelle, which we expect to be mostly unstructured, may represent noise that is enhanced by construction of the map to nanometre resolution. Density is visible within the centre of the L_{12} ring (Fig. 3b, left panel, yellow circle) and probably corresponds to a detergent or lipid plug observed by atomic force microscopy of isolated rings[16]. The map presents the first determination of the ring structure within an intact rotary ATPase, providing insight into how the I subunit affects the L_{12} ring. This information is necessary to assess the likelihood of proposed catalytic models in which the L subunits undergo conformational changes when they contact the I subunit[17]. From the cryo-EM map it is evident that the 12-fold symmetry of the L_{12} ring is not broken significantly, even where the L subunits contact the I subunit (Fig. 3c, d). This preserved symmetry of the ring is inconsistent with models of proton translocation that require major conformational changes in the rotor, but could still be consistent with swivelling of the outer helices of the L subunits if this motion did not distort the ring significantly[17].

Proton translocation facilitated by the I subunit drives rotation of the L_{12} ring, but until now there has been no structural information available for subunit I or its equivalent subunit from any rotary ATPase. Here we observe eight transmembrane densities that can be

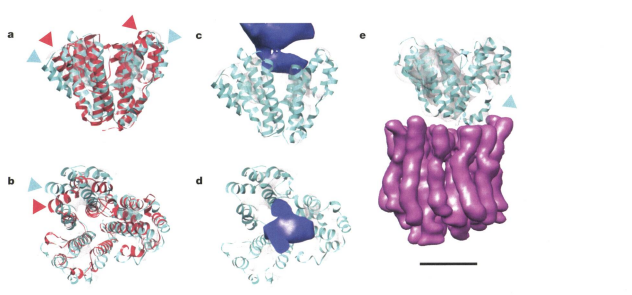

Figure 2 | Fitting of the C subunit crystal structure. a, **b**, Side (**a**) and top (**b**) views comparing rigid body fitting of the C subunit crystal structure (red) to flexible fitting of the crystal structure (cyan) into the corresponding map segment. Arrows indicate regions of major difference between the two atomic models. **c**, **d**, Side (**c**) and top (**d**) views showing that flexible fitting of the C subunit gives it a more open conformation that allows it to accommodate the segment for the DF subcomplex (dark blue) into its central cavity. **e**, A side view of the C subunit, and the segment corresponding to the L_{12} ring (magenta), show that subunit C sits asymmetrically on the ring with its N-terminal α-helix (cyan arrow) mediating most of the contact with the L subunits. Scale bar, 25 Å.

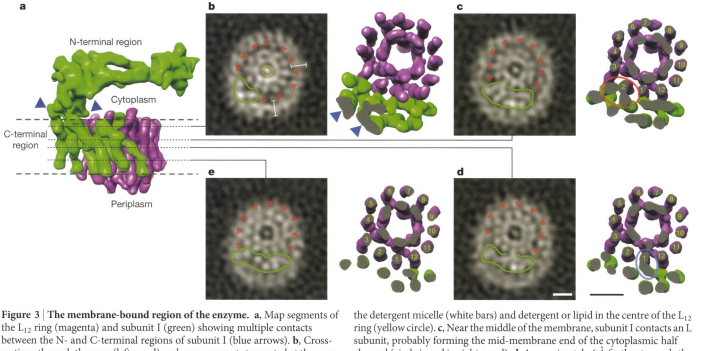

Figure 3 | The membrane-bound region of the enzyme. a, Map segments of the L_{12} ring (magenta) and subunit I (green) showing multiple contacts between the N- and C-terminal regions of subunit I (blue arrows). **b**, Cross-sections through the map (left panel) and map segments truncated at the same height (right panel) show subunit I separated from the L_{12} ring near the cytoplasm. Outer helices of the L_{12} ring are indicated (red arrows) and the transmembrane helices of subunit I are outlined (green). Cross-sections show the detergent micelle (white bars) and detergent or lipid in the centre of the L_{12} ring (yellow circle). **c**, Near the middle of the membrane, subunit I contacts an L subunit, probably forming the mid-membrane end of the cytoplasmic half channel (circle in red in right panel). **d**, Approximately 6 Å further towards the periplasm subunit I contacts a different L subunit, probably forming the mid-membrane end of the periplasmic half-channel (circled in blue in right panel). **e**, Subunit I is separated from the L_{12} ring near the periplasm. Scale bars, 25 Å.

attributed to α-helices in the C-terminal region of subunit I (Fig. 3b–e). This number of transmembrane helices is consistent with an experimentally tested topology map of the *Saccharomyces cerevisiae* V-ATPase a subunit[3], with which the I subunit sequence aligns well (Supplementary Fig. 4). Although we can trace the complete trajectories of the eight transmembrane densities of subunit I, our inability to resolve the helices in the tightly packed inner ring of the L_{12} oligomer means that we cannot rule out the possibility that we have missed a transmembrane helix in our analysis of subunit I. At the cytoplasmic surface of the membrane region, the densities from the N- and C-terminal regions of subunit I appear to be connected in more than one place (Fig. 3a and the right panel of Fig. 3b, blue arrows). These connections show that there must be protein–protein interactions between the N- and C-terminal regions of subunit I involved in keeping the two regions rigidly attached. Within the membrane, subunit I divides into two clusters of helices: one that is mostly perpendicular to the membrane, and another that contains tilted helices adjacent to the L_{12} ring. The first cluster contacts a single L subunit near the middle of the membrane region (right panel of Fig. 3c, circled in red) whereas the second cluster contacts the adjacent L subunit a small distance further towards the periplasm (right panel of Fig. 3d, circled in blue). The maximal separation of the I subunit helices from the outer helices of the L_{12} ring is of around the same distance, approximately 15 Å between helical axes, as is the maximal separation between adjacent outer helices of the L_{12} ring.

Proton translocation in rotary ATPases is thought to involve protonation and deprotonation of conserved mid-membrane glutamic acid or aspartic acid residues in the outer helices of the ring-forming subunits. In the L subunit from the *T. thermophilus* ATP synthase, this conserved protonatable residue is Glu 63. The contact of the I subunit with two different L subunits (Fig. 3c, d) places the two L subunits in distinct chemical environments and establishes the conditions necessary for a two half-channel model for proton translocation[13,18], with one L subunit exchanging protons with the periplasm and another L subunit exchanging protons with the cytoplasm. One cluster of transmembrane helices in the I subunit could conduct protons from the periplasm to the mid-membrane Glu 63 residue of an L subunit (Fig. 4a, blue circle). The other cluster of transmembrane helices in subunit I could conduct protons from the mid-membrane Glu 63 residue of the adjacent L subunit to the cytoplasm (Fig. 4a, red circle). Crystal structures of other membrane proteins indicate that four transmembrane helices are sufficient for forming a proton pore, with available examples showing proton[19] and sodium[20] conducting pores composed of four and three transmembrane helices, respectively. The structure suggests that protons flow from the periplasmic half-channel to the Glu 63 residue of the L subunit in contact with the periplasmic half-channel (the L subunit with an outer helix labelled '1' in Fig. 3c–e). Protonation of this Glu 63 neutralizes the negative charge of the residue and allows the anticlockwise rotation of the ring (viewed from the cytoplasm) that places the Glu 63 in the hydrophobic environment of the lipid bilayer (Fig. 4b). With the negative charge neutralized, Glu 63 can assume the proton-locked conformation seen in a crystal structure of the *Spirulina platensis* c_{15} ring[13]. In this conformation, both oxygen atoms in Glu 63 are involved in hydrogen bonding with other residues in the L_{12} ring and the neutral Glu 63 residue is tucked into the crevice between L subunits. The directionality of the rotation is explained by a Brownian ratchet mechanism where random thermal rotational fluctuations are biased to go in the correct direction by the direction of the proton motive force across the membrane[18]. Rotation of the L_{12} ring brings an L subunit bearing a protonated Glu 63 (on the helix labelled '2' in Fig. 3c–e) out of the lipid environment and into contact with the cytoplasmic half-channel of subunit I. Subunit I contains a conserved and essential arginine residue (Arg 563) of unknown function[21,22]. It has been postulated that Arg 563 causes a decrease in the pK_a of the Glu 63 residue on the L subunit in contact with the cytoplasmic half-channel, thereby causing it to lose its proton to the channel[23]. Arg 563 may also stabilize the deprotonated Glu 63 by forming a salt bridge[12]. This arrangement of half-channels is consistent with a model where L ring rotation could be driven in either direction, depending only on the direction of the proton motive force across the membrane. However, the specific arrangements of amino acids in the structure, which cannot be resolved in this map, could be such that proton translocation from

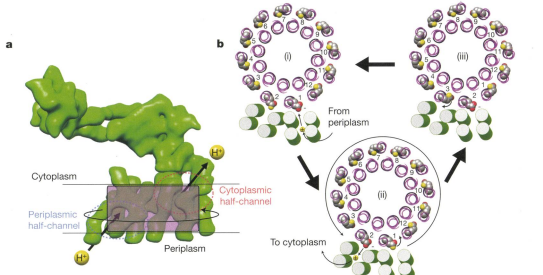

Figure 4 | Model for proton translocation. a, Subunit I (green) is shown parallel to the membrane with the L_{12} ring in front of it indicated by a semi-transparent magenta rectangle. During ATP synthesis, protons enter the periplasmic half-channel in subunit I (dashed blue oval) and are conducted to the centre of the lipid bilayer where they neutralize the Glu 63 residue of an L subunit. The ring rotates to bring a protonated Glu 63 residue into contact with the cytoplasmic half-channel (dashed red oval). **b**, Viewed from the cytoplasm, two half-channels in subunit I are depicted as clusters of green cylinders. Deprotonated Glu 63 residues are shown with two red oxygen atoms whereas protonated Glu 63 residues are shown with one red and one yellow oxygen atom. Protonation of L subunit '1' by the periplasmic half-channel (i) and deprotonation of L subunit '2' by the cytoplasmic half-channel (ii) lead to rotation of the ring, with L subunit '1' assuming a proton-locked conformation as it enters the lipid bilayer. Rotation brings the proton-locked L subunit '3' to the cytoplasmic half-channel (iii) where it assumes an unlocked conformation, allowing the sequence of events to repeat.

the cytoplasm to the periplasm is not able to induce rotation. At 9.7 Å resolution, it is not possible to relate unambiguously the sequence of the C-terminal region of subunit I and predicted transmembrane helices (shown in Supplementary Fig. 4) to the transmembrane densities in the map. Nonetheless, Arg 563 has been proposed to reside on transmembrane helix 7 and form part of the cytoplasmic half-channel[3], which would identify transmembrane helix 7 as one of the two helices in contact with the L subunit labelled '2' in Fig. 3.

At both the cytoplasmic and periplasmic limits of the membrane-embedded region of the map (Fig. 3b, e) all helices from subunit I are well separated from the helices of the L_{12} ring, making it highly unlikely that an entire half-channel could be formed by the interface of helices from the I and L subunits[24]. F-type ATP synthases have been proposed to have five transmembrane helices[25,26]. If true, this topology would suggest that in those enzymes the two half-channels consist of three helices, that one or more helices contributes to both half-channels simultaneously, or that helices from the rotor are involved in formation of the half-channels. The observation that the two L subunits in contact with the I subunit are immediately adjacent to each other indicates that after a Glu 63 residue is deprotonated by the cytoplasmic half-channel it is immediately reprotonated by the periplasmic half-channel with a single 30° rotational step of the rotor. The small contact area between the I subunit and L_{12} ring suggests that these membrane-bound components rely on the two peripheral stalks to hold them together in the precise arrangement necessary for the complex's biological activity. This minimal contact is consistent with an important but fragile interaction that might easily be disrupted by non-physiological conditions such as those needed to make three-dimensional crystals, thus helping to explain why the membrane region of this class of enzyme has not been crystallized, despite significant efforts by many research groups. Knowledge of the precise residues involved in proton translocation will require construction of cryo-EM maps to higher resolution or formation of well-ordered crystals of this hitherto refractory protein complex. At subnanometre resolution, the complete structure of the *T. thermophilus* H^+-driven ATP synthase suggests the mechanism by which the energy stored in a transmembrane proton motive force is converted into rotation in rotary ATPases.

METHODS SUMMARY

T. thermophilus HB8 was grown and the H^+-driven ATP synthase purified as described previously[5]. Specimens were prepared for cryo-EM with a Vitrobot (FEI) and imaged with an FEI Tecnai F20 electron microscope equipped with a field emission gun and operating at 200 kV. An electron exposure of approximately 18 electrons $Å^{-2}$ was used during imaging to optimize the signal-to-noise ratio at relevant spatial frequencies[27]. Images were recorded on Kodak SO-163 film and digitized with a Photoscan densitometer (Intergraph). The previously published cryo-EM map of the *T. thermophilus* V-ATPase[2] was filtered to 30 Å resolution and used as an initial model for refinement of the entirely new data set of 46,105 particle images. Initial particle orientations were determined by projection matching with Frealign[28] using information out to 20 Å resolution. The accuracy of particle orientations was refined further with a new program (Refine_fspace), ultimately using information out to 11.2 Å resolution.

Full Methods and any associated references are available in the online version of the paper at www.nature.com/nature.

Received 18 July; accepted 3 November 2011.
Published online 18 December 2011; corrected 11 January 2012 (see full-text HTML version for details).

1. Muench, S. P., Trinick, J. & Harrison, M. A. Structural divergence of the rotary ATPases. *Q. Rev. Biophys.* **44,** 311–356 (2011).
2. Toei, M. *et al.* Dodecamer rotor ring defines H^+/ATP ratio for ATP synthesis of prokaryotic V-ATPase from *Thermus thermophilus*. *Proc. Natl Acad. Sci. USA* **104,** 20256–20261 (2007).
3. Toei, M., Toei, S. & Forgac, M. Definition of membrane topology and identification of residues important for transport in subunit a of the vacuolar ATPase. *J. Biol. Chem.* **286,** 35176–35186 (2011).
4. Numoto, N., Hasegawa, Y., Takeda, K. & Miki, K. Inter-subunit interaction and quaternary rearrangement defined by the central stalk of prokaryotic V1-ATPase. *EMBO Rep.* **10,** 1228–1234 (2009).
5. Lau, W. C. & Rubinstein, J. L. Structure of intact *Thermus thermophilus* V-ATPase by cryo-EM reveals organization of the membrane-bound V(O) motor. *Proc. Natl Acad. Sci. USA* **107,** 1367–1372 (2010).
6. Abrahams, J. P., Leslie, A. G., Lutter, R. & Walker, J. E. Structure at 2.8 Å resolution of F1-ATPase from bovine heart mitochondria. *Nature* **370,** 621–628 (1994).
7. Lee, L. K. *et al.* The structure of the peripheral stalk of *Thermus thermophilus* H^+-ATPase/synthase. *Nature Struct. Mol. Biol.* **17,** 373–378 (2010).
8. Iwata, M. *et al.* Crystal structure of a central stalk subunit C and reversible association/dissociation of vacuole-type ATPase. *Proc. Natl Acad. Sci. USA* **101,** 59–64 (2004).

9. Srinivasan, S., Vyas, N. K., Baker, M. L. & Quiocho, F. A. Crystal structure of the cytoplasmic N-terminal domain of subunit I, a homolog of subunit a, of V-ATPase. *J. Mol. Biol.* **412,** 14–21 (2011).
10. Murata, T. *et al.* Structure of the rotor of the V-type Na^+-ATPase from *Enterococcus hirae*. *Science* **308,** 654–659 (2005).
11. Stock, D., Leslie, A. G. & Walker, J. E. Molecular architecture of the rotary motor in ATP synthase. *Science* **286,** 1700–1705 (1999).
12. Meier, T. *et al.* Structure of the rotor ring of F-type Na^+-ATPase from *Ilyobacter tartaricus*. *Science* **308,** 659–662 (2005).
13. Pogoryelov, D., Yildiz, O., Faraldo-Gomez, J. D. & Meier, T. High-resolution structure of the rotor ring of a proton-dependent ATP synthase. *Nature Struct. Mol. Biol.* **16,** 1068–1073 (2009).
14. Watt, I. N. *et al.* Bioenergetic cost of making an adenosine triphosphate molecule in animal mitochondria. *Proc. Natl Acad. Sci. USA* **107,** 16823–16827 (2010).
15. Preiss, L. *et al.* A new type of proton coordination in an F_1F_O-ATP synthase rotor ring. *PLoS Biol.* **8,** e1000443 (2010).
16. Meier, T. *et al.* The central plug in the reconstituted undecameric c cylinder of a bacterial ATP synthase consists of phospholipids. *FEBS Lett.* **505,** 353–356 (2001).
17. Fillingame, R. H., Angevine, C. M. & Dmitriev, O. Y. Mechanics of coupling proton movements to c-ring rotation in ATP synthase. *FEBS Lett.* **555,** 29–34 (2003).
18. Junge, W., Lill, H. & Engelbrecht, S. ATP synthase: an electrochemical transducer with rotatory mechanics. *Trends Biochem. Sci.* **22,** 420–423 (1997).
19. Stouffer, A. L. *et al.* Structural basis for the function and inhibition of an influenza virus proton channel. *Nature* **451,** 596–599 (2008).
20. Gonzales, E. B., Kawate, T. & Gouaux, E. Pore architecture and ion sites in acid-sensing ion channels and P2X receptors. *Nature* **460,** 599–604 (2009).
21. Cain, B. D. & Simoni, R. D. Proton translocation by the F_1F_OATPase of *Escherichia coli*. Mutagenic analysis of the a subunit. *J. Biol. Chem.* **264,** 3292–3300 (1989).
22. Kawasaki-Nishi, S., Nishi, T. & Forgac, M. Arg-735 of the 100-kDa subunit a of the yeast V-ATPase is essential for proton translocation. *Proc. Natl Acad. Sci. USA* **98,** 12397–12402 (2001).
23. Pogoryelov, D. *et al.* Microscopic rotary mechanism of ion translocation in the F_O complex of ATP synthases. *Nature Chem. Biol.* **6,** 891–899 (2010).
24. Steed, P. R. & Fillingame, R. H. Aqueous accessibility to the transmembrane regions of subunit c of the *Escherichia coli* F_1F_O ATP synthase. *J. Biol. Chem.* **284,** 23243–23250 (2009).
25. Long, J. C., Wang, S. & Vik, S. B. Membrane topology of subunit a of the F_1F_O ATP synthase as determined by labeling of unique cysteine residues. *J. Biol. Chem.* **273,** 16235–16240 (1998).
26. Valiyaveetil, F. I. & Fillingame, R. H. Transmembrane topography of subunit a in the *Escherichia coli* F_1F_O ATP synthase. *J. Biol. Chem.* **273,** 16241–16247 (1998).
27. Baker, L. A., Smith, E. A., Bueler, S. A. & Rubinstein, J. L. The resolution dependence of optimal exposures in liquid nitrogen temperature electron cryomicroscopy of catalase crystals. *J. Struct. Biol.* **169,** 431–437 (2010).
28. Grigorieff, N. FREALIGN: high-resolution refinement of single particle structures. *J. Struct. Biol.* **157,** 117–125 (2007).

Supplementary Information is linked to the online version of the paper at www.nature.com/nature.

Acknowledgements We thank V. Kanelis, F. Sicheri, P. Rosenthal, L. Kay and R. Henderson for discussions and reading this manuscript, and J. Walker and R. Pomès for discussions. Computations were performed on the general-purpose cluster supercomputer at the SciNet HPC Consortium. W.C.Y.L. was supported by an Ontario Graduate Scholarship. J.L.R. was supported by a New Investigator Award from the Canadian Institutes of Health Research and an Early Researcher Award from the Ontario Ministry of Research and Innovation. This research was funded by operating grant MOP 81294 from the Canadian Institutes of Health Research.

Author Contributions J.L.R. and W.C.Y.L. designed the experiments and J.L.R. supervised the research. W.C.Y.L. performed protein purification and cryo-EM. J.L.R. wrote new computer programs. W.C.Y.L. and J.L.R. performed the image analysis, interpreted the data and wrote the manuscript.

Author Information The cryo-EM map of the *T. thermophilus* H^+-driven ATP synthase is deposited in Electron Microscopy Data Bank under accession code EMD-5335; the docked atomic models are deposited in Protein Data Bank under accession number 3JQJ. Reprints and permissions information is available at www.nature.com/reprints. The authors declare no competing financial interests. Readers are welcome to comment on the online version of this article at www.nature.com/nature. Correspondence and requests for materials should be addressed to J.L.R. (john.rubinstein@utoronto.ca).

LETTER

doi:10.1038/nature10691

An unanticipated architecture of the 750-kDa $\alpha_6\beta_6$ holoenzyme of 3-methylcrotonyl-CoA carboxylase

Christine S. Huang[1], Peng Ge[2], Z. Hong Zhou[2] & Liang Tong[1]

3-Methylcrotonyl-CoA carboxylase (MCC), a member of the biotin-dependent carboxylase superfamily, is essential for the metabolism of leucine, and deficient mutations in this enzyme are linked to methylcrotonylglycinuria (MCG) and other serious diseases in humans[1–4]. MCC has strong sequence conservation with propionyl-CoA carboxylase (PCC), and their holoenzymes are both 750-kilodalton (kDa) $\alpha_6\beta_6$ dodecamers. Therefore the architecture of the MCC holoenzyme is expected to be highly similar to that of PCC[5]. Here we report the crystal structures of the *Pseudomonas aeruginosa* MCC (PaMCC) holoenzyme, alone and in complex with coenzyme A. Surprisingly, the structures show that the architecture and overall shape of PaMCC are markedly different when compared to PCC. The α-subunits show trimeric association in the PaMCC holoenzyme, whereas they have no contacts with each other in PCC. Moreover, the positions of the two domains in the β-subunit of PaMCC are swapped relative to those in PCC. This structural information establishes a foundation for understanding the disease-causing mutations of MCC and provides new insights into the catalytic mechanism and evolution of biotin-dependent carboxylases. The large structural differences between MCC and PCC also have general implications for the relationship between sequence conservation and structural similarity.

The α- and β-subunits of human MCC have 42% and 34% sequence identity with those of human PCC (Supplementary Figs 1 and 2). The α-subunit contains the biotin carboxylase (BC) and biotin carboxyl carrier protein (BCCP) domains (Fig. 1a), and a domain that mediates BC–CT interactions (BT domain)[6]. BC catalyses the MgATP-dependent carboxylation of biotin, and then a carboxyltransferase activity, supplied by the β-subunit, catalyses the transfer of the carboxyl group to the acceptor. The β-subunit contains two domains (Fig. 1a), N and C domains, with the same backbone fold, and its active site is located at the interface of a dimer.

Our initial interest in MCC stemmed from its distinct site of carboxylation in the substrate (Fig. 1b). To understand the molecular

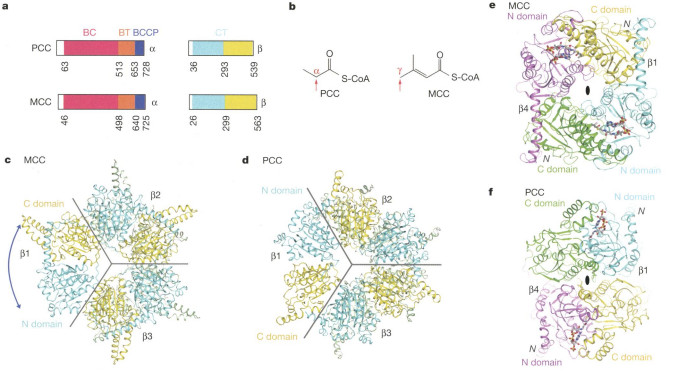

Figure 1 | The domains of MCCβ are swapped compared to PCCβ. **a**, Domain organization of human MCC and PCC. Residue numbers at the boundaries of the domains are indicated. **b**, Distinct carboxylation targets of MCC and PCC, indicated by the red arrow. **c**, Crystal structure of the β_6 hexamer of PaMCC. The subunit beneath β1 is omitted for clarity, and the other two subunits in the bottom layer are coloured in green. The blue arrow indicates the swapping of the positions of the N and C domains relative to PCCβ. Grey lines mark the boundaries of the subunits. **d**, Structure of *Roseobacter denitrificans* PCCβ (ref. 9). **e**, Structure of the β_2 dimer of PaMCC. The N and C domains of the subunit in the bottom layer (β4) are coloured in magenta and green, respectively. *N* indicates N terminus. **f**, Structure of the β_2 dimer of PCC. All the structure figures were produced with PyMOL (http://www.pymol.org) unless stated otherwise.

[1]Department of Biological Sciences, Columbia University, New York, New York 10027, USA. [2]Department of Microbiology, Immunology and Molecular Genetics, California NanoSystems Institute, University of California, Los Angeles, Los Angeles, California 90095, USA.

basis for this activity, we produced crystals of the MCCβ hexamer from *P. aeruginosa* (PaMCCβ) that diffracted to 1.5-Å resolution (Supplementary Table 1). This bacterial enzyme is highly homologous to human MCC, with sequence identities of 47% and 65% for the α- and β-subunits, respectively. To facilitate comparisons between these highly conserved enzymes, we numbered the residues in PaMCC according to their equivalents in human MCC. In *Pseudomonas* organisms, MCC is also involved in terpenoid metabolism[10,11].

We solved the structure of PaMCCβ using *Roseobacter denitrificans* PCCβ as the model[9]. However, subsequent crystallographic analysis revealed that the positions of the N and C domains in PaMCCβ (Fig. 1c) are swapped relative to those in PCCβ (Fig. 1d), even though the overall shapes of the two β_6 hexamers are similar. This distinct domain organization of PaMCCβ is primarily due to a different connectivity between its N and C domains, rather than a swap of these two domains in the primary sequence (Supplementary Fig. 3 and Supplementary Text). This also leads to a large difference in the organization of the PaMCCβ dimer compared to PCCβ (Fig. 1e, f). The closest structural homologue of PaMCCβ is the α-subunit of glutaconyl-CoA decarboxylase (GCDα)[12,13] (Supplementary Fig. 4). However, the sequence conservation between PaMCCβ and GCDα (27% identity) is actually lower than that between PaMCCβ and PCCβ (34% identity). The CoA binding sites, located in the N domain, are swapped between MCCβ and PCCβ as well (Fig. 1e, f). This may be related to the activity of MCC on the γ carbon of the substrate (Fig. 1b), as the activity of GCDα is also on the γ carbon (Supplementary Text).

Most importantly, the change in domain organization of MCCβ suggests that the overall architecture of the MCC holoenzyme may be different as well (Supplementary Text). Therefore, we next determined the structures of PaMCC free enzyme and CoA complex at 2.9- and 3.5-Å resolution, respectively (Fig. 2a and Supplementary Table 1). Like PCC, the holoenzyme of PaMCC contains a central β_6 cylindrical core, with three α-subunits at each end (Fig. 2b). The overall structures of the free enzyme and CoA complex of PaMCC are similar, although there are also recognizable differences (Supplementary Fig. 5 and Supplementary Text).

Notably, the positions of the α-subunits in PaMCC, especially their BC domains, are entirely different from those in PCC (Fig. 2c). Rather than being splayed far apart from each other as in PCC (Fig. 2d), the three BC domains on either end of MCC are in direct contact with each other (Fig. 2b), burying 640 Å^2 of the surface area of each BC domain. Therefore, the BC domain shows trimeric association in the MCC holoenzyme, although this trimer is probably unstable on its own due to the relatively small buried surface area. Overall, the MCC

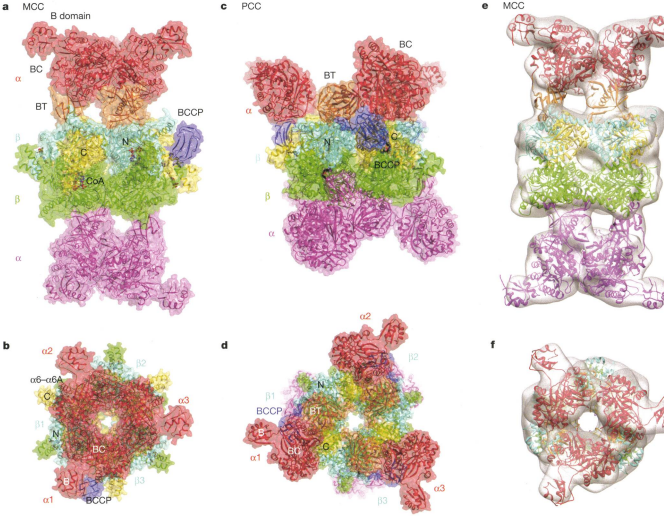

Figure 2 | The MCC holoenzyme has a markedly different architecture compared to PCC. a, Structure of the CoA complex of PaMCC holoenzyme, side view. Domains in the α- and β-subunits in the top half of the structure are coloured as in Fig. 1a. The α- and β-subunits in the bottom half are coloured in magenta and green, respectively. The molecular surface is shown in a semi-transparent rendering. **b**, Structure of the PaMCC holoenzyme, top view. **c**, Structure of the PCC holoenzyme[9], side view. **d**, Structure of the PCC holoenzyme, top view. **e**, Electron microscopy reconstruction of PaMCC at 12-Å resolution, side view. The crystal structure of the PaMCC free enzyme can be readily fit into the electron microscopy density. **f**, Electron microscopy reconstruction of PaMCC, top view. Panels **e** and **f** were produced with Chimera[22].

holoenzyme has the shape of a cylinder, approximately 100 Å in diameter and 200 Å tall, and this shape is remarkably different from that of PCC (Supplementary Fig. 6)[9].

As an independent verification for the crystal structure of PaMCC, we carried out electron microscopy studies on this holoenzyme and produced a reconstruction at 12-Å resolution (Supplementary Text and Supplementary Figs 7 and 8). The crystal structure and the electron microscopy density are in excellent agreement with each other (Fig. 2e, f), confirming the large structural differences between the MCC and PCC holoenzymes.

Interactions between the α- and β-subunits in PaMCC are mediated predominantly by the BT domain, and by the BCCP domain when it is in the active site of the β-subunit for catalysis (see later). Approximately 3,000 Å^2 of the surface area of each α-subunit is buried in the interface of the holoenzyme. The BT domain buries 1,500 Å^2 in the interface with the β-subunit, as well as 200 Å^2 in a contact with the BC domain of a neighbouring α-subunit (see later). The BCCP domain in the active site of the β-subunit contributes 700 Å^2 to the surface area burial, primarily through residues around the biotinylated Lys 681 residue (Supplementary Fig. 1).

The BT domain in PaMCC contains a central α-helix surrounded by a seven-stranded, highly twisted anti-parallel β-sheet (Fig. 3a and Supplementary Fig. 9). The overall structure of this domain is similar to that in PCC, with a root mean squared distance (r.m.s.d.) of 1.8 Å for their equivalent Cα atoms. In addition, sequence comparisons suggest that the BT domain of human MCC and most other MCCs may have an eight-stranded β-barrel, which would be equivalent to that in PCC (Fig. 3a and Supplementary Text).

However, the position of the BT domain relative to the β-subunit and its interactions in the PaMCC holoenzyme are different compared to PCC (Fig. 3b and Supplementary Figs 10 and 11). The hook of the BT domain[9], connecting the central helix to the first β-strand, is crucial for interactions with the β-subunit but has a markedly different conformation in PaMCC (Fig. 3a). The hook interacts with both the N and C domains of the β-subunit in PaMCC, and residues 542–544 in the hook form a parallel β-sheet with strand β1 (residues 95–100) in the N domain of the β-subunit (Fig. 3c and Supplementary Fig. 10 and Supplementary Text). Consistent with these observations, we found that structure-based mutations in the hook could destabilize the PaMCC holoenzyme (Supplementary Fig. 12).

In addition to the hook, there is direct contact between the BT domain of one α-subunit and the BC domain of a neighbouring α-subunit, where residues 604–608 (strand β27 of the BT domain) form an anti-parallel β-sheet with strand β3 of the BC domain (Fig. 3b and Supplementary Text).

Overall, the unique interactions for the BT domain and the trimeric association of the BC domain in the MCC holoenzyme suggest that PCC cannot form a similar architecture, and therefore it is unlikely that the observed structural differences between MCC and PCC represent different stages of catalysis for these enzymes.

The distance between the active sites of BC and CT is approximately 80 Å in MCC (Fig. 4a). Therefore, the entire BCCP domain must translocate during MCC catalysis, as is the case with PCC[9] and pyruvate carboxylase (PC)[14–17]. On the other hand, MCC is distinct from PCC in that although the BT domain of an α-subunit contacts its closest β-subunit, its BCCP domain is actually located in the active site of a neighbouring β-subunit (Fig. 4a), another consequence of the swapping of the N and C domains in the β-subunit of MCC.

We observed the binding of both CoA and BCCP-biotin to the active site of one of the β-subunits (Fig. 4a and Supplementary Fig. 13), and built a model for the bound conformation of methylcrotonyl-CoA (Fig. 4b and Supplementary Fig. 14 and Supplementary Text). The binding modes are consistent with the expected kinetic mechanism of the CT reaction[18]. The N1′ atom of biotin is ~6 Å from the reactive γ carbon of methylcrotonyl-CoA in this model (Supplementary Fig. 14). There is a large conformational change for two helices in the active site upon CoA binding (Supplementary Fig. 15 and Supplementary Text).

The structure of PaMCC provides a foundation for understanding the molecular basis of its disease-causing mutations in human MCC, which represent one of the most frequently observed inborn errors of metabolism[1–4,19–21]. The missense mutations are distributed throughout the holoenzyme (Fig. 4c), but their effects can be interpreted based on the structure (Supplementary Text and Supplementary Table 2). Many of the mutations are located in or near the BC or CT active site (for example R385S in the α-subunit, A218T and V375F in the β subunit;

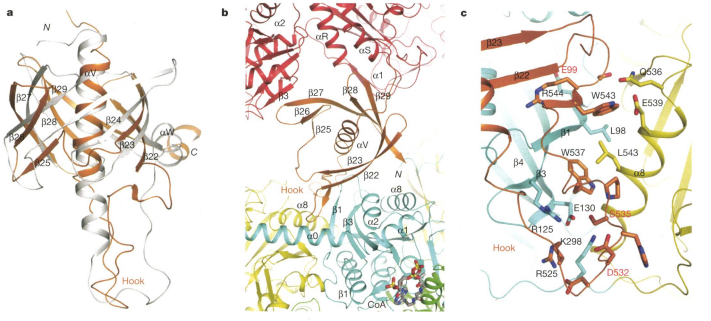

Figure 3 | The BT domain mediates interactions in the MCC holoenzyme. **a**, Overlay of the structure of PaMCC BT domain (in orange) with that of PCC (grey). A large conformational difference for the hook is visible. The exact positions of many of the β-strands are different as well. *C*, C terminus; *N*, N terminus. **b**, The BT domain (orange) contacts a β-subunit (β1, N domain in cyan, C domain in yellow) as well as a neighbouring α-subunit (α2, red) in the PaMCC holoenzyme. **c**, Detailed interactions between the hook of the BT domain and the β-subunit in PaMCC. Three disease-causing mutation sites near this interface are labelled in red. For stereo version of the panels, see Supplementary Figs 9 and 10.

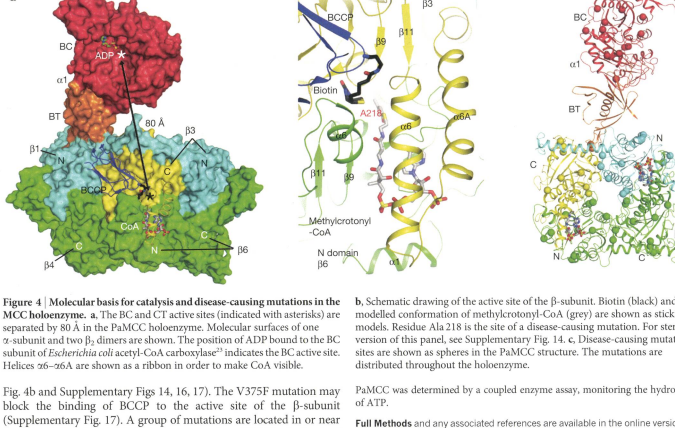

Figure 4 | Molecular basis for catalysis and disease-causing mutations in the MCC holoenzyme. a, The BC and CT active sites (indicated with asterisks) are separated by 80 Å in the PaMCC holoenzyme. Molecular surfaces of one α-subunit and two β_2 dimers are shown. The position of ADP bound to the BC subunit of *Escherichia coli* acetyl-CoA carboxylase[23] indicates the BC active site. Helices α6–α6A are shown as a ribbon in order to make CoA visible. **b**, Schematic drawing of the active site of the β-subunit. Biotin (black) and the modelled conformation of methylcrotonyl-CoA (grey) are shown as stick models. Residue Ala 218 is the site of a disease-causing mutation. For stereo version of this panel, see Supplementary Fig. 14. **c**, Disease-causing mutation sites are shown as spheres in the PaMCC structure. The mutations are distributed throughout the holoenzyme.

Fig. 4b and Supplementary Figs 14, 16, 17). The V375F mutation may block the binding of BCCP to the active site of the β-subunit (Supplementary Fig. 17). A group of mutations are located in or near the subunit interface in the holoenzyme, such as S535F in the hook of the BT domain (Fig. 3c). Additional mutations are located in the hydrophobic core of the structure, and may disrupt folding and/or stability of the enzyme.

Our structure of the PaMCC holoenzyme also has implications for the evolution of biotin-dependent carboxylases. The structural differences between MCC and PCC suggest that there may be two separate lineages of such enzymes that carboxylate CoA esters of organic acids. One lineage includes PCC and acetyl-CoA carboxylase, which carboxylates the α carbon of the acid. The other lineage targets the γ carbon of an α-β unsaturated acid and includes MCC, GCDα and possibly also geranyl-CoA carboxylase (Supplementary Fig. 18)[10,11].

More importantly, the structures of MCC and PCC show that their strong sequence conservation only ensures that the backbone folds of the domains in the two enzymes are the same. On the other hand, the organization of these domains in the individual subunits and especially the architecture of the subunits in the holoenzymes are remarkably different. These observations may also have wide-ranging implications for the relationship between sequence conservation and structural similarity in general.

METHODS SUMMARY

Crystallography. The α- and β-subunits of PaMCC were co-expressed in *E. coli*, with a His-tag on the β-subunit. The PaMCC holoenzyme was purified by nickel affinity and gel filtration chromatography. Crystals were obtained by the microbatch method under oil, and the structures were determined by the molecular replacement method.

Electron microscopy. The PaMCC sample was stained with uranyl acetate and electron micrographs were recorded at ×70,000 magnification in a 200 kV electron microscope. A 12-Å-resolution three-dimensional reconstruction was obtained from ~12,000 particle images.

Mutagenesis and kinetic studies. Site-specific mutants were designed based on the structural information, and their effects on the formation of the holoenzyme were assessed by nickel affinity chromatography. The catalytic activity of PaMCC was determined by a coupled enzyme assay, monitoring the hydrolysis of ATP.

Full Methods and any associated references are available in the online version of the paper at www.nature.com/nature.

Received 22 August; accepted 1 November 2011.
Published online 11 December 2011.

1. Baumgartner, M. R. *et al.* The molecular basis of human 3-methylcrotonyl-CoA carboxylase deficiency. *J. Clin. Invest.* **107,** 495–504 (2001).
2. Gallardo, M. E. *et al.* The molecular basis of 3-methylcrotonylglycinuria, a disorder of leucine metabolism. *Am. J. Hum. Genet.* **68,** 334–346 (2001).
3. Holzinger, A. *et al.* Cloning of the human *MCCA* and *MCCB* genes and mutations therein reveal the molecular cause of 3-methylcrotonyl-CoA carboxylase deficiency. *Hum. Mol. Genet.* **10,** 1299–1306 (2001).
4. Desviat, L. R. *et al.* Functional analysis of MCCA and MCCB mutations causing methylcrotonylglycinuria. *Mol. Genet. Metab.* **80,** 315–320 (2003).
5. Wakil, S. J., Stoops, J. K. & Joshi, V. C. Fatty acid synthesis and its regulation. *Annu. Rev. Biochem.* **52,** 537–579 (1983).
6. Tong, L. Acetyl-coenzyme A carboxylase: crucial metabolic enzyme and attractive target for drug discovery. *Cell. Mol. Life Sci.* **62,** 1784–1803 (2005).
7. Cronan, J. E., Jr & Waldrop, G. L. Multi-subunit acetyl-CoA carboxylases. *Prog. Lipid Res.* **41,** 407–435 (2002).
8. Jitrapakdee, S. *et al.* Structure, mechanism and regulation of pyruvate carboxylase. *Biochem. J.* **413,** 369–387 (2008).
9. Huang, C. S. *et al.* Crystal structure of the $\alpha_6\beta_6$ holoenzyme of propionyl-coenzyme A carboxylase. *Nature* **466,** 1001–1005 (2010).
10. Förster-Fromme, K. & Jendrossek, D. Catabolism of citronellol and related acyclic terpenoids in pseudomonads. *Appl. Microbiol. Biotechnol.* **87,** 859–869 (2010).
11. Aguilar, J. A. *et al.* Substrate specificity of the 3-methylcrotonyl coenzyme A (CoA) and geranyl-CoA carboxylases from *Pseudomonas aeruginosa*. *J. Bacteriol.* **190,** 4888–4893 (2008).
12. Wendt, K. S., Schall, I., Huber, R., Buckel, W. & Jacob, U. Crystal structure of the carboxyltransferase subunit of the bacterial sodium ion pump glutaconyl-coenzyme A decarboxylase. *EMBO J.* **22,** 3493–3502 (2003).
13. Kress, D. *et al.* An asymmetric model for Na$^+$-translocating glutaconyl-CoA decarboxylase. *J. Biol. Chem.* **284,** 28401–28409 (2009).
14. St. Maurice, M. *et al.* Domain architecture of pyruvate carboxylase, a biotin-dependent multifunctional enzyme. *Science* **317,** 1076–1079 (2007).
15. Xiang, S. & Tong, L. Crystal structures of human and *Staphylococcus aureus* pyruvate carboxylase and molecular insights into the carboxyltransfer reaction. *Nature Struct. Mol. Biol.* **15,** 295–302 (2008).
16. Yu, L. P. C. *et al.* A symmetrical tetramer for *S. aureus* pyruvate carboxylase in complex with coenzyme A. *Structure* **17,** 823–832 (2009).
17. Lasso, G. *et al.* Cryo-EM analysis reveals new insights into the mechanism of action of pyruvate carboxylase. *Structure* **18,** 1300–1310 (2010).

18. Knowles, J. R. The mechanism of biotin-dependent enzymes. *Annu. Rev. Biochem.* **58,** 195–221 (1989).
19. Stadler, S. C. *et al.* Newborn screening for 3-methylcrotonyl-CoA carboxylase deficiency: population heterogeneity of *MCCA* and *MCCB* mutations and impact on risk assessment. *Hum. Mutat.* **27,** 748–759 (2006).
20. Nguyen, K. V., Naviaux, R. K., Patra, S., Barshop, B. A. & Nyhan, W. L. Novel mutations in the human *MCCA* and *MCCB* gene causing methylcrotonylglycinuria. *Mol. Genet. Metab.* **102,** 218–221 (2011).
21. Uematsu, M. *et al.* Novel mutations in five Japanese patients with 3-methylcrotonyl-CoA carboxylase deficiency. *J. Hum. Genet.* **52,** 1040–1043 (2007).
22. Pettersen, E. F. *et al.* UCSF Chimera—a visualization system for exploratory research and analysis. *J. Comput. Chem.* **25,** 1605–1612 (2004).
23. Chou, C.-Y., Yu, L. P. C. & Tong, L. Crystal structure of biotin carboxylase in complex with substrates and implications for its catalytic mechanism. *J. Biol. Chem.* **284,** 11690–11697 (2009).

Supplementary Information is linked to the online version of the paper at www.nature.com/nature.

Acknowledgements We thank Y. Shen for carrying out initial studies on MCC; N. Whalen and S. Myers for setting up the X29A beamline at the National Synchrotron Light Source. This research was supported in part by National Institutes of Health (NIH) grants DK067238 (to L.T.) and GM071940 (to Z.H.Z.). C.S.H. was also supported by an NIH training program in molecular biophysics (GM08281).

Author Contributions C.S.H. carried out protein expression, purification and crystallization experiments, mutagenesis and enzymatic assays. C.S.H. and L.T. carried out crystallographic data collection and processing, structure determination and refinement. P.G. and Z.H.Z. carried out electron microscopy experiments. All authors commented on the manuscript. L.T. supervised the project, analysed the data and wrote the paper.

Author Information Atomic coordinates have been deposited in the Protein Data Bank under accessions 3U9R, 3U9S and 3U9T. Reprints and permissions information is available at www.nature.com/reprints. The authors declare no competing financial interests. Readers are welcome to comment on the online version of this article at www.nature.com/nature. Correspondence and requests for materials should be addressed to L.T. (ltong@columbia.edu).

CORRECTIONS & AMENDMENTS

ERRATUM

doi:10.1038/nature10773

Thermalization and its mechanism for generic isolated quantum systems

Marcos Rigol, Vanja Dunjko & Maxim Olshanii

Nature **452**, 854–858 (2008).

In Figs 3b and e of this Letter, there were two points that could have been misinterpreted as outlying data points (they were inadvertently printed parts of a key to the figure that was incompletely removed). These points have been removed in the HTML and PDF versions. We thank David S. Weiss for drawing this to our attention.

International Journal of Obesity

IMPACT FACTOR 5.125*

Publishing the best in obesity research

The *International Journal of Obesity* (*IJO*) provides a multi-disciplinary forum for basic, clinical and applied studies in biochemistry, physiology, genetics and nutrition, molecular, metabolic, psychological and epidemiological aspects of obesity and related disorders. The journal also features a quarterly pediatric highlights issue.

Editors: R L Atkinson and I Macdonald

Author benefits at a glance

- *Quick and easy online submission*
- *Online supplementary material allows you to add greater depth to your article*
- *Fast editorial turnaround*
- *Advance Online Publication within 25 days of acceptance*
- *Open Access option: You now have the option to make your article freely available immediately upon publication.*
- *Increased article visibility to more than 75,000 online recipients of the Table of Contents e-alert for the IJO issue in which your article is published.*
- *Inclusion in the leading abstracting and indexing services.*

With an international editorial board, worldwide recognition and a diverse scope, *IJO* is the ideal outlet to submit your best research.

For more information and to submit your research today visit
www.nature.com/ijo

SMARTPHONE USERS CAN SCAN THIS TAG TO ACCESS THE WEBPAGE.

Download the tag reader app at http://gettag.mobi FREE ONLINE ACCESS

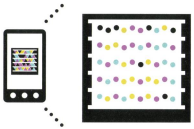

nature publishing group npg

nature REVIEWS CANCER

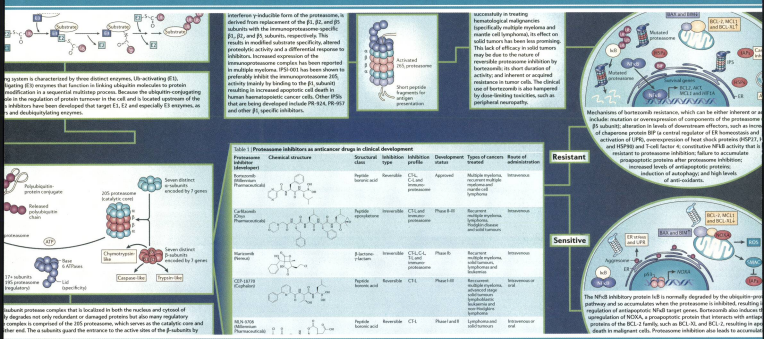

Poster – Proteasome inhibition and cancer therapy

Author: Q. Ping Dou

In recent years the ubiquitin-proteasome system has been identified as essential for maintaining a crucial balance between cell growth and death, the progression of human malignancies, and the development of drug resistance in cancer cells. Emerging evidence shows that targeting the ubiquitin-proteasome degradation pathway is a useful anticancer strategy. The approval of bortezomib by the US Food and Drug Administration (FDA) as the first proteasome inhibitor to be implemented in the treatment of malignant disease, either alone or in combination with other therapies, represents a substantial milestone in this field. Other novel proteasome inhibitors, such as marizomib and carfilzomib, have recently been developed and are being tested in clinical trials. These recent achievements and the development of new drugs that target the ubiquitin–proteasome pathway are highlighted in this poster.

Access the poster **FREE** online!
www.nature.com/nrc/posters/proteasome

This Poster is freely available thanks to sponsorship from

ONYX PHARMACEUTICALS

nature publishing group npg

CAREERS

TURNING POINT Social scientist hopes to engage the public in climate research **p.227**

EUROPEAN UNION Universities urge measures to improve researcher mobility **p.227**

NATUREJOBS For the latest career listings and advice **www.naturejobs.com**

MICHELANGELUS

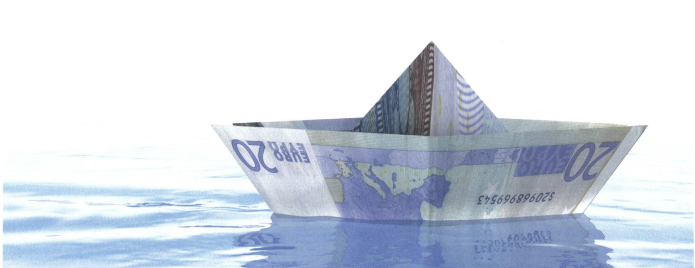

BRIDGE FUNDING

How to stay afloat

When a lab runs out of money, there are a few strategies that it can use to get by.

BY JEFFREY PERKEL

The world's economy is battered and bruised. More than three years after the start of the global recession, the European debt crisis threatens to derail a fragile financial recovery, and funding-agency budgets are suffering. Scientists are feeling the ill effects: many are having to make do with less, and there is a growing risk that researchers and laboratories will soon be caught between grants, unable to find new sources of funding when their current ones expire. "I'm not sure that I'm yet seeing the real impact of what's coming down the road," says John Kirby, dean of the College of the Environment and Life Sciences at the University of Rhode Island in Kingston, referring to the effects on his institution.

Across academia, scientists are planning for shortfalls, with mid-career researchers often the most at risk as funding agencies tailor grant programmes to younger researchers (see *Nature* **471,** 399; 2011). "It is not clear that this development is recession-related, but its emphasis on 'stellar' individuals may have the effect of reducing significantly the funding options for many mid-career scientists," says Charles Dorman, chair of the department of microbiology at Trinity College Dublin.

But young researchers are far from immune: in some cases, university start-up packages are being stretched to allow for the increasing amount of time that a researcher needs to secure a first independent grant. Richard Schultz, associate dean for the natural sciences at the University of Pennsylvania's School of Arts and Sciences in Philadelphia, says that some of his institution's start-up packages, which typically last three years, may soon be recalculated to last for four. "There's a greater likelihood that it may take [new recruits] longer than we anticipated before they get their own extramural funding," he says.

There are steps that researchers can take to make up for deficits. Internal bridge funding can help in the short term, but it is best for scientists to plan ahead, broadening their search for support. Launching collaborations, varying funding sources and extending their work into unfamiliar areas could help anxious researchers to make their way out of the financial doldrums.

CAUGHT BETWEEN GRANTS

Despite their best efforts, researchers can sometimes find themselves without funding for months or even years. In such cases, bridge funding can often be arranged from within the researcher's home institution. Usually cobbled together from overheads and small amounts of money set aside in department and college budgets, such funding is generally limited in availability and quantity, and is awarded on a case-by-case basis. An institution's stopgap resources can vary widely, from a few thousand dollars per researcher to perhaps US$100,000. Before deciding whether to approve bridge funding, a department chair or college dean will assess the researcher's publication and ▶

service record, funding history and likelihood of eventually winning an extramural grant.

Kirby recalls a case that came up when he was working as an associate dean for research at South Dakota State University in Brookings. A private entity funding a research project suddenly went bankrupt, leaving two graduate students bereft of funds. The university stepped in and moved the students into research-assistantship posts so that they could complete their work, he says. In another case, a successful faculty member requested about $50,000 to finalize a data set and strengthen a grant application. Bridge funding allowed him to win the grant and continue his work.

T. HUNT

"The most important thing with a grant is to have a really interesting question."
Mary Collins

But in tough economic times, such opportunities can be difficult to find. In cash-strapped Ireland, for instance, "the ability of universities to offer significant support to researchers facing a funding gap is very limited or even non-existent", says Dorman.

Carl Bauer, chair of the department of molecular and cellular biochemistry at Indiana University in Bloomington, helps to guide labs in his department out of financial straits. When a lab runs into trouble, the first thing Bauer does is to study its books carefully. Typically, such reviews don't entail micromanagement of reagent purchases or other equipment. Rather, the focus is on a lab's biggest expense: personnel. In the United States, graduate students can often be moved into teaching positions that require no funds from the principal investigator, but postdocs and technicians cannot. "Maybe I can keep them going for one more grant cycle, but after that point you have to let them go," says Bauer. Downsizing is almost inevitable at that point, says Mary Collins, dean of the faculty of life sciences at University College London. Bauer adds that he also examines a struggling scientist's past grant applications, gauging whether they have been competitive, because this could affect whether they will be able to gain an independent grant in the future.

A DIVERSIFIED PORTFOLIO

For those who have enough funding in the short term but worry about the medium and long term, experts recommend seeking money from multiple sources. A diverse portfolio of projects enables researchers to apply for a variety of grants. "It's like holding a basket of stocks in different areas," says Bauer. If one grant falls through, research priorities might take a hit, but the lab will survive on the others.

At any one time, Schultz aims to hold multiple grants with staggered start dates, to ensure that his lab's finances are relatively stable. He has several grants from the US National Institutes of Health coming up for renewal in the next few years; but given the current climate, he has "absolutely no confidence that any of them will be renewed. That, psychologically, is a bad place to be." Schultz plans to submit several further grant applications in partnership with colleagues — not his usual practice.

Researchers are increasingly establishing collaborations to hedge their bets. This can improve their chances of getting funding by, for instance, making a project more exciting through the use of innovative approaches and technologies, or more relevant to practical applications, says Collins. "You have to think a bit laterally," she adds. "The most important thing with a grant is to have a really interesting question. The second thing is to demonstrate that you have a clear means to providing some answers to that question. And if you have a technology that you really can't do or have never demonstrably done before, bringing in an expert who can do that as a collaborator is really helpful."

There is a caveat: weak collaborations could put applicants at a disadvantage. Adam Zlotnick, a biochemist at Indiana University, moved to his current post from the University of Oklahoma Health Science Center in Oklahoma City, where he had applied for a grant renewal in collaboration with an organic chemist who was hoping to synthesize a series of antiviral compounds. The application was unsuccessful, in part because the reviewers felt that the collaboration wasn't strong enough. Once at Indiana, Zlotnick found himself working just across the hall from another organic chemist. The two researchers developed a close interaction, talking face-to-face almost daily and sharing graduate students and postdocs. They won a grant on the basis of an application that emphasized teamwork and the interdisciplinary nature of their science. Zlotnick was fortunate: despite missing one grant cycle, he had another grant and start-up funds from Indiana to see him through. However, the start-up money had been intended to jump-start another project, which had to be slowed considerably as he addressed his funding gap. Although he has now regained independent funding, Zlotnick says his enthusiasm for new projects has been tempered.

"If you don't have the track record, you don't stand a chance."
Gareth Leng

Mere marriages of convenience are not enough to ensure funding success for collaborations, says Gareth Leng, head of the School of Biomedical Sciences at the University of Edinburgh, UK. "Grant panels see through them and they don't work out. So you've got to have a kind of a real marriage of love and enthusiasm," he says. "It's not a speed-dating thing." Leng adds that researchers should be careful not to diverge too far from their familiar research path when forming a collaboration or expanding the scope of their grant search. A radical change of direction can be detrimental in the current economic environment. "If you don't have the track record, you don't stand a chance," he notes.

TUITION FEES

Scientists who can not only sell their research, but can also find ways to use its content and methods to contribute to graduate-student training, may be able to tap into sources of funding related to higher education, notes Alan Tessier, an environmental-biology programme officer at the US National Science Foundation (NSF) in Arlington, Virginia. For example, a researcher could apply to lead a grant under a scheme such as the multimillion-dollar NSF Integrated Graduate Education and Research Traineeship Program, or the NSF's Research Experience for Undergraduates initiative. "That includes support for graduate students in their lab," says Tessier.

There are other strategies. For instance, biologists working *in vitro* might attempt to move their research to an *in vivo* model to demonstrate its potential impact and importance for human health, strengthening their case with funders and expanding their technical reach. Scientists in other areas could try to incorporate new informatics or modelling tools into their work to expand their repertoires, show that their work is not stagnant and demonstrate the ability to adapt to new scientific questions, says Collins. In the end, stopgap funding solutions are most useful when they allow the lab to retain personnel. Lab groups can be fragile, notes Schultz. Personnel retain knowledge of the group's past projects and investigative track, so losing just one member can be very disruptive. Even if someone must temporarily work part-time while money is sought, the hope is that the lab will soon recover. "Then they can get moving," says Schultz, "and the lab won't go into what I call that death spiral." Bridge funding is a means of ensuring survival until long-term measures are possible. And whether an investigator has to rely on bridge funding or run a lab on a smaller budget, what ultimately matters, Schultz notes, is that the lab is running. "It's not that you're flourishing," he says. "Your purpose here is to survive." ■

R. LENG

Jeffrey Perkel *is a freelance writer based in Pocatello, Idaho.*

TURNING POINT
Saffron O'Neill

Saffron O'Neill, who studies the interactions between society, policy and climate change at the University of Melbourne in Australia, won the 2011 UK Scopus Young Researcher Award for the Social Sciences on 22 November.

What drew you to study climate change?
I see it as the most pressing environmental issue of our time, and there are lots of policy questions. After my undergraduate degree, my mentors advised me to go to the Tyndall Centre for Climate Research at the University of East Anglia in Norwich, UK. The centre was offering a PhD scholarship to determine how people engage with climate-change information.

Was that meant to be in the social sciences?
It was open-ended, but the abstract focused on the physical sciences — modelling climate in ways that are amenable to public understanding. However, investigating why people didn't engage with this information was more interesting, so my PhD was turned on its head. That was a turning point, realizing that I could contribute from a social-sciences perspective.

How did the 'Climategate' release of e-mails from researchers at the University of East Anglia affect your work?
Climategate happened in November 2009, five months after I left. My former colleagues were in the news all the time. I had moved to the University of Melbourne as a postdoc, but I still received hate mail, including death threats. The experience made me realize that scientists are keen to communicate with the public, but need to do a better job of explaining how scientific discoveries get made.

Why did you decide to go to Australia?
One reason was so I could gain experience in a different country. It was challenging to learn about an unfamiliar policy arena, but it was rewarding to see how Australia and small island states are addressing policy challenges. And I had been working on climate-change mitigation, but had a growing interest in adaptation. My adviser here, Jon Barnett, is an international leader in this area. He focuses on how small island states will have to adapt. I also got a four-year postdoc, which gave me a lot of stability. I didn't have to scrabble around for short-term contracts.

What can your research do to advance climate-change policy-making?
The public has a lot of the scientific information needed to start making decisions, yet isn't doing so effectively. Decision-making is the most important social dimension of any environmental problem, and that is where the most interesting questions lie. My research shows that people embrace climate-change information most if it is relevant to places they care about — for example, how sea-level rise may affect London — or if they can empathize with the affected animals, such as polar bears.

What activities helped to raise your profile?
I served on a panel to assess whether an Australian preparedness strategy, known as Stay or Go, actually put people at increased risk during bush fires in the state of Victoria in 2009, which killed 173 people. Other countries mandate evacuation. The commission reviewing the policy drew on our panel's report when making its final recommendations. It was a rare opportunity to show how science — analysing the forensic data, statements, texts and phone calls made during the bush fires — can help to improve disaster-preparedness policies. I think that experience may have counted in my favour for the Scopus award, which takes citations into account.

What is your next step?
I have a full-time lectureship on public perceptions of climate change lined up at the University of Exeter, UK, which is building a team of climate-change researchers. I've enjoyed being in Australia, but didn't realize how isolated it would feel here. Simply collaborating or going to meetings is really hard. A 24-hour plane ride to Europe is a big deal. Plus I'm trying not to fly too much, being a climate-change scientist. ■

INTERVIEW BY VIRGINIA GEWIN

EUROPEAN UNION

Call for more mobility

A group of universities has made recommendations on how to draw researchers to the European Union (EU). Among other things, the League of European Research Universities (LERU), based in Leuven, Belgium, has called for more transparency about visa regulations that affect researcher mobility, more incentives for companies to give venture funding to scientists and measures to promote gender equality in research. The group published the suggestions on 14 December, in response to a call by the European Commission (EC) for input on its proposal for a European Research Area Framework, to improve the European research environment and help to coordinate funding across the EU, set to be established by 2014. Katrien Maes, LERU's chief policy officer, expects to hear a response from the EC by spring 2012.

COLLABORATION

US–Russian pact

The US National Science Foundation (NSF) has inked an agreement with the Russian ministry of education and science to encourage collaborative research in areas such as energy, nanotechnology and information technology. Early-career scientists applying for NSF grants could improve their chances by collaborating with Russian researchers, suggests John Tsapogas, programme coordinator for the NSF's Office of International Science and Engineering in Arlington, Virginia. The agreement, co-signed on 16 December, allows the Russian ministry to fund US–Russian projects. Tsapogas says that the ministry has a larger budget than other Russian science agencies, so it has a high likelihood of collaborations.

CANCER RESEARCH

New York fellowships

The Memorial-Sloan Kettering Cancer Center in New York is creating ten five-year, early-career research fellowships. They will be funded with US$15 million from $50 million donated to the centre by the Robertson Foundation in New York. Fellows will get tenure-track appointments, says Charles Sawyers, chair of human oncology and pathogenesis at Sloan-Kettering. Investigators will be recruited in oncology and pathogenesis, cancer biology and genetics, pharmacology, and immunology. Sawyers expects much of the research to be translational.

naturejobs

European Head Office, London naturejobs@nature.com
The Macmillan Building, 4 Crinan Street, London N1 9XW, UK
Tel: +44 (0) 20 7843 4961 Fax: +44 (0) 20 7843 4996

European Manager:
Nils Moeller,+44 (0) 20 7843 4953 n.moeller@nature.com

Southwest UK/RoW:
Emma Hare, +44 (0) 20 7843 4944 e.hare@nature.com

Northeast UK/Ireland:
Matthew Ward, +44 (0) 20 7014 4059 m.ward@nature.com

France/Switzerland/Belgium:
Julie Aramburu, +44 (0) 20 7843 4994 j.aramburu@nature.com

Scandinavia/Spain/Portugal/Italy:
Megan Ball, +44 (0) 20 7843 4973 m.ball@nature.com

North Germany/The Netherlands/Eastern Europe:
Kristin Doelling +44 (0) 20 7843 4970 k.doelling@nature.com

South Germany/Austria:
Hildi Rowland, +44 (0) 20 7014 4084 h.rowland@nature.com

Natureevents:
Matthew Clare, +44 (0) 20 7014 4015 m.clare@nature.com

Business Development Manager, Middle East:
Jon Giuliani, +44 (0) 20 7843 4822 j.giuliani@nature.com

USA Head Office, New York naturejobs@us.nature.com
75 Varick Street, 9th Floor, New York, NY 10013-1917
Tel: +1 800 989 7718 Fax: +1 800 989 7103

US Sales Manager:
Ken Finnegan, +1 212 726 9248 k.finnegan@us.nature.com

Japan Head Office, Tokyo
Chiyoda Building, 2–37 Ichigayatamachi, Shinjuku-ku, Tokyo 162-0843
Tel: +81 3 3267 8751, Fax: +81 3 3267 8746

Asia-Pacific Sales & Business Development Manager:
Yuki Fujiwara, +81-3-3267-8765 y.fujiwara@natureasia.com

Business Development Manager, Greater China/Singapore:
Gloria To, +852 2811 7191 g.to@natureasia.com

India
3a, 4th Floor, DLF Corporate Park, Gurgaon, 122 002, India

Advertisement Sales:
Vikas Chawla, +91 1242881057 v.chawla@nature.com

VANDERBILT UNIVERSITY

Endowed Chair - Immunology of Infectious Diseases

Department of Pathology, Microbiology and Immunology
Vanderbilt University School of Medicine

The Department of Pathology, Microbiology and Immunology at Vanderbilt University School of Medicine solicits applications and/or nominations to fill the newly created Major E. B. Stahlman Chair focused on the immunology of infectious diseases. Candidates should have a sustained record of high-impact research publications in this field of study, substantial ongoing extramural research funding and evidence for outstanding academic achievement that merits appointment to the Vanderbilt faculty at the full professor level. Considerable financial resources and space are committed to this position along with the opportunity to lead the recruitment of additional junior faculty.

Vanderbilt University Medical Center, located on the Vanderbilt University campus, is home to internationally recognized programs in bioinformatics, drug discovery, global health, inflammation, imaging science, pharmacology, proteomics, and vaccine science. The School consistently ranks in the Top 20 US Medical Schools and provides outstanding opportunities for scholarship, collaboration, and teaching.

The Vanderbilt University campus is a National Arboretum located in the heart of Nashville, the capital of Tennessee. Known internationally as "Music City USA", Nashville is also the home to professional sports teams, the Nashville Symphony, the Nashville Opera, the Fisk Jubilee Singers, the Frist Center for the Visual Arts, and numerous activities for outdoor enthusiasts. Nashville, Tennessee is a wonderful place to live, work, and raise a family.

Applicants should send a curriculum vitae and a statement of current and future research interests to Samuel A. Santoro, M.D., Ph.D., Dorothy B. and Theodore R. Austin Professor and Chair, Department of Pathology, Microbiology and Immunology, Vanderbilt University School of Medicine, C-3322 Medical Center North, 1161 21st Ave. S., Nashville, TN 37232. Applications and nominations can be directed via email to **samuel.santoro@vanderbilt.edu.**

Vanderbilt University is an Affirmative Action/Equal Opportunity Employer. Women and minority candidates are encouraged to apply.

NW220335R

Faculty Positions: Shanghai Institute of Plant Physiology and Ecology, Chinese Academy of Sciences
中国科学院上海生命科学研究院植物生理生态研究所

Shanghai Institute of Plant Physiology and Ecology (SIPPE) is an internationally recognized national research institution engaged in original, innovative research and technology development in plant, insect and microbial systems. SIPPE has an interactive and vibrant research environment and is fully equipped with a suite of state-of-the-art research facilities. More information can be found at http://www.sippe.ac.cn/eindex.asp.

SIPPE is seeking highly motivated and innovative candidates with strong records of research accomplishments for group leader and supporting principal investigator positions. Candidates of all nationalities who conduct cutting-edge research in one or more of the following areas are encouraged to apply:

Area #1: Crop Genomics and Functional Genomics, Molecular Breeding (mainly rice, maize, cotton and soybean)
Area #2: Plant Metabolism
Area #3: Plant Hormones and Development
Area #4: Plant Cell Biology
Area #5: Plant Stress Biology and Immunity
Area #6: Synthetic Biology (industrial biotechnology)
Area #7: Insect Development and Evolutionary Biology
Area #8: Bioinformatics

The successful applicants for group leaders will establish a vigorous research team that includes graduate students, postdoctoral fellows and research staff. Supporting principal investigators will establish an active research program as well as run a core facility in genomics, cell biology or metabolomics. SIPPE will provide competitive start-up packages for new faculty members including set-up funds, annual laboratory operating funds, and research staff members at various levels. Attractive salary and housing supplements will also be provided by SIPPE.

Candidates must hold a PhD degree, have significant research experience at a major research university or institution, and have demonstrated outstanding achievements in their research field. Qualified candidates should send a cover letter of application, a CV, a statement of present and future research interests, and at least three references to:

Prof. Hong-Wei XUE
Shanghai Institute of Plant Physiology and Ecology, CAS
300 Fenglin Road, Shanghai, China 200032
E-Mail: hwxue@sibs.ac.cn
Tel: 0086-21-54924059

JP220225R

www.nerf.be

Empowered by imec, KU Leuven and VIB

NERF is the new centre for **Neuro-Electronics Research Flanders.** It is a joint basic research initiative, set up by VIB, imec and KU Leuven to understand the function of brain circuits. At NERF basic neuroscientific questions are addressed through collaborative, interdisciplinary research, combining nanoelectronics with neurobiology. The center intends to push the boundaries of science, by zooming in on the functioning of neural circuits at an unprecedented level of detail. In the long run, NERF will generate new insights into the functional capabilities of the circuits of the mind as well as into research methodologies and technologies for medical applications, i.e. diagnostics and treatment of disorders of the central and peripheral nervous system **(see www.NERF.be).**

NERF is housed on the imec campus in Leuven, Belgium, where researchers work in cross-disciplinary teams, benefitting from imec's state-of-the-art clean room infrastructure and a new 800 m² well equipped neuro-science lab, dedicated to NERF. NERF has already recruited 3 teams of top-notch researchers doing world-class basic research in neural circuit analysis and is recruiting 2 additional groups. The focus is on unraveling the input and output signals of individual neurons, which underlie collective computations in neuronal circuits in the brain of living, behaving animals. Devices to do so will be developed in close collaboration with imec research teams on site. By 2014, NERF aims to expand its international team to about 50 excellent researchers, organized in 5 research groups with complementary interests and technical skills, each led by an independent group leader. A long term foundation of financial support is provided by the 3 founders and the Government of Flanders. NERF scientists will be able to work closely with a wide range of over 30 neuroscience research groups covering a wide range of expertise (such as neuronal communication, axon guidance, brain-computer interface, electrophysiology, ...) and core and service facilities (such as genomics, transcriptomics, proteomics, imaging, electronic and mechanical workshops, animal housing...) already established at the 3 founding institutions.

NERF is currently looking for a (m/f)

Scientific Director

As the Scientific Director of NERF, you will be responsible for:

- developing the mission and research strategy of NERF
- creating a stimulating environment and dialectic culture
- fostering talent and triggering excellence.

It is expected that you maintain active research interest in leading your own research program at NERF. Significant long term support will be provided to do so.

You will chair the NERF management committee in which you will have final responsibility for the strategy and the overall success of NERF.

The position will be a dual appointment, consisting of a tenured faculty appointment at KU Leuven and an additional appointment at imec as the Scientific Director and Group Leader of NERF.

Requirements for the position:

NERF is searching for a dynamic, internationally recognized leader taking the challenge of building an exciting centre of excellence in neuro-electronics in Leuven, Belgium. The successful candidate:

• has a Ph.D degree and is an experienced visionary scientist, widely recognized in the field • has demonstrated a strong record of scientific publications in leading scientific journals in the field • has a track record of leading a successful research group, including successful funding support • has an extensive international network with a wide scope of research collaborations • has excellent communication skills • has a strong will for developing a common vision and purpose for NERF.

The package offered will consist of:

• a competitive salary and benefits, including full social security and pension scheme • a long term grant for your own research group • a generous start-up package for your own group • a solid funding program for NERF • full access to local and international competitive grants • dedicated lab space • privileged access to the core facilities of VIB, imec and KU Leuven • an exciting intellectual and research environment.

If you are interested in this position, please send a complete publication list and CV to jo.bury@vib.be. Further information can be obtained from Jo Bury, chair of the NERF board and managing director of VIB +32 92 44 66 11.

Group Leaders

You will investigate the functioning of the brain in a living animal. The focus is on studying information processing in neuronal circuits using experimental and computational methods (with particular emphasis on awake and behaving animals) or theoretical approaches.
In close collaboration with imec research teams you will be involved in the design and development of ground breaking devices, beyond the current state-of-the-art. You will be empowered by working closely together with a wide range of experts from the 3 founding institutions, providing the NERF labs with a unique competitive advantage.

As a NERF Group Leader, you will be responsible for:

• developing an innovative research program, fitting the mission and research objectives of NERF • organizing and managing your own research group • interacting with the other NERF research groups and the research community of imec, VIB and KU Leuven, active in the field.

Requirements for the position:

The successful candidate: • has done at least several years of research as a postdoctoral associate or junior faculty member, with a proven track record of publications in leading journals in the field • is able to set up and manage a research team of postdoctoral and postgraduate researchers and technicians • is enthusiastic, inquisitive, focused on problem solving and a team player • is able to start research activities at NERF within a year after being selected.

The package offered will consist of:

• a competitive group leader salary • a start-up package • continuous funding of your own research group with 3 full time positions • full access to local and international competitive grants • dedicated lab space • privileged access to the core facilities of VIB, imec and KU Leuven • an exciting intellectual and research environment.

Candidates who are interested in this position are asked to send a complete CV, publication list and 3 letters of reference to anke.vannoten@nerf.be. Further information can be obtained from Gustaaf Borghs, NERF Coordinator +32 16 28 12 11 or Jo Bury, Chair of the NERF Board +32 9 244 66 11.

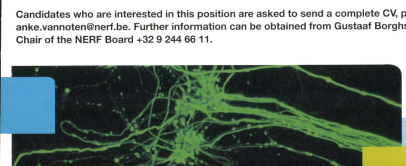

KATHOLIEKE UNIVERSITEIT LEUVEN imec VIB

W2014/SR

Kew
ROYAL BOTANIC GARDENS

Director

The Royal Botanic Gardens, Kew is a global leader in botanical research. Over 250 years, it has developed unrivalled collections that support its scientific aims, and provide opportunities for public engagement, with a focus on scientific discovery, conservation and sustainable use. It is a leading visitor attraction, designated with the World Heritage status. With around 800 employees and 500 volunteers across its two sites and an annual income of over £45m, Kew is one of the largest organisations of its type in the world.

Professor Stephen D Hopper FLS is moving to a new role in Australia in the coming Autumn, and a successor is sought who will provide leadership and vision, directing a team so as to ensure scientific excellence, maximise public impact and deliver effective organisation. The role also has a significant ambassadorial and fundraising component, representing Kew to government, funders and donors, scientists and the broader public.

Ideal candidates will have a distinguished record of achievement in a relevant field, with proven success leading in a complex environment. The appointee will be an outstanding communicator, able to articulate vision, inspire staff and stakeholders, and be comfortable driving strategic fundraising and commercial initiatives. Applicants from outside of directly comparable organisations will need to demonstrate a substantive resonance with the scientific aims and content of Kew's work.

To apply for this position or to receive further particulars, please visit:
www.heidrick.com/kew
Email: kew@heidrick.com
Telephone: +44 (0)20 7075 4079
The closing date for applications is 13 February 2012.

HEIDRICK & STRUGGLES

U220130R

UNIVERSITY OF OXFORD

www.ox.ac.uk/jobs

MEDICAL SCIENCES DIVISION
Department of Pharmacology

University Lecturership in Pharmacology

in association with a Tutorial Fellowship at The Queen's College

Grade: 10a £42,733 - £57,431 p.a.

Applications are invited for a University Lecturership in Pharmacology, in association with a Tutorial Fellowship at The Queen's College. The post holder will be expected to conduct an independent research programme in any area of pharmacology, and to be capable of attracting significant external research funding. Applications will be particularly welcome from individuals with a research interest that includes some aspect of ion channel pharmacology. The successful applicant will also organise and deliver teaching to pre-clinical medical and biomedical science students and provide supervision and research training for graduate students.

Applicants will hold a higher degree in a basic science and/or a medical qualification and will have (or be capable of attaining) international recognition for their research programme. The ability to organise and carry out teaching, supervision and research training to the high standard required by the Department and the College is also essential.

Informal enquiries about the post should be addressed to Professor Antony Galione, Tel: 01865 271633; email antony.galione@pharm.ox.ac.uk

Further particulars, including detailed selection criteria and guidance on applying for this post, is available from **www.admin.ox.ac.uk/fp** or by emailing Carolyn Thackrah on: carolyn.thackrah@pharm.ox.ac.uk

The closing date for applications is 12 noon on Tuesday 31st January 2012.

Applications are particularly welcome from women and black and minority ethnic candidates, who are under-represented in academic posts in Oxford.

Committed to equality and valuing diversity

U220167R

How can you make more informed career or hiring decisions?

- Follow the blog on naturejobs.com to keep up-to-date with the latest scientific employment news from around the world.

What do you think about the news stories affecting scientific careers?

- Start sharing your opinions today on the *Naturejobs* blog.

www.naturejobs.com

Jordan

Exploration and new ventures around the world

Are you up for the challenge?
bp.com/exploration/nt

We're hiring explorers now

The oil and gas industry operates at the forefront of technology and BP is an industry leader. Our award-winning seismic imaging technology, world-class team, sizeable investment in new ventures and our exploration heritage combine to create the perfect environment for explorers.

We're looking for explorers with outstanding technical skills and a passion for exploration that drives them to unlock the hydrocarbons lying within the earth. With BP you'll use technology to explore exciting new frontiers and be part of a world-class team.

BP's exploration success has led to an exciting portfolio of career opportunities. Our roles are largely based at our technology centers in London and Houston with opportunities also available at our other international locations.

We're looking for great Geoscientists in New Ventures, Deepwater Exploration and Unconventional Plays.

Are you up for the challenge?

BP is an equal opportunities employer.

bp

U220467R

Fundación **BBVA**

2012 NOMINATIONS NOW OPEN

The **BBVA Foundation Frontiers of Knowledge Awards** are intended to recognize basic research and creative work of excellence, as embedded in theoretical advances, models and fundamental perspectives for an improved understanding of the natural, social and artificial or technological worlds, technological innovations and developments, and the creation of outstanding works or new artistic or interpretative styles in contemporary classical music. Awards also go to significant achievements that advance our understanding or deliver material progress with regard to two key challenges of the global society of the 21st century: climate change and development cooperation.

BBVA Foundation

Plaza de San Nicolás, 4
48005 Bilbao, Spain

Paseo de Recoletos, 10
28001 Madrid, Spain

www.fbbva.es

Categories

— Basic Sciences (Physics, Chemistry, Mathematics)
— Biomedicine
— Ecology and Conservation Biology
— Information and Communication Technologies
— Economics, Finance and Management
— Contemporary Music
— Climate Change
— Development Cooperation

Award content

Awards in each category will comprise €400,000 prize money, a diploma and a commemorative artwork.

Nominations

Nominations can be made by institutions and organizations working in the knowledge areas covered in each category.

Closing date

The closing date for submissions is 23.00 hours GMT on June 30, 2012.

With the collaboration of:
CSIC

More information: www.fbbva.es/awards · awards-info@fbbva.es

NW220428R

UCL

UCL Faculty of Mathematical and Physical Sciences/
Faculty of Life Sciences

Reader or Chair in Biomolecular Modelling across Multi-scales

UCL has recently embarked on an ambitious strategy to substantially enhance its capabilities in computational life and medical sciences, through the establishment of the UCL Computational Life & Medical Sciences Network (http://www.clms.ucl.ac.uk/). As part of this strategy, UCL is looking to make a number of appointments at all levels. We wish to recruit a Reader/Professor with an outstanding track record in biomolecular modelling. Expansion in this area is critical to a number of ongoing projects in research, undergraduate teaching and postgraduate training. The position is a joint faculty appointment across the Faculty of Mathematical and Physical Sciences and the Faculty of Life Sciences. The successful applicant will be a biomolecular modeller who can address the multi-scale modelling challenge represented by the need to link quantum computations with classical molecular dynamics, feeding again into the more coarse-grained level; and ultimately, into more "traditional" systems biology schemes.

The post holder will have an international research profile in biomolecular modelling, but must have an appreciation of all time and length scales (e.g. quantum, molecular, coarse-grained, systems) and substantial knowledge of High Performance Computing applications.

An exceptional publication record in international, high impact, journals and the ability to attract funding from research councils and charities is essential. The successful candidate will be expected to develop opportunities across Faculties and externally, bringing together expertise in computational, physical and life sciences. UCL has an established culture of interdisciplinary research and therefore an enthusiasm to work in a collaborative, cross-disciplinary manner is essential.

The appointment will be full time. The salary range will be: Reader - £50,902 - £55,362 per annum; Professor – negotiable on the professorial scale but not less than £61,960 per annum, inclusive of London Allowance.

For further details about the vacancy and how to apply online please go to http://www.ucl.ac.uk/hr/jobs/ and search on Reference Number 1226117.

Applicants may make informal enquiries about the post to Peter Coveney, CLMS Director, email: p.v.coveney@ucl.ac.uk, or John Carroll, Associate Dean, Faculty of Life Sciences, email: j.carroll@ucl.ac.uk.

Closing Date: 17th February 2012.

We particularly welcome female applicants and those from an ethnic minority, as they are under-represented within University College London at this level.

U220455R

FUKUSHIMA MEDICAL UNIVERSITY

Fukushima Medical University Center for Disaster Medical Sciences

Fukushima Medical University is now seeking applicants for faculty positions (hereafter described as Project Teacher) at Center for Disaster Medical Sciences, which has been set up within the university-affiliated Center for Medical Education and Career Development (CMECD).

The contract period will be from February 1, 2012 until March 31, 2016. A project teacher will be responsible for planning and implementation of education and training intended for medical students and interns all over the world regarding disaster medicine and medical care after radiation exposure. Applicants who have knowledge of disaster medicine and/or medical care after radiation exposure may be preferred.

Applicants must submit all the documents requested by the CMECD at the following address or via email. The application deadline is January 31, 2012. Visit CMECD's website for more details (http://cmsl01.cc.fmu.ac.jp/cms/cmecd/copy_of_index_html) and please contact FMU HR section for queries.

HR Section, General Affairs Division
Fukushima Medical University
1 Hikariga-oka, Fukushima City, 960-1295, Japan
somu@fmu.ac.jp

JP220335R

UNIVERSITY BASEL Universitätsspital Basel

The Faculty of Medicine of the University of Basel, Switzerland, invites applications for the position of a Research Professorship in

Translational Oncology

The successful candidate will be appointed as research group leader in the Department of Biomedicine and also act as vice head of the Division of Medical Oncology at the University Hospital Basel. The appointment for this position will be at the level of an Assistant or Associate Professorship, depending on the qualification of the candidate.

The position is open to candidates with the following qualifications:

- Medical diploma and Board Certificate in Medical Oncology
- Experience and broad knowledge in translational oncology
- Excellent publication record and innovative research in translational/experimental oncology
- Habilitation or equivalent academic qualification (e.g. PhD degree)
- Experience in management, social competence and strong integrative capabilities
- Experience in translating basic research oncology into clinical practice

In addition, the following profile is desirable:

- Initiative and willingness for interdisciplinary cooperation with the Basel Network of Excellence in Life Sciences
- Visionary qualities and enthusiasm
- Competence and initiative in teaching students of the medical school and residents in Translational Oncology

Teaching at the University of Basel is in German. Successful non-German speaking candidates will be expected to learn German within 2–3 years.

Application deadline is 10.3.2012

For additional information please contact:
Prof. Primo Schär, Head of the Search Committee, Basel, primo.schaer@unibas.ch, phone: +41 61 267 07 67.

Information about how to submit your application is available at: http://medizin.unibas.ch/dekanat/bewerbungen.html. Please send your application as 5 pdf-files to bewerbungen-medizin@unibas.ch

UNI BASEL

W220353R

The NIH is the center of medical and behavioral research for the nation
----making essential medical discoveries that improve health and save lives.

Are you a top-level Administrator seeking a career at the one of the preeminent health institutes in the nation and the world?

The Office of the Director, National Institutes of Health (NIH) in Bethesda, Maryland, is seeking applications from exceptional candidates for the position of Director, Center for Scientific Review (CSR). CSR, with a staff of approximately 450, and a $107M FY'12 budget, is the focal point at NIH for the conduct of peer review of research grants and fellowship applications with the primary goal being that all NIH applications receive fair, independent, expert and timely reviews, free from inappropriate influences, so that NIH can fund the most promising research. The incumbent serves as a principal advisor to the Director, NIH; participates in discussions relative to the development of major policy decisions affecting the research grant and review programs; provides advice and consultation to NIH components, advisory councils and grantee institutions; and assures that effective administrative procedures are established so that program operations and obligations of government funds and other resources are rendered consistent with statutory and regulatory requirements and within limitations imposed by the Department of Health and Human Services (DHHS) and Executive Branch policies. Applicants must possess a Ph.D., M.D., or a comparable doctorate degree in the health sciences field, plus senior level scientific experience and knowledge of research programs in one or more health science areas. Salary is commensurate with experience and a full package of benefits (including retirement, health, life, long term care insurance, Thrift Savings Plan participation, etc.) is available. A detailed vacancy announcement, along with mandatory qualifications and application procedures, can be obtained via the NIH Home Page at: http://www.jobs.nih.gov under Jobs at NIH, Executive Jobs section. Questions on announcement procedures may be addressed to Ms. Regina Reiter at ReiterR@od.nih.gov or discussed with Ms. Reiter by calling 301-402-1130.
Applications must be received by close of business FEBRUARY 17, 2012.

We are looking for applicants with senior level experience who have a commitment to excellence and the energy, enthusiasm, and innovative thinking necessary to lead a dynamic and diverse organization.

NCATS, NIH, AND DHHS ARE EQUAL OPPORTUNITY EMPLOYERS

NIW218520R

Need to find
the ideal
candidate
fast?

Visit
**www.
naturejobs
.com**

to discover
how applicants
can respond
directly to you
by email.

nature jobs
making science work

ÉCOLE POLYTECHNIQUE
FÉDÉRALE DE LAUSANNE

Faculty Position in Materials Science and Engineering

at the Ecole polytechnique fédérale de Lausanne (EPFL)

The School of Engineering of EPFL invites applications from candidates for the position of **tenure-track assistant professor** within its Institute of Materials. We seek exceptional individuals who will develop and drive a research program at the forefront of the discipline, who have a strong dedication to teaching at the undergraduate and graduate levels, and who will be proactive members of a vibrant Materials community.

Top-level applicants in those areas of Materials Science and Engineering that are concerned, in a broad sense, with the following topics are of particular interest:

(i) electrochemistry as applied to the processing, microstructural tailoring or performance of materials,
(ii) the processing, microstructural tailoring, characterization or performance of materials having surface functionality, and
(iii) modeling and simulation as relevant to the processing, microstructural development and performance of materials.

Start-up resources and state-of-the-art research infrastructure will be available. Salaries and benefits are internationally competitive.

The EPFL, located in Lausanne, Switzerland, is a dynamically growing and well-funded institution fostering excellence and diversity. It has a highly international campus at an exceptionally attractive location boasting first-class infrastructure. As a technical university covering essentially the entire palette of engineering and science, EPFL offers a fertile environment for research cooperation between different disciplines. The EPFL environment is multi-lingual and multi-cultural, with English often serving as a common interface.

Applications should include a cover letter with a statement of motivation, curriculum vitae, list of publications and patents, concise statement of research and teaching interests, and the names and addresses of at least five referees. Applications must be uploaded in PDF format to the recruitment web site: **imx-search12.epfl.ch**

Formal evaluation of candidates will begin on **1 March 2012.**

Enquiries may be addressed to:
Prof. Andreas Mortensen
Search Chairman
e-mail: **imx-search@epfl.ch**

For additional information on EPFL, please consult the web sites: **www.epfl.ch, sti.epfl.ch** and **imx.epfl.ch.**

EPFL is committed to increasing the diversity of its faculty, and strongly encourages women to apply.

W220302R

naturejobs **PRESENTS A**

SPOTLIGHT ON BIOTECH/PHARMA

***NATURE* ISSUE DATE:**
26 JANUARY 2012

DEADLINE FOR ADVERTISERS:
AMERICAS: 19 JANUARY 2012 | UK/EU/ROW: 20 JANUARY 2012

Take advantage of an outstanding opportunity to reach *Nature* readers interested in biotechnology and pharmacology. The *Naturejobs* Spotlight on Biotech/Pharma will be published in the 26 January issue of *Nature* and presents an excellent opportunity for organizations to advertise vacancies, promote events and courses, and make important announcements to *Nature* readers.

Bonus distribution	Society for Lab Automation and Screening 2012 – San Diego, USA (4-8 Feb) Imperial College Science Career Fair – London, UK (2 Feb)
Target audience	Biotechnology companies, Pharmaceutical companies, Contract Research Organizations (CRO's), Life Science Technology companies, Chemical companies, Universities offering biotech programs
Examples of suitable job titles	Scientist, Research Scientist/Fellow/Assistant/Associate, Principal Scientist, Principal Investigator, Postdoc, Lab Technician, Lab Assistant, Lab Head, Director, Team Leader, Group Leader, Toxicologist, Bioinformatician

All job advertisements will receive a complimentary 8-week online posting on naturejobs.com and event advertisements will receive a complimentary posting on natureevents.com — the events portal for *Nature*.

Contact your regional sales representative today:

US T: +1 800 989 7718 | Europe T: +44 (0) 20 7843 4961 | Japan T: +81 3 3267 8765 | India T: +91 12 4288 1057
Greater China/Singapore T: +852 2811 7191 | Middle East T: +44 (0)20 7843 4922 | E: naturejobs@nature.com

To advertise events:
US T: +1 202 626 2522 | Europe T: +44 (0) 20 7014 4015 | Japan T: +81 3 3267 8765 |India T: +91 12 4288 1057
Greater China/Singapore T: +852 2811 7191 | Middle East T: +44 (0)20 7843 4922 | E: natureevents@nature.com

naturejobs.com

nature publishing group npg

Bial
ao serviço da sua Saúde

BIAL is a Portuguese-based international pharmaceutical group located in Oporto. Bial is heavily committed to developing innovative medicines as part of its expansion strategy. The Bial Group has an international team of scientists fully committed to the discovery and development of new therapeutic agents. The investment in internationalization is another of Bial's main operating guidelines, whose products are in pharmacies in more than 40 countries.

An opportunity has arisen within our **Laboratory of Chemistry Research** for a:

Head of Chemistry Research (M/F)

Key aspects of this role:
Coordinate and organize the activities of Laboratory of Chemistry Research in order to maximize the human and material resources and for to comply with the objectives
Coordinate the activities of chemical, analytical, therapeutic and technology transfers and process development of API's
Develop strategic plans in accordance with guidelines and objectives
Team management and support other departments.

The successful candidate must have:
PhD in Chemistry
Experience of 5 years in similar positions in Pharmaceutical Industry
Additional Training and experience in Management and Leadership
Good knowledge of English (spoken and written)
Knowledge of patents and regulatory affairs (preferential)
Good Knowledge of GMP and guidelines of quality control (preferential).

Please send your CV and covering letter to:
www.bial.com - working with Bial – Opportunities until January 20th
W220460R

John Innes Centre

INDEPENDENT RESEARCH FELLOWSHIPS

The John Innes Centre (JIC), Norwich, UK is a world leading centre of excellence in plant and microbial sciences based on the Norwich Research Park. We are inviting applications from outstanding researchers who either hold, or wish to apply for Independent Research Fellowships, to attend a Conference at the JIC on 30th April/1st May 2012. At the meeting you will be able to present a talk about your proposed area of research and to discuss your proposals, the development of your group and your future career plans in depth with senior JIC Scientists.

After the Conference we will select and mentor outstanding candidates in writing Fellowship applications and/or offer the opportunity to move existing Fellowships to the JIC.

Further details and particulars can be found at
http://www.jic.ac.uk/corporate/opportunities/vacancies/fellows.htm

Please e-mail a 2-page summary of your research plan, a copy of your CV and arrange for three letters of recommendation to be emailed to dawn.barrett@jic.ac.uk by Friday 16th March 2012

The John Innes Centre is a registered charity (No223852) grant-aided by the Biotechnology and Biological Sciences Research Council and is an Equal Opportunities Employer.

U220480R

MICHIGAN STATE UNIVERSITY

The Reproductive and Developmental Sciences Program (RDSP) at Michigan State University is undergoing a major faculty expansion in conjunction with the Center for Women's Health Research and the Engineering and Health Initiative. This expansion is a joint effort between the Colleges of Human Medicine, Agriculture and Natural Resources, Veterinary Medicine, and MSU AgBioResearch. Applications are invited from outstanding scholars for up to eight tenure track positions at the ranks of Assistant, Associate and Full Professor. The primary areas of emphasis are Stem cells and Regenerative Medicine, Developmental Epigenetics, Environmental Impact on Reproduction and Development and Women's Health and Reproduction. Please see http://www.canr.msu.edu/rdsp/program_expansion for more information.

Michigan State University is an equal opportunity / affirmative action employer.

NW220326R

Damon Runyon Cancer Research Foundation

THE SOHN CONFERENCE FOUNDATION

New Funding Opportunity: Pediatric Cancer Fellowship

The **Damon Runyon Cancer Research Foundation**, supporting the most innovative young cancer researchers, has joined with the **Sohn Conference Foundation**, dedicated to curing pediatric cancers, to establish the Damon Runyon-Sohn Pediatric Cancer Fellowship Award.

Applicants are not required to be pediatricians or members of pediatric departments; however, proposals must have direct relevance to one or more pediatric cancers.

Criteria used to evaluate applicants include:
- **potential impact of research on pediatric cancer**
- **quality of the research proposal (importance of problem, originality of approach, techniques and clarity of presentation)**
- **qualifications, experience and productivity of both the candidate and the Sponsor**
- **quality of the research training environment in which the proposed research is to be conducted**

The award provides $50,000 per year for three years for basic scientists, $60,000 per year for three years for physician scientists, plus an annual $2,000 expense allowance. The Foundation also provides a Dependent Child Allowance of $1,000 per child per year. The award may not be used for institutional overhead or indirect costs.

Application deadline: March 15, 2012. Visit www.damonrunyon.org for further details.

NW220423R

UNIVERSITY of HAWAI'I® MĀNOA

Endowed Chair in Marine Biology.

The Department of Biology at the University of Hawaii at Manoa invites applications from senior scientists across a broad spectrum of research interests in the biology of marine organisms for the Sidney and Erika Hsiao Endowed Chair in Marine Biology.

The successful candidate will join a faculty with diverse research interests, including many with a strong focus on evolutionary biology and native Hawaiian organisms. Teaching responsibilities will include an upper level undergraduate course and a graduate course in the individual's specialty. Applicants must have a Ph.D., strong records of publication with international recognition and extramural funding, be outstanding communicators, and provide evidence of experience equivalent to a university professorship. Individuals interested in developing new initiatives in marine biology are especially encouraged to apply.

To apply, please send a single PDF document that includes a detailed resumé, a statement of research interests and plans, a statement of teaching interests, three publications, and the names and contact information (including email address) for three professional references to HsiaoMB@hawaii.edu; a hard copy should also be mailed to Chair, Hsiao Chair Search, Department of Biology, Rm. 2, Dean Hall, University of Hawaii, 2450 Campus Road, Honolulu, Hawaii 96822.

For a complete job announcement, please refer to: http://workatuh.hawaii.edu.

Review of applications will begin in January 2012 and continue until the position is filled.

The University of Hawaii is an Equal Opportunity/Affirmative Action Institution and encourages applications from women and minority candidates.

NW220429R

www.naturejobs.com

2012 nature conferences

The Salk Institute, *Nature*, *Nature Immunology* and the Fondation IPSEN present:
Symposium on Biological Complexity: **Immunity and Inflammation**
January 18-20, 2012 • La Jolla, CA, USA
www.nature.com/natureconferences/salk2012

Nature Genetics and the *Journal of Investigative Dermatology* present:
Dermatogenetics
February 9-12, 2012 • Miami, FL, USA
www.nature.com/natureconferences/dg2012

The University of Miami, Nature Publishing Group and Scripps Florida present:
Miami 2012 Winter Symposium: **Nanotechnology in Biomedicine**
February 26-29, 2012 • Miami, FL, USA
www.nature.com/natureconferences/miami/mws2012

Nature Reviews Immunology presents:
Resolving Inflammation: Mechanisms and Drug Discovery
April 1-3, 2012 • Keble College, Oxford, UK
www.nature.com/natureconferences/rimdd12

Unique events committed to scientific excellence

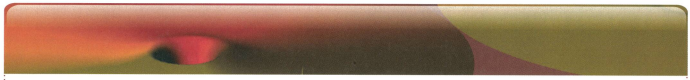

The European Materials Research Society and *Nature Materials* present:
Frontiers in Materials: Spintronics
May 13, 2012 • Strasbourg, France
www.nature.com/natureconferences/spin12

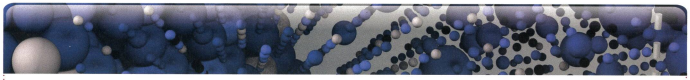

The Jülich-Aachen Research Alliance (JARA) and *Nature Materials* present:
Frontiers in Electronic Materials: Correlation Effects and Memristive Phenomena
June 17-20, 2012 • Aachen, Germany
www.nature.com/natureconferences/fem2012

***Naturejobs* Career Expo- London 2012**
September 20, 2012 • London, UK
www.naturejobs.com/careerexpo

naturejobs CAREER EXPO LONDON 2012

Visit **www.nature.com/natureconferences**
regularly for the updated natureconferences list and more information.

a nature conference

Nature Genetics and the *Journal of Investigative Dermatology* present:

Dermatogenetics

The conference will cover genetic variation, gene expression and cellular mechanisms in this shared area of exceptional interest to basic researchers, biopharma and translational medicine. Lectures and posters are invited in all areas of the field and sessions including: complex dermatological diseases, stem cells and skin cancer, development and regeneration, melanoma and pigmentation, monogenic skin disorders and epigenetics and gene expression.

February 9-12, 2012
JW Marriott Marquis Miami
Miami, FL, USA

KEYNOTE SPEAKERS:
Raphael Kopan
Fiona Watt

SPEAKERS:

Allan Balmain	**Andrzej Dlugosz**	**Anthony Oro**
Greg Barsh	**David Fisher**	**Dennis Roop**
Regina Betz	**Nick Hayward**	**Yardena Samuels**
David (Tim) Bishop	**Valerie Horsley**	**Julie Segre**
Natalia Botchkareva	**Birgitte Lane**	**Eli Sprecher**
Anne Bowcock	**Robert Lavker**	**Richard Spritz**
Pierre Coulombe	**Jianjun Liu**	**Xue Zhang**
James Elder	**Sarah Millar**	

ORGANIZERS:
Myles Axton (*Nature Genetics*, USA)
Angela Christiano (Columbia University, USA)
John McGrath (King's College London, UK)
Irwin McLean (University of Dundee, UK)

Artwork by: Daniel Kohn

For more information and to register, visit:
www.nature.com/natureconferences/dg2012

nature genetics

JOURNAL OF INVESTIGATIVE DERMATOLOGY

THE SOCIETY FOR INVESTIGATIVE DERMATOLOGY, INC.

EUROPEAN SOCIETY FOR DERMATOLOGICAL RESEARCH ESDR

IN216199E

Kenneth Rainin Foundation

2012 INNOVATIONS SYMPOSIUM

NEW INSIGHTS IN HUMAN EVOLUTION & IBD

Four Seasons Hotel Chicago FRIDAY, JULY 20, 2012

Inflammatory Bowel Disease (IBD) is a chronic inflammatory disease of undefined origin. It's our mission to understand it and cure it.

IBD is a complex problem that is not restricted to any field of biology or medicine. That's why we're bringing together the finest minds across multiple disciplines in our first-of-its-kind daylong symposium.

Using IBD as a lens, senior leaders in each discipline will discuss their work with ample time for conversation, connections and setting new directions for the future.

Let's cure IBD.

NW218868E

Register online at www.rainin-symposium.com. Early registration is recommended as seating is limited to 100.

Read *Naturejobs* regularly.
For better career prospects.

naturejobs

Applications are invited from graduates to carry out research at institutions in the USA. Fields of research will include Astronomy, Biophysics, Chemistry, Engineering, Geology, Geophysics, Mathematics and Physics.

Candidacy is open to UK and Commonwealth citizens who graduated from a UK university before 1 September 2009. Candidacy is also open to UK and Commonwealth citizens who are pursuing postgraduate research at a UK university, although not graduates of these institutions.

The fellowship is worth $30,000, is tenable for one year, and should not be regarded as a means of taking up a routine sabbatical.

LINDEMANN TRUST FELLOWSHIP AWARDS 2012

for graduates of Pure and Applied Physical Sciences

Closing date: 15 February 2012
Interview date: 17 April 2012

For more details contact:
Education Department,
The English-Speaking Union
Dartmouth House, 37 Charles Street
London W1J 5ED
education@esu.org T: 020 7529 1550

The English-Speaking Union

Registered Charity No: 273136

U217664A

Small cog, big machine?
Jobs that make a difference.
Each week. *Naturejobs*.

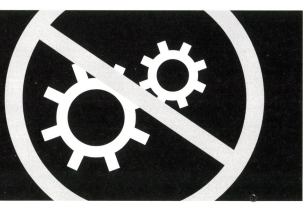

naturejobs

REPROGRAPHICS: CTT, London E17 6BU UK and **The Charlesworth Group,** Wakefield, UK.
PRINTED BY: William Gibbons & Sons Ltd, UK; **Publishers Press**, Lebanon Junction, Ky, USA and **Obun Printing Co. Inc,** Tokyo, Japan

THE DRIVER

On the road to freedom.

BY RAHUL KANAKIA

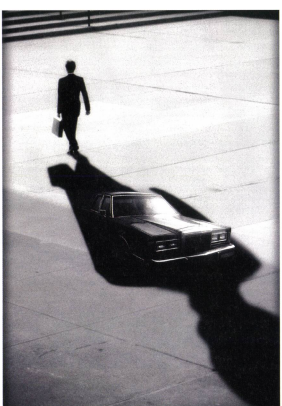

Every day for the past 30 years, Vlad had woken up to find the black Lincoln town car already idling in front of his house. Today was no different. As Vlad made his coffee, the car slowly rolled up and down the block. When he walked to the spot where he'd parked his own car, it rolled along at his side like a well-trained dog. On the freeway, it was three car-lengths behind him. In the university parking lot, it pulled into the space right in front of Vlad, and the professor stared directly into the eyes of the driver. Vlad waved at him. The driver nodded.

The driver was in his late forties, with a neatly trimmed salt-and-pepper beard and receding hairline. He was wearing a white polo shirt with an indistinct company logo over the right breast. Vlad didn't know how tall the driver was, because he had never seen the driver outside the car.

Over the years, Vlad had witnessed the driver ploughing through two pedestrians and ramming four cars off the road in three separate incidents. And once, when the child Vlad was on his bike, deciding which path to take, the window of the car opened up and the man said: "Left." When he got home, Vlad's worried mother told him of the gas explosion on the right-hand path that had killed three people.

By the time Vlad reached his ground-floor office, the car was parked in the quad, right next to the department's doors. It usually stayed there, within spitting distance of Vlad's window, until Vlad left. Bikes wove between it and the wall. Students stepped around it. Sometimes police officers came by and ticketed the car. Once, Vlad checked the citation number on several of these tickets. They were all paid promptly and electronically, within moments of the ticket being registered.

Vlad looked out of his window. It was a wonderful day. The birds were singing. The coeds were wearing sundresses. The sky was clear. The breeze was cool and vigorous. Vlad picked up the folding chair he kept in a corner of his office and decided to eat lunch with the driver.

It had taken years for Vlad to convince the driver to roll the window down at his approach. That had been such a triumph for the young Vlad. Now the driver smiled as Vlad walked up and unfolded his chair.

"How is your reading?" the driver said.

"Don't you know better than me?" Vlad said. He unwrapped the sandwich he'd purchased from the deli and handed half through the open window to the man.

"The directorate has stopped contacting me," the driver said.

"What about the other Vlads? Have they made the breakthrough yet?"

"I don't know. Even the other drivers won't speak to me."

"For how long now?"

"A few months," the driver said. "I think they might have given up on you."

"So you're free now? You can finally leave the car?"

"I think so…" said the driver. "And you're free to start work again."

"I've been sitting in my office doing nothing for so long," said Vlad. "I'm not sure there's any work left in me."

"You've been reading. And you've been thinking," the driver said. "I know this isn't the end for you. I've seen how smart you are."

If anyone had seen Vlad's potential, the driver had. They had spent so many afternoons just like this, with Vlad sitting at the window of the car. First it had been the child Vlad discussing his ambitions and his readings, and then the more adult Vlad seriously proposing grand theories to the driver's smiling face.

"Where will you go?" said Vlad.

"I think maybe I'll stay here, with you," the driver said. "At least for a few more years. Don't I owe that to you?"

Wouldn't that be fine? Vlad had sacrificed his whole future for the man. Didn't the driver owe Vlad something?

"No," said Vlad. "I'm not a slave-owner. You should go out into the world."

"Is that what you want?" said the driver. "It wouldn't be slavery, not really… not if I'm choosing it."

A tear fell from Vlad's left eye. "Do you ever wonder what will happen in the future you left behind?" Vlad said. "Why did they need the products of my mind so much? Why were others willing to kill in order to stop me?

"I don't know," said the driver. "Maybe I wasn't even on the right side. But I did my duty. And I would've kept on doing it. You're the one who chose to set me free."

This tear was just the frailest echo of the thousands of tears the child Vlad had wept when he learned how the man was trapped in this car — perhaps forever — by those cruel directives. The student Vlad had formulated a plan. The adult Vlad had carried it out. And the plan had succeeded.

"Get out," Vlad said. "Go. Live."

The car door opened. The driver exited. He was huge. His shoulder was taller than Vlad's head. He was barefoot. Vlad smiled at that. The man hugged Vlad tightly and then walked to the exit of the quad, leaving his car open and empty.

Vlad slammed the car's door. He folded his chair up. He went back to his office and stood in front of his bookshelf. He put a hand on the last book he'd tried to read, and his fingers came away covered in dust.

All his life, Vlad had possessed a destiny. Now he knew that destiny was gone. He smiled. Tomorrow he'd probably feel empty. But today he felt free. ■

Rahul Kanakia *is an international development consultant based in Oakland, California.*

NATURE.COM
Follow Futures on Facebook at:
go.nature.com/mtoodm

JACEY

npg asia materials

founded in association with the Tokyo Institute of Technology

High Quality - Open Access - Rapid Review - Wide Exposure - Media Coverage - Research Summary - Impact Factor from 2012

Aims and Scope: Novel, high quality, high interest research across materials science - and from around the world.

Reasons to Submit

- Rapid peer review and fast publication times
- Research Summaries maximise interest in your work
- Wide exposure on nature.com to a large global audience
- International Editorial Board of distinguished materials scientists
- Covered by major abstracting and indexing services, with the first impact factor expected in 2012

Submit Now!

Special introductory Article Processing Charge rate for articles accepted before July 31, 2012!

Learn more at: www.nature.com/am

nature publishing group npg

SIGMA-ALDRICH

SIGMA Life Science Where bio begins™

Bioelevate.

Let our Cell Design Studio™ experts simplify your custom cell line engineering while you focus on research.

No matter how obscure or exact your specifications, our custom-engineered cell lines are tailored using CompoZr® ZFN and MISSION® shRNA technologies to fit your application perfectly.

sigma.com/biocells

biocells

©2012 Sigma-Aldrich Co. LLC. All rights reserved. SIGMA and SIGMA-ALDRICH are trademarks of Sigma-Aldrich Co. LLC, registered in the US and other countries. CompoZr and MISSION are registered trademarks of Sigma-Aldrich Co. LLC. Where bio begins and Cell Design Studio are trademarks of Sigma-Aldrich Co. LLC.